# DEFINING NEUROINFLAMMATORY PATHWAYS IN CRYPTOCOCAL MENINGITIS

**By**

**SOFIA ALICIA HAIN PORTER**

A thesis submitted to the University of Birmingham for the degree of

**DOCTOR OF PHILOSOPHY**

Institute of Immunology and Immunotherapy

College of Medical and Dental Sciences

The University of Birmingham

13th June 2024

# Abstract

*Cryptococcus neoformans* is a fungus that is ubiquitous in the environment and can cause lethal meningitis in immunocompromised individuals, with deficits in T cell responses, such as HIV/AIDS, being particularly vulnerable. Cryptococcal meningitis (CM) causes approximately 100,000 deaths per year and those who do survive often suffer from long-term neurological disorders. Tissue-resident macrophage populations in the CNS are the first line of defence against invading pathogens. In this thesis, I have explored the early immune response in the brain when *C. neoformans* first invades, focusing on microglial responses and inflammation in the surrounding meninges. This work has shown that the immune response in the brain and meninges is generally delayed. In the brain, a unique population of microglia develops that hosts live *C. neoformans* and may contribute towards inflammation and interaction with lymphocytes. In the meninges, complement activation and macrophage-platelet interactions coincided with *C. neoformans* proliferation in this tissue. Taken together, this work demonstrates *C. neoformans* has evolved strategies to overcome innate immune responses at the brain borders and within the brain parenchyma. This has important implications for developing immune therapies to treat and prevent cryptococcal meningitis, as targeting adaptive immune defects may not be sufficient to prevent disease.

# Acknowledgments

I would like to thank the Wellcome Trust for providing the funding for my PhD. I would also like to thank the MRC who have provided funding for some of the experimental work in this thesis. Further, I am grateful for the BSI, BMS and Microbiology Society that have provided funding for me to attend conferences and research visits during my PhD.

A massive thank you to my primary super supervisor Rebecca Drummond, whose passion for science and incredible work ethic has been a huge inspiration. Your endless support, patience and guidance have been invaluable for me to get to the end of this PhD. Thank you for always providing interesting and exciting discussions on data, and for your sense of humour which reminded me to not take everything so seriously. Another huge thanks to Julie Rayes, as my second supervisor you've been an amazing mentor who has helped me keep perspective and stay on track, you truly helped to steer this PhD ship away from the rocks exactly when I needed it.

To the Drummond lab – Sally, Sarah, Ebrima, Lorna, Alanoud and Sophie – what an incredible team who have endlessly helped me in the lab and provided emotional support. Thanks to the many amazing Masters and Undergraduate students who have been part of the Drummond lab, I can't wait to see what you all do next. It has been an enormous privilege to be part of the Birmingham Fellows Labs, or "FLABbies", thank you so much to the Maslowski, Dimeloe, Bending and Lu labs for your insightful feedback, collaboration and unbeatable Christmas parties. Thank you to my progress review team – Wei, Andy, Adam, Steve and Guillaume – for your insights and perspective. Big thanks to the MIDAS team; Steve, Robin, Graham, Eva and most importantly Vikki. Thank you to the many others in the III, IMI and wider MDS who have supported me, especially the technicians in the BMSU and the core facilities for all your help in generating and analysing my data. A

special thanks to the Jenne lab in Calgary for hosting my placement and re-invigorating my passion for research right in time to write this thesis.

I couldn't have got through this PhD without the support of the amazing friends I've made along the way. Thank you to the MIDAS gang, or the crème de la crème – Poppy, Lisa, Abbey, Rachel and David – I can't imagine trying to navigate my PhD without you. Thank you to the WAB lot and to my fellow DnD players; special shout out to Gillian, Tom and Tristan for the lunch time hangs and always being on hand for a coffee and a chat. The friendships I've made during this journey are the most rewarding I've ever had. Thank you all for your kindness, positivity and love, you've helped me grow and gain so much confidence. Thanks to the VAC for the chance to discuss one of my favourite things, music, which has been integral in getting me through.

I wouldn't be where I am today without the support of my family. Thank you, Mum, Dad and Amelia, for being there for my whenever I needed you. I know you don't really understand what I do but having you to talk to has been invaluable. A special shoutout to Ricky, who has been with me since I started my A-levels and who always listens without judgement. I miss living with you but thank you for taking care of Mum and Dad for me. And of course, thank you to the light of my life, Sweet Pea, you've made the end of my PhD far more bearable and bring joy to me every day.

Lastly, and most importantly, thank you to my amazing partner Jack, who has held my hand throughout this PhD rollercoaster. Whether we were living apart or together, throughout my PhD you've been there for me to provide a shoulder to cry on and you always know how to make me laugh. I've been incredibly lucky to have a partner who has already finished their PhD as your advice has truly helped me get through this. You've been there for me at my lowest points and helped me to keep my head above water. Your infinite patience, encouragement and love has allowed me to blossom and grow as a

person during my PhD. You also helped me to re-gain a work-life balance and I am so eternally grateful to have the hobbies we share as a much-needed source of joy and relaxation. I am so glad to be on this journey with you.

# Contents

Abstract ..... 1

Acknowledgments ..... 2

Contents ..... 5

List of figures ..... 9

List of tables ..... 11

Abbreviations ..... 12

Chapter 1: Introduction ..... 17

1.1 Human fungal infections ..... 17

1.2 Cryptococcus fungi ..... 21

1.3 Cryptococcosis ..... 21

1.3.1 Clinical features and diagnosis ..... 21

1.3.2 Host susceptibility and risk factors ..... 23

1.4 The host immune response to *Cryptococcus* ..... 25

1.4.1 Innate Recognition of Fungi ..... 25

1.4.2 Innate immune cells in anti-fungal immunity ..... 29

1.4.3 Adaptive Immunity ..... 36

1.5 *Cryptococcus* virulence strategies ..... 40

1.6 Hypotheses and aims. ..... 42

Hypothesis ..... 42

Aims ..... 42

Chapter 2: Materials and Methods ..... 43

2.1 Mice ..... 43

2.2 Sall-1-dTomato mouse model ..... 43

2.3 Cryptococcal meningitis infection model ..... 44

2.4 CFU analysis ..... 44

2.5 Isolation of brain leukocytes ..... 45

2.6 Flow cytometry analysis of brain leukocytes ..... 45
2.7 Intracellular staining assay ..... 46
2.8 Annexin V assay ..... 46
2.9 Fluorescence-activated cell sorting ..... 46
2.10 Ex-vivo fungal killing assay ..... 47
2.11 Flow cytometry analysis of the meninges ..... 47
2.12 CBC analysis ..... 47
2.13 Brain histology ..... 48
2.14 Meninges whole mounts ..... 48
2.15 Immunofluorescence ..... 48
2.16 BV-2 cell culture ..... 49
2.17 MPI cell culture ..... 50
2.18 *In vitro* phagocytosis assay ..... 50
2.19 RNA isolation ..... 51
2.19.1 Cells from *in vitro* culture ..... 51
2.19.2 Cells from *in vivo* experiments ..... 52
2.20 cDNA generation ..... 52
2.21 qRT-PCR ..... 53
2.22 Single-cell RNA sequencing ..... 53
2.23 Bulk RNA-seq ..... 55
2.24 Statistics ..... 56
Materials ..... 57
2.25 General tissue culture reagents ..... 57
2.26 Mouse studies ..... 57
2.27 Mycology ..... 57
2.28 Cell stimulations ..... 58
2.29 Flow cytometry antibodies ..... 58
2.30 Flow cytometry/cell sorting reagents ..... 59

2.31 Microscopy antibodies ..... 60
2.32 Microscopy reagents ..... 60
2.33 qPCR ..... 61
Chapter 3: Defining myeloid cell heterogeneity during cryptococcal meningitis using single cell RNA-sequencing. ..... 62
3.1 Introduction ..... 62
3.1.1 Neuroimmunity in the CNS ..... 62
3.1.2 Microglia identity and function ..... 63
3.1.3 Models for identifying and targeting microglia *in vivo.* ..... 66
3.1.4 Microglia in anti-fungal immunity ..... 68
3.1.5 Microglia heterogeneity ..... 70
Results ..... 73
3.2 Single cell RNA-seq analysis of myeloid populations in an *in vivo* model of cryptococcal meningitis. ..... 73
3.3 Time point analysis of the single-cell RNA-seq data reveals a population of microglia associated with established cryptococcal infection. ..... 77
3.4 scRNA-seq analysis provides clues for the function of IAMs ..... 79
3.5 Flow cytometry confirms IAMs can be identified experimentally. ..... 81
3.6 IAMs derive from microglia. ..... 90
3.7 IAMs are a reservoir for intracellular fungi ..... 95
3.8 Imaging microglia in the fungal-infected brain. ..... 97
3.9 Exploring potential phagocytic receptors expressed by IAMs. ..... 100
3.9.1 GPR84 ..... 101
3.9.2 MSR1 ..... 107
3.10 IAMs are a proliferative microglia population. ..... 109
3.11 Lymphocytes drive IAMs proliferation and recruitment of inflammatory monocytes during *C. neoformans* infection. ..... 111
3.12 Discussion ..... 114

Chapter 4: Exploring meningeal inflammation in cryptococcal infection. 120
4.1 Introduction 120
4.1.1 Immunity at the brain borders 120
4.1.2 The brain borders and cryptococcal meningitis 123
4.1.3 Platelets in anti-fungal immunity 125
Results 128
4.2 Characterising the kinetics of the meningeal immune response during cryptococcal meningitis using RNA sequencing 128
4.3 Transcriptomic analysis of the meninges at day 6 post-infection. 131
4.4 Transcriptomic analysis of the meninges at late infection 135
4.5 Meningeal whole mounts for imaging analysis. 139
4.6 Imaging the immune response to *C. neoformans* infection in the meninges. 145
4.7 Imaging the platelets in the *C. neoformans* infected meninges. 149
4.8 *C. neoformans* infection does not cause changes in platelets in the peripheral blood. 154
4.9 The role of complement in thrombosis and immune lesions in cryptococcal meningitis. 155
4.10 Discussion 163
Chapter 5: Discussion 168
References 173

# List of figures

**Introduction**

Figure 1.1 Schematic of mucosal fungal diseases. 19
Figure 1.2 Innate recognition of fungi. 26

**Chapter 3**

Figure 3.1 Microglia in health and disease. 65
Figure 3.2. Single cell RNA-seq analysis of myeloid populations in an in vivo model of cryptococcal meningitis. 75
Figure 3.3. Classification of cell clusters. 76
Figure 3.4. Time point analysis of the scRNA-seq dataset. 78
Figure 3.5. KEGG pathway analysis and DEG analysis of IAMs and non-IAMs microglia at day 6-post infection 80
Figure 3.6. Single cell RNA-sequencing reveals GPR84 is upregulated in IAMs at day 6. 82
Figure 3.7 Western blot analysis of GPR84 antibody. 83
Figure 3.8 Filipin as an IAMs marker 84
Figure 3.9 CXCL9 and CD206 as IAMs markers. 87
Figure 3.10. Finalising a flow cytometry panel for IAMs. 88
Figure 3.11. CD206 and MSR1 staining enriches for the IAMs population. 89
Figure 3.12. MSR1+CD206+ IAMs have microglia properties 91
Figure 3.13. IAMs in Sall1dTomato mice. 93
Figure 3.14 Adoptive transfer of monocytes. 94
Figure 3.15. IAMs are a reservoir for intracellular fungi. 96
Figure 3.16. Imaging the fungal infected brain. 98
Figure 3.17. Imaging of intracellular fungi. 99
Figure 3.18. GPR84 expression is upregulated in microglia during *in vitro* C. neoformans infection. 102
Figure 3.19. Modulation of GPR84 activation and its effect on *in vitro* phagocytosis of fungi by microglia. 104
Figure 3.20. siRNA knockdown of GPR84 in vitro. 106
Figure 3.21. MPI cell differentiation into microglia or macrophages. 108
Figure 3.22. IAMs are a proliferative microglia population. 110

Figure 3.23. In lymphocyte deficient mice, the dynamics of myeloid cell recruitment and IAMs expansion is altered. 113

**Chapter 4**

Figure 4.1. The brain borders. 122
Figure 4.2. PCA plot of bulk RNA-seq of the meninges from in vivo cryptococcal meningitis samples. 130
Figure 4.3. DEG analysis of the meninges at day 6 post-infection. 132
Figure 4.4. KEGG pathway analysis of the day 6 versus uninfected samples. 134
Figure 4.5. KEGG pathway analysis of the day 8 versus day 6 meninges samples. 137
Figure 4.6. DEG analysis of the meninges at late infection. 138
Figure 4.7. Dissection of the meninges to generate whole mounts for imaging 140
Figure 4.8. Imaging meningeal whole mounts. 142
Figure 4.9. Imaging meningeal whole mounts. 143
Figure 4.10. Imaging meningeal whole mounts from CX3CR1-GFP-CCR2-RFP mice. 144
Figure 4.11. Imaging C. neoformans infection in the meninges. 146
Figure 4.12. Imaging C. neoformans infection in the meninges. 147
Figure 4.13. CD45+ cells are found within fungal lesions. 148
Figure 4.14. Imaging platelets in the meninges. 151
Figure 4.15. Imaging platelets in the meninges. 152
Figure 4.16. Imaging platelets in the meninges. 153
Table 4.17. CBC analysis of uninfected and C. neoformans infected mice. 154
Figure 4.18. CFU analysis of C3 and C1q knockout mice. 156
Figure 4.19. Meningeal whole-mount imaging of the meninges at late infection. 157
Figure 4.20. Meningeal whole-mount imaging of the meninges at day 6 post-infection in C3 knockout mice. 159
Figure 4.21. Meningeal whole-mount imaging of the meninges at day 8 post-infection in C3 knockout mice. 160
Figure 4.22. Meningeal whole-mount imaging of the meninges at day 6 post-infection in C1q knockout mice. 161
Figure 4.23. Meningeal whole-mount imaging of the meninges at day 8 post-infection in C1q knockout mice. 162

# List of tables

## Introduction

Table 1.1 Incidence and risk factors predisposing to invasive fungal infections in humans. 20

## Materials

2.25 General tissue culture reagents 57
2.26 Mouse studies 57
2.27 Mycology 57
2.28 Cell stimulations 58
2.29 Flow cytometry antibodies 58
2.30 Flow cytometry/cell sorting reagents 59
2.31 Microscopy antibodies 60
2.32 Microscopy reagents 60
2.33 qPCR 61

# Abbreviations

°C – Degrees centigrade
µg – Micrograms
µl – Microlitres
µM – Micrometres
18B7 – GXM antibody
6-OAU – 6-n-octylaminouracil
AIDS – Acquired immunodeficiency syndrome
AP-1 – Activator protein 1
APC – Allophycocyanin
APC – Antigen-presenting cell
ApoE – Apolipoprotein E
Arg-1 – Arginase 1
BAM – Border-associated macrophage
BBB – Blood-brain barrier
BCR – B cell receptor
BSA – Bovine serum albumin
BTK – Bruton Tyrosine Kinase
C1q – Complement component 1q
C3 – Complement component 3
C5a – Complement component 5a
CAM – Capillary associated microglia
CARD – Caspase recruitment domain
CARD9 – Caspase recruitment domain-containing protein 9
CCL2 – Chemokine (C-C motif) ligand 2
CCR2 – C-C chemokine receptor type 2
CD – Cluster of differentiation e.g. 4, 8, 11c, 14, 16
CD206 – Mannose receptor
CD40L – CD40 ligand
Cda2 – Chitin deacetylase 2
cDNA – Complementary DNA
CFW – Calcofluor white
CGD – Chronic granulomatous disease
CHO – Chinese hamster ovary
CLEC-2 – C-type lectin-like type II transmembrane receptor
CLR – C-type lectin receptor
CM – Cryptococcal meningitis
CM-IRIS – Cryptococcal immune reconstitution syndrome
CNS – Central nervous system
CPL1 – C-terminal domain phosphatase-like 1
CR3 – Complement receptor 3
CrAg – Cryptococcal antigen
CRD – Carbohydrate recognition domain

CreER – Cre recombinase
CRIg – Complement Receptor of the Immunoglobulin superfamily
CSF – Cerebrospinal fluid
CSF1R – Colony stimulating factor 1 receptor
CX3CR1 – C-X-3-C motif chemokine receptor 1
CXCL – Chemokine (C-X-C motif) ligand-(e.g. 9, 10)
CXCR3 – C-X-C chemokine receptor type 3
DAM – Disease associated microglia
DAMP – Damage-associated molecular pattern
DAPI – 4',6-diamidino-2-phenylindole
DC – Dendritic cell
DEG – Differentially expressed gene
DNA – Deoxyribonucleic acid
EDTA – Ethylenediaminetetraacetic acid
ER – Endoplasmic reticulum
ER – Oestrogen receptor
FACS – Fluorescence-activated cell sorting
Fas/FasL – Fas/Fas ligand
FcR – Fc receptor
GBP – Guanylate-binding protein
GEM – Gel bead-in emulsions
GFP – Green fluorescent protein
GM-CSF – Granulocyte macrophage colony stimulating factor
GPCR – G-protein coupled receptor
GPIb – Glycoprotein Ib
GTP – Guanosine-triphosphate
GWAS – Genome-wide association studies
GXM – Glucuronoxylomannan
HA – Human influenza hemagglutinin
HEPES – 4-(2-hydroxyethyl)-1-piperazineethanesulfonic acid
Hexb – β-hexosaminidase subunit β
HIV – Human immunodeficiency virus
Hr – Hour
HSC – Haematopoietic stem cell
IAM – Infection-associated microglia
IAM – Inflammatory associated microglia
Iba-1 – Ionized calcium-binding adaptor molecule 1
iDTR – Inducible diphtheria toxin receptor
IEG – Immediate early response gene
IFN-γ – Interferon gamma
Ig – Immunoglobulin i.e. IgG, IgD, etc.
IL – Interleukin (i.e. IL-1, IL-4, IL-17a, etc.)
IL12RB1 – Interleukin 12 receptor subunit beta 1
IL-1R – Interleukin 1 receptor
iNOS – Inducible nitric oxide synthase

IRF3 – Interferon regulatory factor 3
IRGs – Immunity-related GTPases
ITAM – Immunoreceptor tyrosine-based activation motif
KEGG – Kyoto Encyclopedia of Genes and Genomes
Ki67 – Marker of proliferation Kiel 67
KIR – Killer cell immunoglobulin-like receptor
KO – Knockout
LPS – Lipopolysaccharide
Ly6C – Lymphocyte antigen 6 complex
Ly6G – Lymphocyte antigen 6 family member G
Lyve1 – Lymphatic vessel endothelial hyaluronan receptor 1
mAb – Monoclonal antibody
Mac-1 – Macrophage-1 antigen
MARCO – Macrophage receptor with collagenous structure
M-CSF – Macrophage colony stimulating factor
MFI – Mean fluorescence intensity
Mg – Milligrams
MHC-I – Major histocompatibility complex 1
MHC-II – Major histocompatibility complex 2
Ml – Millilitres
mM – Millimolar
MPI cells – Max-Planck Institute cells, or continuously growing non-transformed macrophages
MRI – Magnetic resonance imaging
mRNA – Messenger RNA
MSR1 – Macrophage scavenger receptor 1
MyD88 – Myeloid differentiation primary response 88
MZ – Marginal zone
N/A – Not applicable
NADPH – Reduced nicotinamide adenine dinucleotide phosphate
NET – Neutrophil extracellular trap
NET – Neutrophil extracellular trap
NFκB – Nuclear factor kappa-light-chain-enhancer of activated B cells
Ng – Nanograms
NIH – National Institutes of Health
NK – Natural killer
NKp30 – Natural killer cell p30-related protein
NLR – NOD-like receptor
NLR3P – Nucleotide-binding domain, leucine-rich–containing family, pyrin domain–containing-3
NLRC4 – NLR family CARD domain-containing protein 4
NO – Nitric oxide
NOD – Nucleotide-binding oligomerization domain-containing protein
OCT – Optimal Cutting Temperature compound
P2RY12 – Purinergic Receptor P2Y12

PAMP – Pathogen-associated molecular pattern
PBS – Phospho-buffered saline
PCA – Principal component analysis
PE – Phycoerythrin
Pen/Strep – Penicillin/Streptomycin
PF4 – Platelet factor 4
PFA – Paraformaldehyde
PKC – Protein kinase C
PLC – Phospholipase C
PRR – Pattern recognition receptor
qRT-PCR – Quantitative reverse transcription polymerase chain reaction
Raf1 – Raf-1 proto-oncogene, serine/threonine kinase
Rag2 – Recombination activating gene 2
RANTES – Regulated upon Activation Normal T Cell Expressed and Presumably Secreted
RFP – Red fluorescent protein
RFP – Red fluorescent protein
RNA – Ribonucleic acid
RNS – Reactive nitrogen species
ROS – Reactive oxygen species
ROSA – Reverse Orientation Splice Acceptor
Rpm – Revolutions per minute
RPMI – Roswell Park Memorial Institute
RT – Room temperature
Sall1 – Spalt Like Transcription Factor 1
Seq – Sequencing
siRNA – Small interfering RNA
SNP – Single nucleotide polymorphism
SRA1 – Steroid receptor RNA activator 1
STAT – Signal transducer and activator of transcription
SYK – Spleen tyrosine kinase
TAM – Tamoxifen
Th1 – T helper 1
Th17 – T helper 17
Th2 – T helper 2
Th9 – T helper 9
TLR – Toll-like receptor
Tmem119 – Transmembrane protein 119
TNFR – Tumour necrosis factor receptor
TNF-α – Tumour Necrosis Factor alpha
Treg – T regulatory cell
TRIF – TIR-domain-containing adapter-inducing interferon-beta
UV – Ultraviolet
V – Version
VCAM1 – Vascular cell adhesion protein 1

VLA4 – Very Late Antigen-4 / Integrin α4β1
WHO – World Health Organization
X – Times, e.g. 1X, 10X
YPD – Yeast extract peptone-dextrose
α-GalCer – alpha-galactosylceramide
γδ-T – Gamma delta T cells

# Chapter 1: Introduction

I have written and published a book chapter (*Immunity to Fungal Infections, Sofia Hain, Rebecca A. Drummond, Encyclopedia of Infection and Immunity, 2022)* parts of which have been used in the text below. I declare that this is my own work.

## 1.1 Human fungal infections

Human fungal pathogens are often ubiquitous in the environment or are members of the human commensal microbiota[1]. Despite this high exposure rate, fungal infections are largely opportunistic and typically cause disease in individuals who are immunocompromised. Fungal infections represent a wide range of human diseases from common superficial mucosal infections to life-threatening invasive infections. Mucosal fungal infections are the most common human mycoses and include vulvovaginal candidiasis and dermatophytosis (Figure 1)[1–4]. These types of infections can affect apparently immunocompetent individuals, albeit they are often associated with environmental risk factors such as contact with another infected individual or places where ideal growth conditions for the fungi are present. Immunosuppression is also a significant risk factor for mucosal fungal infections such as oropharyngeal candidiasis, and for the development of chronic infections. Whilst they are non-life-threatening, these fungal infections are a significant healthcare burden and can severely affect quality of life and mental health, especially for those with recurrent infections[1]. In contrast, invasive fungal infections predominantly affect people who are immunocompromised because of iatrogenic factors, inherited immunological defects or acquired immune deficiency (Table 1)[3–5].

The incidence of invasive fungal infections has been rising over the last few decades due to a growing at-risk population of immunosuppressed individuals. This is partly due to

significant increases in the use of antibiotics, steroids, and other immune-modulating drugs[6]. Furthermore, there are now several documented congenital risk factors for severe fungal infections, including primary immunodeficiency disorders such as chronic granulomatous disease (CGD) and CARD9 deficiency[1]. Global spread of viral infections which predispose to fungal infections (e.g. HIV) and the recent emergence of SARS-Cov-2 (COVID19) have also contributed to increased numbers of fungal infections and worsened clinical outcome[7,8]. Mortality rates for invasive fungal infections have remained high in part due to inadequate diagnostics and treatments, and limited access to gold-standard antifungal drugs in low-middle income countries which carry the highest burden of infections[3,9–11]. Additionally, the efficacy of currently available antifungal drugs is being eroded by increasing antifungal drug resistance. For example, *Candida auris* is a recently discovered multi-drug resistant species that causes significant mortality and morbidity, which has spread to at least 30 countries following its discovery in 2009[12]. Despite the impact of fungal diseases on human health, there remains much to be learned about the induction and regulation of antifungal immune responses. Yet, a greater understanding of antifungal immunity will be critical for the future development of diagnostics, vaccines and adjunctive immune-based treatments for fungal infection[3,13]. In fact, the WHO recently released its first ever fungal priority pathogens list[14]. This report highlights 19 fungal species ranked based on their threat to public health and need for research and development, with the highest-ranking pathogen on being *Cryptococcus neoformans*.

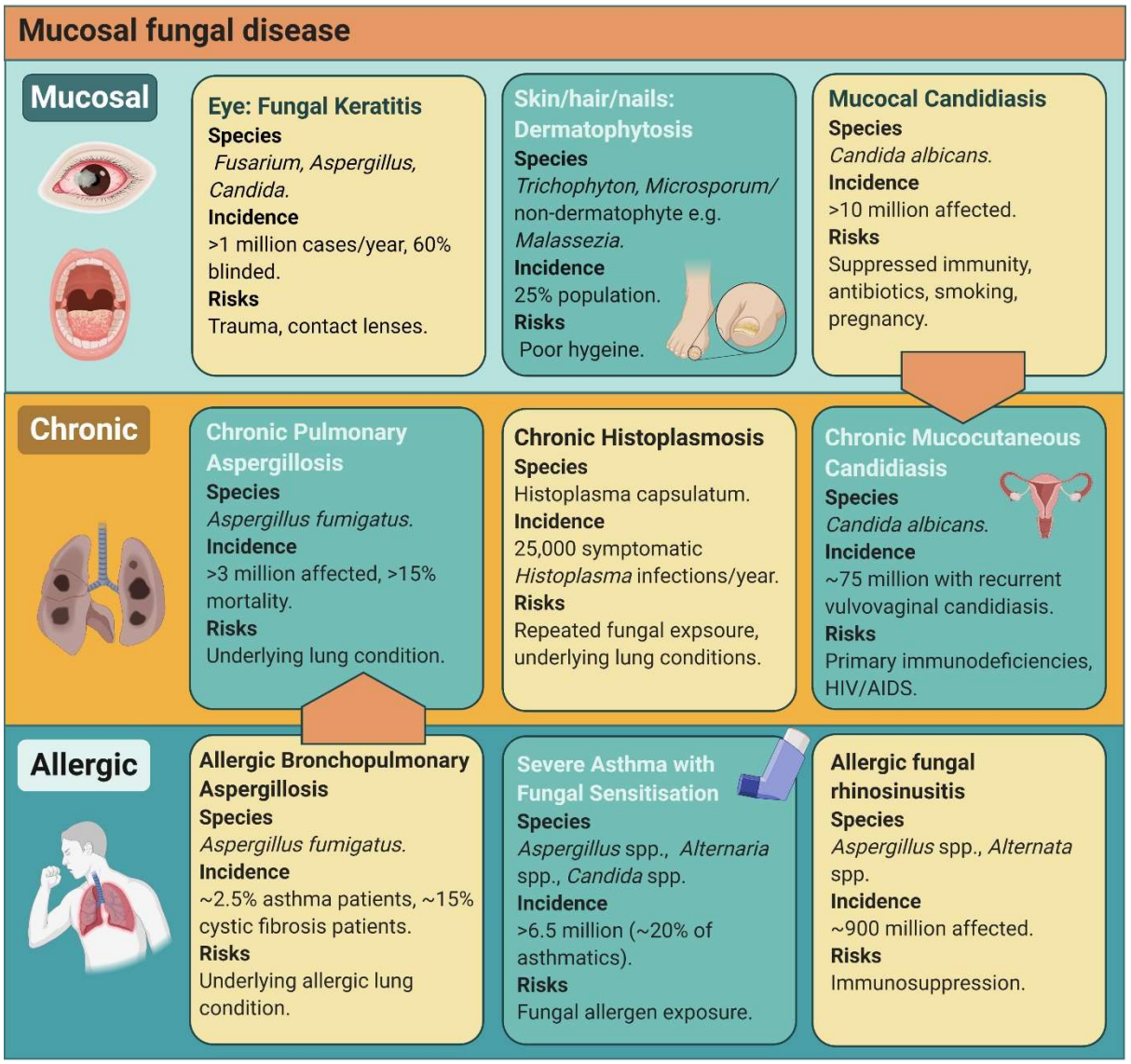


**Figure 1.1 Mucosal fungal diseases.** Published in *Immunity to Fungal Infections*[1]. Non-disseminated mucosal fungal infections are mostly non-life threatening, albeit they have a significant healthcare burden as they are often recurring or chronic in nature. Many are associated with a variety of risk factors and caused by a wide range of fungal species.

| Fungal disease | Infectious Agent | Disease burden | Fatality rate | Number of deaths | Tissues affected | Risk factors |
|---|---|---|---|---|---|---|
| Cryptococcal meningitis | *Cryptococcus neoformans*, *Cryptococcus gattii* | 194,000 | 60-100% | 147,000 | CNS | HIV/AIDS, leukemia, organ transplant, immunosuppressants |
| Invasive aspergillosis | *Aspergillus* spp., | >2 million | 43-95% | ~1.7 million | Lung, CNS, kidney, heart, skin, eye, bone | Cancer, organ transplant, COPD |
| Invasive candidiasis | *Candida* spp. | ~1.5 million | 35-90% | ~1 million | Lung, CNS, kidney, heart, skin, eye, bone, abdominal, liver, spleen | Cancer, organ transplant, surgery, hospitalisation |
| Disseminated histoplasmosis | *Histoplasma capsulatum* | ~70,000 | 30-100% | ~66,000 | Any, mostly liver, spleen or gastrointestinal | HIV/AIDS |
| Pneumocystis pneumonia | *Pneumocystis jirovecii* | 105,000 (non-AIDS)<br>400,000 (AIDS) | 15-100% | ~210,000 | Lung | HIV/AIDS, immunosuppressants |
| Mucormycosis | Mucormycetes | ~200,000 | 25-100% | 84,000 | Multiple, mostly lung and skin, kidney exclusively in India | Diabetes, organ transplant, trauma, COVID-19 |

**Table 1.1 Incidence and risk factors predisposing to invasive fungal infections in humans.** Adapted from figure published in *Immunity to Fungal Infections*[1]. Data derived from Bongomin et al. [4]and Denning[5].

## 1.2 Cryptococcus fungi

*Cryptococcus* species are fungi of the phylum Basidiomycota. Whilst most basidiomycetes are known to form large visible multi-cellular structures by sprouting mushroom fruiting bodies, *Cryptococcus* species are microscopic yeast-forming fungi. They can reproduce asexually and sexually, with the latter forming tiny basidiospores enabling efficient dispersal. *Cryptococcus* species are pathogenic yeasts ubiquitous in the environment, and can commonly be found in the soil, trees, and bird droppings[15–17]. There are many *Cryptococcus* species, for which the taxonomy is frequently evolving[18,19], however the main human disease-causing species can be divided into variants of either *Cryptococcus neoformans* or *Cryptococcus gattii*[16,20]. The major global cause of cryptococcal infection (known as cryptococcosis) is *C. neoformans* serotype A, causing systemic disease in immunocompromised patients. *C. deneoformans* or serotype D and the serotype AD hybrid strain have predominantly been found in Europe and are associated with milder skin infections. The members of the *C. gattii* species complex are differentially distributed across the continents, with some rarer species particularly associated with HIV patients[20,21].

## 1.3 Cryptococcosis

### 1.3.1 Clinical features and diagnosis

*Cryptococcus* spores or yeasts can easily be inhaled into the lungs due to their microscopic size[15]. The fungus can then become lodged in the alveoli, resulting in colonialisation and asymptomatic infection. The fungus is often contained by a granuloma and remains dormant or is cleared entirely[21]. However, in an immunocompromised host exposure to cryptococcus, or reactivation of a latent infection by entering an immunosuppressed state, can result in disease[16,21]. Human cryptococcosis is an invasive

infection with heterogeneous presentation depended on patient background, underlying conditions and cryptococcal species. Cryptococcus, like many other invasive fungal infections, has tropism for specific tissues, in this case the brain and the lungs. Spores or yeast that have been trapped in the lungs can disseminate to the CNS, resulting in cryptococcal meningitis. Disease can also occur in the lungs themselves in pulmonary cryptococcosis. Patients may present with both lung and brain disease, and in other rare instances of cryptococcus infection may occur in other organs, for example in the bone[15,22].

Cryptococcal lung infection presents with pneumonia-like symptoms, with patients experiencing severe lung inflammation resulting in symptoms including coughing, fever, and shortness of breath[23]. However, a subset of patients will experience lung failure with no prior symptoms. The generic clinical presentation of pulmonary cryptococcosis combined with a lack of clinical suspicion for fungal infections can cause delays in diagnosis, resulting in worse disease outcomes[23,24]. Furthermore, a definitive diagnosis often cannot be made from diagnostic imaging alone as the lungs of a pulmonary cryptococcosis patient can have similar features to other lung infections and even lung cancer[23]. Additional laboratory testing is therefore required, with the lateral flow test for cryptococcal antigen (CrAg) being the gold standard[21,23].

Cryptococcal meningitis (CM) symptoms include headaches, nausea, fever, vomiting, confusion, behavioural changes and altered vision[25]. If left untreated, patients develop increasingly severe symptoms of cognitive impairment, seizures and ultimately become comatose[25]. Mortality from CM varies depending on geographical location and the underlying condition of the patient, but can be as high as 70%, and those that do survive often experience long-term neurological defects and disability[26,27]. Diagnosis of CM is confirmed through lumbar puncture and collection of a CSF sample for CrAg testing[25,28].

The development of the CrAg test has had a significant impact on the speed of diagnosis for cryptococcosis as testing can be performed on fluids such as blood which are quicker to collect than CSF[29]. The specific testing of CSF enables diagnosis of the presence of the fungus in the CNS. Additional tests that can be performed on CSF include the India Ink test, which detects cryptococcal capsule, and culturing the CSF on agar to check for fungal growth. However, in some patients, fungal burdens in the CSF can be very low, so the increased sensitivity of the CrAg test is vital to prevent the infection from being missed[25,28]. Imaging analysis such as MRI and histological examination of post-mortem tissue have enabled characterisation of hallmarks of CM in the brain. These include enlarged perivascular spaces, infarctions, hydrocephalus, meningeal inflammation, pseudocysts, and cryptococcomas[25,30,31]. Histopathology of these cryptococcomas has revealed they are tumour-like masses of fungi surrounded by capsule and which may or may not be surrounded by inflammatory cells [25,30,31]. Cryptococcal cells may also be found in small clusters with inflammatory cells in the enlarged perivascular spaces, and in areas of cryptococcal growth there may be neuronal death resulting in a 'Swiss cheese' morphology, which is replicated in animal models of CM[25,30–32]. The extent of fungal infiltration and growth in the brain and meninges, along with the recruitment of leukocytes, varies depending on patient background, with HIV patients tending to have more fungi distributed across the brain, often extracellularly[25]. To effectively diagnose and predict cryptococcosis patient outcomes, and determine the best course of treatment, it is therefore vital to understand the patient's immune background.

### 1.3.2 Host susceptibility and risk factors

As described above, cryptococcosis is typically seen in patients with some form of immunosuppressive state. Cryptococcus is ubiquitous in the environment, so if exposure alone was sufficient to result in disease, then cryptococcosis would be far more common.

However, cryptococcosis is also seen in patients described as apparently immunocompetent; that is, the patient has no known background of immunosuppression, but may have, for example, genetic polymorphisms that have not been diagnosed. Cryptococcosis can affect several different immunocompromised populations, however it is particularly common in HIV/AIDS patients. This is reflected in the spike in incidence of cryptococcosis around the same time the worldwide HIV pandemic was at its peak[28,33]. Whilst antiretroviral therapy is now widely available, in low and middle-income countries this is not necessarily the case, and it is in these regions that HIV-associated cryptococcosis cases are the most prevalent. In high-income countries, the at-risk populations have been evolving in the last 20 years as the use of immunosuppressive therapies has grown. These include those undergoing solid organ transplantation, bone marrow transplant recipients and cancer patients. Furthermore, there has been an increase in iatrogenic risk factors for cryptococcosis due the increasing use of immune-modulating drugs in modern medicine[6]. Advances in genomics testing and the increase of GWAS has enabled the identification of primary immunodeficiencies that increase the risk of cryptococcosis, for example *IL12RB1* deficiency[34–36].

Whilst a large percentage of cryptococcal lung infections occur in immunocompetent patients, immunosuppression is still a key risk factor, and this is certainly the case for CM. Pulmonary cryptococcosis in immunocompromised individuals is seldom asymptomatic and diagnostic imaging often reveals distinct clinical pathophysiology, likely reflecting the increased severity of the disease in these patients[23]. As described above, CM presentation in imaging analysis often differs between patients that are HIV positive or negative. Disease severity in CM can vary widely depending on the patient background, the geographical location, and the cryptococcal species causing the infection. HIV-positive CM patients generally present with symptoms more rapidly, and these symptoms may be more severe, however this can in fact aid diagnosis[25]. A potential complication of

CM is CM-IRIS (immune reconstitution inflammatory syndrome). In a subset of patients, reversal of immunosuppression is followed by a more severe inflammatory response to cryptococcal infection and worse outcomes, and this is most often seen in HIV-positive CM cases[25,37,38]. In these patients there are two main types of IRIS, which centres around the timing of anti-retroviral and antifungal therapies. Unmasking IRIS is when patients only develop CM symptoms after antiretroviral therapy is administered; paradoxical IRIS is when beginning antiretroviral therapy results in worsened CM symptoms after an initial period of recovery following anti-fungal therapy [25,37,38]. It is therefore thought that the inflammation caused by the fungal infection, rather than the fungus itself, is the main driver of morbidity and mortality from cryptococcal meningitis. Understanding the immune response to this fungus us therefore vital to develop immunotherapies to better treat this disease.

## 1.4 The host immune response to *Cryptococcus*

The susceptibility of patients with immunosuppression to *Cryptococcus* infection highlights the importance of an appropriate immune response to the fungus. Below I will outline what we know about the role of different immune cells and receptors in protection against cryptococcosis.

### 1.4.1 Innate Recognition of Fungi

The immune response to fungal pathogens begins with innate recognition of the fungi by PRRs expressed by myeloid cells[1]. Fungal recognition is mediated by several classes of PRRs including the C-type lectin receptors (CLRs), Toll-like receptors (TLRs) and NOD-like receptors (NLRs) which bind to components of the fungal cell wall and nucleic acids leading to the activation of intracellular signalling cascades and antifungal immune responses (figure 1.2)[39–41].

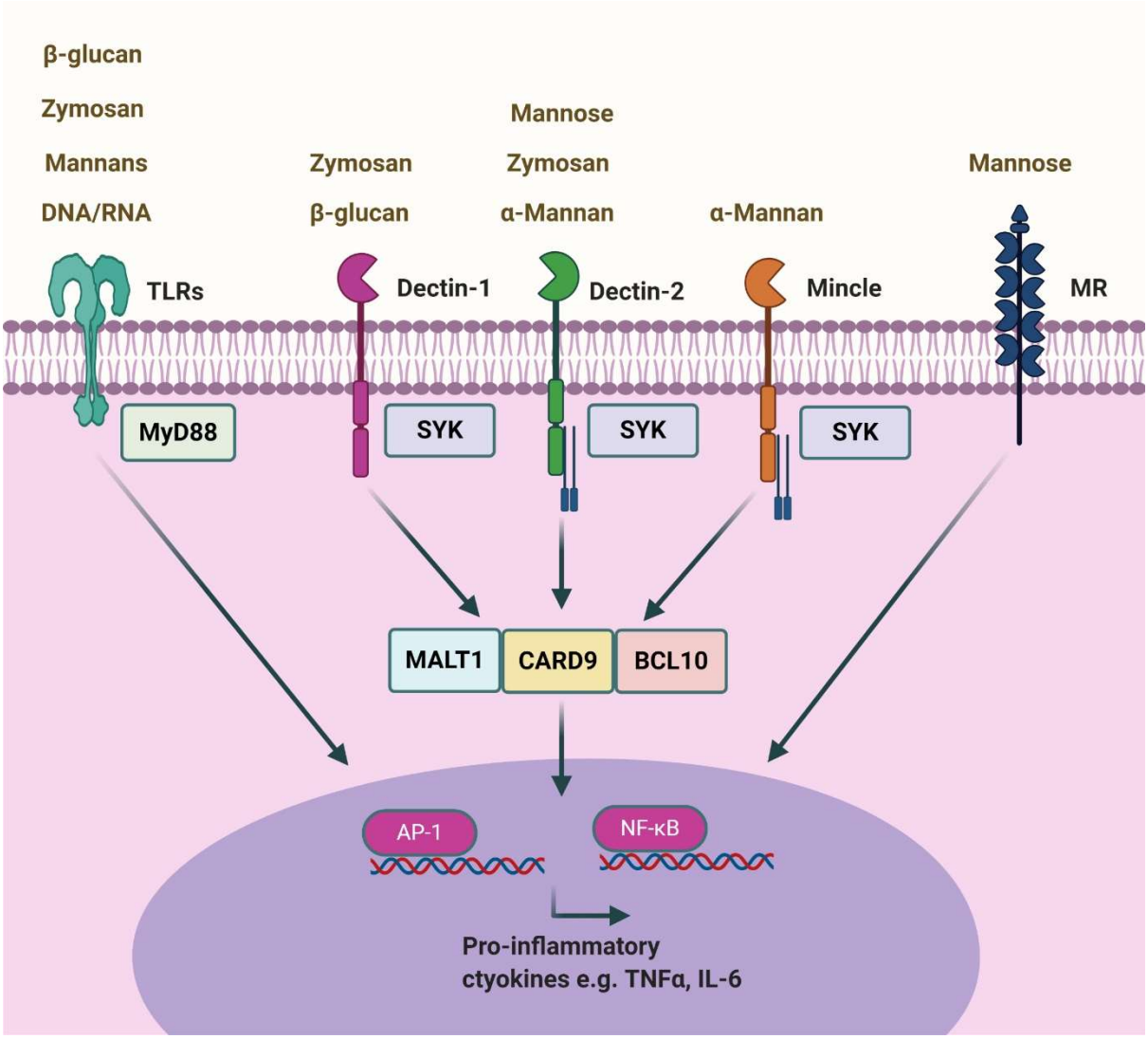


**Figure 1.2. Innate recognition of fungi.** Published in *Immunity to Fungal Infections*[1]. Fungal PAMPs deriving from the fungal cell wall are bound by TLRs or CLRs expressed by myeloid cells. Recognition by these receptors activates intracellular signalling cascades mediated by MyD88 (TLRs) or SYK/CARD9 (CLRs), culminating in a cellular immune response (e.g. cytokine production).

#### 1.4.1.1 CLRs

The CLRs are a large family of transmembrane receptors which share a carbohydrate recognition domain (CRD) that is either calcium-dependent (C-type lectin) or calcium-independent (C-type lectin-like)[42]. Several CLRs have been shown to activate antifungal immunity in mice and humans, particularly the CARD9-coupled CLRs Dectin-1, Dectin-2, Dectin-3, and Mincle[40]. Dectin-1 is the best-studied CLR in the context of antifungal immunity and recognises β-glucan in the fungal cell wall. Upon β-glucan binding, the ITAM signalling motif within the cytoplasmic tail of Dectin-1 (or FcRγ, the signalling partner of Dectin-2/3) becomes phosphorylated, resulting in the recruitment and activation of Syk kinase. This initiates a signalling cascade via the kinases PLCγ and PKCδ leading to the formation of the CBM signalling complex, composed of CARD9, BCL10 and MALT1. This activates phagocytosis and fungal killing pathways and drives the production of pro-inflammatory cytokines through activation of transcription factors (e.g. NFκB and AP-1) and the NLRP3 inflammasome. Dectin-1 can also alternatively activate the Syk-independent Raf1 signalling pathway, driving IL-23 production to promote Th17 differentiation[13,40,41,43].

The importance of CLR signalling in antifungal immunity has also been demonstrated by studies in mice deficient in CARD9 or CARD9-coupled receptors, which have increased susceptibility to *A. fumigatus, C. albicans* and *C. neoformans* infection[43]. This is partially replicated in humans where deleterious mutations in *CARD9* result in a primary immunodeficiency disease that specifically causes increased susceptibility to fungal pathogens – excluding *C. neoformans* – but not bacterial or viral infections. CARD9 deficiency presents with an organ-specific pattern of susceptibility with patients predominantly presenting with either subcutaneous skin infections, CNS candidiasis or extra-pulmonary aspergillosis[8,44,45]. Human deficiencies in single CLRs have also underscored the importance of this receptor family in antifungal immunity, for example

Dectin-2 deficiency has been shown to promote susceptibility to pulmonary cryptococcosis[46].

#### 1.4.1.2 TLRs

TLRs are a family of PRRs consisting of 12 members in mice and 10 in humans, which are expressed at the cell surface or on intracellular organelles. All TLRs have a PAMP-recognising ecotodomain, a transmembrane domain and a Toll/IL-1 receptor domain for signalling[47]. TLRs bind a diverse array of fungal ligands including cell wall components (TLR2), mannans (TLR4) and fungal DNA (TLR9)[40]. Extracellular TLRs recruit the signalling adaptor MyD88 to activate AP-1 and NF-κB resulting in production of inflammatory cytokines, while intracellular TLRs signal through the adaptor TRIF to activate interferon responsive transcription factors, such as IRF3[47]. MyD88-deficient mice have an increased susceptibility to multiple fungal infections, including *A. fumigatus*, *C. albicans*, *C. neoformans*, and *Histoplasma capsulatum*, while deficiencies in single TLRs promote susceptibility in a context-dependent manner[39]. However, MyD88 deficiency in humans does not appear to be associated with an increased susceptibility to fungal infections. Instead, MyD88-deficient patients die in early childhood from profound bacterial infections, presumably because CLR-CARD9 signalling is sufficient to protect against fungal infection in the absence of the TLRs[48].

#### 1.4.1.3 NLRs

NLRs are an intracellular family of PRRs which can be divided into inflammasome forming (e.g. NLRP3 and NLRC4) and non-inflammasome forming (e.g. NOD1 and NOD2). Inflammasomes are large protein complexes that drive proteolytic cascades mediated by caspase enzymes culminating in the production of bioactive cytokines IL-1β and IL-18. In mice, deficiencies in NLRP3 and NLRC4 promotes susceptibility to several fungal pathogens including *C. albicans, C. neoformans* and *A. fumigatus*[40]. Until recently, the fungal ligands responsible for inflammasome activation were unknown, but new studies

have shed light on how these pathways become activated by *Candida* and *Aspergillus* fungi. *Candida* hyphae secrete a peptide toxin called Candidalysin which supports the fungal invasion of epithelial barriers and establishment of mucosal infections[49]. Candidalysin was recently found to activate the NLRP3 inflammasome in macrophages, promoting both fungal escape (by driving macrophage death)[50] and the induction of IL-1β-dependent protective immunity by microglia in the brain[51]. Fungal activation of inflammasomes can therefore have diverse consequences that are organ- and cell type-specific. Galactosaminogalactan, a component of the *Aspergillus* cell wall, was recently found to bind mammalian ribosomes and block translation, which acted as a trigger for NLRP3 inflammasome activation and induction of protective immunity[52]. Thus, by studying fungal-mediated activation of these pathways, we have discovered novel mechanisms controlling inflammasome function.

### 1.4.2 Innate immune cells in anti-fungal immunity

#### 1.4.2.1 Macrophages

Macrophages are myeloid cells of the innate immune system with a range of functions including tissue repair, removing dead cells, maintaining homeostatic organ function and uptake and clearance of invading microbes. During embryonic development, macrophages first arise from progenitors in the yolk sac, some of which seed developing organs to generate specialised tissue-resident macrophage populations. Thereafter, hematopoietic stem cells (HSCs) in the foetal liver and the bone marrow give rise to monocytes which circulate in the blood and differentiate into macrophages upon entering tissue. The phenotype and function of monocyte-derived macrophages is shaped by environmental signals and the nature of the inflammatory insult [53–55]. For example, high concentrations of IFN-γ due to intracellular *C. neoformans* infection drives upregulation of the transcription factor STAT1 which supports polarisation towards a pro-inflammatory

and phagocytic phenotype, termed M1 or classical activation. M1 macrophages are particularly important for protective immunity against intracellular bacteria and fungi. On the other hand, exposure to IL-4 or IL-10 stimulated by extracellular pathogens such as parasites and dimorphic fungi, upregulates STAT6 resulting in an anti-inflammatory/tissue repair macrophage phenotype termed M2 or alternative activation [56,57].

Macrophages detect fungal pathogens via PRRs (see figure 1.2). Once activated by PRRs, macrophages initiate fungal uptake and killing by phagocytosis and produce pro-inflammatory cytokines and chemokines. Macrophages phagocytose fungi using either opsonic receptors (e.g. CR3, FcγR) or non-opsonic receptors (e.g. Dectin-1) [58,59]. Following uptake, fungi-containing phagosomes fuse with lysosomes to form an acidic phagolysosome compartment, which contains a milieu of anti-microbial enzymes and drives nutrient starvation within the fungus, facilitating fungal death. To kill fungi, macrophages produce toxic compounds such as reactive oxygen species (ROS) which is generated by the enzyme NADPH oxidase. In addition to ROS, macrophages produce reactive nitrogen species (RNS) and nitric oxide (NO) following activation of the iNOS enzyme [60]. M1 macrophages express high levels of iNOS which enables the conversion of arginine to NO and citrulline. In contrast, M2 macrophages alternatively upregulate arginase to convert arginine to ornithine and urea, and so produce little NO[61]. Nitrogen-dependent fungal killing by M1 macrophages has been shown to be protective in many fungal infections including cryptococcosis. STAT1 knockout mice, which lack an M1 response, are highly susceptible to pulmonary *C. neoformans* infection resulting in increased lung/brain fungal burden and accelerated mortality[62]. Further work has shown that these STAT1 knockout mice are deficient in their production of NO by lung macrophages, and iNOS knockout mice are deficient in controlling intracellular *C. neoformans* infection[63–65]. STAT1 regulates expression of CXCL9 and CXCL10, which

drive recruitment of CXCR3$^{+}$ Th1 CD4+ T cells that promote fungal clearance by enhancing phagocytic and killing functions of macrophages[32,62].

Macrophages are critical antifungal immune cells since individuals with genetic mutations that disrupt macrophage responses have been shown to be more susceptible to invasive fungal infections[39]. In the case of cryptococcosis, autoantibodies against GM-CSF have been identified as a risk factor for cryptococcosis[25,66]. GM-CSF is important for surfactant clearance by alveolar macrophages, and signals via phosphorylation of STAT5 which activates macrophage inflammatory signalling; therefore, autoantibodies disrupt this process which results in a rare lung disease, pulmonary alveolar proteinosis[35,67]. In mouse models, macrophage depletion results in higher fungal burden and decreased survival following infection with *C. neoformans*[68,69]. However, there are some contexts in which macrophages may promote fungal infection. For example, depletion of macrophages at a late stage of *C. neoformans* infection reduced dissemination of the fungus to the spleen and brain in mice, indicating that *Cryptococcus* may utilise macrophages for immune evasion and trafficking to distant organs[70].

Tissue-resident macrophages often act as the front-line defence against invading fungi and promote rapid responses via chemokine production, which recruit and activate leukocytes. For example, microglia are CNS-resident macrophages that have been shown to signal via pro-inflammatory cytokines upon *C. neoformans* infection but are unable to effectively control intracellular growth of the fungi[71]. The role of tissue resident macrophages in CM will be discussed in further detail in **chapter 3**.

#### 1.4.2.2 Monocytes

Monocytes are circulating myeloid cells that differentiate into macrophages or dendritic cells (DCs) following recruitment into tissues[57]. However, monocytes can also act as immune effector cells, mediating fungal uptake and producing inflammatory cytokines.

Monocytes are classed into three subtypes: classic (inflammatory), intermediate, and non-classical (patrolling). These subsets are identified by expression of surface receptors, in which "classic" are identified as $CD14^{high}CCR2^{+}CD16^{int}CX3CR1^{+}$, "intermediate" as $CD14^{high}CCR2^{+}CD16^{int}CX3CR1^{+}$ and "non-classical" as $CD14^{low}CCR2^{-}CD16^{high}CX3CR1^{+}$. Equivalent subsets exist in mice which are defined by expression of Ly6C in addition to CCR2 and/or CX3CR1[57,72]. Classical monocytes are the main circulating monocyte population that seeds inflammatory macrophages/DCs. The functions of patrolling and intermediate monocytes are less well defined; patrolling monocytes are believed to be involved in homeostatic functions and tissue repair, while intermediate monocytes have been observed to perform both classical and non-classical functions, dependent on context[57,72].

Monocytopenia, where patients have a reduced number of circulating monocytes, promotes susceptibility to systemic fungal infections including cryptococcosis[39,73]. Furthermore, dysfunctional monocytes have been associated with worse outcomes in both HIV positive and non-HIV CM patients, and with development of CM-IRIS[72,74]. In these studies, monocyte dysfunction was defined by defective phagocytosis, reduced production of pro-inflammatory cytokines such as TNF-α and a decrease in antigen presentation[72]. Once cryptococcal infection occurs in the tissue, monocytes are recruited to the site of infection[72,75,76]. *In vivo* studies have shown that in the lung, this process occurs in a CCR2-dependent manner, and most of the monocytes recruited are $Ly6C^{high}$ inflammatory monocytes[72,75]. In CCR2 knockout mice, the decreased recruitment of monocytes to the lung results in fewer macrophages and dendritic cells in the lung to control the fungal burden. Furthermore, monocytes can present antigen to T cells and drive a beneficial Th1 response in the lung (discussed in more detail below). In the brain, patrolling $Ly6C^{low}$ monocytes are the main recruited population, with the interaction

between TNFR-driven monocyte VLA4 and vascular endothelial VCAM1 being a key driver of this recruitment[76].

Although monocytes exert many protective functions in the context of fungal infection, there is evidence to suggest that their role can also be detrimental to fungal clearance. For example, monocyte depletion during early *C. neoformans* infection was found to be protective by preventing an accumulation of M2 macrophages which support *C. neoformans* proliferation and survival[72,75]. Furthermore, *C. neoformans* has also been shown to hijack monocytes and use them as 'Trojan Horses' to invade the blood-brain-barrier[77].

#### 1.4.2.3 Dendritic cells

DCs are professional antigen-presenting cells that interact with T-cells and activate the adaptive immune response. DCs possess long dendrites decorated with PRRs which enable them to sample their surroundings and rapidly detect an inflammatory insult or infection, often resulting in the release of cytokines to activate other effector cells[78]. DCs can be found circulating in the blood but are also resident in lymphoid tissues and in various mucosal tissues such as the skin and gut[79]. Once activated via PRRs, DCs migrate to lymph nodes where they present antigenic peptides to CD8 and CD4 T cells on MHC-I or MHC-II molecules, respectively [78]. This process of antigen presentation leads to the development of the adaptive immune response which is critical for the clearance of fungal pathogens such as *C. neoformans*[80]. DCs are divided into different subsets based on developmental origin, location and immune function[79]. HSCs in the bone marrow give rise to the common DC precursor, which can then go on to become conventional DCs (cDC, further subdivided into cDC1 and cDC2) or plasmacytoid DCs (pDC). Alternatively, monocytes can give rise to monocyte-derived DCs (moDCs), or embryonic precursors give rise to tissue-resident DC populations (e.g. Langerhans cells in the skin)[79,81].

Early *in vivo* work showed the key DC populations in *C. neoformans* infection are moDCs and Langerhans cells[82]. Using an inducible depletion model of CD11c-expressing cells – which depleted DCs and alveolar macrophages in the lung – showed decreased survival in mice infected with *C. neoformans* strain 52D (a mildly virulent strain that is used in chronic infection models)[83]. Whilst no significant difference in CFU was seen, there was an increase in neutrophil infiltration into the lung, and the inflammation in the lungs was more disseminated, likely reflecting the importance of DCs and alveolar macrophages in controlling the infection by granuloma formation[83]. As discussed above, a major source of DCs in the lung during cryptococcal infection are inflammatory monocytes, which is dependent on CCR2[72,75]. DCs have also been shown to be highly efficient in phagocytosis, killing, and antigen presentation to T cells during cryptococcal lung infection, however these processes can be disrupted by the fungal capsule (discussed in the next section)[64,65]. However, DCs have also been shown to significant in the induction of a Th2 T cell response, which is typically detrimental to *C. neoformans* clearance[64,65]. In a murine vaccination model of *C. neoformans*, it was shown that DCs exhibited trained immunity, that is immune memory by innate immune cells as opposed to adaptive immune cells[84,85]. DCs in the lung were shown to be 'M1'-like and had increased pro-inflammatory cytokine signalling upon re-challenge with *C. neoformans*[85].

#### 1.4.2.4 Neutrophils

Neutropenia and inherited defects in neutrophil function are strongly associated with an increased risk for candidiasis, aspergillosis and mucormycosis in humans[86]. Neutrophils are short-lived phagocytes specialised for pathogen killing, particularly extracellular pathogens, that are rapidly recruited in large numbers to the site of infection[87]. Neutrophils release granules that contain microbicidal enzymes such as elastase and myeloperoxidase, and produce large amounts of ROS; these effectors are defined as non-oxidative and oxidative killing mechanisms, respectively[87]. Furthermore, neutrophils can

form neutrophil extracellular traps (NETs), a mesh of chromatin containing citrullinated histones and antimicrobial proteins (e.g. calprotectin) to trap and kill pathogens[88].

Early studies showed that *in vitro*, human neutrophils can kill *C. neoformans* both through ROS and granule release[89]. Myeloperoxidase knockout mice infected with *C. neoformans* were shown to have decreased survival, increased lung fungal burden, polarisation towards a Th2 response, and increased dissemination of the infection to the brain[90]. Neutrophil phagocytosis and killing of *C. neoformans in vitro* is dependent on opsonisation by the complement protein C5a[91], whilst *in vivo* imaging through intravital microscopy has shown that in the brain microvasculature, neutrophils have an important function in the uptake of *C. neoformans* and this is mediated by C3[92].

Nevertheless, the evidence of beneficial functions for neutrophils in cryptococcosis specifically is still limited, and it seems they may be more significant in other invasive fungal infections such as candidiasis. A study using neutropenic mice found that these mice responded better to cryptococcal infection, and one mechanism later identified was that by depleting neutrophils, the production of IL-17A by γδ-T cells is increased which is protective in *C. neoformans* lung infection[93,94].

#### 1.4.2.5 NK Cells and NK T cells

NK (natural killer) cells are lymphoid cells that do not have rearranged antigen receptors and respond rapidly to inflammatory stimuli in an innate-like fashion[58]. NK cells are cytotoxic cells involved in the direct killing of fungal pathogens; however, they also secrete inflammatory mediators to activate and recruit other immune cells including macrophages. NK cells recognise fungal pathogens via their expression of TLRs, CLRs and NK activation/inhibitory receptors[95]. The latter includes Ly49 and KIR receptors, which mediate either activation or inhibition signals in NK cells[96]. For example, NKp30 directly recognises β-glucan on the surface of *C. neoformans*[97]. These recognition events lead to

NK cell activation, resulting in the release of perforin-containing granules and fungal killing[95].

NK T cells are a subtype of T cell which express the invariant T cell receptor (TCR) through which they recognise lipid antigens presented by CD1d (an MHC-like molecule) on antigen presenting cells[98]. NK T cells produce significant amounts of IFN-γ and are particularly important in *C. neoformans* infection where Th1 responses are protective[99]. Indeed, a specific subset of NK T cells expressing TCR chain Vα14 was found to accumulate in the lungs of *C. neoformans*-infected mice in a CCL2-dependent manner, and depletion of these cells (e.g. using CCL2 KO mice) resulted in reduced Th1 immunity and increased fungal burden[99,100] . Furthermore, non-specific activation of NK T cells using the lipid α-GalCer was shown to increase IFN-γ production by NK T cells resulting in enhanced fungal clearance[99,100].

### 1.4.3 Adaptive Immunity

#### 1.4.3.1 T cells

CD4 T-cells recognise specific peptide antigen via their TCR in the context of MHC-II expressed on the surface of antigen-presenting cells (such as DCs, B-cells and macrophages). The importance of CD4 T-cells in cryptococcosis is evidenced by the susceptibility of HIV/AIDS patients for whom loss of CD4 T-cells is a defining characteristic of the disease. Furthermore, primary immunodeficiencies associated with increased risk of cryptococcosis often involve dysfunctional adaptive immunity, such as idiopathic CD4 lymphopenia and anti-IFN-γ autoantibodies[25,101,102].

CD4 T-cells differentiate into several subtypes (including Th1, Th2, Th9, Th17 and Treg) in response to environmental signals and APC-derived instructions, which are classified based on expression of master transcription factors and cytokine profiles[80]. Th1 cells are defined by their production of pro-inflammatory cytokines such as TNF-α and IFN-γ and

are associated with intracellular infection, for example by bacteria and fungi. Th2 cells on the other hand produce cytokines including IL-4, IL-5 and IL-13 and are associated with extracellular pathogens such as parasites. IFN-γ secreted by Th1 cells drives macrophages towards an M1 phenotype, which is protective in *C. neoformans* as discussed above[103]. Adjunctive immune-based therapy with recombinant IFN-γ has been shown to improve clinical outcome in patients with cryptococcal meningitis[104]. Indeed, mice deficient in IFN-γ or its receptor are highly susceptible to pulmonary infection with *C. neoformans*[105]. Th2 responses on the other hand are considered detrimental in cryptococcosis and have been associated with worse outcomes, including increased dissemination of the fungi and uncontrolled inflammation[101]. To determine the mechanism by which *C. neoformans* induces a Th2 response in the lungs, Nielsen and colleagues developed an assay to identify reactive T cells that expressed antigen specific for *C. neoformans*[106]. Using the cryptococcal-specific antigen chitin deacetylase 2 (Cda2) (a component of the fungal cell wall), they developed an MHC-II tetramer that would bind and therefor identify all Th cells with the Cda2 antigen [106]. This assay confirmed that most antigen-specific T cells in the lung where Th2 which allowed the fungus to establish a pulmonary infection. Tregs are a subset of CD4 T-cells that suppress inflammation to limit potential tissue damage[107]. In cryptococcosis, Tregs have been shown to be beneficial by downregulating Th2 responses, thus induction of Treg expansion could be one method to treat cryptococcal infection[102]. γδT cells on the other hand have been shown to be the main source of IL-17A in a model of *C. deneoformans* lung infection, and IL-17A knockout mice have enhanced Th1 responses and improved fungal clearance[108]. This study by the Kawakami lab built on the previous work on cryptococcal-specific Th cells to create the CnT-II mouse line, a transgenic mouse that expresses *Cryptococcous*-specific TCR on CD4 T cells, enabling the researchers to explore the effect of IL-17A stimulation on T cells responding to the fungus specifically [108].

Due to the susceptibility of HIV patients to cryptococcal meningitis, the function of CD4 T-cells in the CNS tissue has begun to be explored. It has been established that like the lung, in the CNS CD4 T-cell recruitment and Th1 polarisation are significant in the antifungal response, including by recruiting effector cells such as inflammatory macrophages and in activating tissue resident macrophages, i.e. microglia[71]. However, CD4 T-cells may also be harmful to the anti-cryptococcal response, seeing as HIV patients who are given anti-retroviral therapy which restores some CD4 T-cell function can go on to develop CM-IRIS. An *in vivo* model of CM-IRIS has been developed by adoptively transferring CD4 T-cells into mice defective in adaptive immunity that had previously been infected with the fungus, confirming the key role of CD4 T-cells in this condition[109]. Another *in vivo* study showed that depletion of CD4 T-cells increased fungal burdens in the brain, however fatal inflammation was reduced[110] . A Th1 polarised pro-inflammatory response to *C. neoformans* therefore may provide effective fungal killing but also drive deleterious inflammation in the brain.

CD8 T-cells are cytotoxic T cells activated by recognition of cognate antigen presented in the context of MHC-I, upon which they secrete pro-inflammatory cytokines and cytotoxic granules containing perforins and granzymes, resulting in killing of target cells and driving inflammation. CD8 T cells can also induce apoptosis of infected cells through Fas/FasL, and they are therefore important for killing viruses and cancers. CD8 T-cell cytotoxicity occurs rapidly but is controlled and limited by their antigen specificity[111]. CD8 T-cells secrete several protective antifungal cytokines such as IFN-γ and IL-17 and can also directly exert cytotoxic effects on fungal pathogens[112]. It has been shown that CD8 T-cells may be able to compensate for a loss of CD4 T-cells. In an *in vivo* model of CD4 T-cell depletion, the number IFN-γ producing CD8 T-cells was found to increase which helped to control fungal growth in the lung. Interestingly, the protective capacity of CD8 T-cells appears to be organ-specific as they could not compensate for the lack of CD4 T-

cells within the brain[113–115]. Since CD8 T-cells may be able to provide protection in a CD4 depleted environment, albeit in a context-dependent manner, there has been interest in stimulating CD8 T-cell responses as a therapeutic strategy in patients at risk for fungal infections with compromised CD4 T-cell function[112]. However, other studies have shown that CD8 T-cells need CD4 T-cells to be effective in killing *C. neoformans*[102].

#### 1.4.3.2 B cells

B cells provide humoral immunity and act as antigen-presenting cells. Once B cells exit the bone marrow, they can either circulate through the blood and secondary lymphoid tissues, searching for antigen, or become resident subsets such as spleen marginal zone (MZ) B cells[116]. Antigen recognition occurs via the B cell receptor (BCR) and subsequently results in activation and differentiation into antibody-secreting plasma cells. Naïve B cells express IgM/IgD antibodies, and upon activation undergo T-cell-dependent somatic hyper-mutation and class-switching resulting in the production of high-affinity functional antibodies. Alternatively, activated B cells can develop into memory cells, a self-renewing population that remains in the body for many years and enables a rapid humoral response upon re-exposure to antigen[117].

Patients with defects in humoral immunity, such as X-linked agammaglobulinemia or hypogammaglobulinemia (in which patients have a mutation in the BTK gene resulting in low numbers of mature B cells and therefore produce little or no antibodies), have increased susceptibility to cryptococcosis caused by both *C. neoformans* and *C. gattii*[80,118–120]. Studies using B cell and/or IgM deficient mice have demonstrated a protective role for these cells in controlling *C. neoformans* infection, since animals lacking B-cells exhibited increased fungal burdens in the lung and brain and reduced survival rates[121–123]. Antifungal antibodies, which most commonly target cell wall components such as β-glucan, promote protection against infection by enhancing macrophage phagocytosis and killing by binding

Fc receptors expressed by myeloid cells[13,80,118]. This appears to be particularly important for *C. neoformans* infection, where antibodies are needed to overcome the resistance of these encapsulated yeast to phagocytosis, and likely explains the susceptibility of B-cell-deficient mice to this fungal infection[124]. Antibodies may also directly bind the fungal surface, disrupting *C. neoformans* growth and virulence[125]. Antibody binding to the fungal cell surface can further activate complement and induce antibody-dependent cellular cytotoxicity mediated by NK cells[126].

These protective mechanisms have resulted in optimism for vaccine development for fungal pathogens, as well as providing an opportunity to boost immunity in immunocompromised patients (specifically those lacking T cell responses) using immunoglobulin therapy. There have been a small number of clinical trials testing the efficacy of anti-fungal mAbs against fungi including *C. neoformans* that have yielded promising results, however none have yet resulted in a licensed therapy in humans[127].

## 1.5 *Cryptococcus* virulence strategies

Whilst we can examine the antifungal immune response from a host perspective, it is also important to understand the virulence strategies *Cryptococcus* fungi have evolved to evade the host immune system.

The virulence of *Cryptococcus* is firstly facilitated by its ability to form microscopic spores which are easily dispersed through the environment and can become airborne, thereby enabling the fungi to be inhaled by the host into the lungs. The fungus can also survive at a range of temperatures, enabling it to survive in a range of hosts from amoeba to humans. For the latter, the ability of *Cryptococcus* to grow at 37°C is particularly critical[21,128]. *Cryptococcus* has adapted to survive an acidic pH, for example it is able to survive passing through the digestive system of pigeons (one of the main environmental niches for

cryptococcus) and can survive in acidic soil[21,128]. This consequently presents a challenge for killing of *Cryptococcus* by phagocytes, as fusion of phagosomes with lysosomes to forms an acidic phagolysosome compartment.

*Cryptococcus* fungi have evolved several strategies to perturb killing by phagocytes such as macrophages. Evidence from *in vitro* and *in vivo* studies has shown that *C. neoformans* can alter its morphology to form giant cells termed Titan cells, which are resistant to phagocytic uptake due to their size[129]. The capsule that surrounds the cell wall of *Cryptococcus* fungi is a significant virulence factor as it shields the PRRs in the fungal cell wall from immune recognition and phagocytosis[15,21]. The contents of the capsule, including glucuronoxylomannan (GXM) and chitin, have also been shown to downregulate pro-inflammatory signalling[21,130]. Phagocytosis of *Cryptococcus* fungi does still occur; however, this does not necessarily result in killing of the fungus. The capsule of *C. neoformans* has been shown to disrupt or reverse phagosome acidification, enabling its survival[131,132]. *C. neoformans* has also been shown to reduce the production of NO by LPS/IFNγ stimulated macrophages *in vitro*, thereby disrupting macrophage phagocytic killing[133]. This survival within phagocytes has been implicated in enabling dissemination of *C. neoformans* in the 'Trojan Horse' theory, for example persistence within lung interstitial macrophages has been indicated to drive dissemination to the CNS[134]. Work by the Drummond lab has further shown that uptake by microglia in the CNS can in fact enable *C. neoformans* survival by providing copper, a key nutrient[135]. In *in vivo* pulmonary infection, *C. neoformans* has been shown to drive an M2-like phenotype in interstitial macrophage, measured by expression of IL-4 and arginase, and this is in fact independent of the fungal capsule[136]. The study found *C. neoformans* secretion of the protein CPL1, which signals via TLR4 on the macrophages, is the mechanism by which the fungus drives macrophage polarisation. *Cryptococcus* fungi are therefore highly dynamic in their ability to adapt to their environment and persist in the host.

## 1.6 Hypotheses and aims.

### Hypothesis

The myeloid response to CNS *C. neoformans* infection is highly heterogenous.

### Aims

1) Identify novel activation states and/or subsets of tissue-resident macrophage populations in the brain that interact with *C. neoformans*.

2) Define and investigate function of previously uncharacterised receptors for *C. neoformans*.

3) Investigate invasion of *C. neoformans* and subsequent development of inflammation within the meninges.

# Chapter 2: Materials and Methods

## 2.1 Mice

All mouse work was approved by the Animal Welfare and Ethical Review Board and UK Home Office under Project Licence PBE275C33 and PP7564605. Mice were used for experiments at 7-12 weeks old. A maximum of 5 mice per cage were housed in individually ventilated cages under specific pathogen-free conditions in the Biomedical Services Unit at the University of Birmingham. Mice had continuous access to standard chow, drinking water and environmental enrichment. C57BL/6 wild-type mice (males and females) were purchased from Charles River. Cx3cr1-GFP-Ccr2-RFP mice (strain number 032127) were purchased from Jackson Laboratories and colonies bred and maintained at the University of Birmingham. Rag2-/-, C3-/- and C1q-/- mice were bred and maintained at the University of Birmingham. For experiments with homozygous transgenic mice, age-matched C57BL/6 wild-type mice were used as controls. Mice were euthanised by cervical dislocation at indicated experimental time points, or when humane endpoints (for example 20% weight loss) had been reached, whichever occurred earlier.

## 2.2 *Sall1*-dTomato mouse model

*Sall1*-Cre$^{ER}$ mice were a generous gift from Melanie Greter (University of Zurich). *Rosa26*$^{Ai14}$ mice were purchased from Jackson Laboratories. Breeding and maintenance of *Sall1*-Cre$^{ER}$*Rosa26*$^{Ai14}$, mice was performed at the University of Birmingham. *Sall1*-Cre$^{ER}$*Rosa26*$^{Ai14}$ mice stably express tdTomato fluorescence in cells expressing the *Sall1* gene following tamoxifen-induced recombination. Male and female CreER-expressing mice and their negative litter-mate controls were used for experiments at 7-12 weeks old. Mice were dosed with 10mg of Tamoxifen in 100µl via oral gavage. The tamoxifen was prepared by adding 100µl of RNA-grade 100% ethanol followed by 900µl of corn oil per

100mg of Tamoxifen powder in an Eppendorf. This was dissolved by vortexing overnight. For experiments, two tamoxifen doses were administered 48 hours apart prior to infection with *C. neoformans*. Where indicated, multiple doses of tamoxifen were administered throughout the course of infection.

## 2.3 Cryptococcal meningitis infection model

The *Cryptococcus neoformans* strains used were H99 and KN99α-mCherry[137]. *C. neoformans*-GFP strain FD651 was provided by Robin May. Fungal stocks were stored in 50% glycerol at -80°C. For infection, the yeast was placed in YPD broth (2% peptone, 2% glucose, 1% yeast extract) at 30°C with 200rpm shaking for 24 hours, or the yeast was first streaked onto YPD agar plates (2% peptone, 2% glucose, 1% yeast extract, 2% bacteriological agar, 1% Pen/Strep) before transferring some of the fungal colonies to YPD broth overnight. The fungus was washed twice in sterile PBS and counted using a haemocytometer. $2x10^4$ CFU was injected intravenously via the lateral tail vein. Mice were monitored daily, and mice sacrificed at the indicated time points or when humane endpoints (e.g., 20% weight loss, meningitis, hypothermia) were reached. The inoculum dose was confirmed by diluting the injected sample and plating $1x10^2$ CFU on a YPD agar plate and incubated at 30°C for 24-48 hours before counting the fungal colonies.

## 2.4 CFU analysis

Brains were collected into 1.5ml Eppendorf tubes in 1ml of PBS, which were weighed before and after tissue collection. After homogenization of the sample, 750µl was used for FACS analysis with the remaining 250µl used for CFU analysis. In a 96-well flat-bottomed plate, 25µl of brain homogenate was added to 225µl of PBS for each sample. A serial 1:10 dilution was done by taking 25µl from the first well an adding to 225ul of PBS in the next well, and so on, from 1:10 to 1:10000. The diluted tissue homogenate was then

plated onto YPD agar and incubated at 30°C for 48 hours prior to counting the number of fungal colonies. The organ fungal burden (CFU/g) was then calculated using the following formula:

[Count x (25µl x 40) x dilution factor] / weight (g)

## 2.5 Isolation of brain leukocytes

Brains were carefully dissected out and placed in ice-cold sterile PBS. Brains were manually homogenized prior to myelin removal by Percoll gradient centrifugation. 10ml of 30% Percoll/tissue homogenate was underlaid with 1.5ml 70% Percoll, and the gradients were centrifuged at 2450rpm for 30 minutes at 4°C with the brake off. The interphase layer containing the cellular component was then removed and washed in PBS or FACS Buffer (PBS, 0.5% BSA, 0.01% sodium azide, 2mM EDTA). The samples were then re-suspended in ice-cold PBS and filtered through a 100uM filter into FACS tubes in preparation for staining.

## 2.6 Flow cytometry analysis of brain leukocytes

Isolated leukocytes were re-suspended in 100µl of PBS were live/dead stained with the Zombie UV dye (0.5µg/ml) for 10 minutes on ice in the dark. Fc receptors were blocked with anti-CD16/31 (24G2, purified in house) and stained with fluorochrome-conjugated antibodies for surface markers (CD45, CD11b, CX3CR1, Ly6G, Ly6C, CD206 and MSR1, see table 2.26) for 15-30 minutes on ice in the dark. Samples were then washed in FACS buffer/PBS prior to immediate analysis or fixed in 4% PFA/BD Cytofix and stored at 4°C until analysis. Samples were run on the BD LSRFortessa X-20 with BD FACSDiva software. Final analysis was performed using the FlowJo software (v10). See figure 2.1 for the gating strategy.

## 2.7 Intracellular staining assay

Samples were processed as described above. After surface staining and washing, samples were fixed with 100µl of BD Cytofix on ice for 1 hour. Samples were then washed three times with 200µl of the BD Cytofix Fix/Perm kit 1X perm buffer at 1700rpm for 5 minutes. After discarding the supernatant, 1ul of intracellular antibody was added (e.g. Ki67-PerCPCy5.5, Arg1-APC) and staining was performed overnight at 4°C in the dark. The following day, samples were washed twice with perm buffer and once with FACS buffer before acquiring on the flow cytometer.

## 2.8 Annexin V assay

Samples were processed rapidly and always on ice as this is an active process. The brain samples were processed as above, but sterile PBS was used instead of FACS buffer to prevent apoptosis caused by sodium azide. After surface staining, samples were washed with 1ml of Annexin V binding buffer. Staining with 1ul of Annexin V-APC was performed in 100µl of binding buffer at RT in the dark for 15 minutes. 200µl of binding buffer was then added and samples acquired immediately.

## 2.9 Fluorescence-activated cell sorting

For cell sorting experiments of brain samples, the Miltenyi GentleMACS Brain Dissociation Kit was used according to the manufacturer's instructions. Briefly, after collecting brain samples in 1ml of ice-cold PBS, samples were cut into ~8 pieces using a scalpel. An appropriate volume of enzyme mix 1 (enzyme P and buffer Z) was prepared and 1950ul added to a gentleMACS C tube before adding the brain tissue. Note: for experiments with 8 samples or less, one C tube was used per brain sample; for larger experiments, multiple samples were combined into one C tube and the volume of enzyme mix 1 and 2 multiplied accordingly. 30µl of enzyme mix 2 (enzyme A and buffer Y) was added per C tube/per

sample. The C tubes were then placed in the gentleMACS Octo Dissociator (with heaters) and incubated at 37°C for 30 minutes with agitation. The samples were then centrifuged briefly to collect the tissue homogenate, before proceeding with brain leukocyte isolation protocol as above.

## 2.10 Ex-vivo fungal killing assay

Brain samples from mice infected with GFP-Cryptococcus were collected and processed and surface stained as described in sections **2.5** and **2.6**. Cells were sorted on GFP positive populations of IAMs, non-IAMs microglia and macrophages. At least 1000 events were collected for each population. The samples were then plated at 200-500 events per YPD agar plate in 100µl and spread across the plate. The plates were incubated at 30°C for 24-48 hours and the fungal colonies counted.

## 2.11 Flow cytometry analysis of the meninges

After cervical dislocation, the mouse skull cap was removed. Using fine forceps, the dural meninges were scraped from the inside of the skull and placed in 400µl of meninges digest buffer (RPMI medium, 1mg/ml collagenase, 1mg/ml dispase, 40µg/ml DNAse) containing 10mM EDTA to prevent platelet activation. The samples were incubated at 37°C with shaking for 30 minutes. The sample was then passed through a 70µM filter and re-suspended in FACS Buffer/PBS before spinning at 1500rpm for 5 minutes. Samples were then stained with surface antibodies as described in section **2.6**.

## 2.12 CBC analysis

Up to 300µl of blood was collected using cardiac puncture into tubes containing 50µl of 100mM EDTA. The blood was kept at room temperature and rapidly analysed using the Horiba Pentra ES 60 Haematology analyser.

## 2.13 Brain histology

Mice were sacrificed by cervical dislocation and perfused via cardiac puncture with 10-20ml of PBS, followed by 10ml of 4% PFA. The brain was then carefully dissected out and placed in ice cold 4% PFA overnight. The tissue was briefly washed in PBS and then placed in 30% sucrose in the fridge for 24 hours, or until the tissue sinks. The excess sucrose was removed before orienting the tissue in a mounting mould with OCT medium. The sample was allowed to sit at room temperature for 5 minutes to ensure the OCT surrounded the tissue properly. The sample was then rapidly frozen on dry ice or using an ice bath, then stored at -80°C until required. The tissue was cryosectioned using the Bright Instruments Clinicut at 30μM and mounted onto poly-lyseine slides prior to drying overnight to ensure adhesion. If not staining immediately, slides were stored at -20°C.

## 2.14 Meninges whole mounts

After skull cap removal, the entire skull cap was placed in 2% PFA/PBS/10mM EDTA for 2 hours. The dural meninges were then carefully dissected from the inside of the skull cap, ensuring the tissue remains intact. The meninges were then placed in ice-cold PBS/10mM EDTA in a 24-well plate, allowing the tissue to flatten.

## 2.15 Immunofluorescence

For brain tissue slides, the slides were first air dried at room temperature for 30 minutes (if using slides that had been frozen). Slides were then washed in PBS to remove excess OCT medium. An oil pen was used to draw around tissue sections. The samples were then blocked in brain blocking buffer (0.1M Tris-HCL, 1% BSA, 1% Donkey/Goat serum, 0.5% Triton-X100, 0.01% Saponin) for 30 minutes to 1 hour at RT. For meninges whole mounts, blocking was done in meninges blocking buffer (PBS, 1% BSA, 5% Donkey serum, 10mM EDTA) in a 24-well plate for 30 minutes. Antibodies were added in blocking buffer and

incubated overnight at 4°C or at room temperature for 2 hours. Samples were washed 3 times in PBS for 20 minutes. If secondary antibodies were required, these were diluted in PBS and incubated at room temperature for 2 hours prior to repeating the washing step. If required, samples were counter-stained with DAPI for 5 minutes at room temperature, then washed. For brain samples, autofluorescence was quenched with the TrueVIEW Autofluorescence Quenching Kit. For meninges whole mounts, the tissue was carefully placed on slides and flattened using forceps. Slides were mounted using the Pro-Long Gold Mounting media and cured at room temperature overnight. If not imaging immediately, slides were stored at -20°C. Fluorescence imaging was performed using the Zeiss Axio Scan Z1 slide scanner or the Leica DM6000 fluorescence microscope. Confocal imaging was performed using the Zeiss LSM 780 Confocal microscope or the Zeiss LSM 880 Confocal with Airyscan Fast. Image analysis was performed using the Zen Blue (v3.1) software.

## 2.16 BV-2 cell culture

BV-2 cells, a murine microglial cell line, were provided by Michail Lionakis (NIH). The cells were cultured in complete RPMI (RPMI with GlutaMAX and HEPES, 10% FBS, 1% Pen/Strep) in T175 flasks. Once 80-90% confluent, cells were split by removing the media and applying 5ml of 10% Trypsin in PBS to the flask for approximately 1 minute before neutralising the Trypsin with media. Adherent cells were then removed from the flask plastic using a cell scraper and the supernatant/cells collected into a Falcon tube. The cells were pelleted by spinning at 1500rpm for 5 minutes at 4°C, the supernatant was discarded, and pellet re-suspended in 10ml of complete RPMI. Cells were then counted and diluted accordingly to use for experiments or added to a fresh T175 flask at a 1:6 to 1:10 dilution. BV-2 cells proliferate rapidly so were passaged every 2-3 days to a maximum of 10 passages.

## 2.17 MPI cell culture

Both WT and SRA1-KO MPI cells[138–140] were provided by Robin May and cultured for experiments. All reagents were pre-warmed to RT. If splitting cells from flasks, these were first checked to ensure 70-90% confluence had been reached. Cells were cultured T25 flasks immediately after defrosting, before being transferred to T75 flasks. The culture medium was removed and transferred to a 50ml Falcon tube (MPI cells are semi-adherent so floating cells may still be viable). The remaining cells in the flask were washed twice with sterile PBS, with the supernatant collected into the same 50ml Falcon tube. Enough 1X sterile PBS-EDTA was added to the flask to cover the surface (5ml for T75, 2ml for T25) and incubated at 37°C for 10-20 minutes (until cells detached). The flask was washed with PBS to collect the cells, which were then transferred to the 50ml tube. Cells were centrifuged at 200g for 5 minutes to, before carefully discarding the supernatant to avoid disturbing the delicate pellet. The cells were re-suspended in 5ml of complete RPMI (10% FBS, 2mM L-Glutamine, 100U/ml Pen/Strep) and the cells counted using a haemocytometer. Cells were re-seeded in complete RPMI (for T75 flasks: 1-2x$10^5$ cells/ml in total 10ml) with X-63–GM-CSF conditioned medium (provided by the May lab) at 1% (10µl per 1mL of medium) for macrophage differentiation or M-CSF (50ng/ml) plus IL-34 (100ng/ml) for microglia differentiation and incubated at 37°C, 5% $CO_2$, humidified atmosphere.

## 2.18 *In vitro* phagocytosis assay

The day prior to the assay, a YPD culture of mCherry *C. neoformans* was prepared. BV-2 cells were detached as described above and counted using Trypan Blue exclusion. Cells were plated into 24-well plates at 1x$10^5$ cells/well in 500µl, and incubated overnight at 37°C, 5% $CO_2$, humidified atmosphere. If pre-stimulation with cytokines was required, these were added at 10ng/ml to the relevant wells. On the day of the assay, the *C.*

*neoformans* YPD culture was prepared by spinning down and washing twice in PBS before counting with a haemocytometer. The fungal cells were resuspended at $10x10^6$/ml in 10 µg/ml 18B7 antibody (Sigma) and incubated at RT for 15 minutes to allow the 18B7 to opsonise the fungus. 50µl (10%) of the opsonised *C. neoformans* cells were added to each well containing BV-2 cells, and the plate(s) spun down at 1500rpm for 1 minute to ensure the fungus was in contact with the adherent BV-2 cells at the bottom of the well. This was incubated at 37 °C for 1 hour. The supernatant was then removed from the cells, they were washed with PBS then detached from the wells using 200µl of 10% Trypsin/PBS on ice for 5 minutes. The cells were lifted by pipetting and transferred to FACS tubes, washed twice with PBS, then stained with 0.5µl Zombie-UV dye for 10 minutes on ice. 24GZ Fc block was added (0.5µl/sample) in 50µl of FACS buffer, followed by 0.5 µl (from a 1mg/mL stock to get 5µg/ml final) of calcofluor white (CFW) and 1µl anti-CD11b-APC-Cy7. Antibodies were incubated on ice for 15-30 minutes prior to washing with FACS buffer before acquisition by flow cytometry.

## 2.19 RNA isolation

### 2.19.1 Cells from *in vitro* culture

Trizol samples were thawed at RT and allowed to sit for 5 minutes after thawing. 200µl of chloroform was added to each 1ml Trizol sample and gently mixed by inverting the tube. The sample was left to settle for up to 5 minutes prior to centrifugation at 12,000g for 15 minutes at 4°C. Up to 500µl of the top clear phase was transferred to an RNAse-free Eppendorf and 500µl of 70% ethanol was added to each sample. 700µl of this mixture was added to a Qiagen column (from the RNeasy kit) and pulse spun for 15 seconds, discarding the flow through. This step was repeated with the remaining sample in the Eppendorf. 350µl of RW1 wash buffer was added to the column spun for 15 seconds prior to discarding the flow-through. DNase digest was performed using the Qiagen RNase-

Free DNase set; 70-80µl of DNase mix was added to each column and samples incubated at RT for 30 minutes. The column was washed with RW1 buffer as above before moving to a fresh collection tube and washing with 350µl RPE buffer, then washing again with 500µl of RPE buffer for 2 minutes at 10,000g. The column was transferred to an RNase-free Eppendorf and 30µl of RNase-free water added to the column membrane. The samples were spun at 10,000g for 1 minute to pellet the RNA into the Eppendorf. The RNA was stored at -80°C.

### 2.19.2 Cells from *in vivo* experiments

After cells had been sorted, they were centrifuged at 300g for 10 minutes to pellet the cells. The samples were re-suspended in 1ml PBS and transferred to RNAse-free Eppendorf tubes, before centrifugation for 5 minutes at 5000rpm. The supernatant was carefully removed and the pellet re-suspended in 50µl of Trizol before bringing the final volume to 1ml. If not extracting RNA immediately, samples were stored at -80°C. For RNA extraction, samples were thawed and 200µl of chloroform added. Samples were inverted and then centrifuged at 12000rpm for 15 minutes at 4°C. The upper phase was removed and transferred to a new Eppendorf, then gently mixed with 500µl of isopropanol and 5µl of GlycoBlue. After overnight incubation at -20°C samples were centrifuged at 12,000g for 15 minutes. The supernatant was carefully removed and 700µl of ice-cold 70% ethanol added before spinning at 12,000g for 5 minutes. The supernatant was removed, and the pellet was air-dried for 5 minutes to remove any remaining ethanol prior to re-suspending in 10µl of RNase-free water.

## 2.20 cDNA generation

For cDNA generation, the High-Capacity RNA-to-cDNA kit was used. A master mix of the 2X RT-Buffer and Reverse Transcription enzyme was prepared according to the number of samples. For each sample, 9µl of RNA was added to 10µl of RT-buffer and 1µl of RT-

enzyme in a PCR tube. After a brief spin the tubes were placed in a thermal cycler and run at 37°C for 1 hour followed by 5 minutes at 95°C. After the run had completed, the samples were stored at -20°C long-term or used straight away for qRT-PCR.

## 2.21 qRT-PCR

1-2µl of cDNA was used for qRT-PCR analysis with SYBR Green. 2X SYBR green master mix was combined with forward and reverse primers, RNase-free water and cDNA to a final volume of 20µl in 96 or 384 well plates. All primers were provided by Merck: mouse GPR84 (Fwd: TGTGAGGTGAGGAGAATAGTGG, Rev: ATAGCCAGGCTGGTCTTAGC), mouse Tmem119 (Fwd: AATGACAGCTCTTCACCGGG, Rev: GCATGCACCGCTATATTGGC). The housekeeper genes used were RPL13a (Fwd: GCGGATGAATAC CAACCCCT, Rev: CCACCATCCGCTTTTTCTTGT) and GAPDH (Fwd: AACTTTGGCATTGTGGAAGG, Rev: ACACATTGGGGGTAGGAACA). Analysis was performed on the QuantStudio 5 system including melt curve determination. Data was analysed using the ThermoFisher Cloud software prior to exporting for analysis in Microsoft Excel using the comparative CT method.

## 2.22 Single-cell RNA sequencing

*Cell sorting and RNA Isolation – performed by Rebecca Drummond*

Brains from mice were collected at the time points indicated and processed as described in **2.9**. Cells were sorted on live singlets that were CD45+ and CD11b+ and collected into cold complete media (RPMI, 10% FBS, 1% Pen/Strep). Sorted cells were pelleted and resuspended in PBS supplemented with 0.04% BSA at a concentration of approximately 1000 cells/ul. Cells were loaded on a GemCode Single-Cell Instrument (10X Genomics) to generate single-cell gel bead-in emulsions (GEMs). scRNAseq libraries were prepared

using a Chromium Next GEM Single-Cell 3' Library and Gel Bead Kit v2 (day 0/3 samples) or v3.1 (day 6 sample) (10X Genomics).

*RNA-Sequencing*

RNA sequencing was performed by Genomics Birmingham. Sequencing libraries were loaded onto the Illumina NextSeq500 with the following settings: 1.6pM initial loading concentration, 28 cycles read 1, 98 cycles read 2, 8 cycles index, v2.5 150 cycle flow cell. The demultiplexing of raw sequencing data was performed using CellRanger v3.0.1 (10X Genomics), using function mkfastq. Reads obtained from mkfastq were used as the input for 'cellranger count' (10X Genomics), in which reads were aligned to the mouse reference genome (mm10, v3.0.0; Ensembl 93). Pooling of the different samples was completed using 'cellranger aggr' (10X Genomics), in which the different chemistries used for different samples was accounted for and corrected. For analysis of day 6 samples, the same analysis was performed but on 'Sample 2' only, which contained the pooled day 6 samples.

*Data Pre-processing and Filtering*

Sequenced data was filtered, processed and analysed using Partek Flow (v9.0.20). H5 files (generated by CellRanger as described above) were imported into Partek, and the following filters applied: total reads per cell 500-12,000, number of expressed genes 250-3,000, percentage of mitochondrial reads maximum 8%. These filters retained 99.18% of cells (15,398 out of 15,526). Normalisation was then performed, using the recommended settings (counts per million, +1, log2 transform). A noise reduction filter was then applied to remove non-expressed genes (of 31,017 genes, 12,460 genes were removed). For analysis with all time points together, correction steps had to be performed to remove batch effects. For this, clustering analysis was performed and visualised by tSNE (using the following parameters: Louvain clustering, 30 nearest neighbours [K-NN], 10 principal

components). Cells were classified using a feature list of selected genes manually imported into Partek and applied to the data; microglia were defined as cells expressing Cx3cr1, Sall1 and Tmem119, and macrophages as expressing high levels of H2-Aa, Cd163 and F13a1. We then used the 'Remove Batch Effect' function, removing the attribute 'time-point' and the interaction between this attribute and the cell classifications applied previously. The clustering analysis was then re-run and plotted by tSNE to evaluate the removal of the batch effect. Graph-based clustering, detailed cellular classifications and downstream analyses (pathway analysis, differential gene expression) were performed on this clustering result. For analysis of the day 6 samples only, the H5 file generated for these samples was input into Partek and the same filtering and processing steps followed, except no batch correction steps were required.

## 2.23 Bulk RNA-seq

Meninges were collected from mice at the indicated time points and placed directly into 1ml of Trizol. Samples were collected from two independent experiments. RNA extraction was performed as described in **2.19**. The RNA quality and concentration was checked using the Nanodrop 2000, and it was determined that all samples were of sufficient quality to proceed with sequencing analysis. Samples were then plated into V-bottom PCR plates, with one plate prepared for additional QC testing and another for the library preparation. Samples were then submitted to Genomics Birmingham for sequencing using the Lexogen QuantSeq 3. Data was uploaded to the Illumina BaseSpace online software. The BlueBee online software by Lexogen was used to convert the FASTq files from BaseSpace into counts files, which were then collated into a counts matrix file which was imported into RStudio for further analysis by R (version 4.1.0). The BiocManager (version 3.13) and DESeq2 packages from the Bioconductor software were installed. The count matrix data was filtered by removing counts fewer than 10 and normalised using the rlog

(regular log) function. PCA analysis was performed by comparing the different experimental groups; uninfected, day 3 infected, day 6 infected, and day 8/9 infected, with the latter were combined to a late infection group. The significantly differentially expressed genes between experimental groups were determined using lfcShrink with ashr to determine log2 fold change with adaptive shrinkage[141]. Differentially expressed genes (DEGs) were plotted using the EnhancedVolcano package[142]. The adjusted p value and log2 fold change were plotted with an FC cutoff of 1.5. The biomaRT package was then used to extract gene identifiers for KEGG pathway analysis using the packages DOSE and clusterProfiler. DEGs were first filtered to remove "NA" adjusted p values and by genes with a log fold change above or equal to 1.5. The minimum gene set size was set to 10 to ignore gene sets (i.e. pathways) with fewer than 10 genes.

## 2.24 Statistics

All statistical analysis was performed using GraphPad Prism software (version 10). Details of individual tests are included in the figure legends. In general, data were tested for normal distribution by Kolmogorov-Smirnov normality test and analysed accordingly by unpaired two-tailed t-test or Mann Whitney U-test. In cases where multiple data sets were analysed, two-way ANOVA was used with Bonferroni correction. In all cases, P values $< 0.05$ were considered significant. P value levels indicated on data plots are as follows: *p<0.05, **p<0.01, ***p<0.001, ****p<0.0001.

# Materials

## 2.25 General tissue culture reagents

| Reagent | Supplier | Catalogue # |
|---|---|---|
| 1X DPBS, 500mL | Gibco (Fisher Scientific) | 11503387 |
| PBS tablets | VWR | 6501-200TAB |
| Percoll | Merck | GE17-0891-01 |
| RPMI 1640 with GlutaMax and HEPES, 500mL | Gibco (Fisher Scientific) | 61870036 |
| DMEM (low glucose) | Sigma | D5546 |
| Heat-inactivated FBS | Sigma | F9665 |
| Penicillin/Streptomycin | Gibco | 15140-122 |
| UltraPure™ 0.5M EDTA | Gibco | 15575020 |
| Trypsin-EDTA 10X | Sigma | T4174 |
| Fungizone ( Amphotericin B) | Gibco | 11510496 |

## 2.26 Mouse studies

| Reagent | Supplier | Catalogue # |
|---|---|---|
| Tamoxifen | Sigma | T5648-5G |
| Corn Oil | Sigma | C8267-500ML |
| RNA grade ethanol | Fisher | BP2818-212 |
| Oral gavage needles | Sigma | CAD9920-100EA |

## 2.27 Mycology

| Reagent | Supplier | Catalogue # |
|---|---|---|
| Agar | Fisher Scientific | 10351303 |
| Peptone | | 11413603 |
| Glucose | | 10767844 |
| Yeast extract | Sigma | Y1625-1KG |

## 2.28 Cell stimulations

| Reagent | Supplier | Catalogue # |
|---|---|---|
| IFN-γ | | |
| IL-1β | | |
| TNF-α | | |
| LPS | | |
| Recombinant Mouse IL-34 (carrier free) | Biolegend | 577602 |
| M-CSF | Biolegend | 576406 |
| GM-CSF | Generated in-house by the May lab | |
| Anti-Glucuronoxylomannan (GXM) Antibody, clone 18B7 | Merck | MABF2069 |
| Mouse serum | | |
| 6-OAU | Cayman Chemical Company | 17687 |

## 2.29 Flow cytometry antibodies

| Target | Fluorophore | Supplier | Clone | Catalogue # | Conc.( µg/ml) |
|---|---|---|---|---|---|
| CD45 | PE | BioLegend | 30-F11 | 103106 | 1 |
| CD11b | APC-Cy7 | BioLegend | M1/70 | 101226 | 1 |
| CX3CR1 | BV605 | BioLegend | SA011F1 | 149027 | 1 |
| CD206 | BV421 | BioLegend | MMR | 141717 | 1.2 |
| CD206 | PerCPCy5.5 | BioLegend | C068C2 | 141715 | 1 |
| MSR1(CD204) | PE-Cy7 | eBioscience | M204PA | 25-2046-80 | 4 |
| MHC-II | FITC | eBioscience | M5/114 | 11-5321-82 | 2.5 |
| Ki67 | PerCPCy5.5 | BioLegend | 16A8 | 652423 | 2 |
| Annexin V | APC | BioLegend | N/A | 640919 | 1 |
| Ly6G | PerCPCy5.5 | BioLegend | 1A8 | 127616 | 1 |

| | | | | | |
|---|---|---|---|---|---|
| Ly6C | Alexa Fluor 700 | BioLegend | HK1.4 | 128024 | 1 |
| CX3CR1 | Alexa Fluor 647 | Biolegend | SA011F11 | 149004 | 1 |
| CXCL9 (MIG) | Alexa Fluor 647 | Biolegend | MIG-2F5.5 | 515606 | 2.5 |
| Filipin complex from Streptomyces filipinensis | N/A | Sigma | N/A | F9765 | |

## 2.30 Flow cytometry/cell sorting reagents

| **Reagent** | **Supplier** | **Catalogue #** |
|---|---|---|
| Fc block (24GZ) | Made in-house | N/A |
| Compensation beads | BD Biosciences | 552845 |
| Accucheck Counting Beads | Invitrogen | PCB100 |
| Zombie UV Fixable Viability Kit | Biolegend | 423108 |
| Zombie Violet Fixable Viability Kit | Biolegend | 423114 |
| Sodium Azide 10% | Sigma | S2002-5G |
| Bovine Serum Albumin | Sigma | A8022-50G |
| Paraformaldehyde 4% | Thermo Scientific | J19943-K2 |
| BD Cytofix Fixation Buffer | BD Biosciences | 554655 |
| BD Cytofix/Cytoperm Kit | BD Biosciences | 554714 |
| eBioscience FOXP3/Transcription Factor Staining Buffer Set | Invitrogen | 00-5523-00 |
| Annexin V Binding Buffer | BioLegend | 422201 |
| ArC™ Amine Reactive Compensation Bead Kit | Thermofisher | A10346 |
| 10X DPBS | Gibco | 70011-044 |
| Adult Brain Dissociation Kit | Miltenyi | 130-107-677 |

| | | |
|---|---|---|
| Monocyte Isolation Kit | | 130-100-629 |
| CD4+ T Cell Isolation Kit | | 130-104-454 |

## 2.31 Microscopy antibodies

| Target | Fluorophore | Supplier | Clone | Catalogue # | Conc.( µg/ml) |
|---|---|---|---|---|---|
| CD41 | PE | BioLegend | MWReg30 | 133906 | 1 |
| CD45 | APC | BioLegend | 30-F11 | 103112 | 1 |
| CD31 | Alexa Fluor 488 | BioLegend | 390 | 102414 | 2 |
| Iba-1 | Unconjugated polyclonal antibody | Wako | N/A | 019-19741 | 1 |
| Goat anti-Rabbit IgG (H+L) Secondary | Alexa Fluor 647 | Thermofisher | N/A | A-21244 | 4 |

## 2.32 Microscopy reagents

| Reagent | Supplier | Catalogue # |
|---|---|---|
| ProLong Gold antifade reagent | Invitrogen | P36930 |
| OCT | Epredia | 6502 |
| Advanced PAP Pen | Sigma | Z672548-1EA |
| Sucrose | Fisher | S/P770/53 |
| TrueView Autofluorescence Quenching kit | VectorShield | SP-8400 |
| Donkey Serum | Sigma | D9663 |
| Goat Serum | SLS | G9023 |
| Triton-X 100 | Sigma | X100-100ML |

## 2.33 qPCR

| Reagent | Supplier | Catalogue # |
|---|---|---|
| Trizol | Invitrogen | 15596018 |
| Qiagen RNAeasy Mini Kit | Qiagen | 74106 |
| cDNA synthesis kit, 50 rxn | Thermofisher | 4388950 |
| RNase-free DNAse set | Qiagen | 79256 |
| Biopure 1.5ml Eppendorfs | SLS | E0030121589 |
| Chloroform | MP Biomedicals | 194002 |
| SYBR Green | Applied Biosystems | A25742 |

# Chapter 3: Defining myeloid cell heterogeneity during cryptococcal meningitis using single cell RNA-sequencing.

## 3.1 Introduction

### 3.1.1 Neuroimmunity in the CNS

The brain was historically thought of as a tissue where immune responses were suppressed to preserve brain function. Whilst the CNS has highly sophisticated borders, including the blood-brain barrier (BBB) and the barriers of the choroid plexus and meninges (discussed further in **chapter 4**), we now understand that pathogens, cells and small molecules can cross these barriers and the brain is not entirely shut off from the periphery. Circulating immune cells can enter the brain during inflammation and mediate antimicrobial immune responses as well as drive autoinflammatory diseases in this tissue. Furthermore, the CNS contains highly specialised tissue-resident immune cells, such as microglia, perivascular macrophages, meningeal macrophages and T cells. Our understanding of how infectious organisms including bacteria, viruses, parasites, and fungi have evolved to cross CNS barriers and overcome the resident immune cells, causing meningitis and brain infection, is key to preventing and treating these often-fatal infections. Furthermore, understanding the mechanisms of inflammation in the CNS could provide treatments for other CNS diseases such as multiple sclerosis and Alzheimer's disease. Here, I discuss how CNS-resident myeloid cells contribute towards the brain immune response, and how heterogeneity in these cells is thought to develop in different inflammatory contexts. In this chapter, I focus on microglia since these are the most numerous CNS resident macrophages, and my data centres on this cell type.

### 3.1.2 Microglia identity and function

The cells of the brain can be divided into two major groups, neurones and glia. Glial cells include astrocytes, oligodendrocytes, and microglia, all of which have specialised functions in brain health and disease[143]. Microglia are a type of macrophage and are the most numerous tissue-resident immune cells in the brain, compromising around 10% of all brain cells. They are recognisable by their distinct morphology; they are large cells with numerous dendrites that enable extensive sampling of the tissue environment[144]. Similar to other tissue-resident macrophage populations, microglia first arise from the yolk sac and populate the CNS early in development. However, microglia are unique in that they are derived entirely from this first wave of macrophage tissue population, and throughout life are replenished solely by clonal expansion, whereas other tissue macrophages renew through hematopoietic progenitors from the bone marrow[145,146]. However, some *in vivo* models of microglia depletion have shown that myeloid precursors from the periphery can enter the brain and differentiate into "microglia-like" cells, albeit these cells have a distinct genetic signature compared to "normal" microglia[147,148].

Microglia have a significant role in the brain during haemostasis through the development and maintenance of healthy neurological function. Once microglia populate the developing CNS, they begin guiding the establishment of neuronal networks[149]. Microglia are subsequently required for neuronal pruning and elimination of apoptotic neurones in neurogenesis[149]. Microglia also perform synaptic pruning, mediated by CX3CR1/CX3CL1 and C1q/C3-CR3 interactions, thus removing unused synapses[149]. Furthermore, microglia assist in the regulation synaptic signal strength and in protecting neurones from damage caused by excessive neurotransmitter release[149].

Microglia also have a significant role as immune sentinels of the brain. Microglia can recognise pathogens through PRRs, then release chemokines/cytokines and present

antigen to trigger further immune cell recruitment and activation[149,150]. Like other macrophage populations, microglia express PRRs including TLRs and NLRs and some CLRs (see **chapter 1** for more detail on these receptors), that enable them to respond to a range of PAMPs and DAMPs[149,151]. Microglia also express several scavenger receptors, such as MARCO and CD36, for phagocytosis and elimination of pathogens as well as uptake of apoptotic cell debris and removal of Aβ plaques in the context of Alzheimer's disease[149,152]. TREM-2 is another phagocytic receptor that is highly expressed by microglia and is important for protection against Alzheimer's Disease[153]. As mentioned above, microglia also express the complement receptor CR3, which can detect complement opsonised pathogens for phagocytosis [149]. Microglia respond to both pro-inflammatory and anti-inflammatory cytokine signalling, including type I interferons, IFN-γ, IL-10 and TNF-α[149]. The receptors required for microglia immune functions are amongst those that can be used to identify and target microglia experimentally.

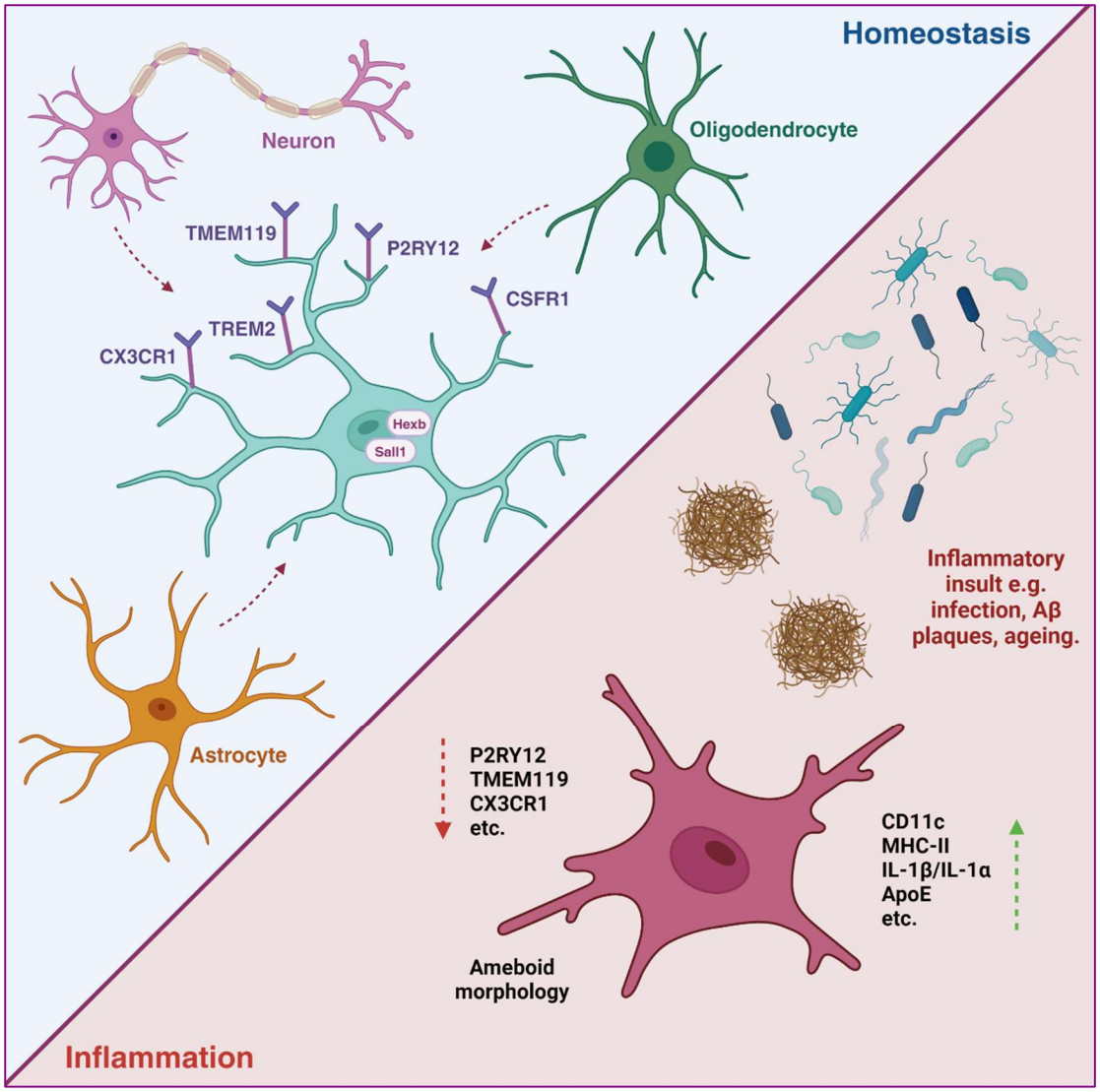


**Figure 3.1 Microglia in health and disease.** Under homeostatic conditions, microglia have important functions as sentinels of the brain. Homeostatic microglia can be identified by their expression of surface receptors including CX3CR1, Trem2, Tmem119, P2Ry12 and CSFR1 which have important roles in microglia sensing signals from the brain environment and other CNS cell populations, including neurones, astrocytes and oligodendrocytes. Microglia also express intracellular markers including Sall1 and Hexb. In inflammatory conditions, microglia can become activated and alter their morphology and downregulate expression of homeostatic markers whilst upregulating antigen presentation, scavenger receptors for phagocytosis and other inflammatory markers.

### 3.1.3 Models for identifying and targeting microglia *in vivo.*

The prominent homeostatic microglia surface markers are CX3CR1, P2YR12, Tmem119, Trem2 and CSF1R that enable communication between microglia and neurons, astrocytes, and oligodendrocytes[150](figure 3.1). Microglia can also be identified by their expression of intracellular marker genes including *Hexb* (β-hexosaminidase subunit β) and the transcription factor *Sall1*[150]. Defining microglial markers has enabled the development of experimental models to specifically target this cell population.

CX3CR1 is the chemokine receptor for CX3CL1, also known as fractalkine, which is released by neurones[146,154]. CX3CR1 is a marker for several macrophage populations, however it is particularly highly expressed in microglia. Consequently, in flow cytometry analysis homeostatic microglia can be distinguished from other myeloid populations in the brain by their intermediate expression of CD45 and high expression of CX3CR1[146]. This was utilised to generate one of the first murine models for studying microglia, the $CX3CR1^{+/GFP}$ mouse where all cells expressing CX3CR1 also express green fluorescent protein[155]. This model was subsequently used to generate a CX3CR1 knockout mouse by further crossing the heterozygous $CX3CR1^{+/GFP}$ mouse to create $CX3CR1^{GFP/GFP}$ mice where both CX3CR1 alleles were replaced[154–157]. This enabled further studies to explore the function of CX3CR1 in microglia, which found that in models of neuroinflammation such as LPS injection, in CX3CR1 knockout mice microglia activation is increased which induced excessive neurone death and cognitive defects[154–158].

In the following ~20 years, more sophisticated models to employ CX3CR1 to study microglia have been developed. $CX3CR1^{GFP}CCR2^{RFP}$ mice enable cells that are derived from circulating monocytes, which specifically express CCR2, to be distinguished from those derived from CNS-resident macrophages including microglia[159]. The generation of several $CX3CR1^{CreER}$ mouse lines has enabled temporal and spatial-specific knockout of

CX3CR1[160]. In these models, Tamoxifen is administered to the mice, this results in the ER (oestrogen receptor) domain being released from the Cre, which can then translocate to the nucleus resulting in recombination of loxP loci in the DNA and therefore knockdown of the gene target. These models have been used for fate-mapping studies and can also be combined with Rosa26$^{mTmG}$ mice to generate a fluorescent gene knock-in to convert CX3CR1-expressing cells into fluorescent cells[157,160,161]. The use of CX3CR1 targeted mouse models to study microglia is somewhat limited by the fact that CX3CR1 is not exclusively expressed by microglia and thus is non-specific. However, due to their longevity and renewal by clonal expansion, approximately a month after TAM administration CNS macrophages, including microglia, will be the only cells maintaining the knock-out/in[157,160].

To differentiate between microglia and other CNS-resident macrophages (namely perivascular macrophages) more sophisticated Cre models have been developed. Using a split Cre system, CX3CR1 can be targeted along with Sall1, which is specific to microglia[162], whilst combining with Lyve1 is specific for perivascular macrophages[163]. Reporter mice have been developed targeting several other purportedly microglia-specific genes, including Tmem119, Hexb, P2ry12 and Sall1[164], with varying success. Issues have arisen when applying these models to different inflammatory disease contexts, where expression of signature genes is altered in activated microglial and other macrophage populations can begin expressing these genes (figure 3.1). For example, it was found that in a model of traumatic brain injury, microglia downregulate Tmem119 expression, whilst infiltrating inflammatory macrophages may upregulate this gene thus causing complications when differentiating between these two populations[164–166]. However, other studies of neurodegeneration using Hexb$^{dTomato}$ mice have shown microglia maintain fluorescence even in the disease state, thus selection of appropriate reporter mice to study microglia in disease must be carefully considered depending on the

context[164]. In addition to generation of reporter mice, microglial surface markers have been used to develop antibodies for imaging analysis and quantification by, for example, flow cytometry. Iba-1 is highly specific to microglia and is commonly used for fluorescent labelling of microglia[157,164]. Iba-1 has been shown to be upregulated in activated microglia, making it a useful marker to study microglia in inflammatory contexts[167].

In addition to genetic knockouts and knockdowns, alternative tools for microglia depletion are also available. Clodronate liposomes can be injected into mice to deplete macrophages as phagocytosis of these liposomes induces apoptosis[164]. However, in order to target a specific macrophage population the injection has to occur in an anatomically appropriate area, which in the case of microglia means intra-cerebral injection. Unfortunately, this model is "leaky" as the injection itself can cause trauma and thus non-specific microglial activation, and uptake and depletion can occur in other macrophage populations in the brain[164]. To address this, CSFR1 (colony-stimulating factor-1 receptor) inhibitors have been developed, including PLX3397 and PLX5662, which can be administered to mice using a special diet[164,168,169]. These models show robust depletion of microglia and have demonstrated the importance of CSFR1 in microglial development and viability, which aligns with evidence from human studies which have found SNPs in this receptor are associated with the development of neurodegenerative disorders such as Alzheimer's disease[169]. However, these models are limited by their inability to deplete 100% of microglia, and work by the Drummond lab[170] (under review) and others has shown that these drugs can have off-target effects including depletion BAMs and peripheral macrophage populations[164].

### 3.1.4 Microglia in anti-fungal immunity

We know microglia have a role in cryptococcal meningitis as patient brain samples have shown significant uptake of the fungus by these cells[171,172]. However, microglia are likely

detrimental to the clearance of the fungus. Early studies showed that microglia can respond to *C. neoformans* infection and produce pro-inflammatory cytokines, upregulate antigen presentation through expression of MHC-II, and increase expression of CD11c which is a marker of microglial activation associated with increased phagocytosis[71,173]. However, it has also been demonstrated that microglia are not the predominant expressors of iNOS, which is associated with a M1-like pro-killing phenotype[71,174]. In a model of 'chronic' cryptococcal meningitis, using the clinical isolate 52D which is a less virulent strain, microglia activation did not occur until fungal growth in the brain was well-established[173], at which point it is too late to prevent mortality. Recent work by the Drummond lab[135] has shown microglia phagocytosis of *C. neoformans* enables the fungus to establish an intracellular niche. In fact, the microglial intracellular environment contains a supply of copper, a metabolite important for *C. neoformans* survival which is otherwise difficult to find in the brain[135]. This provides a clear rationale for *C. neoformans* to evolve to disseminate to the brain, and in fact depletion of microglia provides improved outcomes of infection [135].

Whilst there is much to learn about the role of microglia in cryptococcal meningitis, evidence from other infectious contexts reveals their importance in the pathogen response and provides clues for what mechanisms may be relevant in a *Cryptococcus* infection context. In humans, deficiency in the CLR CARD9 results in increased susceptibility to fungal infections in the CNS, particularly those caused by *Candida albicans*[175,176]. It has been shown that the expression of CARD9 by microglia is pivotal in the anti-fungal response, as CARD9 signalling activation by candidalysin drives the production of IL-1β and CXCL1 by microglia which in turn recruit neutrophils to the brain[175]. If CARD9 expressing microglia are removed, then CNS infection by *Candida* cannot be controlled effectively [175]. In the context of parasite infection with *Toxoplasma gondii*, microglia signal through IL-1α rather than IL-1β which is instead produced by inflammatory

macrophages[177]. Microglial release of IL-1α is required for immune cell recruitment and parasite clearance, as IL-1R is predominantly expressed on the vascular endothelium in the brain, thus IL-1α signalling is likely driving immune cell adhesion and extravasation[177]. Microglia have also been shown to be important in intracellular infections, for example in models of viral encephalitis depletion microglia has shown to worsen disease outcomes, however it has also been shown that Zika virus-induced IFN-γ production by CD8 T cells drives excessive microglial activation and removal of neurons[150,178,179]. The role of microglia in the infection response is therefore highly context dependent.

### 3.1.5 Microglia heterogeneity

The importance of the inflammatory context in understanding microglial immune mechanisms has been demonstrated by the discovery of microglial subsets. Single cell RNA-sequencing analysis, combined with spatial analysis techniques such as Image-Seq, has allowed researchers to begin to uncover these microglial subsets, and has aided in our understanding of BAM subpopulations and the interactions between the CNS resident immune cells and infiltrating leukocytes from the periphery. Firstly, it is becoming increasingly clear that even under homeostatic conditions, there is heterogeneity in microglia across the different regions of the brain[180]. Studies (largely in mice) have shown that microglia numbers and cell morphology differ depending on the brain region, as well as differing in features such gene expression, cell turnover rate, and metabolism [180]. For example, microglia in the subventricular zone – an area surrounding the brain ventricles where substantial neurogenesis occurs – have fewer dendrites, increased expression of regulatory 'M2-like' cytokines such as IL-4 and reduced expression of surface receptors required for phagocytosis such as P2YR12[180,181]. Another recent study found that there is a subpopulation of microglia which localise to the capillaries and mediate regulation of capillary diameter, which have been termed capillary-associated microglia (CAMs)[182]. This

regional heterogeneity is important to consider when studying microglia in different inflammatory contexts. For instance, when modelling traumatic brain injury, how might the site of injury affect the microglial response observed? In infection models, how might the route of infection affect what microglia encounter the pathogen first, and what capacity do these microglia have to clear effectively deal with the pathogen?

Microglial subsets have also been identified in the context of ageing and neurodegeneration. In early development, a subpopulation of microglia defined by their high CD11c expression are vital for myelination of neurones, however over the course of development into adulthood this population is vastly reduced[183]. *In vivo* studies of neurodegeneration models such as Alzheimer's disease revealed a subset termed disease-associated microglia (DAM)[184–187]. In the DAM population there is a reduction of expression of microglia markers including P2YR12, CX3CR1 and Tmem119, whilst inflammatory markers and expression of ApoE and Trem2 (both genes associated with increased risk of Alzheimer's disease in humans) were upregulated [184–187]. Furthermore, these DAMs have been found to localise to Aβ plaques and to be the main microglial population that phagocytoses these plaques [184–187]. Interestingly, DAMs can be defined experimentally by their increased CD11c surface expression, thus showing the expression of this molecule on microglia throughout life can have significant outcomes on cognitive function.

Whilst these DAMs have been replicated in various neurodegeneration models, the term "disease-associated" is non-specific and thus more precise terminology may be required as microglial subsets continue to be studied in different disease contexts. This has been demonstrated using LPS as the inflammatory stimulus which generates inflammatory-associated microglia (IAM) that are distinct from the published DAM signature, albeit there is some overlap including the downregulation of microglia genes associated with

homeostasis[188,189]. LPS-stimulated microglia were shown to upregulate expression of inflammatory markers such as the chemokine CCL2, whilst in contrast to DAMs these microglia downregulated Trem2[188].

Whether microglia form similar subsets in the context of other infectious diseases including fungal CNS infection, has not been explored. I therefore sought to define microglial heterogeneity in an *in vivo* model of cryptococcal meningitis.

# Results

## 3.2 Single cell RNA-seq analysis of myeloid populations in an *in vivo* model of cryptococcal meningitis.

To study the heterogeneity of myeloid cells during cryptococcal meningitis, we used an *in vivo* model of the disease. Mice were infected intravenously with *C. neoformans* strain H99 as using this method ensures rapid and reliable dissemination of the fungus to the brain. Brain samples were collected at day 0 (uninfected controls), day 3 and day 6 post-infection (figure 3.2a). The brains were gently digested using the Miltenyi Brain Dissociation Kit (see **Methods 2.9**) to maximize the number of viable cells extracted from each brain sample. The samples were then stained and FACS sorted to collect CD45+CD11b+ myeloid cells for single-cell RNA-sequencing analysis. As our focus was on the myeloid response to fungal infection, we sorted the cells before the sequencing analysis to avoid having to remove a significant number of unwanted cells such as neurons from our sequencing analysis. Including all brain cells could have masked the complexity of our myeloid populations, and sorting the cells enabled us to ensure we had enough of our cells of interest. Once Illumina sequencing was performed, analysis files were processed including aligning reads to the reference genome, and then further analysis was performed using Partek Flow and RStudio. Partek Flow is an online software platform for sequencing data analysis, whilst RStudio is an integrated development environment for coding by R.

After performing quality control steps including filtering and normalisation, which removes elements that can falsely skew a single-cell data set such as counts from dying cells and genes that were not expressed in any cells, we performed graph-based clustering. This analysis clusters similar cells together, thus providing a baseline to determine what different cell populations are present in a single cell sequencing dataset. The analysis of

our data revealed that across all samples, 14 clusters of cells could be identified, visualised using a t-SNE plot (figure 3.2b). To classify these clusters by cell type, we used feature lists of signature genes an applied these to the t-SNE plot to see in which clusters these genes were expressed (figure 3.2c). Microglia signature genes were defined as *P2ry12, Hexb, Tmem119, Cx3cr1, Sall1* and were highly expressed in clusters 1-6, 9, 10 and 12 (figures 3.2c and 3.3). The neutrophil signature genes were *S100a8, S100a9, Lcn2, Ngp, Camp*, expressed in cluster 8 (figures 3.2c and 3.3). Monocyte and macrophage populations were initially defined by expression of *Ly6c2, Plac8, Ccr2, F13a1, H2-Aa, Mgl2* and aligned with clusters 7, 11 and 14 (figures 3.2c and 3.3), with cluster 11 also expressing some NK cell signature genes. In conclusion, the data showed that in a model of cryptococcal meningitis, many different subsets of myeloid cells are present in the brain.

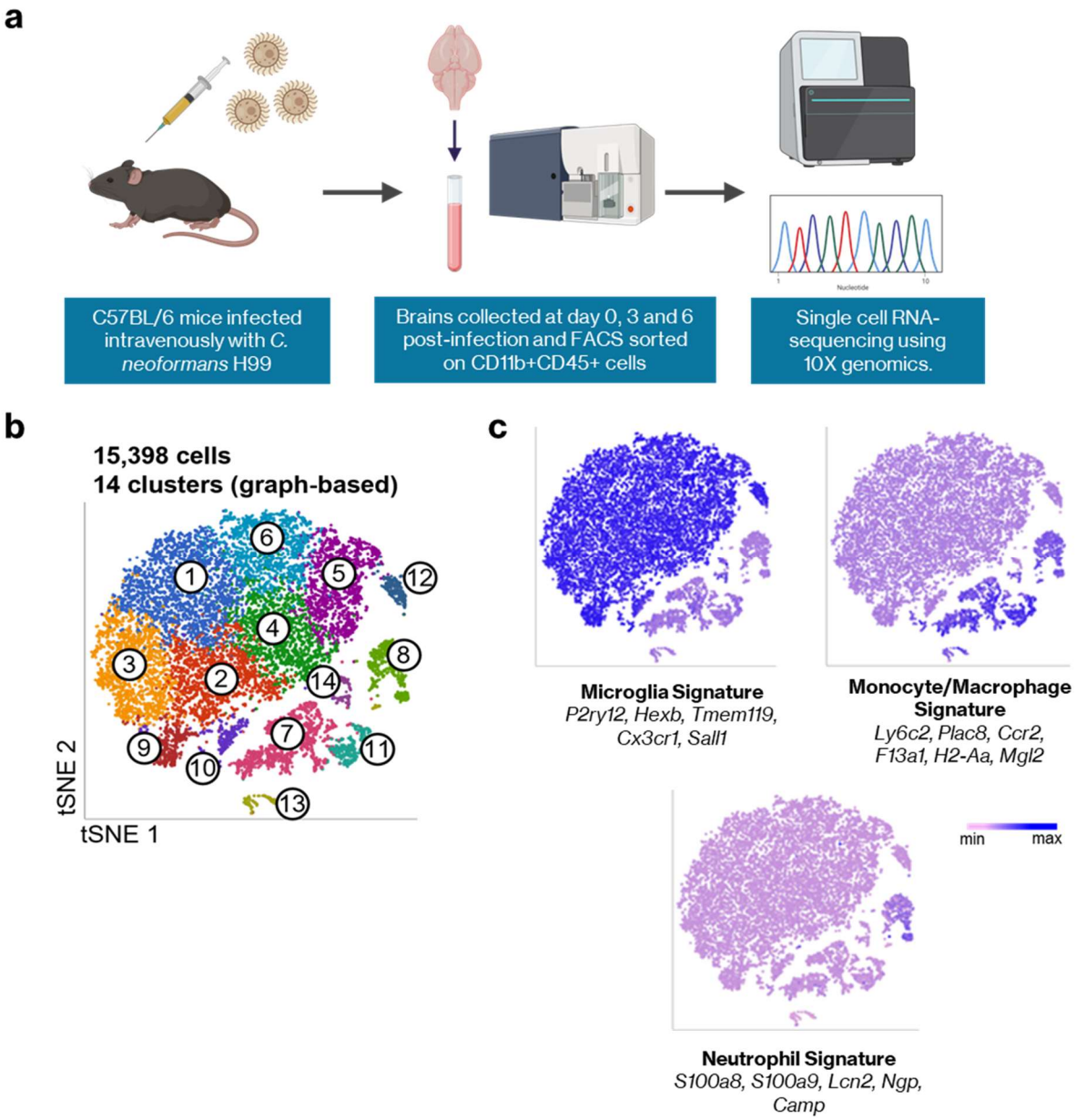


**Figure 3.2. Single cell RNA-seq analysis of myeloid populations in an *in vivo* model of cryptococcal meningitis.** **(a)** Schematic of the workflow of the RNA-seq experiment. **(b)** tSNE plot of the 14 graph-based clusters identified within the dataset. **(c)** The same tSNE plot coloured by expression of gene feature lists associated with the indicated cell types.

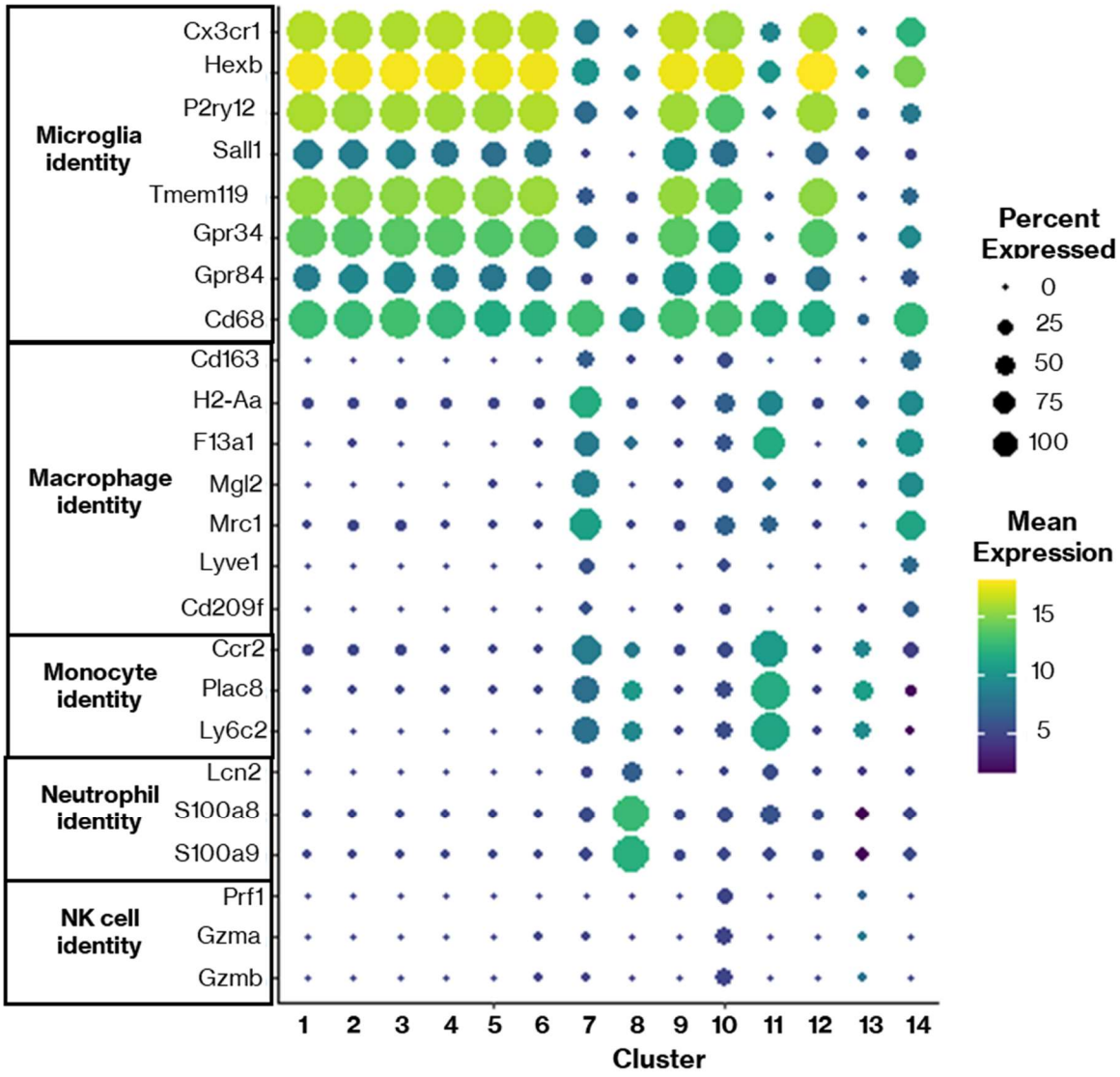


**Figure 3.3. Classification of cell clusters.** Expression of the indicated signature genes within each of the cell clusters generated by graph-based clustering. The data shows the percentage of cells within each cluster with transcripts for that gene and the mean value.

## 3.3 Time point analysis of the single-cell RNA-seq data reveals a population of microglia associated with established cryptococcal infection.

Once the cell clusters had been defined, we wanted to determine whether certain myeloid clusters were enriched at specific time points of infection. First, we used the t-SNE plot produced in figure 3.2b and coloured the plot by each time point sample (figure 3.4a). we observed that the clusters we had previously defined as neutrophils or monocyte/macrophages were largely from the day 6 post-infection samples, indicating that these cells are inflammatory cells that have arrived in the brain from the periphery to respond to the infection (figure 3.4a). We next wanted to define the microglial clusters and found that whilst most of the clusters had similar proportions of cells associated with each time point, cluster 10 was largely present at day 6 post-infection (figure 3.4b). We confirmed that cluster 10 did not highly express the immediate early response genes (IEGs) *Fos, Jun, Rhob, Atf3, Klf2, Egr1, Dusp1, Ubc, Hspa1a, Nfkbia, Tnf* (figure 3.4c) as microglia can upregulate these genes because of sample processing for single-cell RNA-seq[190]. We therefore hypothesised that the cluster 10 microglial population was a subpopulation of microglia specifically associated with fungal infection and termed this population infection associated microglia (IAM). To conclude, this data showed that at early time points of infection there is little change to the myeloid populations, with heterogeneity only evident at the later time point post-infection.

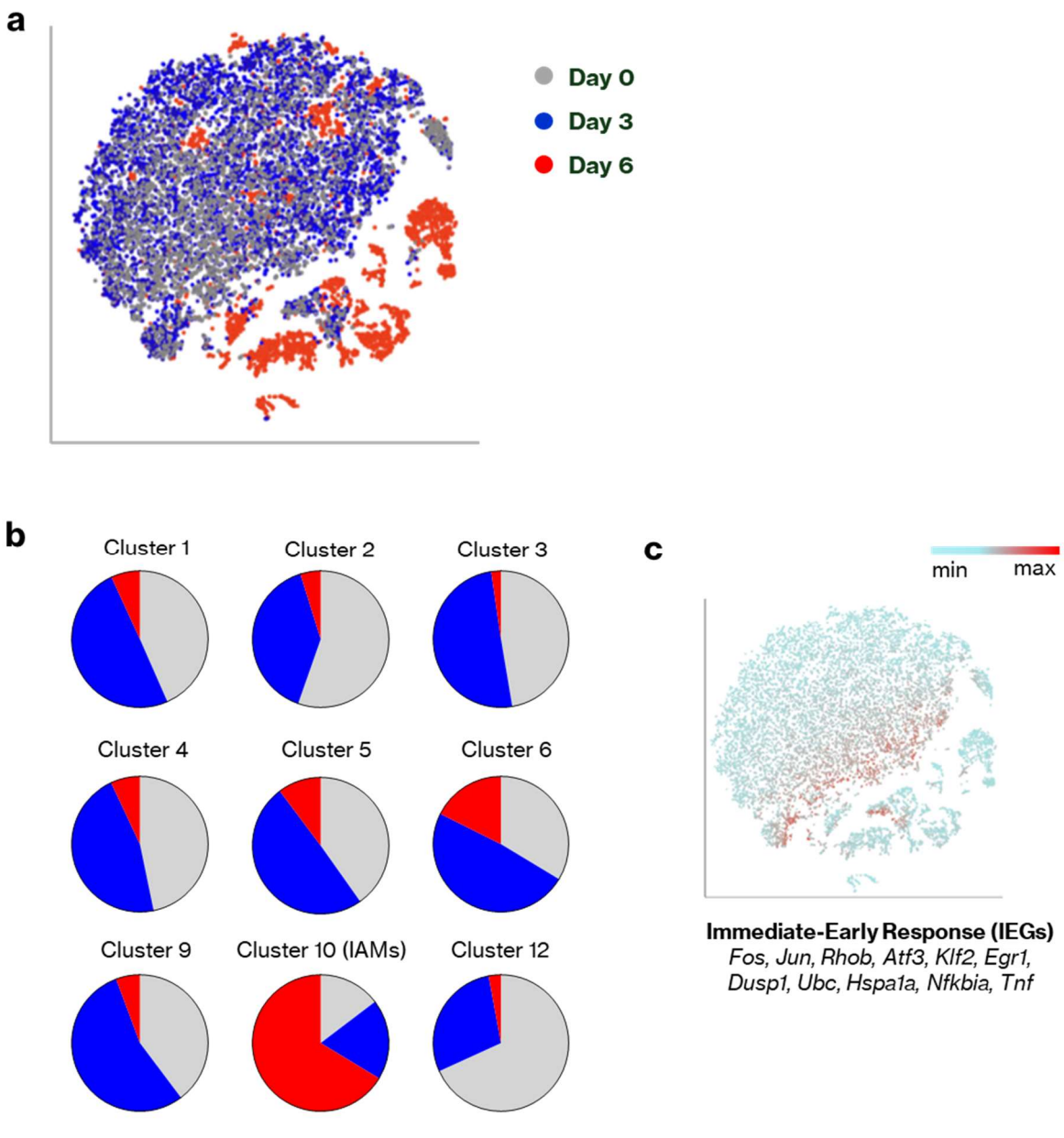


**Figure 3.4. Time point analysis of the scRNA-seq dataset. (a)** tSNE plot of the graph-based clustering analysis coloured by time point of sample collection (day 0, 3 and 6). **(b)** Pie charts of the clusters defined as microglia showing the percentage of each cluster that belongs to each experimental time point. **(c)** tSNE plot coloured by expression of immediate-early response genes.

## 3.4 scRNA-seq analysis provides clues for the function of IAMs.

Once I had established the IAMs cluster as a cell population of interest for further exploration, I first wanted to determine the genes and pathways were upregulated in the IAMs population compared to non-IAMs microglia. I performed this analysis on the day 6 samples only as this is when the majority of IAMs were present (figure 3.4b), but also in anticipation of future functional experiments for the IAMs which would utilise the day 6 post-infection time point. KEGG pathway analysis enables the top differentially expressed pathways between two cell populations to be identified. This analysis draws on a database of known gene pathways and can include both downregulated and upregulated pathways. The pathway analysis revealed that IAMs upregulated genes in the proteosome pathway, which was largely immunoproteasome genes (e.g. *Psmb8, Psme1*) which are upregulated during antigen presentation[191] (figure 3.5a). IAMs also upregulated metabolism and cell cycle pathways (figure 3.5a), indicating these microglia may be more proliferative and metabolically active than non-IAMs microglia. Genes in the pathway phagosome, lysosome and endocytosis were also upregulated by IAMs, indicating that they may be more phagocytic than other microglia. Analysis of the top 25 DEGs showed IAMs upregulate expression of inflammatory chemokines and cytokines including IL-1α and CCL12 (figure 3.5b). Indeed, the upregulation of pathways of Salmonella and Epstein-Barr infection (figure 3.5a) align with IAMs being an infection-responsive microglia population, as these infections drive IFN-γ signalling which is also important in *C. neoformans* infection, and IFN-γ GTPases such as *Ifitm3* are highly expressed in the IAMs (figure 3.5b). The top 25 DEGs also revealed that IAMs downregulate homeostatic microglia genes including *P2yr12* and *Tmem119*, aligning with previous studies that have shown activated microglia alter their expression of these markers.

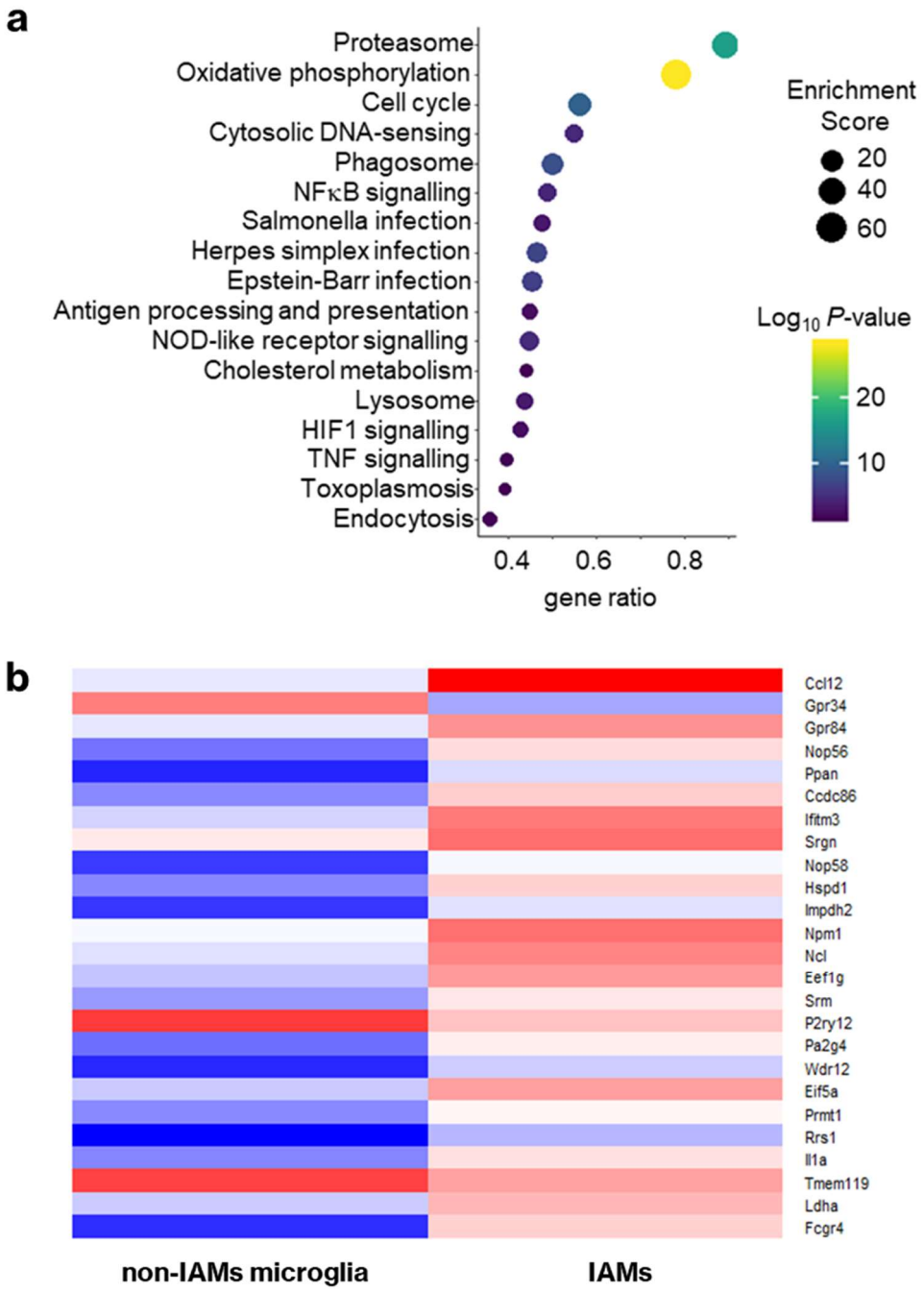


**Figure 3.5. KEGG pathway analysis and DEG analysis of IAMs and non-IAMs microglia at day 6-post infection. (a)** KEGG pathway analysis of upregulated genes by IAMs (compared to non-IAMs), showing gene ratio of detected genes within indicated pathways, P-value and enrichment scores. **(b)** Heatmap of the top 25 differentially expressed genes in IAMs versus non-IAMs microglia: *Ccl12, Gpr34, Gpr84, Nop56, Ppan, Ccdc86, Ifitm3, Srgn, Nop58, Hspd1, Impdh2, Npm1, Ncl, Eef1g, Srm, P2yr12, Pa2g4, Wdr12, Eif5a, Prmt1, Rrs1, Il1a, Tmem119, Ldha, Fcgr4*.

## 3.5 Flow cytometry confirms IAMs can be identified experimentally.

Since microglia subsets are poorly understood and have never been explored in the context of cryptococcal meningitis, I decided to focus on the IAMs cluster for further analysis to better understand these cells. I decided to develop a strategy to identify the IAMs using flow cytometry, with the aim of using this to perform functional assays. First, I used the RNA-seq analysis to identify potential markers that may be used to design a flow cytometry panel. Ideal markers would include surface-expressed proteins that were specific to IAMs and not expressed by non-IAMs microglia or by monocytes/macrophages and had commercially available antibodies for those markers.

The top differentially DEGs that were highly expressed by IAMs but not other microglia (figure 3.5b) included GPR84, a member of the G-protein coupled receptor (GPCR) superfamily. GPR84 is termed an orphan GPCR as its endogenous ligand(s) have not been definitively identified, however initial studies have found medium chain fatty acids can activate GPR84[192–194]. GPR84 expression has been reported throughout the body, including in the brain, the colon, and bone marrow[195–197]. Importantly, multiple studies have shown GPR84 is primarily expressed in leukocytes, including circulating monocytes/macrophages, neutrophils, and microglia[195,196]. GPR84 has been shown to be upregulated by microglia during inflammation and may have roles in CNS dysfunction such as chronic pain and multiple sclerosis[198,199]. I performed graph-based clustering analysis on the day 6 samples and observed that GPR84 expression was highly specific to the IAMs population (figure 3.6a and 3.6b). Whilst this would have made GPR84 an ideal candidate for identifying IAMs by flow cytometry, my tests of the commercially available murine GPR84 antibodies showed that these were not reliable. We did purchase a human antibody that had been published for use in mice, however after testing this antibody by

Western blotting using CHO cells engineered to express HA-tagged GPR84 courtesy of collaborators in the Greaves lab (University of Oxford), we determined that it was non-specific (figure 3.7a and 3.7b).

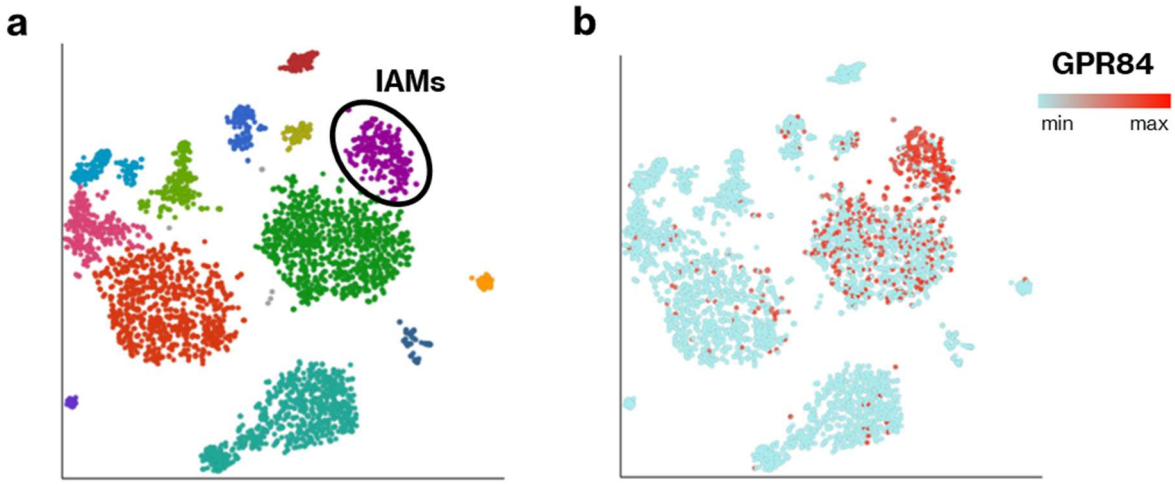


**Figure 3.6. Single cell RNA-sequencing reveals GPR84 is upregulated in IAMs at day 6. (a)** tSNE plot of the day 6 time point single cell RNA-seq data, with the IAMs population highlighted. **(b)** The same tSNE plot as in (a) but with the plot coloured by the expression of GPR84, with high expression indicated in red.

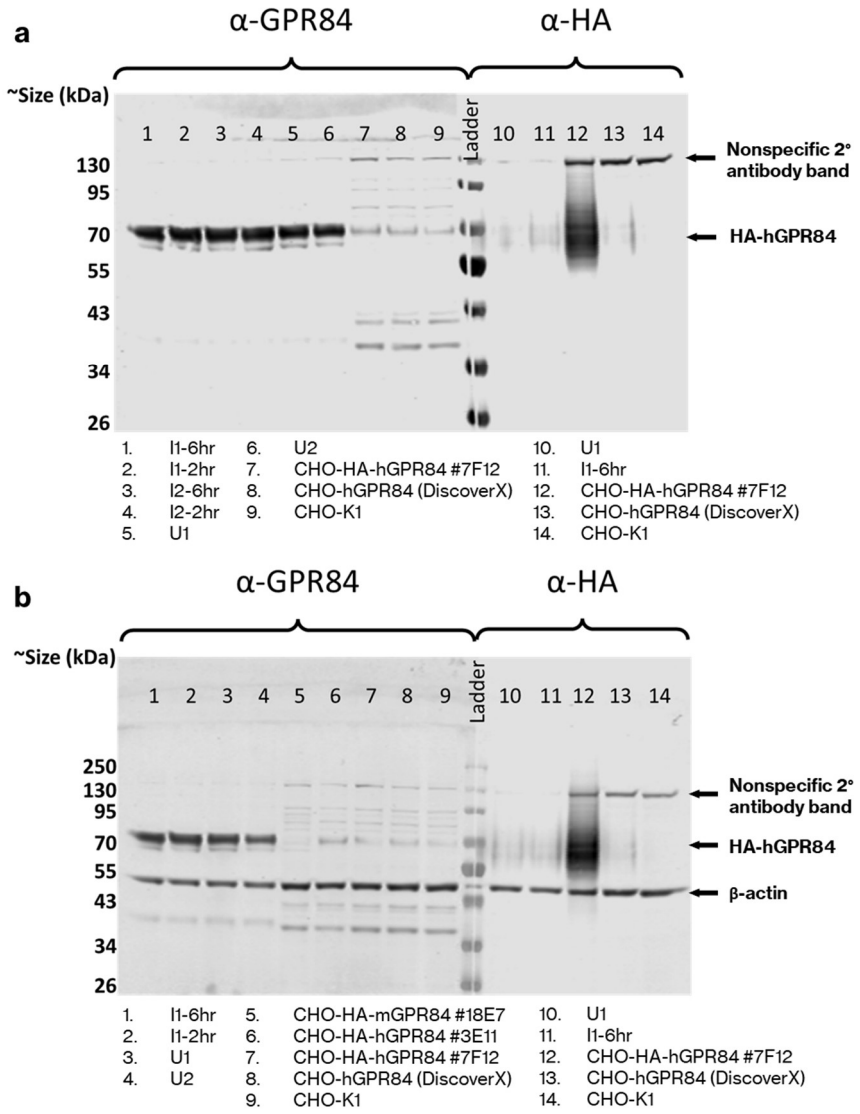


**Figure 3.7 Western blot analysis of GPR84 antibody.** The rabbit polyclonal GPR84 antibody from Bioss was purchased from Thermofisher (Cat#BS-15353R). The BV-2 microglial cell line was seeded and infected with *C. neoformans* for 2 and 6 hours before collection of protein lysates. Samples were in duplicated (indicated as I1 and I2). Uninfected controls (U1 and U2) were also prepared. Samples were sent to the Greaves lab at the University of Oxford and Western blotting analysis kindly performed by Vincent Luscombe. The Greaves lab have developed a CHO cell line that expresses GPR84 (human or mouse) tagged with HA, thereby GPR84 expression can be probed using an anti-HA antibody. The CHO-K1 samples are negative controls. **(a)** Western blot of the BV-2 samples and CHO cell line samples probed with the GPR84 antibody and an anti-HA antibody, showing the former producing a different band to that of the cell lines. **(b)** Probing of the samples with β-actin as an endogenous control to check protein levels across the samples. CHO cell lines expressing human and mouse GPR84 were probed to check the GPR84 antibody binding was not due to mouse/human eptiope differences.

Cholesterol metabolism was one of the top upregulated KEGG pathways in IAMs (figure 3.5a) so I next decided to use Filipin, a marker for cholesterol, to stain for IAMs. This is an intracellular stain, so samples were processed accordingly (see **Methods 2.7**), and staining was performed overnight. In some of the infected samples, it appeared that a CD45$^{high}$Filipin+ microglia population was present (figure 3.8a), and once quantified it was found that there were a significantly higher number of CD45$^{high}$Filipin+ microglia in infected mice versus uninfected mice (figure 3.8c). However, the MFI of Filipin was not significantly different between uninfected and infected mice (figure 3.8b), reflecting the fact that almost all microglia were positive for Filipin, likely reflecting the large percentage of cholesterol present in the brain.

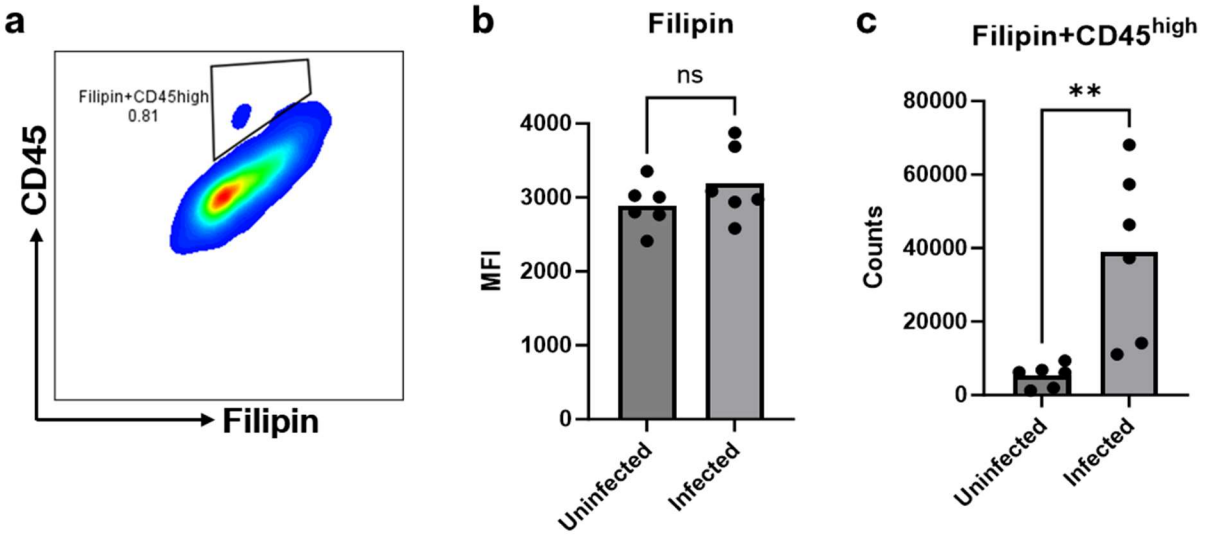


**Figure 3.8 Filipin as an IAMs marker. (a)** Representative flow cytometry plot of CD45 and Filipin staining within microglia in an infected mouse. Cells were gated on live singlets, and on CD45+CD11b+ myeloid cells prior to gating microglia as CD45intCX3CR1high. **(b)** Quantification of the mean fluorescence intensity (MFI) of Filipin in microglia from uninfected and infected mice. **(c)** Counts of CD45highFilipin+ microglia in uninfected and infected mice. Data plotted are the individual samples as data points and the mean per condition represented by a bar. 6 mice per condition, corresponding to one sample per mouse, were obtained from two independent experiments. Statistical analysis performed using Student's t-test.

I also included an antibody for the chemokine CXCL9 in this panel, as it required the same intracellular cytokine staining protocol and CXCL9 was upregulated in IAMs compared to non-IAMs microglia in the RNA-seq data (figure 3.9a). The CLR CD206 (*Mrc1* gene) was also upregulated in the IAMs (figure 3.9a), and as this has previously been shown to be upregulated in activated microglia, this was also included in the flow cytometry panel. I first gated the brain samples on CD45+CD11b+ myeloid cells and identified a population of CD206+CXCL9+ cells in the infected samples (figure 3.9b). Counts analysis revealed this population was significantly increased in the brains of infected mice (figure 3.9c). However, this gating strategy did not gate on microglia specifically. Initially as we had seen a decrease in microglia homeostatic markers such as CX3CR1 in the RNA-seq data, I opted to exclude this marker in my analysis. However, upon re-gating the CD45+CD11b+ myeloid population into macrophages ($CD45^{high}CX3CR1^{int}$) and microglia ($CD45^{int}CX3CR1^{high}$), it became clear that the CXCL9 staining was present exclusively in macrophages (figure 3.9d).

Since neither CXCL9 staining or Filipin staining were suitable for accurately gating on the IAMs population, I next tried the macrophage scavenger receptor 1 (MSR1) combined with staining for CD206 as these receptors were both upregulated in IAMs (figure 3.10a). Furthermore, the known functions of CD206 and MSR1 in pathogen recognition and uptake would make for interesting functional studies, for example recent work by the May lab has shown MSR1 is involved in phagocytosis of *C. neoformans* by macrophages[200]. As previously, the gating strategy I used began with gating on live singlet cells and then on CD45+ CD11b+ myeloid cells (figure 3.10b). I incorporated Ly6G and Ly6C staining to exclude neutrophils and inflammatory monocytes (figure 3.10b). Then, macrophages and microglia were gated based on CD45 and CX3CR1 expression. Due to the altered expression of these markers in the RNA-seq data (figure 3.10a), I applied a generous microglia gate that included a small intermediate population which expressed higher

CD45, but that was still lower than the CD45high macrophage population. Within this gate, I then used CD206 and MSR1 to gate on double positive cells as IAMs and double negative cells as non-IAMs microglia (figure 3.10b). Counts analysis showed CD206+MSR1+ cells were significantly higher in infected mice (figure 3.11a), aligning with the RNA-seq data. Whilst some double positive cells were still present in the uninfected samples, the flow cytometry analysis likely represents an enrichment of the IAMs population that may include small numbers of other cells such as macrophages. Aligning with the RNA-seq data (figure 3.10a), the expression of MHC-II was higher in the CD206+MSR1+ population, whilst the CX3CR1 expression decreased (figure 3.11b).

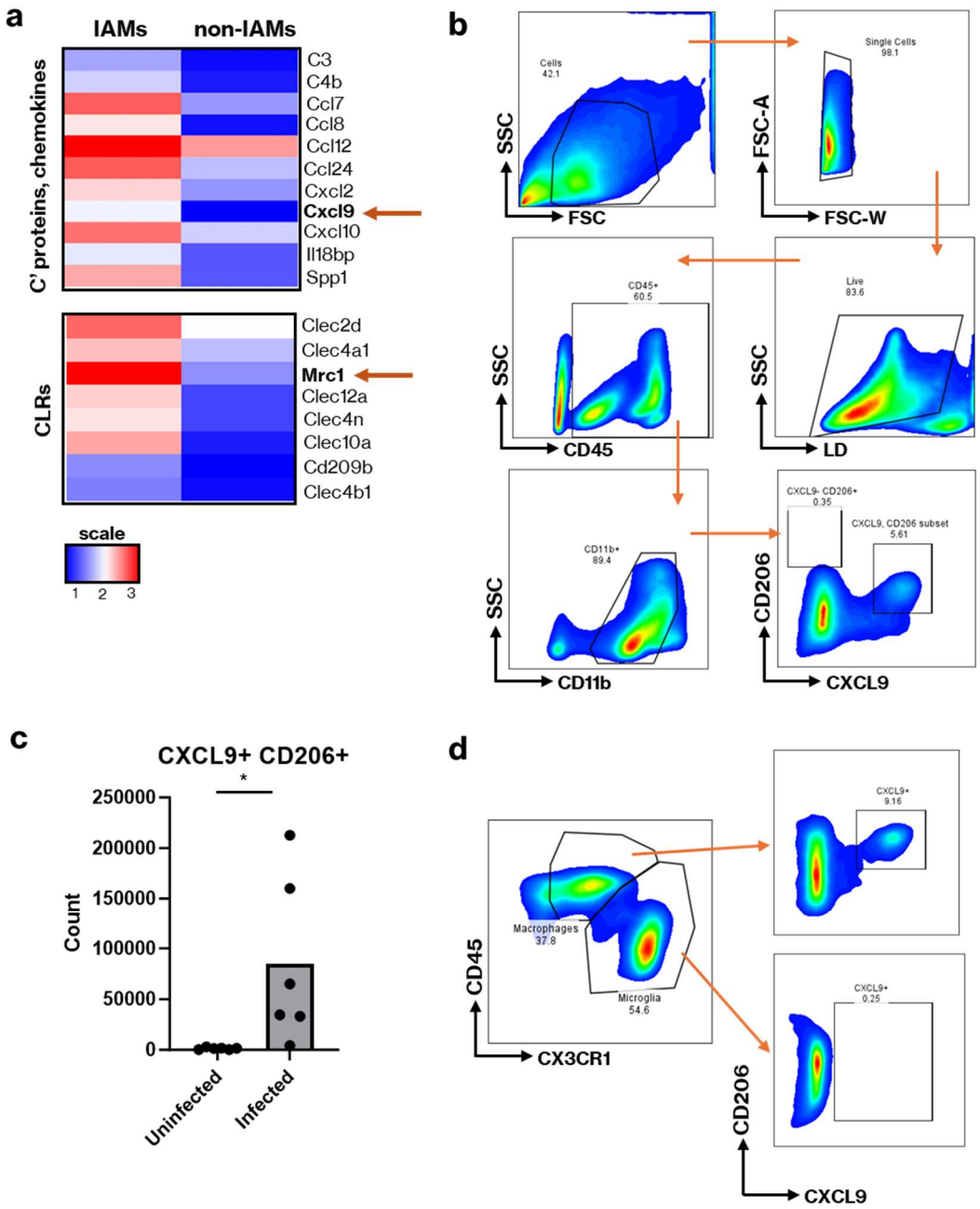


**Figure 3.9 CXCL9 and CD206 as IAMs markers. (a)** Heatmap plots of selected differentially expressed genes at day 6 post-infection between IAMs and non-IAMs microglia. **(b)** Representative flow cytometry plots showing the gating strategy in an infected mouse. After gating on singlet live cells, myeloid cells were gated as CD45+ and CD11b+. Within this population, the CD206 and CXCL9 double positive cells were gated. **(c)** Counts of CXCL9+CD206+ cells in uninfected and infected mice. Data plotted as individual samples and the mean per condition. N=6 mice per condition, obtained from two independent experiments. Statistical analysis performed using Student's t-test. **(d)** After gating on myeloid cells as described in (b), samples were gated as macrophages and microglia using CD45 and CX3CR1. Representative flow plots show the expression of CXCL9 within the microglia and macrophage populations.

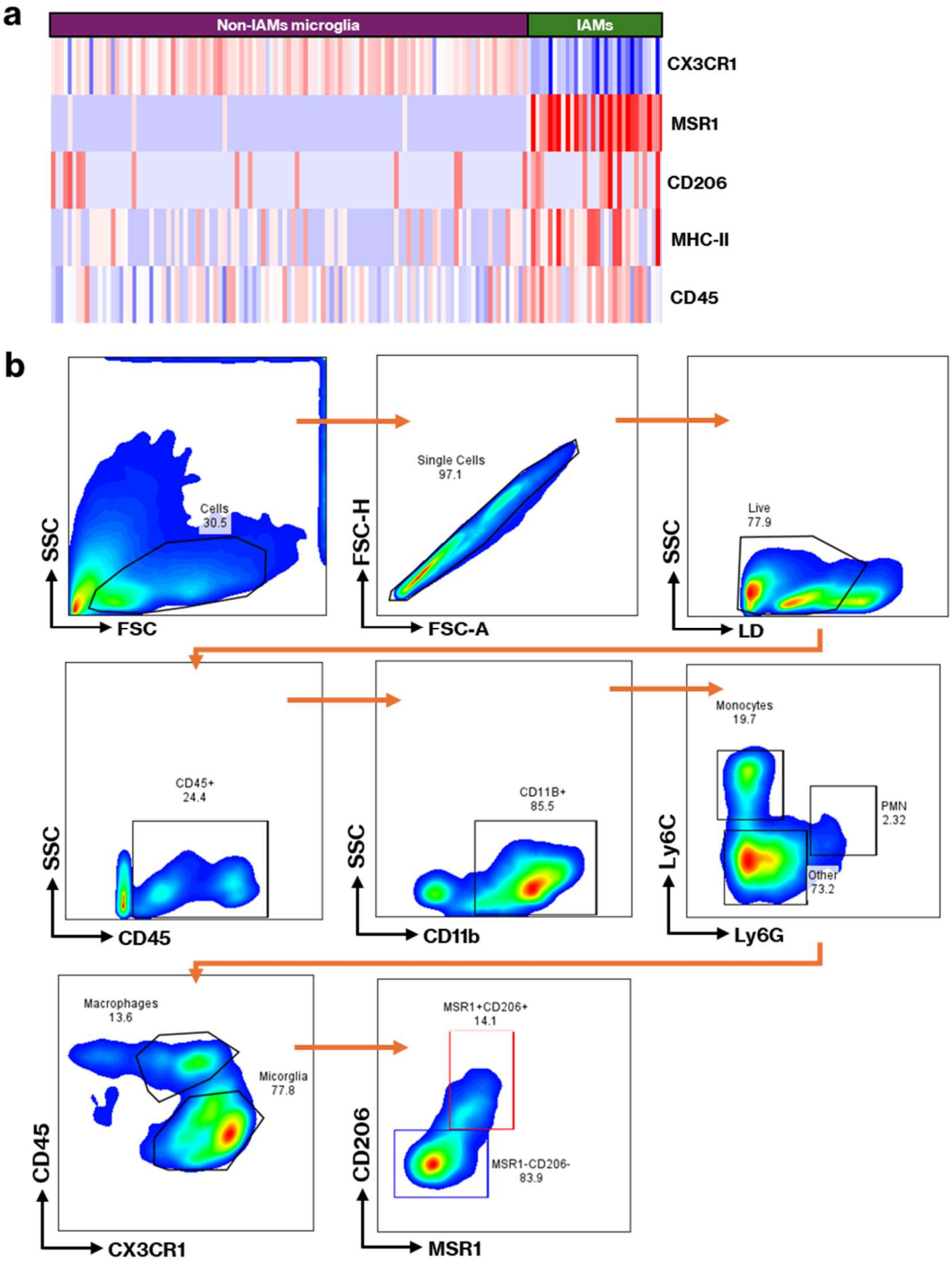


**Figure 3.10. Finalising a flow cytometry panel for IAMs. (a)** Heatmap of all cells in the IAMs and non-IAMs microglia populations at day 6-post infection showing the differential expression of CX3CR1, MSR1, CD206, MHC-II and CD45. **(b)** Representative flow plots of the gating strategy for IAMs.

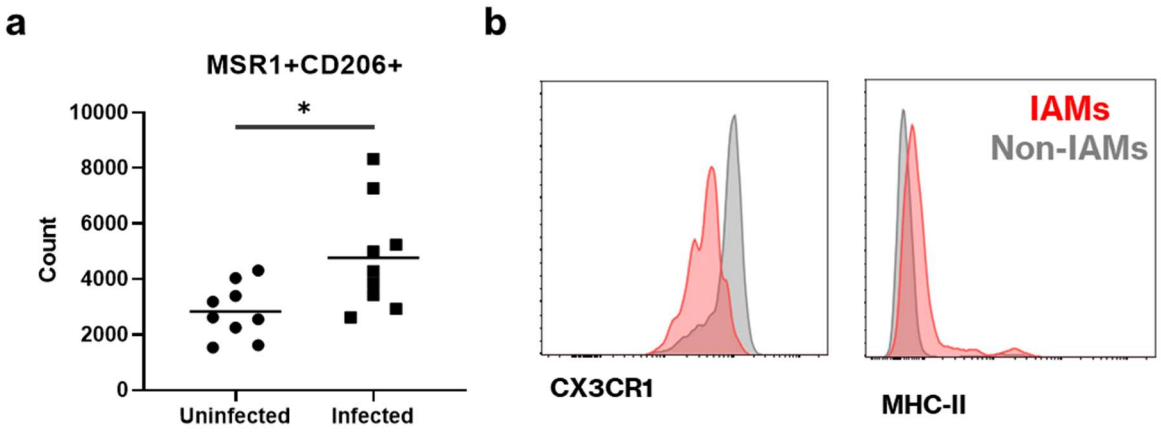


**Figure 3.11. CD206 and MSR1 staining enriches for the IAMs population (a)** Counts analysis of MSR1+CD206+ (IAMs) in uninfected versus infected mice. Analysis performed on n=9 mice per condition, taken from 3 independent experiments. Data are plotted as individual values and with mean per condition. Statistical analysis is Student's t-test. **(b)** Representative flow cytometry histograms showing MHC-II and CX3CR1 staining in IAMs versus non-IAMs microglia.

## 3.6 IAMs derive from microglia.

Once I had established that MSR1 and CD206 could be used as cell surface markers for IAMs, I wanted to further confirm the identity of this population was indeed microglial, as these markers can be expressed by macrophages in the brain such as perivascular macrophages. Within the macrophage gate defined by the flow cytometry data there is a small population of CD206+ cells, which express higher CD206 than the cells in the microglia gate (figure 3.12a).

I next used FACS sorting to sort macrophages, CD206-MSR1- microglia and CD206+MSR1+ microglia from the brains of uninfected and infected mice. I extracted RNA from sorted cells and performed qRT-PCR analysis to determine the expression of homeostatic microglia marker Tmem119 (figure 3.12b). The results showed that Tmem119 gene expression was significantly higher in non-IAMs microglia than macrophages, whilst in IAMs Tmem119 expression trended higher than macrophages but lower than non-IAMs microglia. This aligns with our RNA-seq data that shows IAMs downregulate Tmem119 expression compared to other microglia (figure 3.5b). Furthermore, previous studies have shown macrophages can upregulate Tmem119 during inflammation[164–166], whilst in microglia subpopulations such as DAMs Tmem119 is downregulated[184–187]. I performed the qPCR analysis using other microglia genes such as Hexb and Sall1, however no expression could be detected in the samples. I then analysed GPR84 gene expression as in the RNA-seq data this was specifically expressed by microglia, and particularly IAMs (figure 3.6). Gene expression analysis revealed macrophage expression of GPR84 was significantly lower than in non-IAMs microglia, whilst in IAMs the expression of GPR84 trended higher than macrophages but did not reach significance (figure 3.12c).

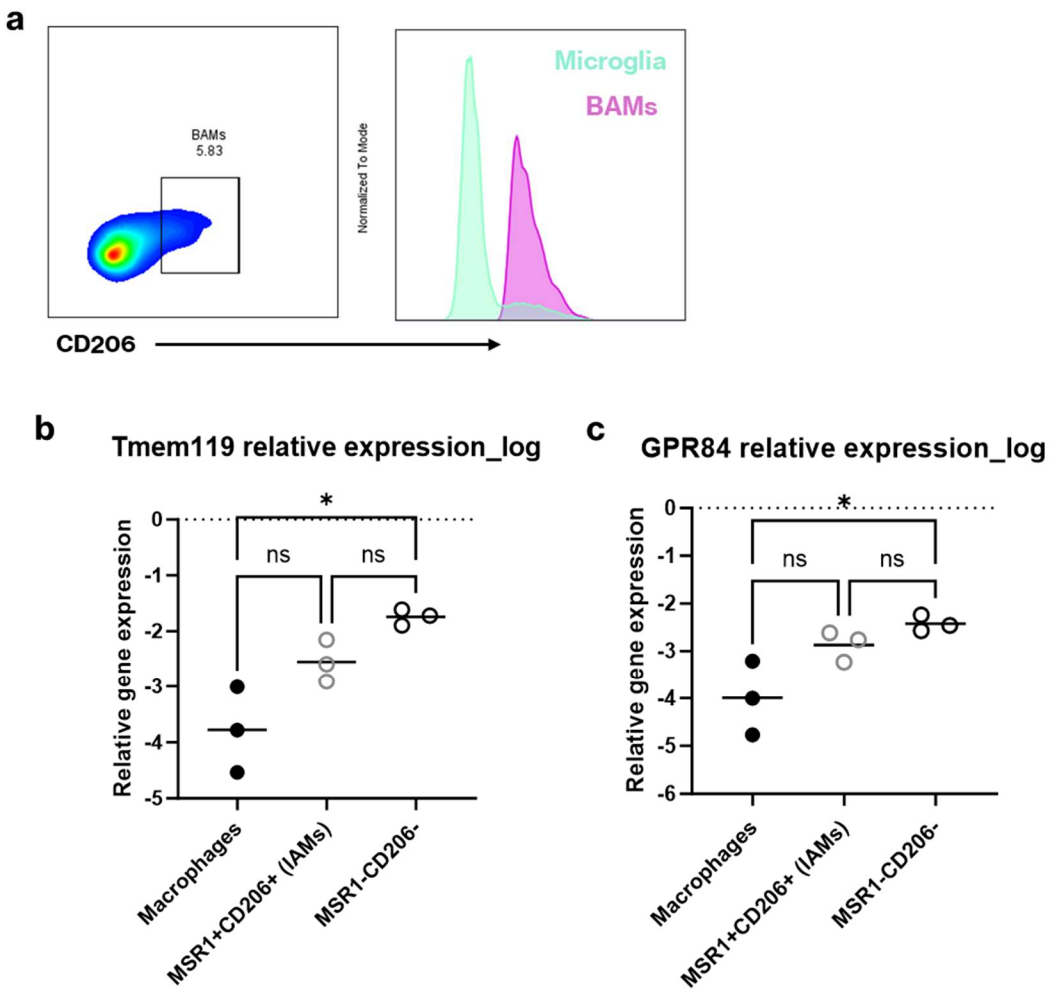


**Figure 3.12. MSR1+CD206+ IAMs have microglia properties. (a)** Representative flow cytometry plot of CD206+ cells, defined as border-associated macrophages (BAMs) from the macrophage gate defined in figure 3.10b. Histograms of CD206 staining in the BAMs versus microglia shows a higher shift in CD206 expression in the BAMs. **(b)** Brains from mice I.V. infected with *C. neoformans* strain H99 or *C. neoformans* GFP were collected at day 6 post-infection and processed for cell sorting. Cells were sorted as live singlet CD45+CD11b+Ly6C-Ly6G- cells. Macrophages were gated as CD45highCX3CR1int, whilst microglia were sorted as CD45intCX3CR1high. Within microglia, cells were sorted as non-IAMs (CD206-MSR1-) or IAMs (CD206+MSR1+). ~5000 cells were collected for each population, then processed for qRT-PCR analysis of Tmem119 and **(c)** GPR84 gene expression. Relative expression determined using comparative CT (ΔCt) normalised to the housekeeper RPL13a, relative to the uninfected controls. For each experiment, brain samples were pooled from 5-6 mice/condition. Data points indicate 3 independent experiments. Data are plotted as log relative gene expression with the mean per condition. Statistical analysis performed using Two-way ANOVA with multiple comparisons.

Whilst the qPCR analysis indicated that IAMs do express higher GPR84 and Tmem119 than macrophages, the differences did not reach significance. This may be due to limitations in cell numbers as there were far more non-IAMs microglia than macrophages or IAMs in both uninfected and infected mice, and despite normalisation and use of a housekeeper gene, biases could still be introduced. I subsequently used our transgenic Sall1dTomato mouse model to determine if IAMs are indeed microglia. In this model, mice are treated with tamoxifen which induces genetic recombination resulting in all Sall1+ cells, namely microglia, becoming dTomato+ by removing the stop codon. In these experiments I employed a strategy of dosing mice every 2 days with tamoxifen to ensure dTomato expression was maintained. Flow cytometry analysis confirmed that Sall1dTomato expression was significantly higher in the microglia population than in macrophages or monocytes (figure 3.13a). Within the Sall1+ microglia, there was a significantly higher frequency of MSR1+CD206+ IAMs than in Sall1- cells (figure 3.13b and 3.13c). This data showed that IAMs mostly Sall1+ and are therefore derived from microglia and not macrophages.

Finally, I wanted to determine if the IAMs population could be derived from inflammatory monocytes that had differentiated into 'microglia-like' cells. I performed adoptive transfer of monocytes from CX3CR1$^{GFP}$CCR2$^{RFP}$ mice into wild-type mice. If IAMs are derived from peripheral monocytes that have entered the brain I hypothesised they would be CCR2+, as this is a specific marker for monocytes. Flow cytometry analysis indicated that the IAMs population were largely present in CCR2- cells (figure 3.14a). I also did an adoptive transfer of monocytes from wild-type (CD45.2) mice into BoyJ (CD45.1) mice, for which IAMs were largely CD45.1+ and therefore not derived from the transferred monocytes (figure 3.14b).

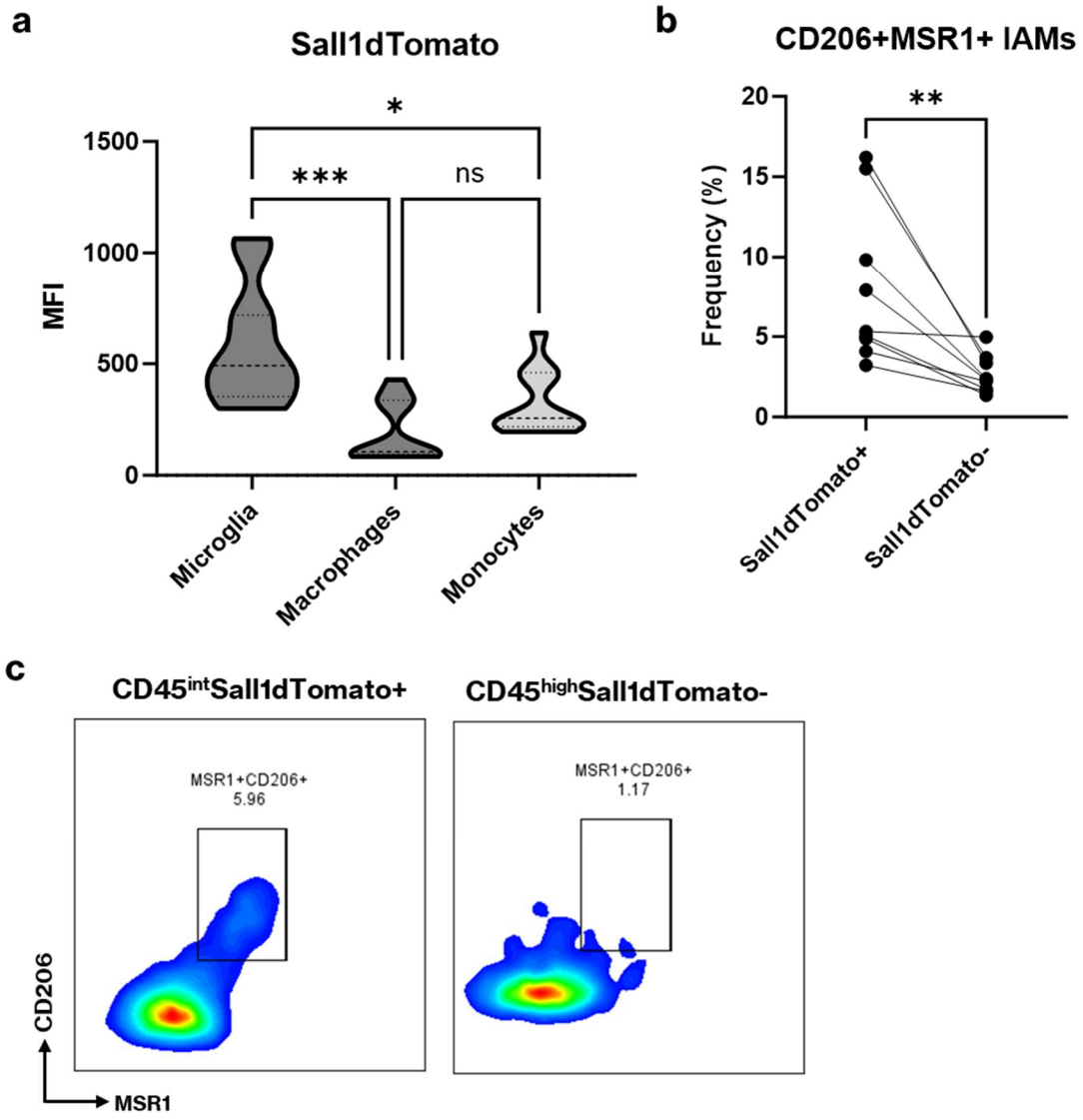


**Figure 3.13. IAMs in Sall1dTomato mice. (a)** Geometric mean fluorescence intensity (MFI) of Sall1dTomato in microglia, macrophages and monocytes in the brains of day 6 infected mice. Gating was performed as described in figure 3.10b. N=11 mice from two independent experiments. Data are plotted as a violin plot. Statistical analysis was ordinary one-way ANOVA with multiple comparisons. **(b)** Percentage frequency of Sall1dTomato+ and Sall1dTomato- cells in IAMs (CD206+MSR1) from infected mice. Data are plotted as individual values with lines pairing the Sall1+ and Sall1- frequency from the same IAMs sample. Statistical analysis by paired t-test. **(c)** Representative flow cytometry plots from CD45 intermediate Sall1dTomato+ cells (microglia) and CD45 high Sall1dTomato- cells (macrophages) showing MSR1 and CD206 expression.

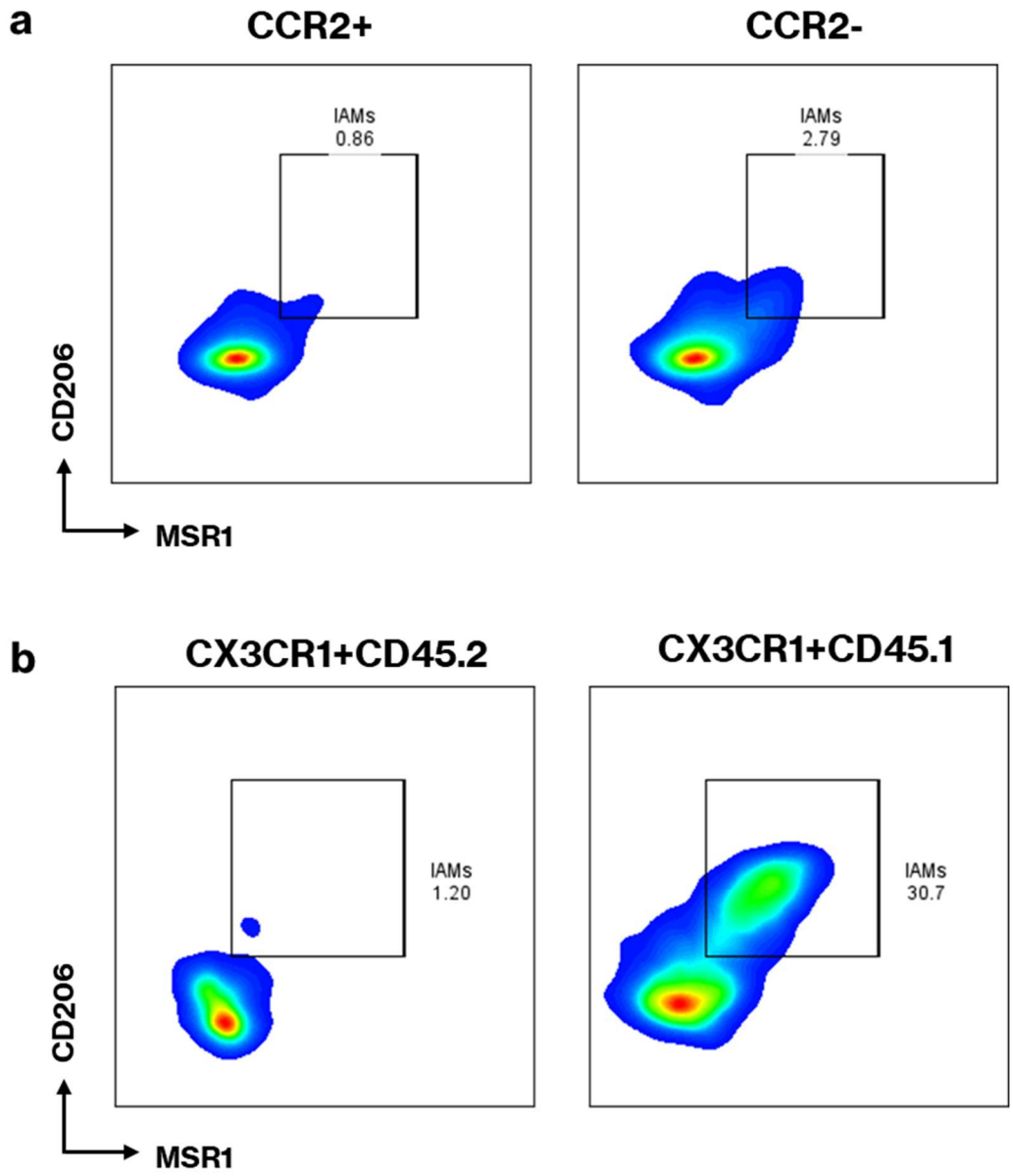


**Figure 3.14 Adoptive transfer of monocytes. (a)** Monocytes derived from CX3CR1GFPCCR2RFP mice were injected into C57BL/6 mice prior to infection with *C. neoformans* and brain samples collected at day 6 for flow cytometry analysis. The data from 4 injected mice were pooled prior to analysis due to the small number of adoptively transferred monocytes in individual samples. Representative flow cytometry plots show CD206 and MSR1 expression in CCR2+ and CCR2- myeloid cells. **(b)** The same adoptive transfer experiment was performed but using monocytes from CD45.2 mice injected into CD45.1 BoyJ mice. Data from 4 infected samples was pooled and the flow plots show the CD206 and MSR1 expression in CX3CR1+ myeloid cells that or CD45.2+ and CD45.1+.

## 3.7 IAMs are a reservoir for intracellular fungi.

After confirming that my flow cytometry strategy for identifying IAMs was robust, I used this approach to explore the function of these cells. Pathway analysis had revealed that one of the top upregulated pathways in IAMs was the phagosome (figure 3.5a) indicating that IAMs may have a role in phagocytosis and killing of *C. neoformans* during cryptococcal meningitis. To explore this, I used the flow cytometry assay I developed to identify IAMs and examined the association of these cells with *C. neoformans* using a fluorescent marker. For this, we infected mice with a GFP-expressing strain of *C. neoformans* which enables tracking of infected cells and extracellular yeast in the brain during infection[135]. Using this approach, I found a significantly higher frequency of GFP+ cells in the IAMs population versus non-IAMs microglia at day 6 post-infection (figure 3.15a and b), indicating at greater levels of fungal association by IAMs. This result could be interpreted in two ways. First, this could indicate a higher fungal killing rate by the IAMs, as the RNA-seq analysis showed increased expression of IFN-γ regulated genes and genes related to phagocytosis (figure 3.5). However, previous work by the Drummond lab has shown that the fungus can be taken up by microglia and resides there to access key nutrients for survival[135]. To discern between these two outcomes, I developed an *in vivo* killing assay by FACS sorting equal numbers of *C. neoformans* infected IAMs and non-IAMs from mouse brains, plating these cells on fungal growth media (YPD agar), then counting the viable CFUs to calculate the percentage viability. Surprisingly, I saw that fungal viability was higher in IAMs (figure 3.15c).

To understand why IAMs may be less effective at killing the fungus, I used flow cytometry to analyse arginase expression. Upregulated arginase (Arg-1) is associated with an M2-like phenotype resulting in reduced fungal killing, enabling the fungus to survive and replicate. Previous work by the Dang lab has shown CLP-1 secretion by *C. neoformans*

drives this M2 polarisation[136]. In line with this, arginase expression was significantly increased in the IAMs population (figure 3.15d).

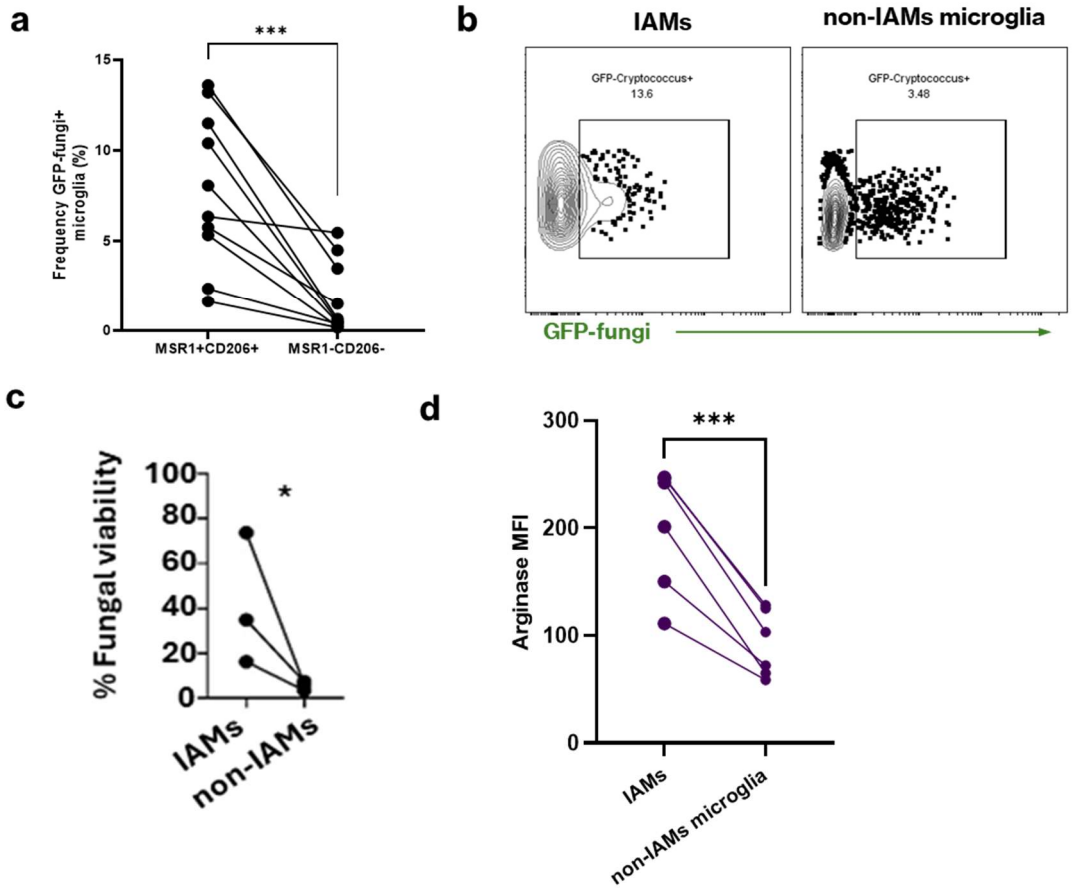


**Figure 3.15. IAMs are a reservoir for intracellular fungi. (a)** Frequency of GFP+ fungi positive microglia measured by flow cytometry in IAMs (MSR1+CD206+) and non-IAMs (MSR1-CD206-). For each sample, the frequency for each population is plotted as two joined data points. Statistical analysis by paired t-test. N=10 mice, taken from 3 independent experiments. **b)** Representative flow cytometry plots of GFP+ fungi in IAMs and non-IAMs microglia. **(c)** Percentage viability of fungi collected from GFP+ IAMs and non-IAMs microglia. 100-400 GFP+ cells were plated and the number of CFUs counted after 24-48 hours. Each set of joined data points represents a single experiment, for which 5-6 brains were collected and pooled prior to sorting. Statistical analysis by paired t-test. **(d)** The mean fluorescence intensity (MFI) or Arginase staining measured by flow cytometry in IAMs and non-IAMs. Each set of joined data points corresponds to a single mouse. N=6, taken from two independent experiments. Statistical analysis by paired t-test.

## 3.8 Imaging microglia in the fungal-infected brain.

I next wanted to determine the location of infected microglia in the brain to understand where in relation to the fungus the IAMs are located. I performed imaging analysis of brains from day 6 post-infection mice, using GFP-*C. neoformans* to visualize the fungus and Iba-1 to stain microglia. I found that in the fungus is mostly confined to large circular fungal lesions, reminiscent of the cryptococcomas seen in patients (figure 3.16a and c). These lesions were found to be distributed throughout the brain rather than localised to any specific region (figure 3.16c). The Iba-1 staining showed microglia that highly express Iba-1 can be found at the border of the fungal lesions (figure 3.17a and b). These microglia also appear to have an ameboid morphology, indicating that they are activated. When zooming in on these microglia further, I observed microglia with internalised fungi (figure 3.17c). Taken together, these images indicate the IAMs are likely the microglia surrounding the fungal lesions.

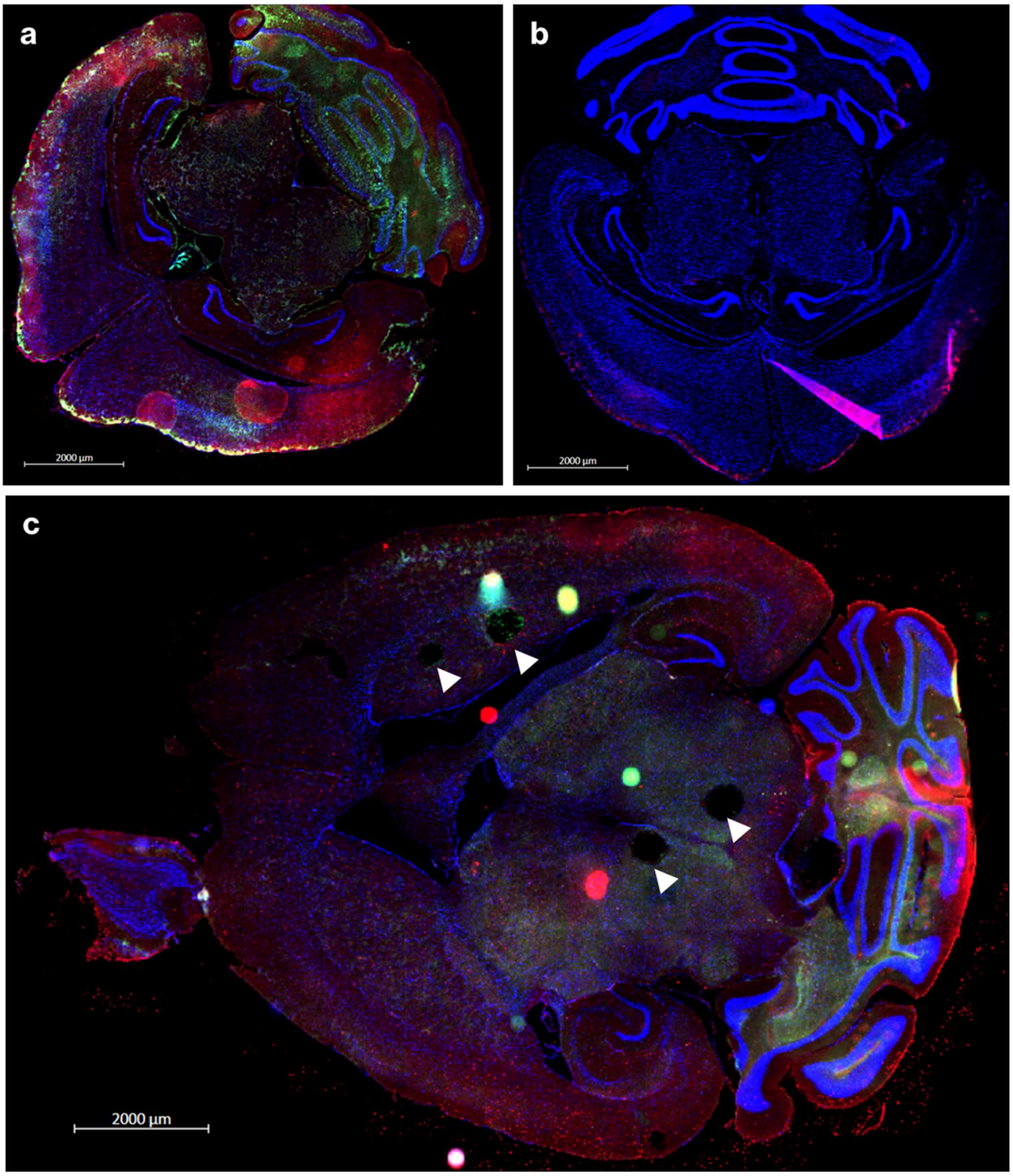


**Figure 3.16. Imaging the fungal infected brain.** Fluorescence imaging of horizontal brain slices from **(a)** uninfected and **(c)** *GFP-C.neoformans* infected mice. GFP fungi are in green, Iba-1 microglia in red and DAPI nuclear staining in blue. **(b)** Iba-1 unstained control from an uninfected mouse. Images taken on the Zeiss Axio Slide Scanner at 20X.

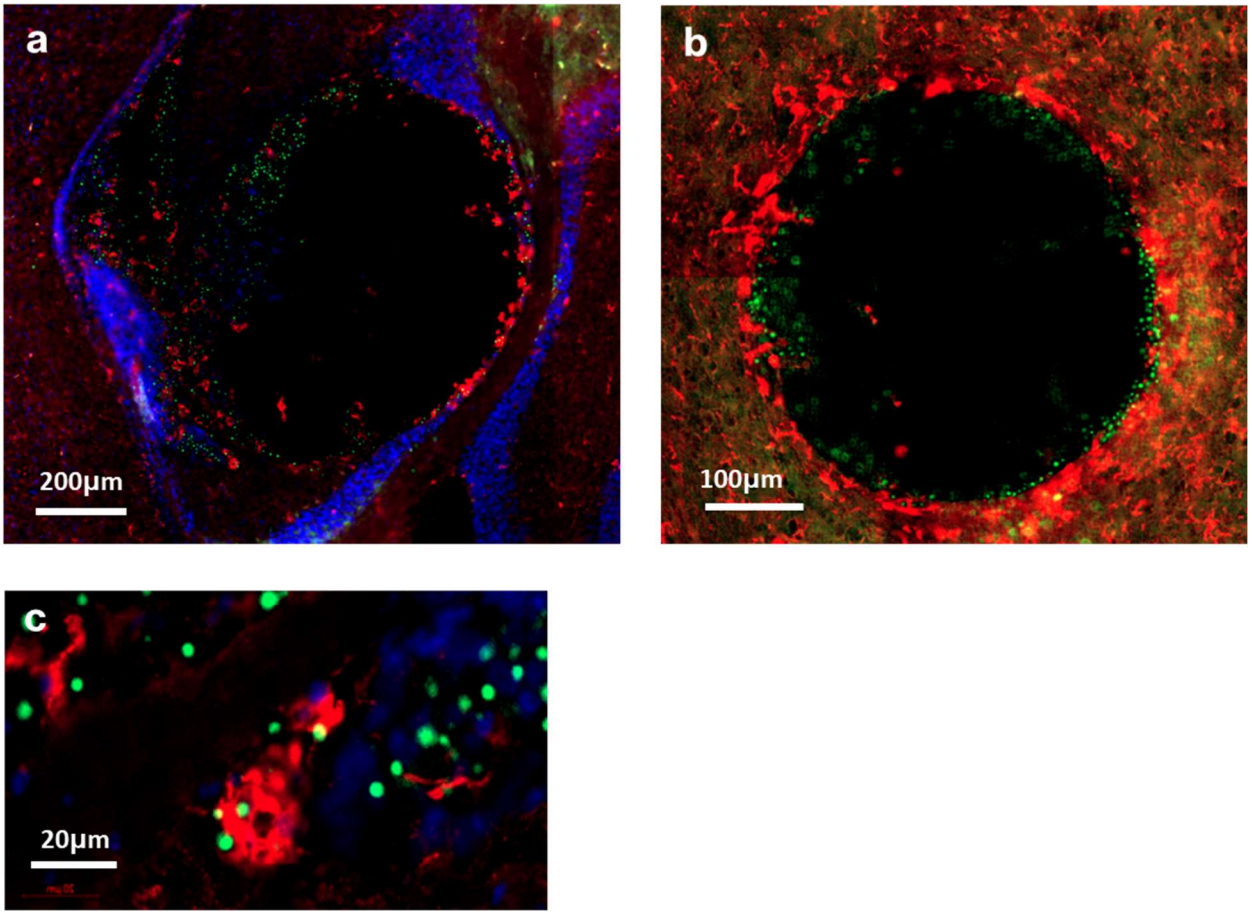


**Figure 3.17. Imaging of intracellular fungi.** Confocal images of brains from GFP-*C. neoformans* mice. GFP fungi are shown in green, Iba-1 microglial staining in red and DAPI nuclear staining in blue. Images taken at **(a) (b)** 25X and **(c)** 40X magnification.

## 3.9 Exploring potential phagocytic receptors expressed by IAMs.

Thus far I have determined that significantly more IAMs are GFP+ than non-IAMs microglia in the context of GFP-*C. neoformans* infection, and fungal viability is increased in IAMs. This raises two possibilities; IAMs are more phagocytic but have poor killing resulting in an intracellular reservoir for the fungi, or phagocytosis is similar across all microglia populations but for IAMs more of the fungi remain viable. I therefore wanted to explore the possible function of two suspected phagocytic receptors expressed by these IAMs, MSR1 and GPR84.

Previous *in vitro* studies have shown that GPR84 is involved in the modulation of pro-inflammatory signalling by macrophages, for example upregulation of TNFα production by LPS-stimulated macrophages[201]. Further work by the Greaves lab (University of Oxford) found that GPR84 expression was increased *in vivo b*y LPS stimulation, and that activating GPR84 *in vitro* upregulated phagocytosis by macrophages[194]. Upregulation of pro-inflammatory signalling by GPR84 occurs through several pathways, including NFκB and the NLRP3 inflammasome[194,197]. Additionally, GPR84 has been shown to be upregulated by microglia during inflammation and may have roles in CNS dysfunction such as chronic pain and multiple sclerosis[198,199]. These studies have been enabled by the agonists and antagonists of GPR84 have been developed, including 6-OAU (6-n-octylaminouracil) and GLPG1205, which have been trialled for the treatment of diseases including atherosclerosis and pulmonary fibrosis. Whilst previous studies have explored the function of GPR84 in the context of bacterial stimuli such as LPS, GPR84 function in the context of a fungal infection has not yet been explored.

MSR1 is also known as CD204 or SR-A1 is part of the class A macrophage scavenger receptor family[200,202]. The ligands MSR1 has been shown to bind are extensive, and include LPS, β-glucans (important components of the fungal cell wall) and viruses, and therefore

MSR1 is important for the immune response to a range of pathogens[202]. In models of Alzheimer's disease, MSR1 has been shown to mediate microglial binding and uptake of β-amyloid, which is beneficial in preventing build-up of β-amyloid and therefore plaque formation, but detrimental in that it drives microglial activation and tissue damage[202]. Work by the May lab has shown that *in vitro C. neoformans* infection of MSR1 knockout cells results in a significant decrease in phagocytosis[200]. They found that TLR4 modulated the expression of MSR1 on the macrophage cell surface, as TLR4 knockout macrophages increase expression of MSR1[200]. Furthermore, they showed MSR1 specifically drove phagocytosis of non-opsonised fungi[200]. Whilst in our experience, efficient microglial uptake of *C. neoformans in vitro* requires opsonisation of the fungus, previous studies have shown that microglia can take up non-opsonised *C. neoformans*[203] and thus the role of MSR1 expression by microglia is therefore an area of interest for further study.

### 3.9.1 GPR84

I began exploring the function of GPR84 in microglia by developing an *in vitro* assay to measure GPR84 expression, as I did not have access to GPR84 knockout mice for *in vivo* studies. I used BV-2 cells, a mouse microglia cell line. I sought to determine whether infecting these cells with *C. neoformans* induced GPR84 gene expression measured by qPCR, and the kinetics of this expression. I found that infecting with *C. neoformans* at CFU $4x10^5$ for 2 hours induced a robust increase in GPR84 gene expression in BV-2 cells (figure 3.18a). Co-stimulation with a range of inflammatory molecules either did not yield as much of an increase, or was too variable, so *C. neoformans* alone was the most effective GPR84 stimulant (figure 3.18b). Using heat-killed *C. neoformans* and the a-capsular mutant strain Δ*cap10* did not result in a significant decrease in GPR84 expression (figure 3.18b), indicating that the upregulation of GPR84 in microglia is not dependent on the fungus being alive or having an intact capsule. As previously described, *in vivo C.*

*neoformans* infection resulted in a significant upregulation of GPR84 in microglia compared to macrophages, and a non-significant increase in the IAMs population (figure 3.12c).

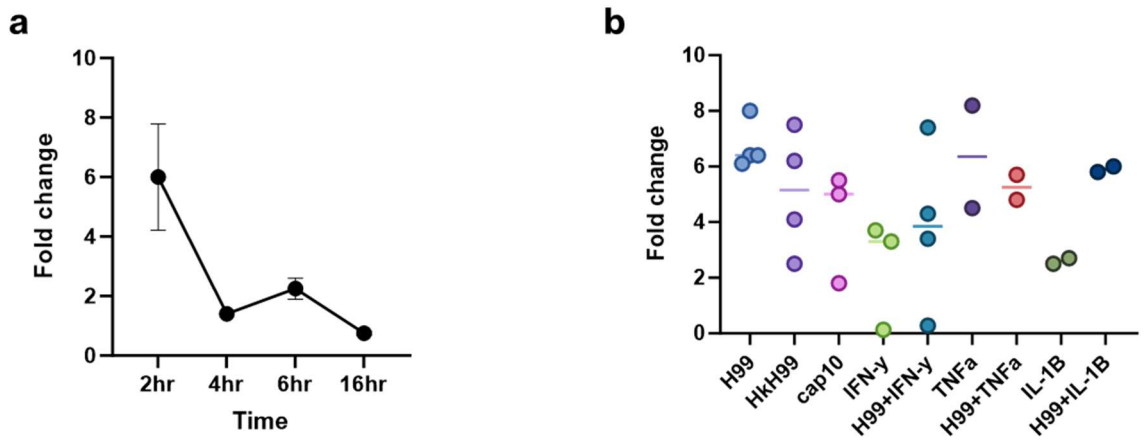


**Figure 3.18. GPR84 expression is upregulated in microglia during *in vitro C. neoformans* infection.** BV-2 cells were plated and infected with *C. neoformans* H99 (H99), heat-killed *C. neoformans* H99 (HkH99) or the a-capsular mutant strain *cap10* (cap10) at a ratio of 1:1 of cells:fungus and analysed by qRT-PCR. The fold change of GPR84 mRNA expression was determined using the comparative CT (2^ΔΔCt) method normalised to the housekeeper GAPDH, relative to the uninfected controls in each experiment. **(a)** The fold change of GPR84 for the indicated time points of infection. Data are plotted as mean ± standard deviation. n=1-5 independent experiments, in which different experiments tested different time points (2hrs n=5, 4hrs n=1, 6hrs n=2, 16hrs n=2). **(b)** The fold change of GPR84 after a 2-hour infection with the indicated strains and stimuli. All cytokine stimulations were performed at 10ng/ml for 2 hours prior to the infection. Each data point represents a single experiment, plotted with the mean per condition, for which the fold change was calculated from 2-3 technical replicates. Statistical analysis using an ordinary one-way ANOVA with multiple comparisons (no significance found).

I then investigated the function of GPR84 in fungal infection, and whether it could be a novel receptor involved in fungal uptake, particularly given the previous literature on GPR84 stimulation upregulating phagocytosis[194]. I developed an *in vitro* assay to measure phagocytosis by BV-2 cells using flow cytometry. I infected BV-2 cells with mCherry-*C. neoformans* and then stained with CFW (calcofluor white), and antibody that binds fungal chitin. BV-2 cells interacting with the fungus were defined as mCherry+, and internalised fungi were defined as CFW- as the antibody cannot access the fungi to stain them if they have been taken up by the cell. Once I optimised the assay, I then applied the GPR84 agonist 6-OAU and the antagonist GLPG1205 to modulate GPR84 activation and determine its effect on phagocytosis, with the view that these could then be applied to studies in mice. I found that 6-OAU induced a subtle increase in mCherry+ BV-2 cells (figure 3.19a), whilst the antagonist trended towards a lower frequency of internalised fungi (figure 3.19b). However, this data was difficult to interpret without effective positive controls.

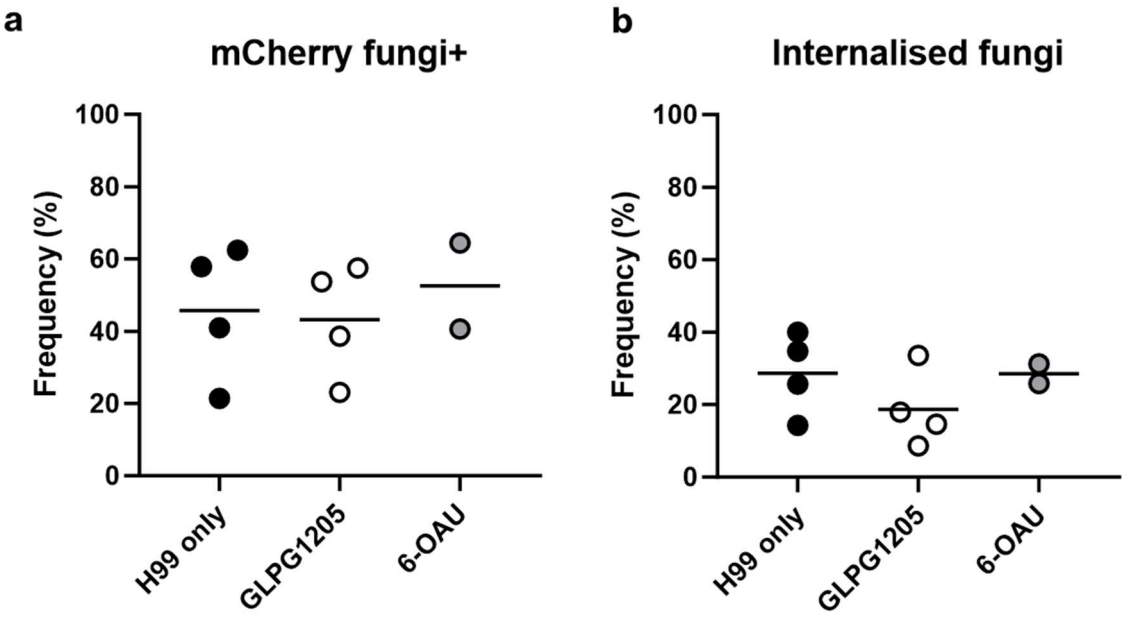


**Figure 3.19. Modulation of GPR84 activation and its effect on *in vitro* phagocytosis of fungi by microglia.** BV-2 cells were plated and infected with mCherry+ *C. neoformans* at a ratio of 5:1 of fungi:cells ($10x10^6$ CFU/ml) for 1 hour. Fungi were opsonised with 10ng/ml GXM antibody prior to infection. The conditions tested were fungi only (H99 only), GPR84 antagonist (GLPG1205) and GPR84 agonist (6-OAU). Flow cytometry analysis was performed and **(a)** the percentage frequency of mCherry+ BV-2 cells and **(b)** the frequency of internalised fungi (mCherry+CFW-) are plotted. Each data point represents the mean of a biological replicate where conditions were tested in duplicate (n=2 technical replicates). N=2-4 biological replicates.

I next wanted to explore whether I could inhibit GPR84 more potently to determine if it is indeed a phagocytic receptor. To do this, I developed an siRNA knockdown of GPR84 expression. Due to the lack of antibodies, I used qRT-PCR to measure the reduction in gene expression. I optimised this assay by testing different concentrations of siRNAs, siRNAs in combination or individually, and different time points. At a 4-hour transfection time point (figure 3.20a), both the siRNA cocktail and siRNA 1 alone induced around 90% downregulation of GPR84 expression. At 18 hours (figure 3.20b) siRNAs 1 or 3 induced a ~95% knockdown in GPR84, whilst at 24 hours (figure 3.20c) the siRNA cocktail induced a 50-90% knockdown and siRNA 1 and 3 a 70-95% knockdown. This data requires further repeats to confirm that the knockdown is significant, however this can then be used for phagocytosis assays as described above to observe the effect on the knockdown on fungal uptake.

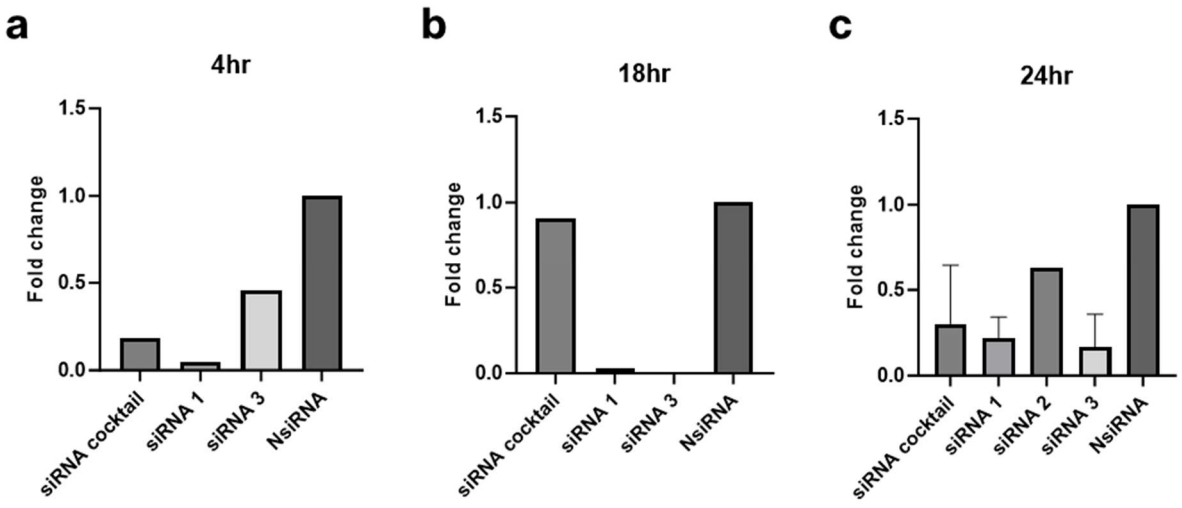


**Figure 3.20. siRNA knockdown of GPR84 *in vitro*.** BV-2 cells were transfected with 30nM of siRNA per condition. 3 siRNAs for GPR84 were tested as a cocktail and individually and incubated for **(a)** 4 hours **(b)** 18 hours and **(c)** 24 hours. Cells were collected and GPR84 gene expression analysed by qRT-PCR, and the fold change calculated using the comparative CT (2^ΔΔCt) method. For each condition, 2-3 technical replicates were plated. The bars on the graph represent the mean from 1-2 experiments ± standard deviation. For each condition, controls transfected with scramble siRNA (NsiRNA).

### 3.9.2 MSR1

I did not have access to the MSR1 knockout mouse line, so I instead used knockout cell lines kindly donated by the May lab from their MSR1 work[200]. I used MPI (Max-Planck Institute) cells from wild-type and SR-A1 (MSR1) knockout mice (see Methods **2.17**). MPI cells are generated by culturing cells from the foetal liver in the presence of GM-CSF results in an immature macrophage-like cell that is capable of self-renewal and thus these cell lines can be generated from knockout mice[139]. For my project I wanted to explore MSR1 function in microglia, and thus began by attempting to differentiate the MPI cells into microglia-like cells using IL-34 and M-CSF stimulation, with GM-CSF stimulated cells to generate macrophages used as controls. Cells were removed from flasks for flow cytometry analysis after an early passage (passage 2 or 3) and after a further two passages (passage 4 or 5). In these experiments I found that beyond passage 5/6, the cells began to die, and the growth rate vastly decreased. Flow cytometry staining for CD45 showed the MFI in the GM-CSF stimulated cells increased at the later passages, but for the M-CSF+IL-34 cells no conclusive result could be obtained (figure 3.21a). In the GM-CSF stimulated cells, the increase in CD45 likely reflected their progressing differentiation into a more mature macrophage cell. There was a slight increase in CX3CR1 in the M-CSF+IL-34 cells indicating a possible change towards a more microglial-like cell (figure 3.21b), however there were no clear changes in the macrophage marker F4/80 (figure 3.21c). Finally, the Ly6C MFI was higher in the M-CSF-IL-34 cells which could indicate differentiation into a monocyte-like cell population (figure 3.21d). Overall, I could not conclusively differentiate the MPI cells into microglial-like cells, so I decided to not pursue further work with these cells including MPI MSR1 knockout cell lines.

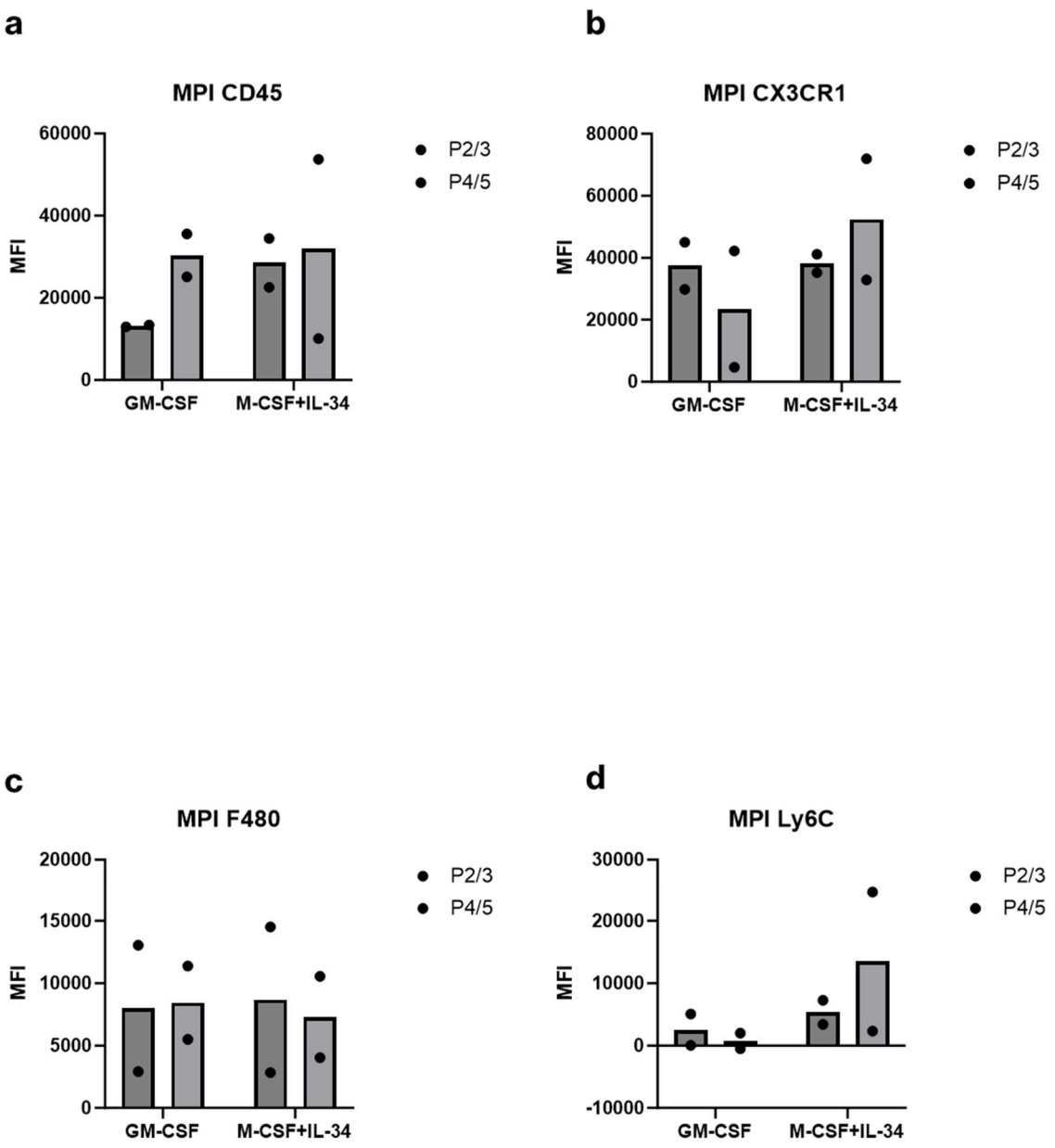


**Figure 3.21. MPI cell differentiation into microglia or macrophages.** MPI cells derived from WT mice were seeded at 1x10$^5$ cells/ml in T75 flasks and stimulated with GM-CSF or M-CSF plus IL-34. Cells were collected at the indicated passage numbers (P=passage) and stained for flow cytometry analysis. The mean fluorescence intensity (MFI) is plotted for **(a)** CD45, **(b)** CX3CR1, **(c)** F4/80 and **(d)** Ly6C. Each data point represents an individual cell flask, and analysis was performed across two independent experiments (n=2).

## 3.10 IAMs are a proliferative microglia population.

In the pathway analysis, the cell cycle was one of the top upregulated pathways in IAMs (figure 3.4a). Microglia proliferation is called microgliosis and contributes towards neurodegeneration in models of Alzheimer's disease[204]. In the context of cryptococcal infection, microglia proliferation has not been studied and is poorly understood. As I had identified a population of microglia that were the main intracellular infection reservoir for the fungus and were also the proliferating population, I decided to further explore the dynamics of microglia proliferation during infection. I used flow cytometry panel and included a stain for Ki67, a marker of cell proliferation, to quantify and measure the dynamics of proliferation of IAMs and other microglia at various time points during infection. The data showed that most of the Ki67+ microglia were IAMs (figure 3.22a) and that the frequency of Ki67+ cells is significantly higher in IAMs compared to other microglia (figure 3.22b), in line with the predictions made by the single cell RNAseq data and pathway analysis. I also performed Annexin V staining, a marker of apoptosis, and found there was no significant increase in apoptotic microglia in the infected mice that could be driving the cell proliferation (figure 3.22c). I next measured Ki67+ microglia over the course of infection, including at day 8/9 (the lethal end point of infection in this model) and compared this to the number of IAMs over the same time course (figure 3.23d and 3.23e). The data shows that microglia proliferation initially increases but increases significantly towards the end of the infection, when disease is most pronounced. The number of IAMs also increased over time (figure 3.22e) albeit was variable between experiments. Taken together, these data show microgliosis occurs in the *C. neoformans* brain occurs in a cell-death independent manner and coincides with the onset of lethal neuroinflammation, and that the main proliferating microglia population is the IAMs.

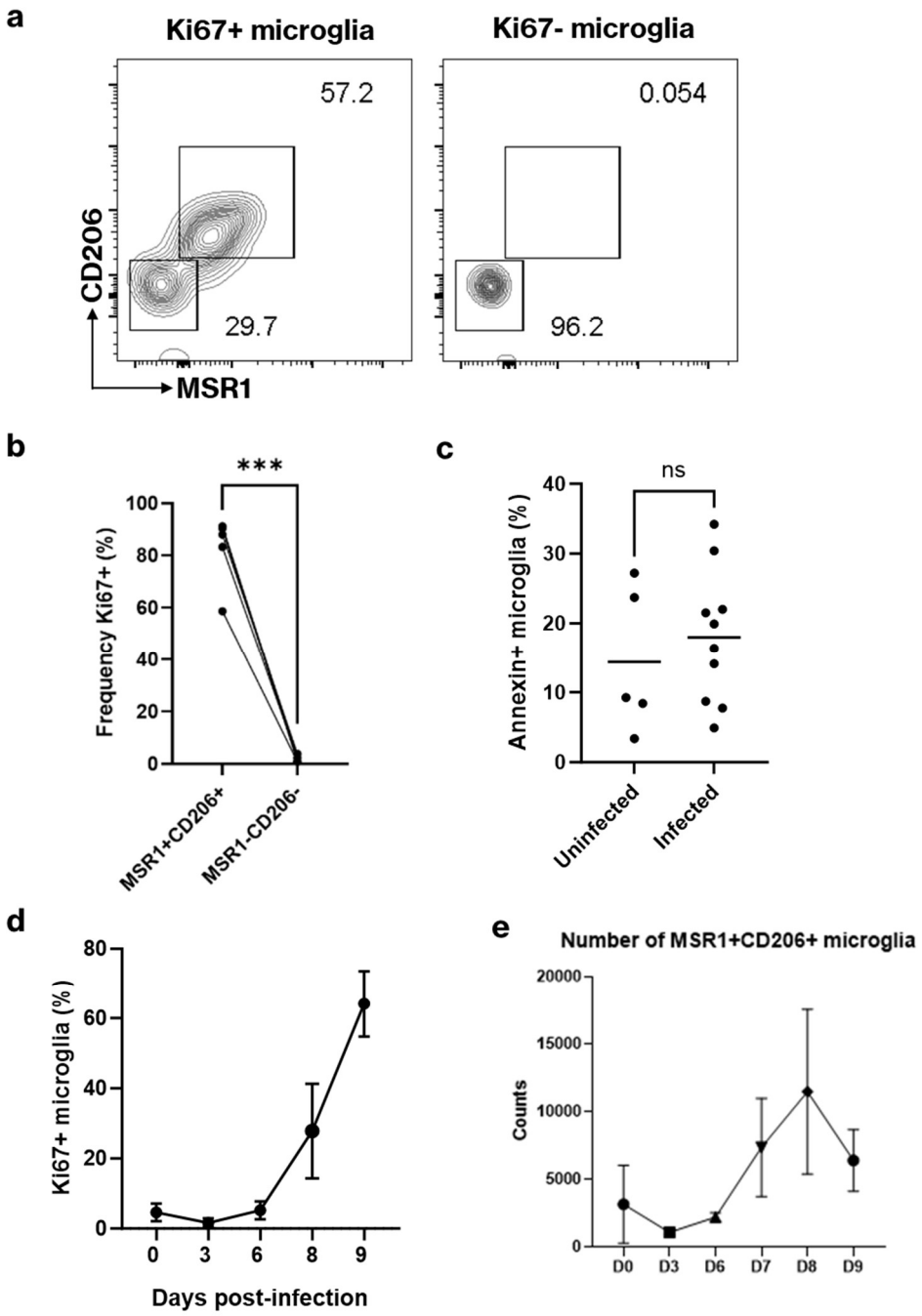


**Figure 3.22. IAMs are a proliferative microglia population. (a)** Representative flow cytometry plots of MSR1 and CD206 staining in Ki67+ versus Ki67- microglia. **(b)** Percentage frequency of Ki67+ cells in IAMs (MSR1+CD206+) and non-IAMs microglia at day 6 post-infection. Paired data points indicate one sample. Statistical analysis by paired t-test. N=6 from three independent experiments. **(c)** Frequency of Annexin+ microglia at day 6 post infection in uninfected and infected samples. n=5 mice for uninfected and n=10 for infected, taken from two independent experiments. Statistical analysis by Student's t-test. **(d)** Percentage frequency of Ki67+ microglia and **(e)** number of IAMs across different time points of infection. Data plotted as mean ± standard deviation. N=3-8 samples per time point from 4 independent experiments.

## 3.11 Lymphocytes drive IAMs proliferation and recruitment of inflammatory monocytes during *C. neoformans* infection.

I next wanted to explore the mechanisms that drove IAMs generation, proliferation and the uptake of fungi by these cells. Since IAMs appear late in infection, this coincides with the arrival of CD4 T cells into the *C. neoformans* infected brain, and work by the Drummond lab has shown that CD4 T cells are the main source of IFN-γ which I know from the RNA-seq data is involved in IAMs signalling. We used $Rag2^{-/-}$ mice which lack lymphocytes and therefore CD4 T cells. I first quantified the number of all microglia in the brains of wild-type and $Rag2^{-/-}$ mice in uninfected and day 6 post-infection brains and found there were no significant changes in the overall microglia numbers (figure 3.23a). This showed that the $Rag2^{-/-}$ mice did not have alterations in the tissue-resident macrophage populations under homeostatic conditions which could have implications for interpreting microglia populations in the infected conditions. Quantification of IAMs at day 6 post-infection also showed no significant differences in numbers between the wild-type and $Rag2^{-/-}$ mice (figure 3.23b). However, when I performed the same analysis at day 8 post-infection, the expansion of IAMs seen in the wild-type mice did not occur in the $Rag2^{-/-}$ mice (figure 3.23c). I then performed Ki67 analysis and found that in the $Rag2^{-/-}$ mice the expansion of microglia at day 8 post-infection did not occur (figure 3.23d). Analysis to characterise other myeloid populations in the $Rag2^{-/-}$ mice revealed that recruitment of these cells to the brain was reduced, particularly in the case of inflammatory monocytes (figure 3.23e). Finally, the frequency of GFP-*C.neoformans*+ monocytes, macrophages and IAMs was significantly reduced in the $Rag2^{-/-}$ mice, indicating a loss of the intracellular fungal reservoir. These data show that lymphocytes are important for recruitment of myeloid cells to the brain in *C. neoformans* infection, which is somewhat surprising given that we would normally expect innate immune cells to arrive first before the induction of adaptive responses. Whilst the removal of lymphocytes may benefit the host immune

response by reducing microgliosis-driven neuroinflammation and the intracellular niche for the fungi to escape the immune system, this could be due to a broad range of effects. For example, $Rag2^{-/-}$ mice lack B cells and therefore antibody opsonisation of fungi for uptake would not occur in these mice.

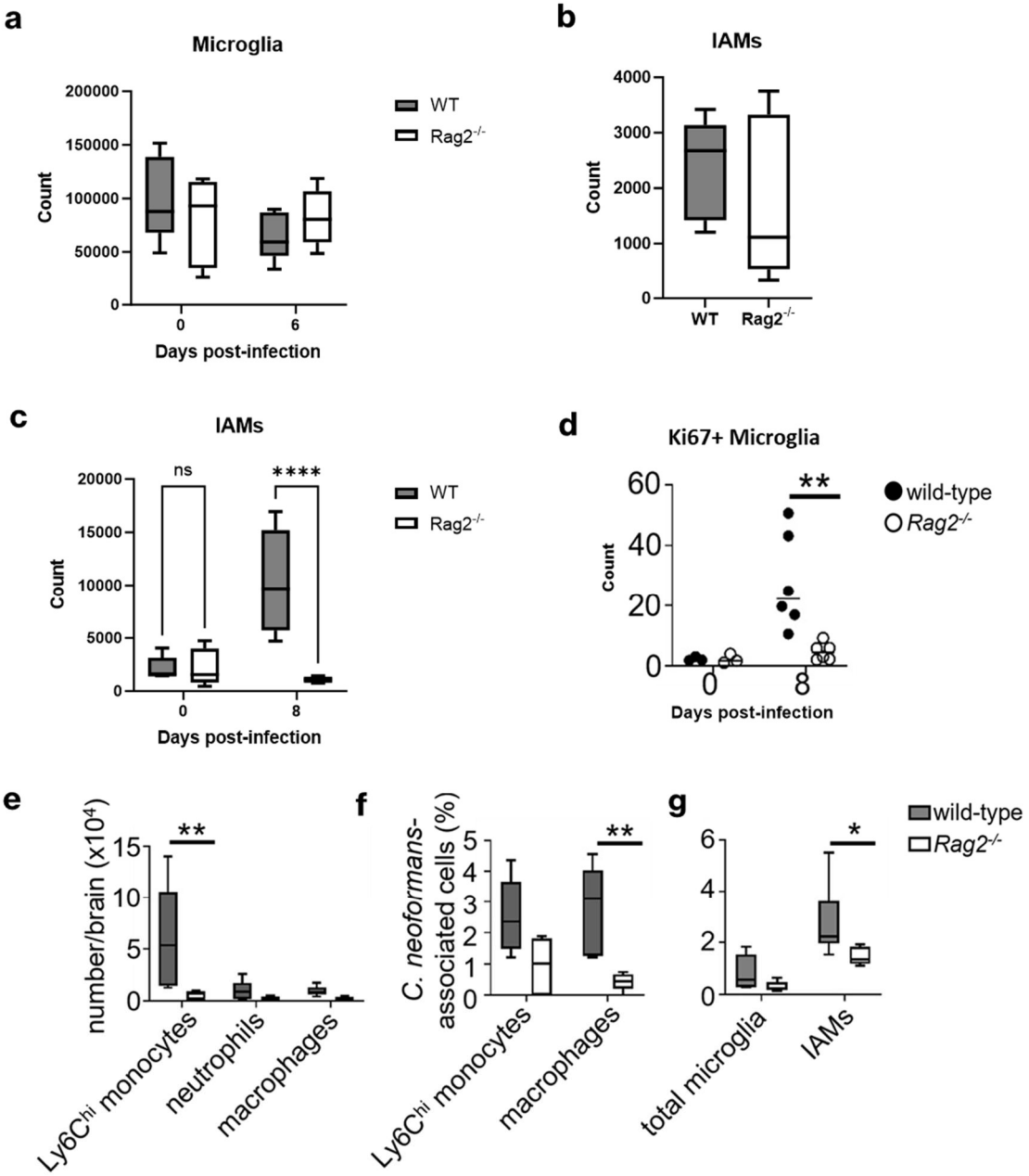


**Figure 3.23. In lymphocyte deficient mice, the dynamics of myeloid cell recruitment and IAMs expansion is altered. (a)** Counts analysis of all microglia and **(b)** IAMs at day 0 and 6 post-infection in wild-type (WT) and Rag2-/- mice. **(c)** IAMs counts at day 0 and day 8 post-infection in WT and Rag2-/- mice. **(d)** Number of Ki67+ microglia at day 0 and day 8 post-infection in WT and Rag2-/- mice. **(e)** Counts of monocytes, neutrophils and macrophages at day 6 post-infection in WT and Rag2-/- mice. **(f)** Frequency of monocytes and macrophages and **(g)** IAMs that are GFP+ from mice infected with *GFP-C. neoformans* for 7 days. Data are plotted in a box-and-whisker plots or scatter plots. In each plot there are n=5 mice per condition, taken from two independent experiments. Statistical analysis is two-way ANOVA.

## 3.12 Discussion

In this chapter I identified and characterised a population of inflammatory microglia that harboured live fungi and proliferated during infection, particularly towards the end stages of disease. Two previous studies have shown that using LPS challenge, a model for bacterial infection, also induces a subset of inflammatory microglia[188,189]. In the first study[188] the authors injected mice with LPS and collected brains 24 hours later, and like our study they first FACS sorted their samples before single cell RNA-seq analysis, however they sorted on CD11b+CD45$^{int}$ microglia only, whereas we analysed all CD11b+CD45 cells. In line with our data, they showed a downregulation of microglia homeostasis genes in their LPS-treated microglia compared to saline controls, including *Tmem119*, *Gpr34* and *P2ry12*[188]. They also identified several inflammatory genes upregulated in the LPS-stimulated microglia, which akin to our IAMs included *Gpr84* and *Msr1* [188]. Whilst in this chapter I have shown these receptors are also expressed by microglia in a fungal infection context, more work is needed to understand their function in microglia specifically.

The authors further analysed their LPS-stimulated microglia and identified a small subset (defined as “subset-LPS”) with higher expression of homeostatic genes and lower expression of pro-inflammatory genes, including those associated with antigen presentation and the complement pathway[188]. They performed pseudo time modelling of their data and found that inflammatory markers were upregulated prior to the downregulation of homeostatic markers, and that the subset-LPS were likely cells in an intermediate state between the unstimulated and LPS-stimulated microglia[188]. In contrast, our RNA-seq analysis indicates that IAMs are a defined subpopulation. Whilst graph-based clustering analysis showed multiple microglial clusters, for most of these we did

not find a biological reason to define them as separate clusters, and have been careful not to over-interpret our data.

Another study used primary microglia stimulated with LPS or LPS and IFN-γ for 6 hours prior to bulk RNA-seq analysis[189]. They found that there were differences between the two treatment conditions, for example in the LPS only stimulated microglia they found increased expression of the phagocytic receptor Trem1 and pro-inflammatory cytokines and markers of cell proliferation, whilst the LPS+INF-γ microglia downregulated these genes and instead upregulated pathways such as oxidative phosphorylation[189]. Both LPS studies compared their results to published DAM gene signatures and found both unique and overlapping features[188,189]. In comparison to our IAMs data, DAMs similarly downregulate homeostatic genes such as *Cx3CR1*, however for others, particularly *Trem2*, these are highly upregulated in DAMs[187]. In terms of inflammatory markers, a similar pattern is seen, whereby overlapping upregulated genes include *ApoE* and *Cd11c*, whilst genes such as *Mrc1* are uniquely expressed in IAMs [187]. Imaging analysis of DAMs shows they localise to Aβ plaques [187] which aligns with our imaging data showing activated microglia at the site of fungal lesions. It can therefore be argued that both DAMs and IAMs provide evidence of microglial capacity to localise to the site of the inflammatory insult and perform phagocytosis. Unfortunately, this does not necessarily benefit the host, as Aβ uptake can drive harmful neuroinflammation, and in our work fungal uptake by IAMs seems to allow the establishment of a fungal niche, likely reflecting the evolution of survival strategies by *C. neoformans.*

As previously discussed, evidence from pulmonary *C. neoformans* infection has shown that interstitial macrophages provide an intracellular niche for the fungus, driven by fungal secretion of CLP1 which polarises these macrophages to an M2-like phenotype[136]. This polarisation increases Arginase expression, which is known to downregulate phagocytic

killing. In macrophages, the metabolism of arginine can occur through Arginase or iNOS (inducible nitric oxide synthase), the latter generating NO (nitric oxide) which can then be converted into ROS (reactive oxygen species) that enable pathogen killing in the phagocytic compartment[205]. Previous work by our lab has shown that *C. neoformans* uptake and survival inside microglia benefits the fungus by providing access to copper, a nutrient that is otherwise in short supply in the brain[135]. The IAMs therefore likely represent the main target of the fungus for uptake and survival given that we have found arginase expression is increased in this population.

Despite the increased arginase expression in IAMs, our initial hypothesis based on the RNA-seq and fungal uptake data was that this population would have a higher killing capacity than other microglia. This is due to the increased expression of genes regulated by IFN-γ in the IAMs population, which are typically associated with an M1-like phenotype of macrophages and enhanced killing[56]. Numerous studies have shown the importance of IFN-γ-regulated GTPases – which include guanylate-binding proteins (GBPs) and immunity-related GTPases (IRGs) – in the host immune response viral, bacterial and parasitic pathogens[206–209]. When pathogens such as *Toxoplamsa gondii* infects and enters the cell through vacuoles, GBPs and IRGs bind the vacuole and target it for degradation, resulting in the release of the pathogen into the cytosol which can again be bound by GTPases resulting in inflammasome activation and death of the infected cell [206–209]. It was therefore surprising that despite the upregulation of several IFN-regulated GTPases in the RNA-seq data for the IAMs population, our functional assays showed decreased fungal killing and no significant increase in apoptosis.

There have been clinical trials testing IFN-γ as a therapy for cryptococcal meningitis[210], as a major risk factor is defective T cell responses (i.e. HIV/AIDS patients) and IFNγ-driven Th1 responses are thought to be protective. However, our data indicates that IFN-γ

signalling is important for establishing the IAMs population, and therefore IFN-γ treatment could drive the establishment of a fungal intracellular niche. This is further shown by our Rag2$^{-/-}$ data which removed lymphocytes and therefore the main source of IFN-γ in the brain, CD4 T cells. Whilst further work is needed using models that more specifically remove these cells, such as treating mice with a CD4-depleting antibody, our data has interesting implications for CM patients with HIV/AIDS. HIV causes dysfunctional CD4 T cells, so it is possible that in these patients intracellular survival of the fungus in microglia is not as much of an issue, and instead treatment would need to target extracellular fungi. However, our Rag2$^{-/-}$ also showed a reduction in the recruitment of monocytes to the brain, so we cannot conclusively say whether the subsequent reduction in IAMs proliferation and fungal uptake is a direct effect of the lymphocyte removal or an indirect effect through loss of inflammatory myeloid cells. A similar study by the Olszewski lab[173] showed depletion of CD4 T cells in mice infected retro-orbitally with *C. neoformans* strain 52D showed reduced IFNγ production and accumulation of inflammatory myeloid cells resulting in increased survival despite fungal clearance being impaired. CCR2 knockout mice which lack monocytes showed reduced inflammatory monocyte accumulation in the brain during *C. neoformans* infection, and this was associated with improved disease outcomes by reducing neuroinflammation[211]. Interestingly, CCR2 knockout mice showed increased arginase and reduced iNOS expression by microglia, implying that monocyte recruitment is important for inducing microglia phagocytic killing, and in fact in their knockout mice fungal burdens increased despite the reduction in inflammation [211]. This potentially supports the hypothesis that based on our IAMs data where in the Rag2$^{-/-}$ microglia proliferation at late infection is reduced, along with the number of IAMs, that monocyte recruitment is required for the microgliosis and expansion of IAMs that coincides with lethal neuroinflammation.

The CCR2KO study does however differ to our work in the method of modelling CM in that they used a retro-orbital intravenous injection route and a less virulent strain of *C. neoformans*, 52D, meaning their time course of infection was much longer than ours. In fact, it is important to note that a limitation of our IAMs work is that I did not test other infection routes. *C. neoformans* infection intranasally is the main other infection route used to model cryptococcosis, which is arguably more clinically relevant as *C. neoformans* infects humans through inhalation of fungal spores. This model allows a longer time course of infection – up to 30 days – however dissemination to the brain is not as efficient and reliable. It is possible that mice that do develop cryptococcal meningitis from intranasal infection would also have IAMs, although perhaps this population would be smaller given the reduced exposure to the fungus. This model could also generate different microglial populations given that entry of the fungus into the brain could occur through the olfactory bulb. Olfactory bulb microglia are a population of increasing research interest in the context of airway infections, for example a recent study showed these microglia were central in driving protective T cell responses to restrict viral infection[212]. There is still more work to be done to understand the mechanisms of *C. neoformans* entry into the brain, and therefore how different infection models may affect outcome.

Another factor to consider when modelling cryptococcal meningitis is the strain of fungus used. In this study we used *C. neoformans* H99 which is a highly virulent strain. I have previously discussed models that utilise strain 52D, however there are also other clinical isolate models such as strain 1841 which has been used to model C-IRIS[213]. C-IRIS has been modelled *in vivo* using lymphocyte deficient mouse strains, such as $Rag^{-/-}$, then adoptively transferring CD4 T cells into the mice[214]. In the 1841 study, the authors found that induction of C-IRIS *in vivo* did not require IFN-γ signalling by CD4 T cells, however in another model using *C. neoformans* H99 it was found that mice adoptively transferred

with CD4 T cells from IFNγ$^{-/-}$ mice had improved disease outcome, indicating Th1 responses were key drivers of disease[215]. Both strains were originally isolated from patients, therefore variations in *C. neoformans* in the environment could potentially lead to different patient outcomes. Future work for this project could therefore be to test if IAMs are generated with different *C. neoformans* strains as this could have significant clinical implications.

In this chapter, I have begun to examine the mechanisms by which microglia may phagocytose fungi. This is an area that needs further investigation, although previous studies have implicated GPCRs such as GPR34 and opsonisation of fungi, for example by complement proteins, as important factors in cryptococcal uptake[172]. In this chapter, I have explored the role of MSR1 and GPR84 in fungal uptake of microglia. Important future experiments would be to use GPR84 and/or MSR1 knockout mice to determine if there is a phenotype in these mice when infected with *C. neoformans*, which could therefore guide functional studies. If I had been able to obtain these mice during my PhD, I would have performed similar flow cytometry analysis to determine if IAMs were also present in these mice, and importantly I would use GFP-*C. neoformans* infection to determine any differences in fungal uptake and viability.

In summary, in this chapter, I have used genomics analysis to determine that microglial responses in cryptococcal meningitis are critically delayed. I identified a context-specific subset or activation state of microglia which is highly proliferative, phagocytic but does not effectively kill the fungus enabling its survival.

# Chapter 4: Exploring meningeal inflammation in cryptococcal infection.

## 4.1 Introduction

### 4.1.1 Immunity at the brain borders

Whilst the discovery of the blood-brain barrier (BBB) was initially interpreted as evidence for the brain being an immune privileged organ, we now understand that the BBB is just one of the anatomical locations where neuroimmune interactions take place in health and disease (figure 4.1)[216,217]. Beginning at the skull, the bone marrow has been shown to be connected to the meninges and the brain through specialised channels. Recent work has shown that there is bi-directional traffic in these channels, allowing the movement of CSF, blood and pathogens between the skull bone marrow to the meninges and then to the brain[218–221]. Furthermore, the skull bone marrow can provide a local source of leukocytes such as monocytes and neutrophils to the brain[218–221].

The meninges are the protective layer that surrounds the brain and spinal cord and sit just under the skull bone (figure 4.1). They are composed of an outer dura mater layer that is connected to the skull, the subarachnoid space which contains much of the meningeal vasculature and the CSF, and the innermost layer, the pia mater which sits directly on the brain parenchyma. Importantly, recent advances in our understanding of the meninges lead to the discovery of lymphatic vessels within this tissue[222]. This, along with the discovery of resident T cells in the brain[223], demonstrated that the brain has lymphatic drainage and therefore is not “immune privileged”. Further studies have since explored the lymphoid cells present under different inflammatory conditions such as autoimmunity and infection, and that lymphatic drainage from meningeal vasculature connects the brain

with the cervical lymph nodes[217]. The meninges vasculature and tissue also contain resident and circulating myeloid cells which can interact with the brain parenchyma. Additional barriers exist in the perivascular spaces, which are spaces that surround the brain vasculature containing CSF and resident macrophages, and in the choroid plexus, which surrounds the inner brain ventricles[216,217]. The choroid plexus is largely composed of epithelium and connective tissue allowing for crosstalk between resident immune cells and the circulation [216,217]. There are therefore many highly specialised borders within the CNS, and understanding how pathogens such as fungi can overcome these borders and enter the brain could generate treatment strategies whereby entry into the CNS is prevented.

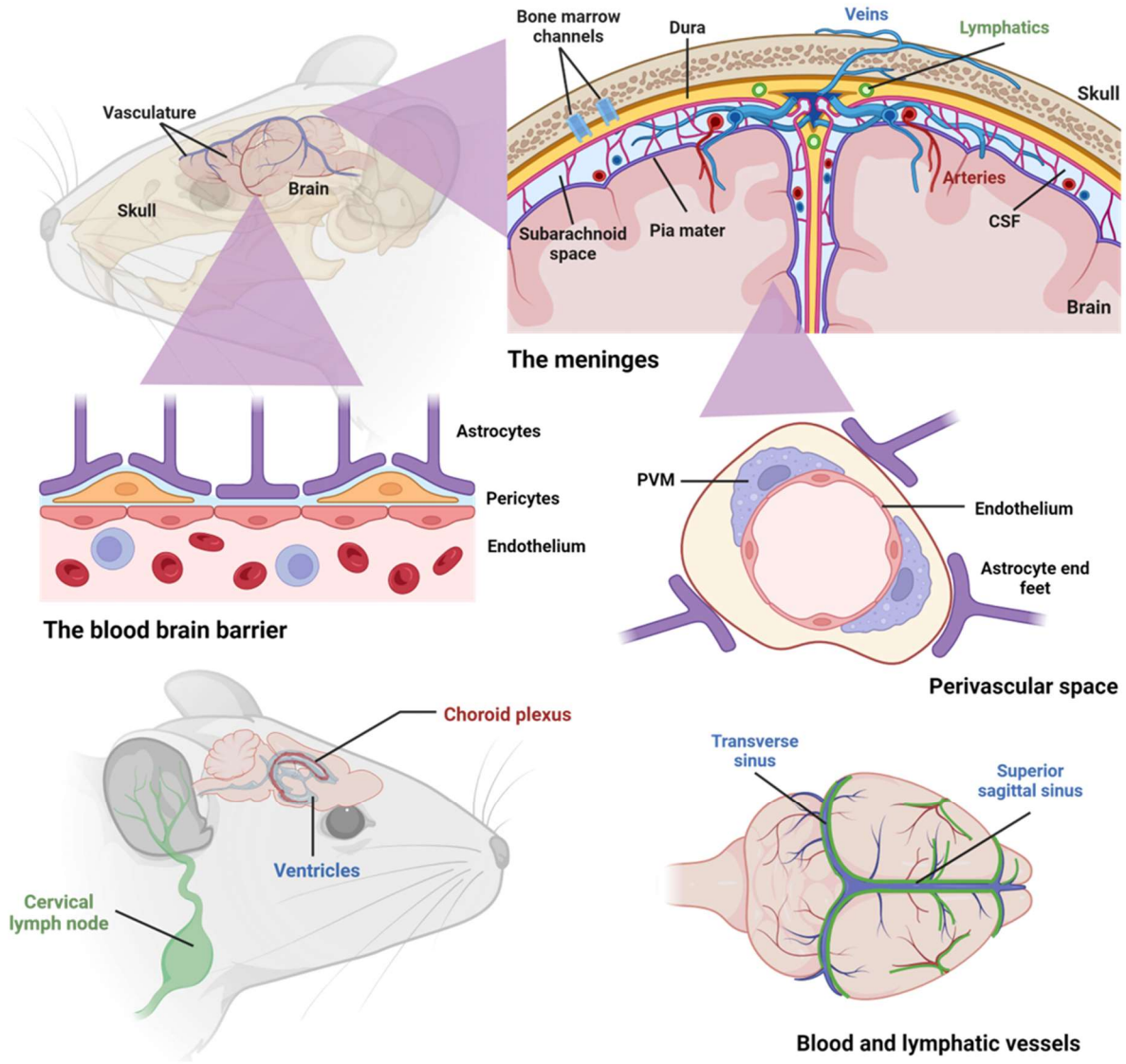


**Figure 4.1. The brain borders.** The meninges are the protective layer that surrounds the brain and spinal cord and sits between the brain and skull bone. It is composed of three layers. The dura mater is the outermost layer located just below the skull that is largely composed of fibroblasts and connective tissue. The subarachnoid space is the middle layer that contains cerebral spinal fluid and extensive vasculature. The pia mater sits just on top of the brain parenchyma. The skull bone marrow is connected to the meninges through specialised channels. The brain vasculature includes veins that surround the skull that connect down into the meninges and the brain, arteries and lymphatic vessels. The major veins of the meninges are the dural venous sinuses, which are composed of the transverse sinus and superior sagittal sinus. The lymphatic vessels sit adjacent to the veins and arteries, and lymphatic drainage from the brain occurs at the cervical lymph nodes. . The brain vascular endothelium is surrounded by pericytes and astrocytes which make up the blood-brain barrier. Perivascular spaces are found along the blood vessels of the brain, where perivascular macrophages (PVM) surround the blood vessels. Astrocytes in the brain connect to the outside of these perivascular spaces. The ventricles are located within the brain. These cavities where the cerebrospinal fluid is produced contain the choroid plexus vasculature.

### 4.1.2 The brain borders and cryptococcal meningitis

Despite the anatomical relevance of the meninges in cryptococcal meningitis, most studies into the immune mechanisms of the disease have largely focused on the brain parenchyma. Nevertheless, recent advancements in microscopy techniques have enabled researchers to begin to understand how *C. neoformans* crosses the brain borders to enter the brain.

Three mechanisms have been suggested for how *C. neoformans* can cross the BBB. The first is that *C. neoformans* crosses the vascular endothelium at the BBB by transcytosis through endothelial cells. Evidence for this mechanism include *in vitro* studies using human brain endothelial cells where *C. neoformans* has been shown to adhere and enter these cells, drive cellular reorganization such as changes in the actin cytoskeleton, and is able to cross a cell monolayer[224–226]. It has been further shown that this process can occur without damaging the tight junctions in the model BBB, thus the fungus arguably crosses through the cells rather than in between them[227]. There is little *in vivo d*ata to support this mechanism, however one study showed purified brain vascular endothelial cells from infected mice contained *C. neoformans* fungi, and the extent of uptake increased with a more virulent *C. neoformans* strain[228].

The second mechanism of *C. neoformans* invasion is the “Trojan horse” hypothesis, which is that the fungus is phagocytosed, mainly by monocytes, that then cross the BBB, after which *C. neoformans* escapes into the brain[226,229–231]. This has been demonstrated using *in vitro* models of the brain vascular borders to show that macrophages/monocytes containing fungi are able to cross the model barrier[226,231]. *In vivo* evidence for this mechanism comes from studies where monocyte depletion reduces brain fungal burden, and through imaging of the perivascular spaces which *C. neoformans* containing cells in this location, most of which were monocytes[226,229,230]. The latter study also showed

extensive invasion and proliferation by *C. neoformans* in the subarachnoid layer of the meninges[230]. A similar mechanism has been proposed whereby monocytes containing fungi arrive at the brain borders and laterally transfer the fungi to endothelial cells[226]. This could provide a model of *C. neoformans* brain invasion through a combination of Trojan horse and transcytosis. The *C. neoformans* containing cells in the perivascular spaces also included neutrophils, which have been shown to be able to take up *C. neoformans* and release it at the BBB in a non-apoptotic manner[232]. In contrast to monocytes, neutrophil depletion has been shown to increase brain fungal burden[233]. Intravital imaging has shown that neutrophils are able to enter the brain microvasculature and take up *C. neoformans* prior to re-entering the peripheral circulation, demonstrating a mechanism for fungal removal from the brain[233].

The third mechanism is through paracellular crossing, whereby *C. neoformans* can cross the BBB due to barrier damage such as deterioration of tight junctions[226]. Intravital imaging studies have shown *C. neoformans* entering the brain vasculature and travelling through down to the small capillaries, where the fungus becomes arrested before traversing the capillary endothelium to enter the brain tissue[234,235]. This process was found to be dependent on fungal expression of the urease enzyme, which has been shown to be important for *C. neoformans* virulence[234,236]. It has been suggested that production of toxic ammonia by urease activity, along with other fungal secreted virulence factors, drives damage of the endothelium thus enabling the fungus to exit the blood vessels and disseminate[226,234,235]. Another study using a zebrafish model also found *C. neoformans* arrests in brain vasculature, after which the fungus proliferates extensively causing dilation of the blood vessels and vascular occlusion[237]. This causes vascular endothelial damage and bleeding, which enables further dissemination of the fungus [237].

Further studies using zebrafish, which enable high resolution imaging due to the transparent nature of the organism, have demonstrated a complex mechanism for *C. neoformans* crossing the brain borders which likely involves all three of the mechanisms described above. These studies have shown that fungi arrive in the vasculature and interact with endothelial cells which can result in uptake and persistence within endothelial cells or transcytosis[238,239]. The fungal-endothelial interactions then likely drive recruitment and activation of phagocytes including inflammatory macrophages and neutrophils, but also activation of microglia adjacent to the blood vessels [238,239]. This results in fungal uptake by these cells, which can then either promote crossing of BBB inside the phagocytes or removal of fungi from the vasculature depending on the specific cell type that takes up the fungus, for example uptake by neutrophils is more likely to drive clearance [238,239]. This process could prevent loss of vascular integrity (for example, microglia removal of fungi from the vasculature could prevent the proliferation of fungi and subsequent vascular damage) or, if the recruited phagocytes remove infected endothelial cells, then this would disrupt the barrier [238,239]. Further work is needed to establish whether this model is replicated in mice and humans. Furthermore, the current literature often focuses on general models of the brain vasculature rather than specific anatomical borders such as the meninges.

### 4.1.3 Platelets in anti-fungal immunity

Whilst studies on CNS invasion in cryptococcal meningitis have implicated vascular damage, the response to this vascular damage has not been explored. Platelets are short-lived anucleate blood cells with a significant role in preventing bleeding when vascular damage occurs[240]. Platelets are recruited to the site of damage upon which they are activated, adhere to the endothelium, and recruit more platelets to adhere thus forming a clot to prevent bleeding [240]. Furthermore, activated platelets release an array of cytokines

and chemokines through their α-granules, including platelet factor 4 (PF4), RANTES and IL-1β, which recruit and activate immune cells. Activated platelets also express specific surface receptors including P-selectin, CD40L and GPIb which enable their interaction with leukocytes[241,242].

The role of platelets in fungal infection has not been extensively explored. Patient risk factors for fungal infection, such as leukaemia and organ transplantation, are also associated with thrombocytopenia (low blood platelet count), which could be argued as indirect evidence of platelet dysfunction increasing the risk of invasive fungal infection[243,244]. An i*n vitro* study showed Thrombocidin-1, a component of human platelet α-granules, has a potent antifungal effect against *C. neoformans*, therefore platelets may have direct fungicidal capabilities[245]. The receptors that could mediate direct interactions between fungi and platelets are still poorly understood. An *in vitro* study showed that *Mucor circinelloides* potently induced platelet aggregation and activation, mediated by recognition through GPIIb/IIIa and the platelet Fc receptor FcγRIIA[246]. Furthermore, platelets can activate complement via P-selectin which enhances fungal clearance by driving opsonisation and phagocytosis[247,248]. However, excessive complement activation has been associated with pathologic thrombosis and infarction, serious complications that have been observed in patients with angioinvasive fungal infections such as mucormycosis and aspergillosis, particularly those with CNS involvement [249,250].

In addition to direct fungicidal functions, platelets may mediate fungal killing indirectly via the recruitment of phagocytes. For example, neutrophils are strongly attracted to thrombi formed *in vitro* with *A. fumigatus* conidia and human whole blood [251]. Platelet/macrophage interactions can also boost antimicrobial immunity. For example, CLEC-2/podoplanin interactions, which mediate platelet-macrophage binding, has been shown to be protective since CLEC-2$^{-/-}$ mice have excessive inflammation and increased mortality

following the induction of bacterial sepsis[252]. Indeed, GP1b/Mac-1 (CR3/complement receptor 3) interactions between platelets and macrophages can help drive an M1 phenotype which helps to promote bacterial clearance[253]. Further research is needed to establish whether similar interactions occur during fungal infection and what effect they exert on disease outcome. Furthermore, studies involving *C. neoformans* are limited, and the role of platelets in a model of cryptococcal meningitis has not previously been explored.

In this chapter, I aimed to examine the inflammatory response in the meninges following *C. neoformans* infection using RNA sequencing and imaging analysis, with a particular focus on the role of platelets and blood vessel integrity.

# Results

## 4.2 Characterising the kinetics of the meningeal immune response during cryptococcal meningitis using RNA sequencing

To broadly investigate the inflammatory response in the meninges using our *in vivo* CM model, I first performed bulk RNA sequencing analysis to determine which genes and pathways changed during infection over early and late time points. I collected meninges from mice at day 3, 6 and 8/9 post-infection, along with uninfected controls, and processed the samples to extract RNA for sequencing. Once sequencing was performed, I used the data for analysis in R (see Methods **2.23** for further detail). I first analysed the broad changes across the different time point samples using a PCA (principal component analysis) plot (figure 4.2). A PCA plot allowed me to visualise how similar the samples were by how closely they clustered together. My results show that the day 3 post-infection samples and the uninfected controls samples clustered closely, indicating that very few changes in gene expression occurred between these two time points (figure 4.2a). I confirmed this by quantifying the gene changes between uninfected and day 3 samples, which found 1 gene increased in expression (*Gm8292*), and 15 genes were downregulated (including *Mis18bp1, Atp1a3, Snord13*).

In contrast, the day 6 samples clustered away from the day 3 and uninfected samples, showing that changes in gene expression did occur in these samples (figure 4.2a). When comparing the uninfected and day 6 samples, I found 1524 genes where the log fold change increased, and 1084 genes where it had decreased. From this point forward, I decided not to perform further analysis on the day 3 samples as there were no significant changes. The PCA plot further showed that the day 8 and day 9 samples also clustered away from the uninfected samples but also the day 6 samples (figure 4.2a). The day 8 and

9 samples clustered very closely, so I redefined all these samples as a single 'late infection' group and re-plotted the PCA (figure 4.2b). A total of 3333 genes were upregulated and 3438 genes downregulated in the late infection samples compared to uninfected controls, whilst between the day 6 and late infection samples, 1956 were upregulated and 2148 downregulated. Overall, these data show that during early *C. neoformans* infection there are no genetic changes in the meninges, however by day 6 there are extensive changes, and this trend continues into late infection at day 8/9.

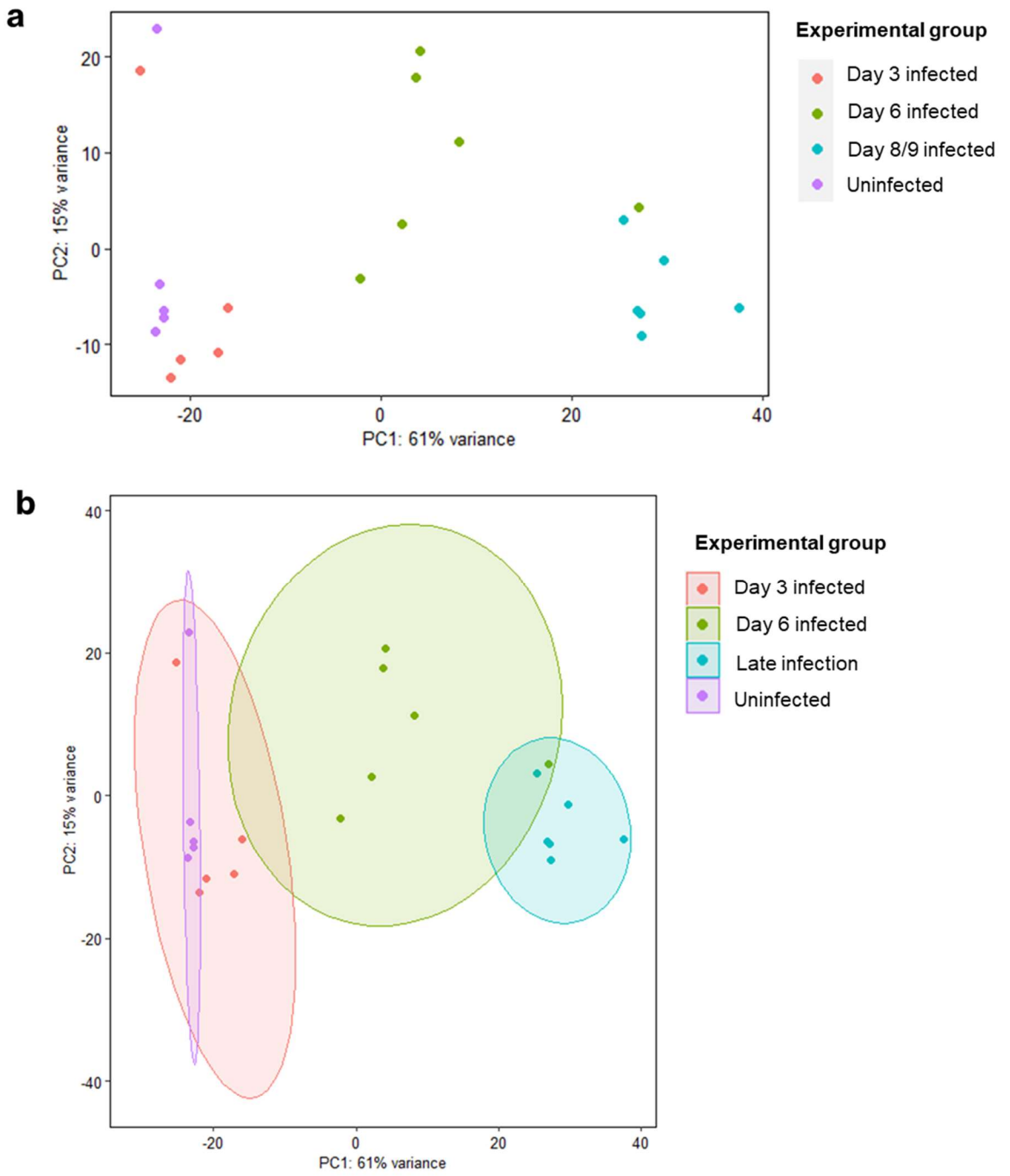


**Figure 4.2. PCA plot of bulk RNA-seq of the meninges from *in vivo* cryptococcal meningitis samples.** RNA-seq analysis was performed on the meninges of mice infected with *C. neoformans* using the intravenous route. Tissue was collected at day 3, 6, and 8/9 along with uninfected controls. **(a)** PCA plot showing the clustering of different experimental groups. **(b)** PCA analysis was re-done with the day 8 and day 9 samples grouped together as 'late infection' samples, and with polygons drawn around each sample group. Each dot on the PCA plot represents a single sample/mouse. Meninges were collected from 3 mice per time point across two independent experiments (n=6 per time point total).

## 4.3 Transcriptomic analysis of the meninges at day 6 post-infection.

I next analysed the day 6 samples further to understand what immune changes were occurring at this time point. I began by comparing the uninfected and day 6 samples and determining what the top differentially expressed genes were between these two data sets. I first determined what genes changed significantly (i.e. had a p value above 0.05) between the two samples. I then calculated the adjusted p value (padj), a method which removes any false positives that can be generated by multiple testing performed in RNA seq data set analysis[254]. Finally, I ordered the DEGs by the padj value to determine the top DEGs between the day 6 post-infection and uninfected samples. I plotted this as a volcano plot to visualise the upregulated and downregulated genes (figure 4.3a). Within the top 25 DEGs, genes included various chemokines such as *Cxcl10* and *Ccl22*, and cytokine signalling such as IL-1β (*Il1b*) and the IL-1 receptor (*Il1rn*) (figure 4.3b). Other upregulated genes included the complement protein C3, and P-selectin (*Selp*) which is expressed and activated platelets and vascular endothelium (figure 4.3b).

**a**

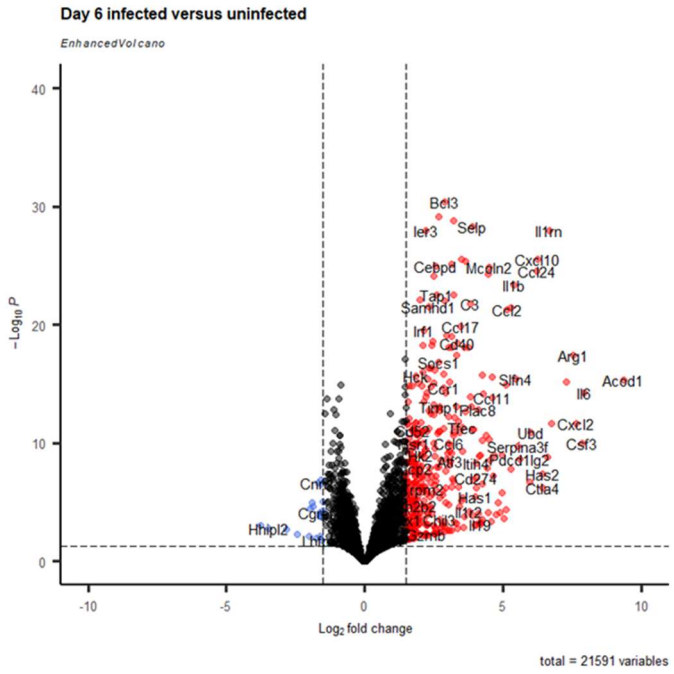


**b**

| Gene | log2FoldChange | padj |
|---|---|---|
| Bcl3 | 2.883317382 | 4.28E-31 |
| Csf2rb | 2.683549537 | 7.50E-30 |
| Slc15a3 | 3.226194344 | 1.51E-29 |
| Selp | 3.899295691 | 5.31E-29 |
| Ier3 | 2.203156867 | 9.88E-29 |
| Il1rn | 6.683574958 | 9.88E-29 |
| Ccl22 | 3.518394784 | 2.77E-26 |
| Cxcl10 | 6.257230465 | 2.95E-26 |
| Socs3 | 3.636093485 | 3.92E-26 |
| Gm49339 | 3.149734012 | 7.97E-26 |
| Cebpd | 2.555109163 | 1.08E-25 |
| Mcoln2 | 4.509212459 | 1.44E-25 |
| Ccl24 | 6.221523032 | 3.02E-25 |
| Ccl7 | 4.468508619 | 5.01E-25 |
| Slfn2 | 2.51517511 | 8.10E-25 |
| Il1b | 5.391236638 | 4.41E-24 |
| Tap1 | 2.60538699 | 2.74E-23 |
| Csf2rb2 | 3.200946795 | 3.17E-23 |
| Lrg1 | 1.999062558 | 7.83E-23 |
| Arid5a | 2.896902304 | 9.73E-23 |
| C3 | 3.838953943 | 1.52E-22 |
| Samhd1 | 2.305805559 | 2.84E-22 |
| AA467197 | 5.280871901 | 3.58E-22 |
| Ccl2 | 5.135891441 | 5.43E-22 |
| Ccl17 | 3.451119143 | 1.52E-20 |

**Figure 4.3. DEG analysis of the meninges at day 6 post-infection. (a)** Volcano plot of the DEGs between day 6 and uninfected meninges samples. Data are plotted as log fold change against $\log_{10}$ of the p value. Downregulated genes with a fold change below -1.5 are indicated in blue, whilst upregulated genes with a fold change above 1.5 are indicated in red. **(b)** Table of the top 25 DEGs in day 6 versus uninfected samples, ordered by adjusted p value (padj). Data shown are the log fold change and the padj.

I then looked beyond individual genes to what gene pathways were significantly upregulated between uninfected and day 6 samples using KEGG pathway analysis (figure 4.4). The top upregulated pathways are “Cytokine-cytokine receptor interaction” and “Viral protein interaction with cytokine and cytokine receptor” which are large pathways that includes genes of cytokine and cytokine receptor interactions associated with pro-inflammatory immune responses and host defense (e.g. *Il6, Cxcl9, Cxcl10 Ccl24*) (figure 4.4). These pathways are also similar to “Chemokine signalling pathway”, whilst other upregulated pathways highlight the importance of specific signalling pathways including the TNF pathway and IL-17 signalling. The osteoclast differentiation pathway also contains many pro-inflammatory markers (e.g. *Tnf*, *Il-1*), along with genes involved in vascular and platelet adhesion (e.g. *Itgb3*). The Rheumatoid arthritis pathway includes genes involved in antigen presentation, inflammation, Th17 responses, and infiltration of inflammatory cells and angiogenesis (e.g. *Vegf, H2-Aa*). Both the osteoclast differentiation and rheumatoid arthritis pathways also indicate tissue damage occurring in the meninges and the skull. Finally, the malaria pathway is upregulated due to the increased expression of the prior discussed inflammatory genes, along with markers of platelet and vascular activation (e.g. *Icam1*, *Selp*). To conclude, the pathway analysis shows that at day 6 post-infection, there is increased pro-inflammatory cytokine and chemokine signalling, immune cell activation, and genes related to platelet and vascular activation in response to vascular damage also seem to be upregulated.

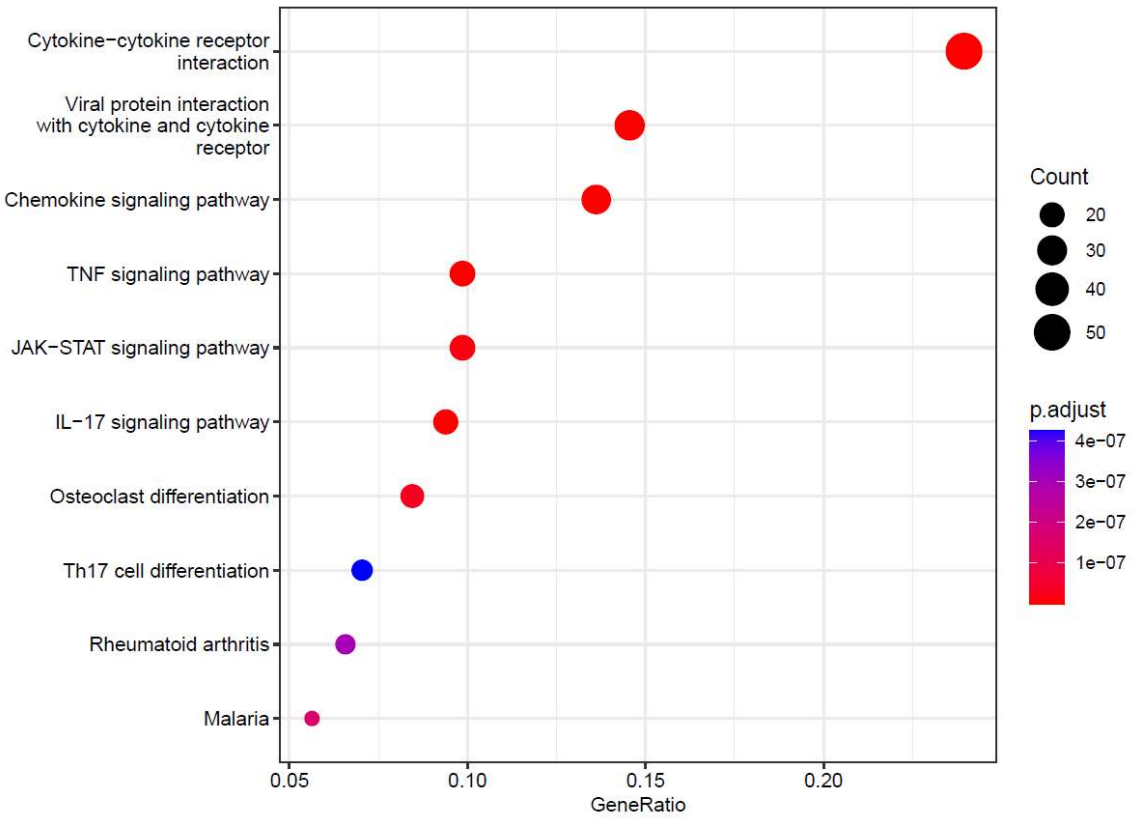


**Figure 4.4. KEGG pathway analysis of the day 6 versus uninfected samples.** The top 10 KEGG gene pathways significantly upregulated (above 1.5 log2 fold change) at day 6 post-infection compared to uninfected controls are plotted. Points are coloured by the adjusted p value, and the size of the point corresponds to the count.

## 4.4 Transcriptomic analysis of the meninges at late infection.

I next wanted to explore the genetic changes in the meninges between the day 6 and late infection samples, as these clustered separately in the PCA plot (figure 4.2b). KEGG pathway analysis revealed the top upregulated pathway was antigen processing and presentation, likely indicating the activation of the adaptive immune response at this time point (figure 4.5). Pathway analysis also showed upregulation of complement and coagulation genes, which are also present in the Chagas disease pathway. Other upregulated pathways such as allograft rejection corresponded to expression of MHC genes. The top differentially expressed genes at late infection included *C1qa* and *C1qb* which encode complement proteins (figure 4.6b). Further, whilst C3 was not in the top DEGs, in contrast to the uninfected versus day 6 samples, the C3 receptor *C3ar1* was upregulated in the late infection samples, indicating that complement signalling is a key pathway in the meningeal response to cryptococcal meningitis.

The second top DEG is *Grn* the gene for progranulin (figure 4.6b). Interestingly, mutations in this gene have been associated with increased risk of developing frontotemporal dementia in humans, and CNS macrophages in *Grn* knockout mice have been shown to upregulate pro-inflammatory cytokines and phagocytosis[255]. In the case of microglia, *Grn* knockout mice have excessive neuronal synaptic pruning by microglia which was found to be mediated by C1qa[255]. This study found that in the *Grn* knockout mice, deposits of C1qa and C3 increased with ageing, and this occurred specifically in the thalamus region of the brain, whilst knocking out C1qa prevented the synaptic pruning by *Grn* knockout microglia [255]. My data therefore shows a similar interaction may be occurring in the meninges, which may relate to the neurological defects seen in cryptococcal meningitis. Within the upregulated genes at late infection there are also chemokines such as *Ccl8* and MHC-II antigen presentation genes (e.g. *H2-Ab1*). *Ctsb* (cathepsin B) is also

upregulated, and this protein has been shown to degrade ECM, and its expression in the brain is associated with cancer[256]. Further, in an *in vitro* study of infection with the parasite *Leishmania major*, knocking out *Ctsb* in macrophages resulted in a protective type 1 response[257].

To conclude, in the meninges at the late infection time point, pro-inflammatory signalling and antigen presentation are highly upregulated, along with genes that have previously been explored for their role in neurodegenerative diseases. Furthermore, the upregulated genes indicate increased ECM remodelling, which may be indicative of tissue damage. Finally, the complement pathway seems to continue to play a significant role in the meninges at the late stage of infection, albeit the specific complement proteins upregulated at this stage are different to those at day 6.

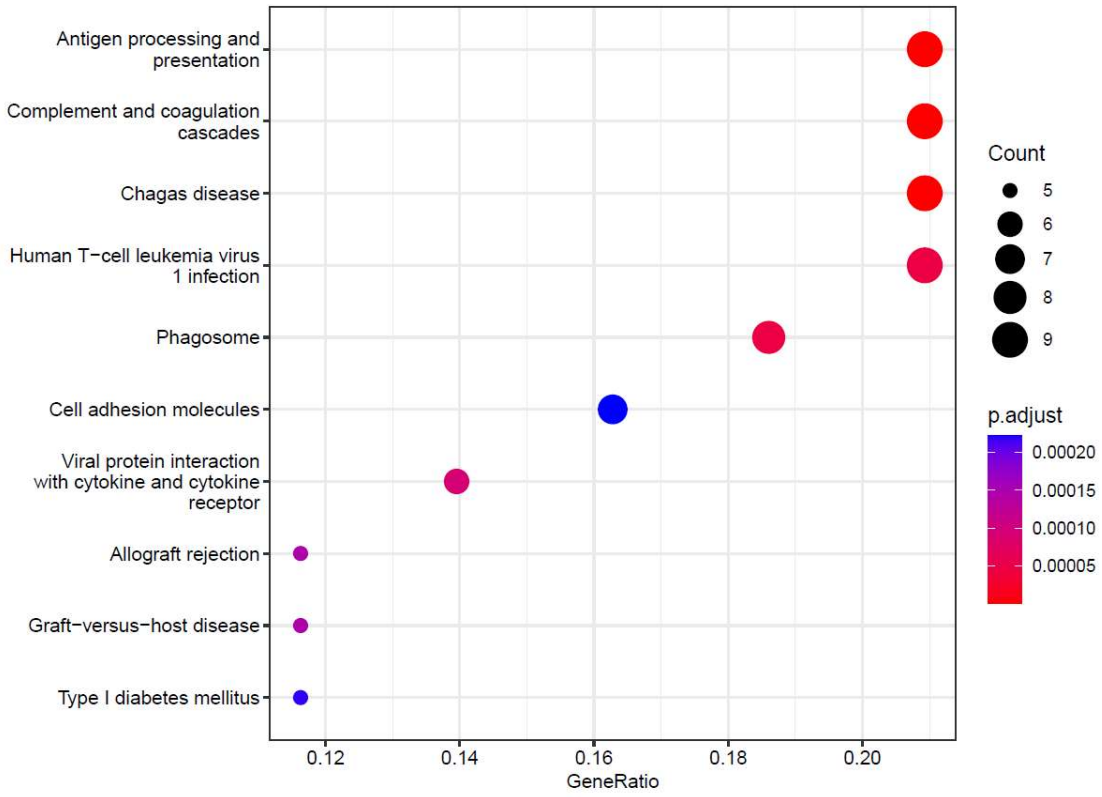


**Figure 4.5. KEGG pathway analysis of the late infected versus day 6 meninges samples.** The top 10 KEGG gene pathways significantly upregulated (above 1.5 log2 fold change) at late infection compared to day 6 post-infection are plotted. Points are coloured by the adjusted p value, and the size of the point corresponds to the count.

**a**

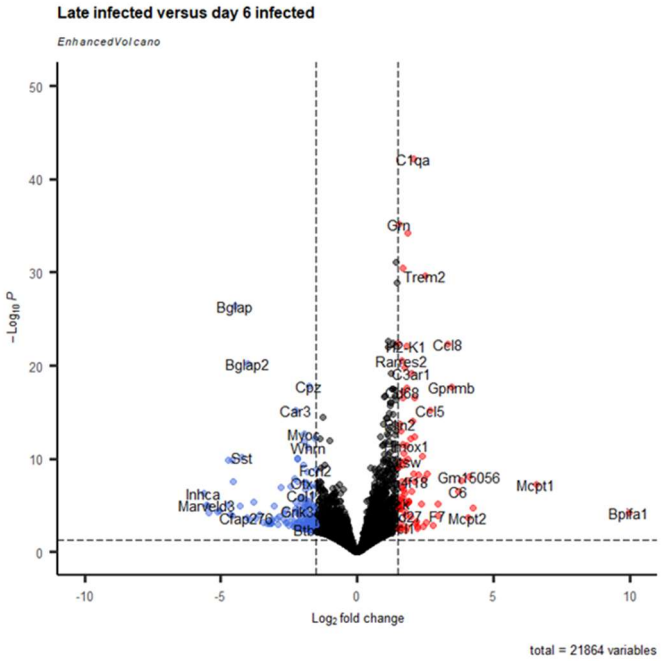


**b**

| Gene | log2FoldChange | padj |
|---|---|---|
| C1qa | 2.077638947 | 6.56E-43 |
| Grn | 1.530271663 | 6.95E-36 |
| C1qc | 1.868834521 | 5.73E-35 |
| Ctsb | 1.427681274 | 7.13E-32 |
| C1qb | 1.661867319 | 3.09E-31 |
| Trem2 | 2.491471185 | 2.22E-30 |
| Pld4 | 1.465668535 | 1.37E-29 |
| Bglap | -4.488870009 | 4.55E-27 |
| Npc2 | 1.135476603 | 2.27E-23 |
| H2-D1 | 1.501293972 | 3.43E-23 |
| H2-Ab1 | 1.333223446 | 3.44E-23 |
| Ccl8 | 3.338679155 | 4.42E-23 |
| H2-K1 | 1.818545254 | 6.98E-23 |
| Cxcl16 | 1.435691973 | 7.22E-23 |
| Ctsh | 1.151290576 | 1.08E-22 |
| Rarres2 | 1.63371509 | 3.26E-21 |
| Bglap2 | -3.99751137 | 6.66E-21 |
| Ecm1 | 1.756083651 | 1.60E-20 |
| C3ar1 | 1.999184623 | 6.71E-20 |
| Rasa4 | 1.239306522 | 7.03E-20 |
| Sftpd | -21.41397922 | 5.48E-19 |
| Cpz | -1.767790599 | 1.65E-18 |
| Gpnmb | 3.447915685 | 2.13E-18 |
| Lgmn | 1.820201208 | 2.43E-18 |
| Slc29a3 | 1.266639571 | 3.30E-18 |

**Figure 4.6. DEG analysis of the meninges at late infection. (a)** Volcano plot of the DEGs between late and day 6 infected meninges samples. Data are plotted as log fold change against $\log_{10}$ of the p value. **(b)** Table of the top 25 DEGs in late versus day 6 infected meninges samples, ordered by adjusted p value (padj). Data shown are the log fold change and the padj.

## 4.5 Meningeal whole mounts for imaging analysis.

To further explore inflammation in meninges and begin analysing the increase in complement and platelet pathways seen in my sequencing data, I set up an imaging protocol to examine meningeal whole mounts that would allow me to stain for immune cells, platelets and blood vessels and compare these across different mouse backgrounds (such as those lacking complement proteins).

To collect meninges tissue, the skull cap is first carefully removed, and the dural meninges are then peeled from the inside of the skull thus providing the tissue whole mount. I first optimised different fixation methods, as fixation provided tissue stiffness which made peeling easier and breakage of the tissue less likely, albeit extensive fixation could potentially impact antibody binding. I first tried using the skull as a 'well' for antibody staining, then fixing the samples after antibody incubation. However, I found cell death begins in the meninges within 30 minutes to an hour after collection, which along with the unevenness of the skull surface resulted in extensive variation in antibody staining between samples. Furthermore, as I was interested in imaging platelets, I had to determine a method that would keep them intact and not result in accidental platelet activation. I next tried fixing the tissue first but only for a brief period, which prevented the previous variation in platelet clotting I had previously seen. Finally, I optimised a method to peel the meninges after fixation, then placing them in a well plate containing the staining solution. This ensured even antibody penetration and placing the meninges in the staining solution helped to flatten out the tissue for easier mounting (figure 4.7). This method has been adapted into a book chapter, which I published as corresponding author [258].

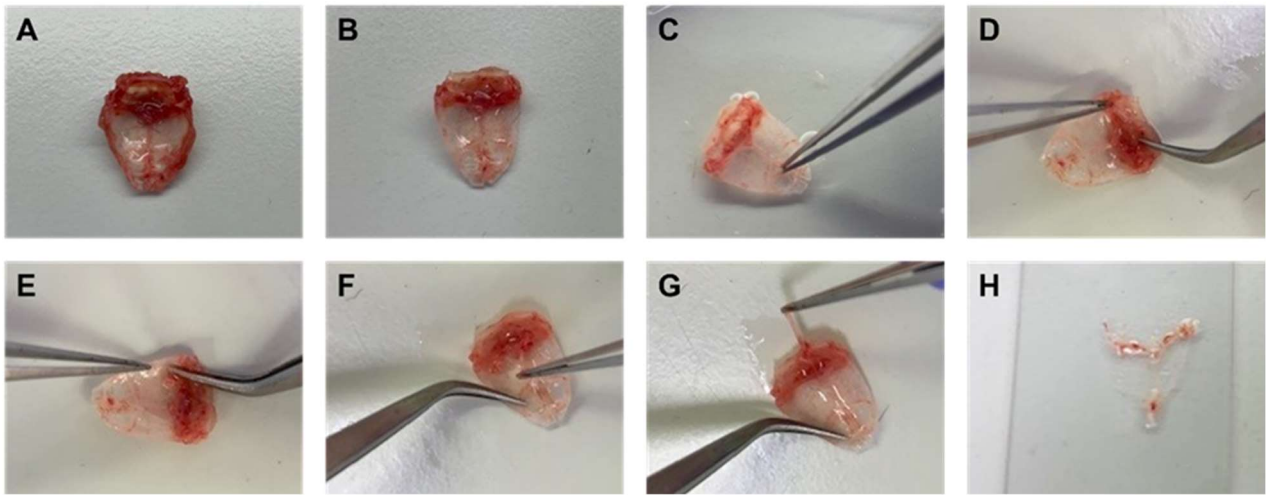


**Figure 4.7. Dissection of the meninges to generate whole mounts for imaging. (A)** The skull cap of a mouse. **(B)** The skull cap after trimming the outer edge. **(C)** The meninges are first detached at the base of the superior sagittal sinus. **(D)** The fleshy outer ends of the transverse sinuses are next detached. **(E)** The ultrafine forceps can then be slid under the entire outer edge of the meninges. **(F)** To peel the meninges, we begin where we started by holding the end of the superior sagittal sinus and pulling it towards the back of the skull. **(G)** As the meninges is peeled it will roll up. The final step is to gently detach it from the very back of the skull. **(H)** The meninges can then be flattened on a slide. Figure adapted from *Meningeal Whole Mounts for Imaging CNS Fungal Infection.*

To check the protocol for making meningeal whole mounts worked correctly, I first imaged the tissue to confirm the anatomy was correct and the tissue remained intact. Staining a sample with DAPI alone revealed the expected morphology of the tissue (figure 4.8a). I further confirmed this by staining with CD31 for endothelium, which revealed the main meninges vasculature, namely the superior sagittal sinus and transverse sinus, remained intact (figure 4.8b). I also confirmed that the CD31 staining worked sufficiently to be able to image the smaller blood vessels in the meninges (figure 4.9a). I had to optimise the CD31 concentration as the Alexa-488 directly conjugated antibody provided the brightest staining out of any colours, however most of the tissue autofluorescence occurred in the 488 channel (figure 4.9b). Finally, I used a CD45 antibody to confirm I could visualise leukocytes within the meninges (figure 4.9c). The imaging showed extensive CD45 staining which could be seen throughout the tissue including within the dural sinuses (figure 4.9c). I also collected meninges from CX3CR1-GFP-CCR2-RFP transgenic mice, and found my protocol maintained the fluorescence of the cells, enabling visualisation of CX3CR1+ macrophages and CCR2+ monocytes (figure 4.10).

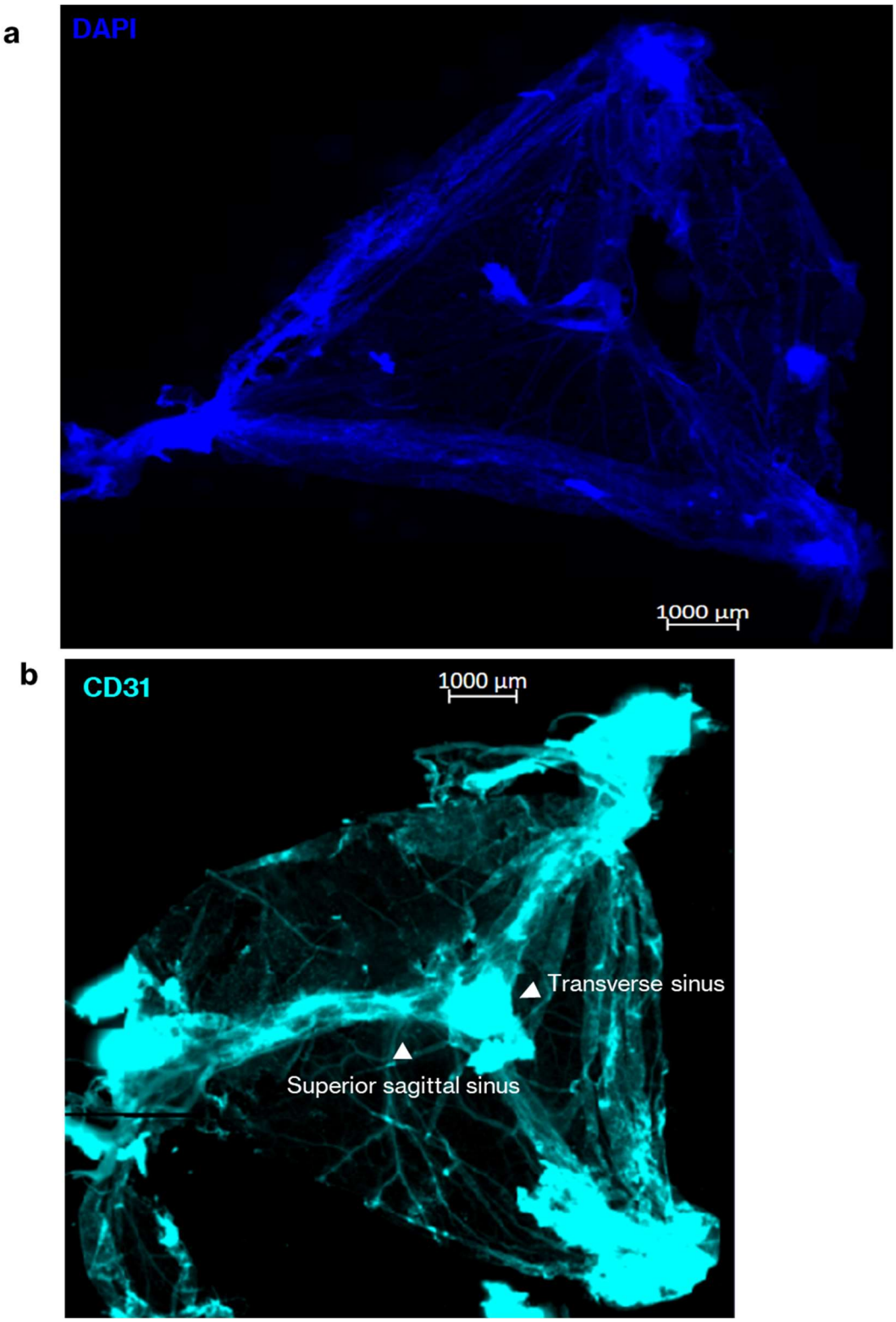


**Figure 4.8. Imaging meningeal whole mounts.** Single images of whole meninges tissue taken at 10X on the ZEISS Axio Slide Scanner. **(a)** DAPI nuclear staining in an uninfected mouse **(b)** CD31 staining, with the meningeal dural sinuses labelled, from an infected mouse. Images selected to clearly demonstrate the desired anatomy. Whole meninges were collected from two independent experiments with n=2-3 mice per group (uninfected and infected) and stained for DAPI, CD31, CD41 and CX3CR1, with one sample used as a DAPI-only control.

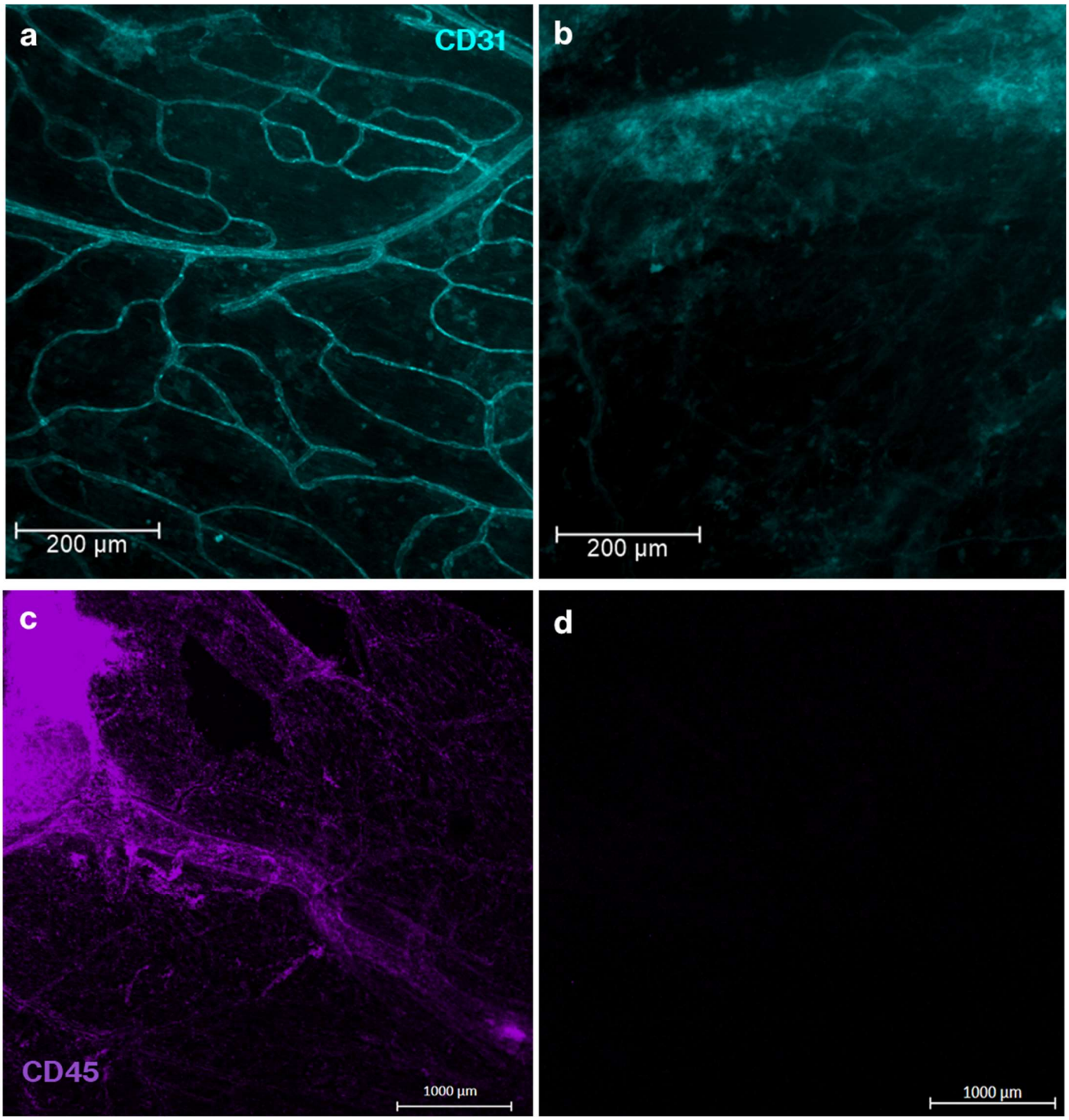


**Figure 4.9. Imaging meningeal whole mounts. (a)** Snapshot of CD31 staining taken at 10X on the Leica DM6000 fluorescence microscope. **(b)** Snapshot of the CD31 channel in an unstained control. Whole meninges were collected from two independent experiments with n=2-3 mice per group (uninfected and infected) and stained for DAPI, CD31, CD41 and CX3CR1, with one sample used as a DAPI-only control. 3 images were taken per sample across different areas of the tissue. **(c)** Confocal microscopy tile scan images taken at 10X magnification on the LSM880 of CD45 staining and **(d)** unstained control meninges. A single tile scan image was taken to cover most of the whole mount per sample, n=4 mice.

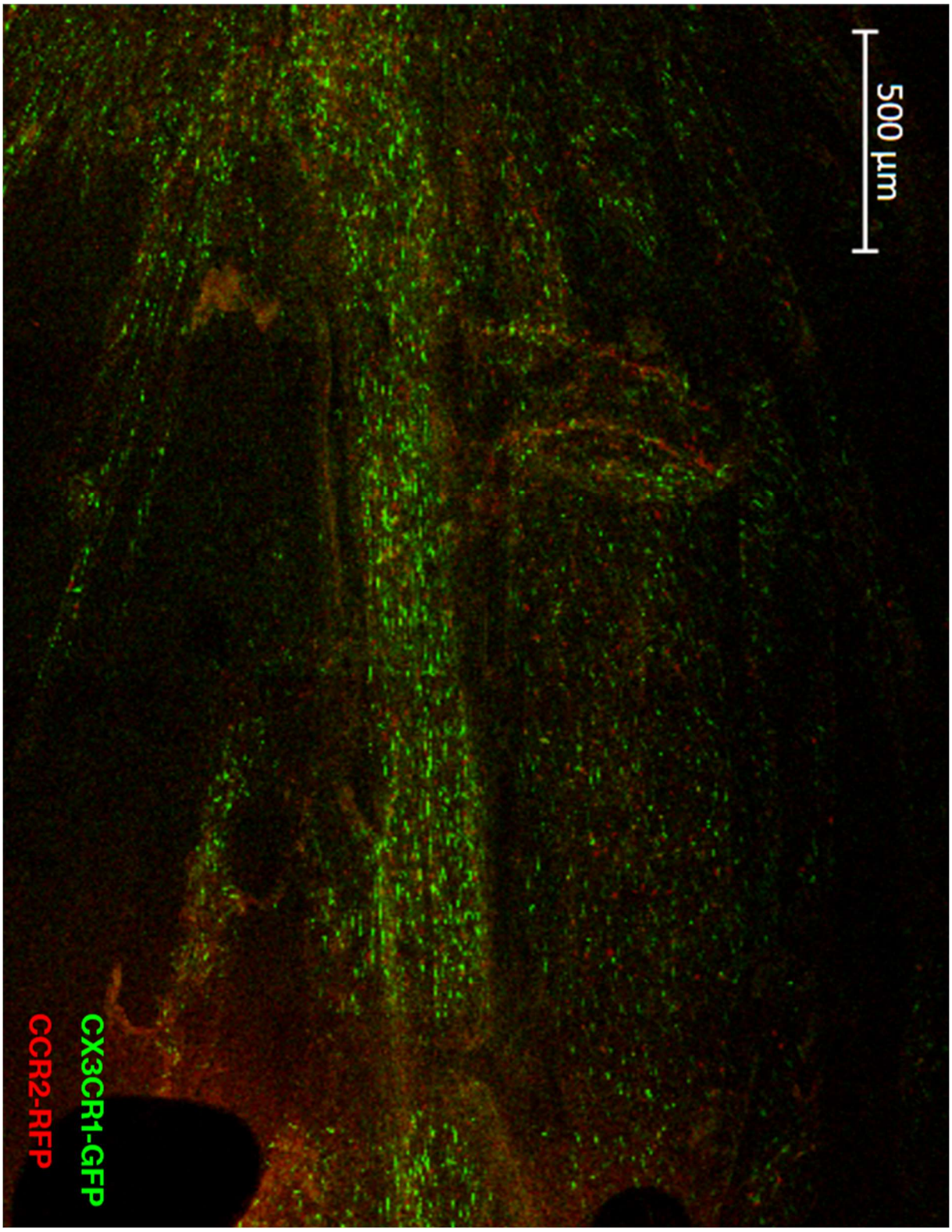


**Figure 4.10. Imaging meningeal whole mounts from CX3CR1-GFP-CCR2-RFP mice.** Representative confocal microscopy tile scan image taken at 10X magnification on the LSM880 of the meninges at day 6 post-infection. Transgenic mice expressed GFP on CX3CR1+ cells (macrophages) and RFP on CCR2+ cells (monocytes).

## 4.6 Imaging the immune response to *C. neoformans* infection in the meninges.

To visualise the response to cryptococcal meningitis in the meninges, I used GFP labelled *C. neoformans* to infect mice and collected tissue from day 6/7 post-infection. I initially imaged the tissue on a 20X magnification and scanned the entire tissue to determine where the fungus was located (figure 4.10b). I observed fungal cells in the dural sinuses and in the tissue adjacent to these vessels (figure 4.10b). I imaged the fungus more closely and found that the fungi within the meninges tissue formed distinct lesions containing large numbers of fungal cells, reminiscent of cryptococcomas (figure 4.10c). DAPI staining revealed there were other non-fungal cells present in these lesions (figure 4.10c). To determine whether immune cells were present in these lesions I stained for CD45 (figure 4.11). This data shows extensive CD45 staining in the infected meninges, with bright staining seen next to blood vessels and surrounding areas of fungi (figure 4.11). Using a higher magnification showed extensive CD45+ cells within the fungal lesions, with staining on cells with a rounded morphology and on larger cells that contain intracellular fungi (figure 4.12a and b).

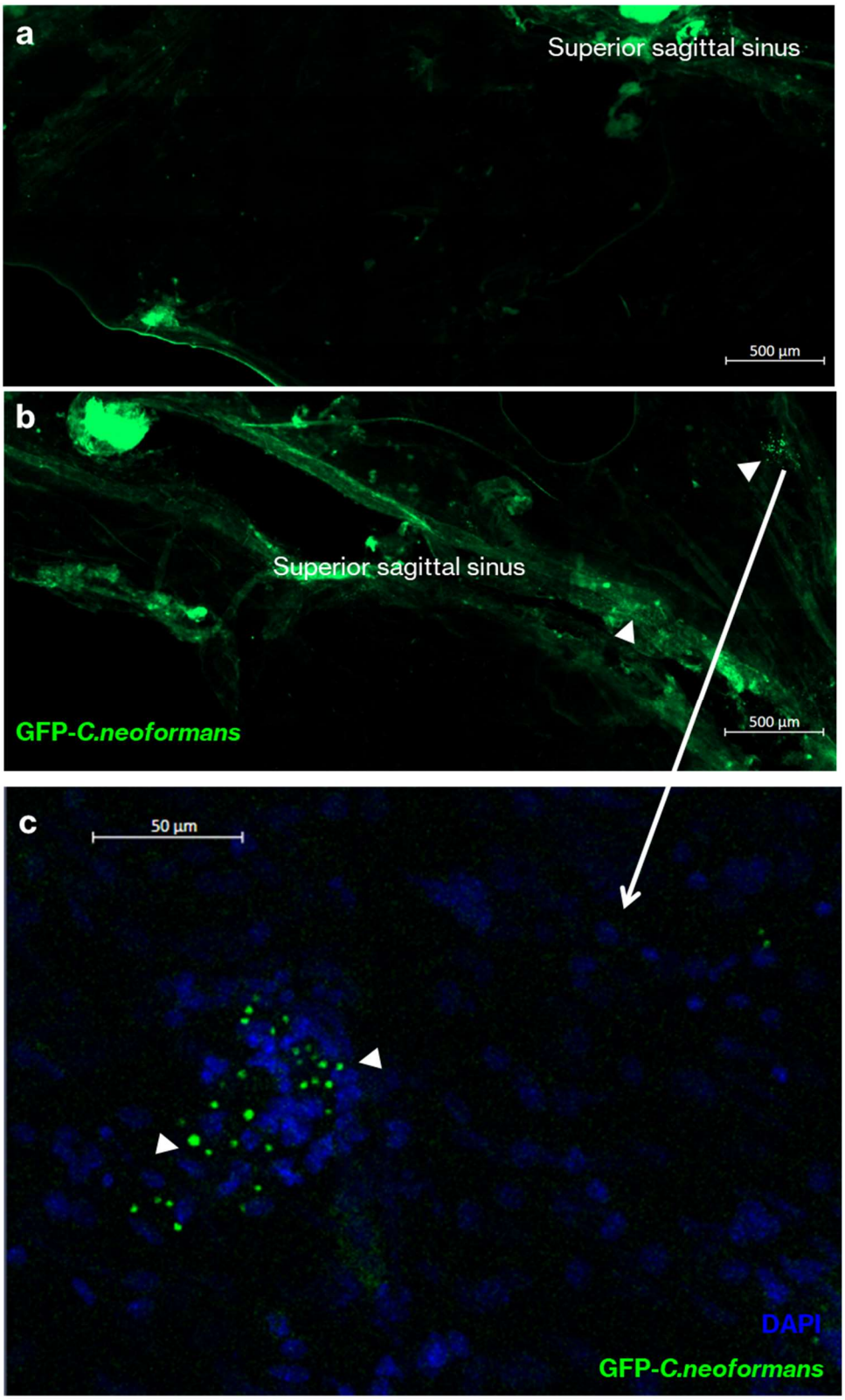


**Figure 4.11. Imaging *C. neoformans* infection in the meninges.** Mice were infected with *GFP-C. neoformans* and meninges collected at day 6/7 post-infection. Fluorescence images of meningeal whole mounts at 20X were taken using the ZEISS Axio Slide Scanner of **(a)** uninfected and **(b)** infected mice. **(c)** Representative confocal microscopy image of a fungal lesion, taken at 25X (4 images taken per tissue). N=2-3 mice per condition.

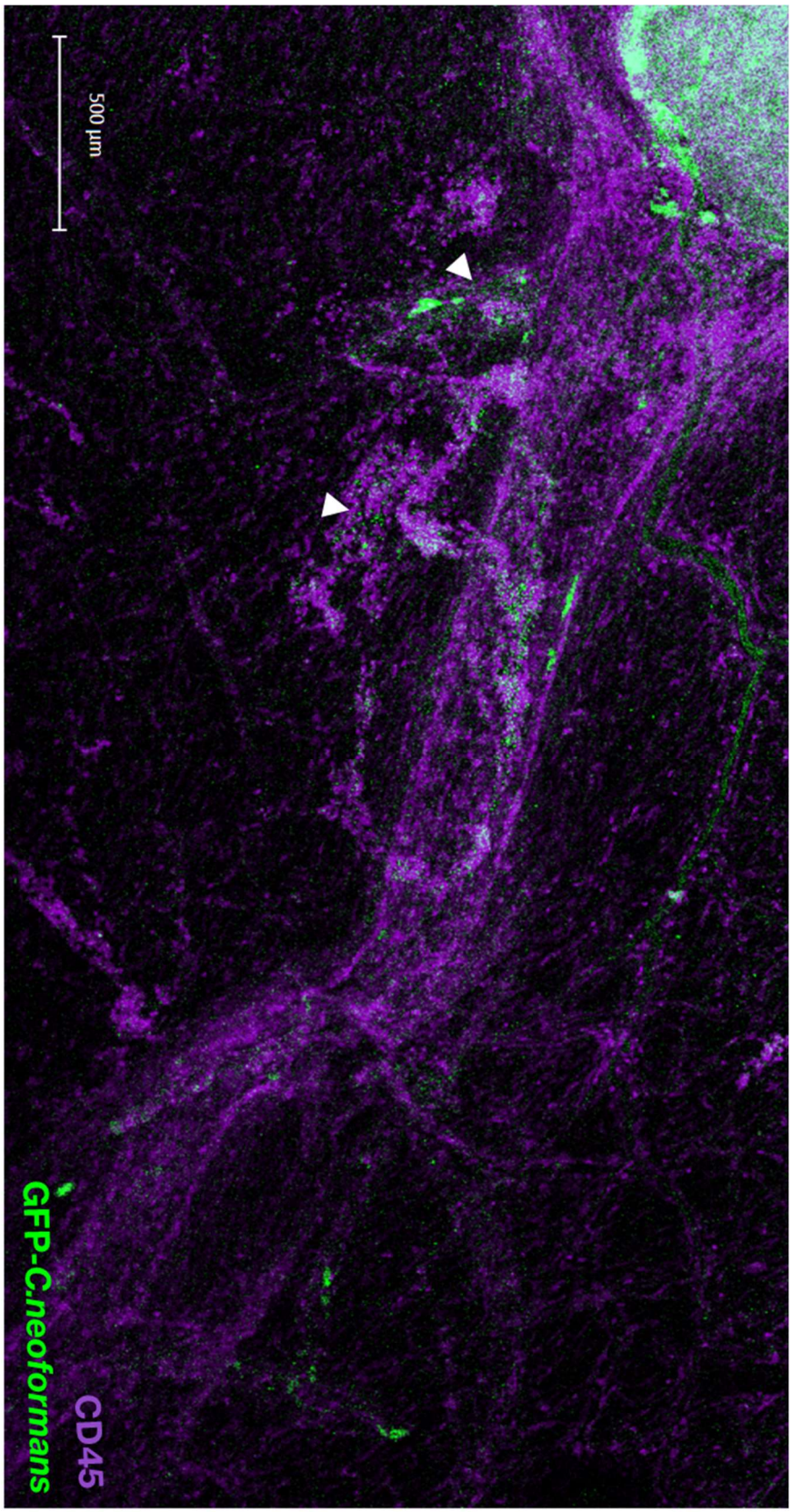


**Figure 4.12. Imaging *C. neoformans* infection in the meninges.** Representative confocal microscopy tile scan of *GFP-C. neoformans* taken at 10X magnification on the LSM880 of GFP-*C. neoformans* and CD45-APC staining. Examples of fungal lesions are indicated by the arrows.

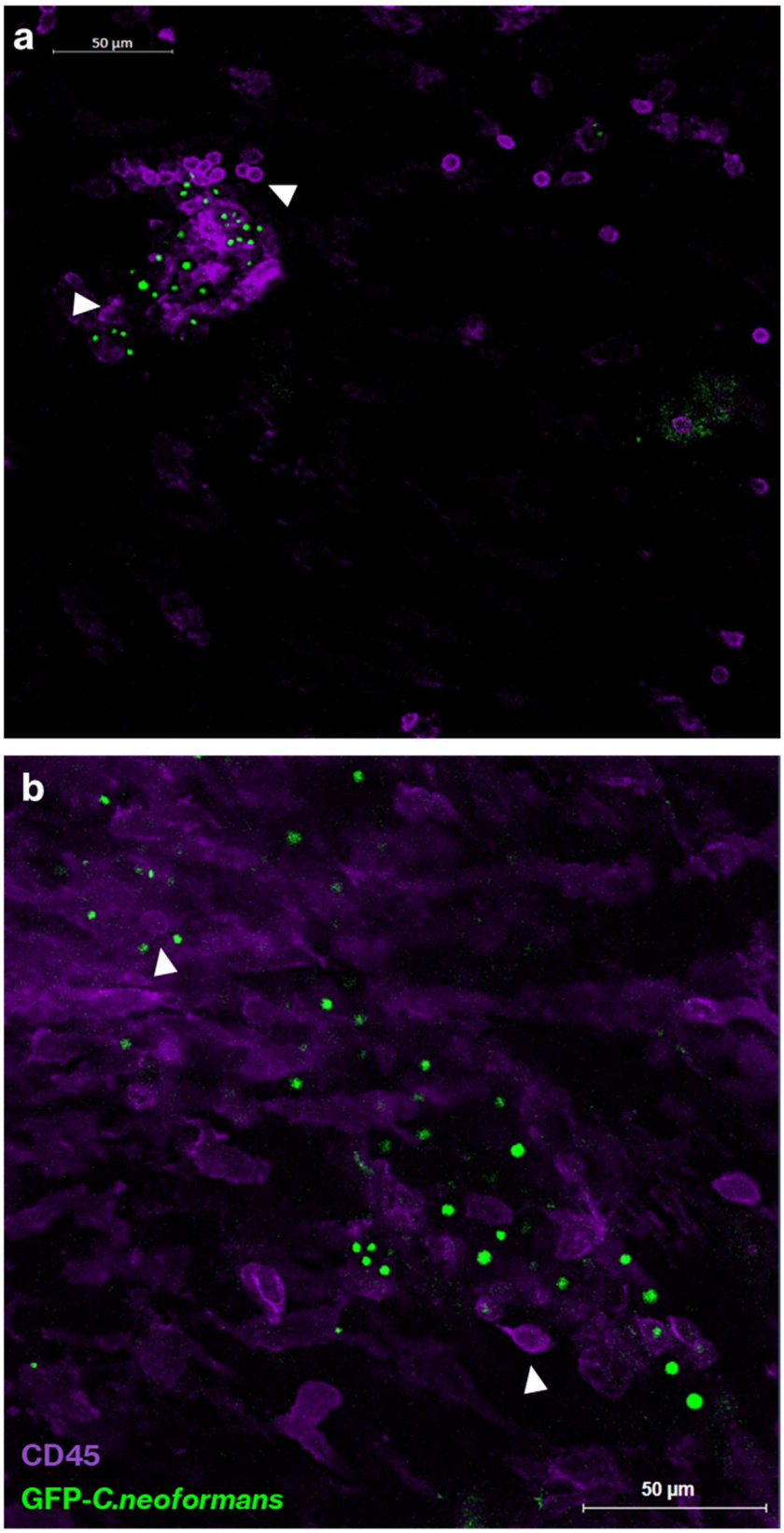


**Figure 4.13. CD45+ cells are found within fungal lesions.** Confocal images taken on the LSM880 of GFP-*C. neoformans* and CD45-APC-stained meninges at **(a)** 25X and **(b)** 40X magnification. Arrows indicate areas of intense CD45 staining surrounding small, rounded cells and larger cells which appear to contain fungi.

## 4.7 Imaging the platelets in the *C. neoformans* infected meninges.

One of the genes of interest that came up in RNA-seq analysis at day 6 post-infection was P-selectin (figure 4.3). I therefore wanted to explore the role of platelets in *C. neoformans* infection using imaging for platelet CD41. As previously discussed, I had optimised the meningeal whole mount protocol to ensure platelet interactions were maintained in the tissue for imaging, which included fixing the samples immediately and adding EDTA to prevent further platelet activation. Removal of the meninges from the skull could cause trauma to the vasculature, hence fixing and incubation with EDTA was performed prior to peeling the meninges. Imaging of CD41 and CD31 confirmed platelets could be seen throughout the meninges, including within blood vessels as would be expected (figure 4.14b).

I next compared platelet staining between uninfected and infected mice to determine if there were any differences. Whilst both uninfected and infected meninges contained platelet staining and some clotting could be seen in both samples (possibly due to the sample preparation), in the infected mice I saw more extensive clotting, including in the tissue outside of the blood vessels (figure 4.15a and b).

To determine whether platelets were interacting with the fungus itself, I infected mice with GFP-*C. neoformans* and collected meninges at day 7 post-infection prior to confocal imaging (figure 4.16). I observed platelets appear to be bound to the endothelium adjacent to the lesions containing fungi (figure 4.16a). I also observed some CD41 staining within the lesions, and platelet thrombi adjacent to the fungal lesions that did not contain any fungi (figure 4.16a). when combined with CD45 staining, CD41 platelets could be seen bound to the edge of CD45+ immune cells within the fungal lesions (figure 4.16b). Taken together, these data show an increase in platelet aggregation within the fungal-infected meninges. Platelets appear to line the blood vessels adjacent to fungal lesions, likely

driving immune cell recruitment and extravasation. It is possible that platelets are recruited in response to the fungal infection and/or vascular damage due to the fungus entering the tissue. CD45 cells within the fungal lesions appeared to have platelets bound to their surface, however platelets don't seem to be interacting with the fungus directly. Finally, platelet clots within the tissue are sterile and therefore may be driven by the fungus indirectly or by immune cell activation.

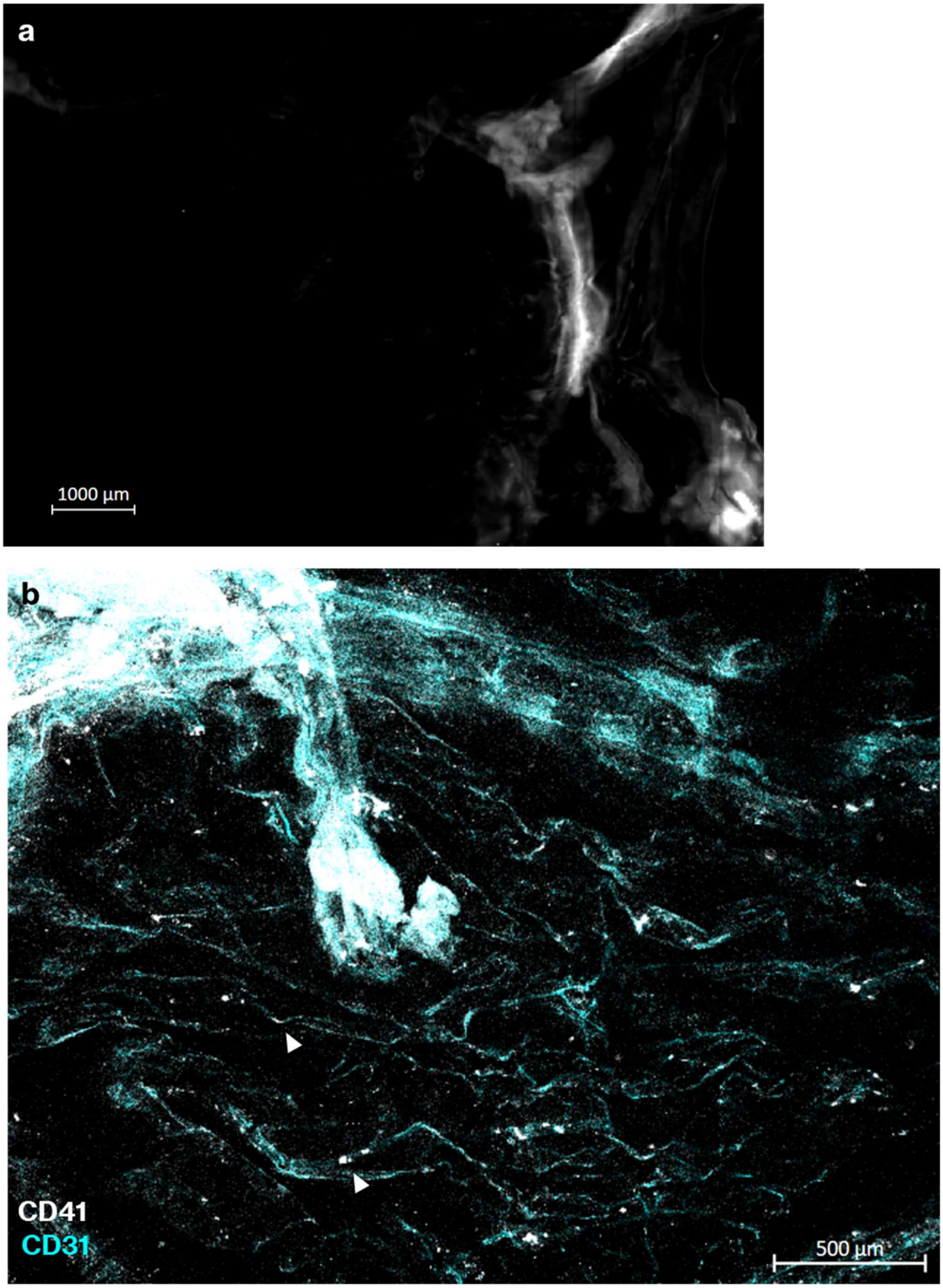


**Figure 4.14. Imaging platelets in the meninges. (a)** Slide scanner image taken at 10X of CD41 unstained control meninges whole mount. **(b)** Representative confocal microscopy tile scan taken at 10X magnification on the LSM780 microscope. The image shows staining for endothelial CD31-AF488 and CD41-PE. Arrows indicate areas of platelets within blood vessels. Samples from both images were from the same experiment with n=6 mice.

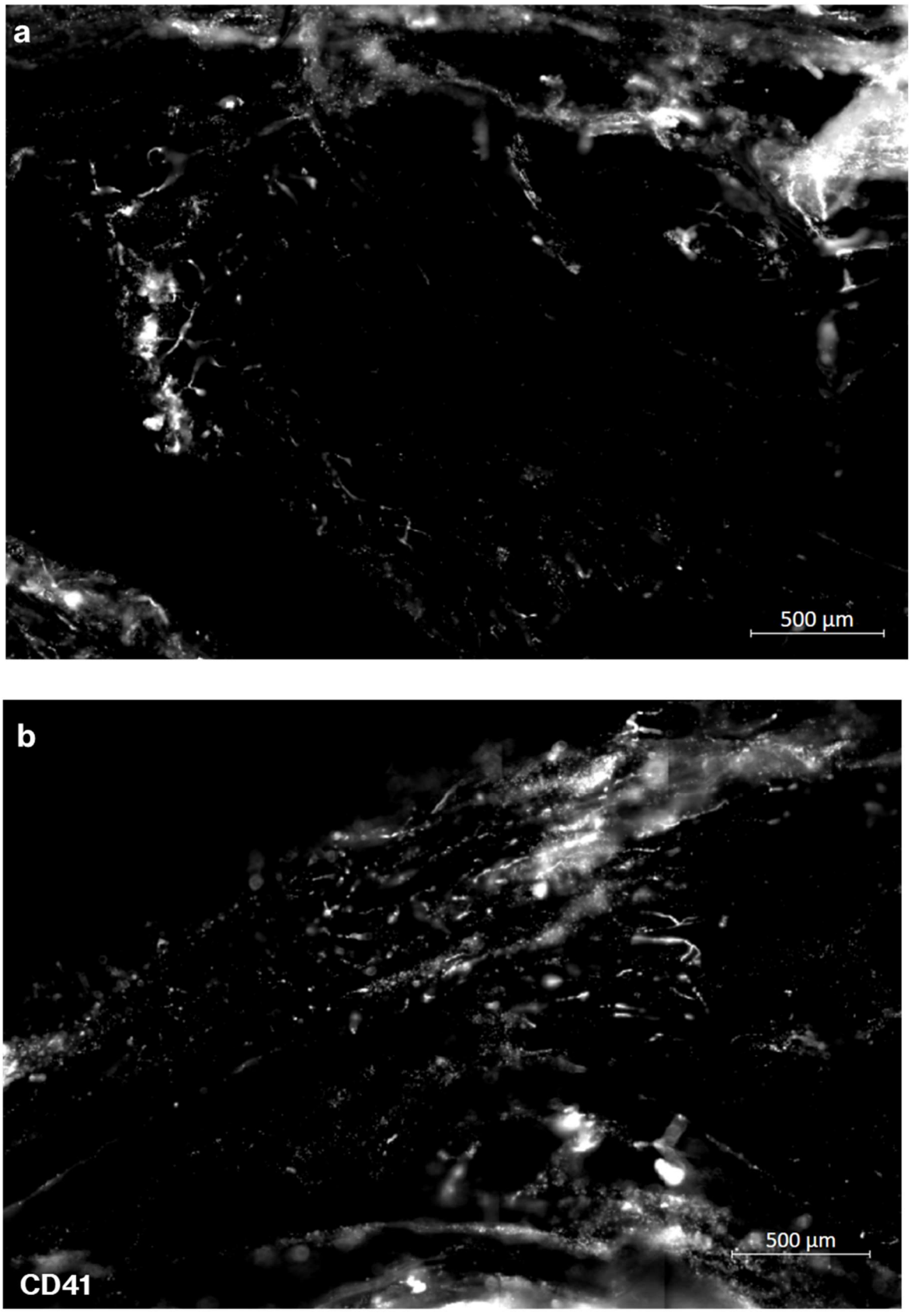


**Figure 4.15. Imaging platelets in the meninges.** Representative confocal microscopy tile scan taken at 10X magnification on the LSM880 microscope of **(a)** uninfected and **(b)** infected meninges stained for platelet CD41-PE.

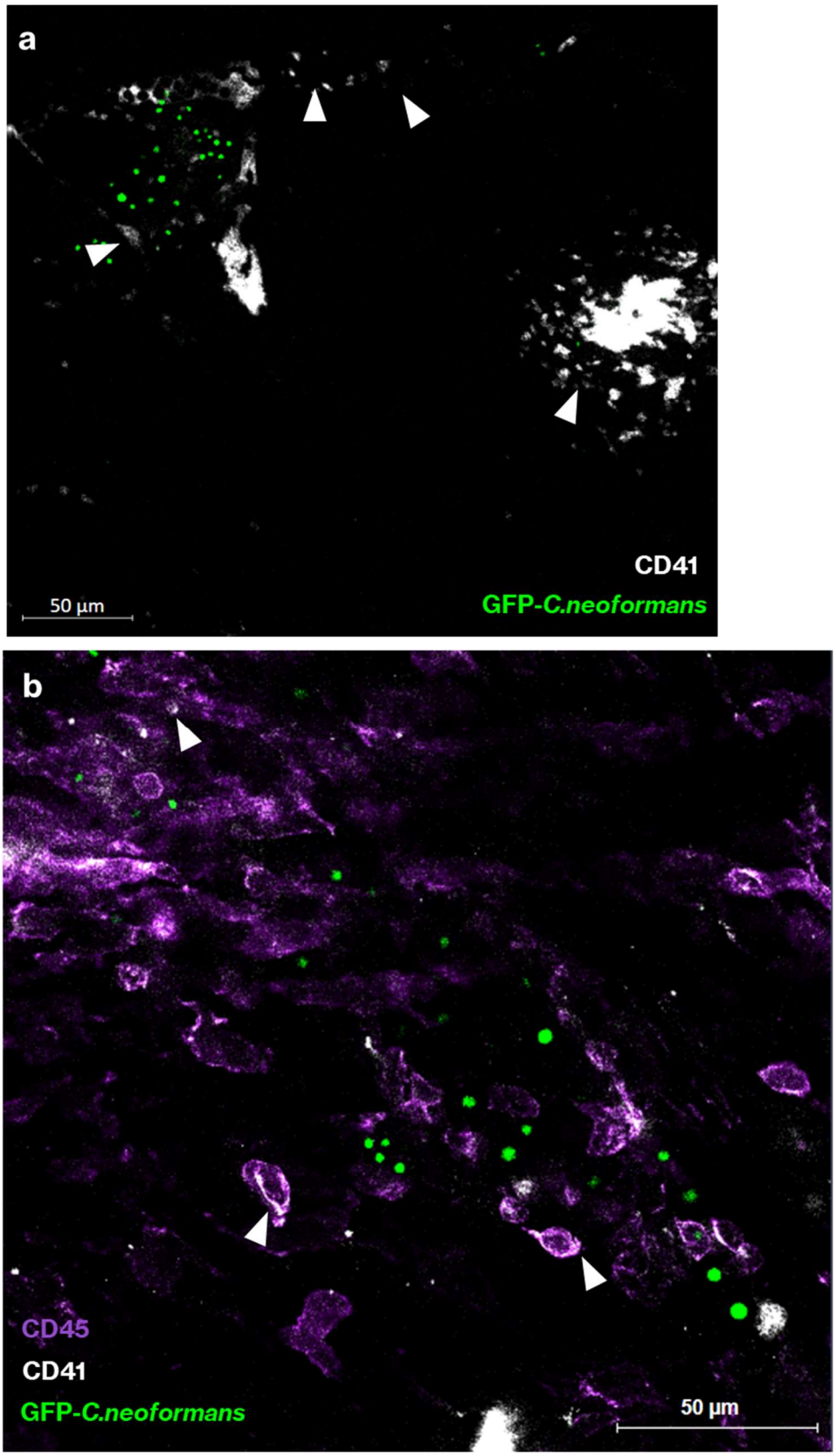


**Figure 4.16. Imaging platelets in the meninges.** Representative confocal microscopy images of infected meninges. **(a)** 25X magnification of GFP-*C. neoformans* and platelet CD41-PE. **(b)** 40X magnification image of an immune lesion showing platelet CD41 staining around CD45+ cells and on individual platelet cells within the lesion.

## 4.8 *C. neoformans* infection does not cause changes in platelets in the peripheral blood.

Whilst alterations in platelet number or function have not been extensively reported in cryptococcal meningitis patients, I sought to determine whether platelet numbers and were increased in the peripheral blood in our *in vivo* model, which could therefore be driving the phenotype seen in the meninges. I performed complete blood count (CBC) analysis of uninfected and infected mice. The data showed no significant changes in platelet count (PLT) or mean platelet volume (MPV) between uninfected and infected mice (figure 4.16a and b). These data show that the phenotype seen in the infected meninges is likely tissue-specific and not driven by platelet dysfunction in the periphery.

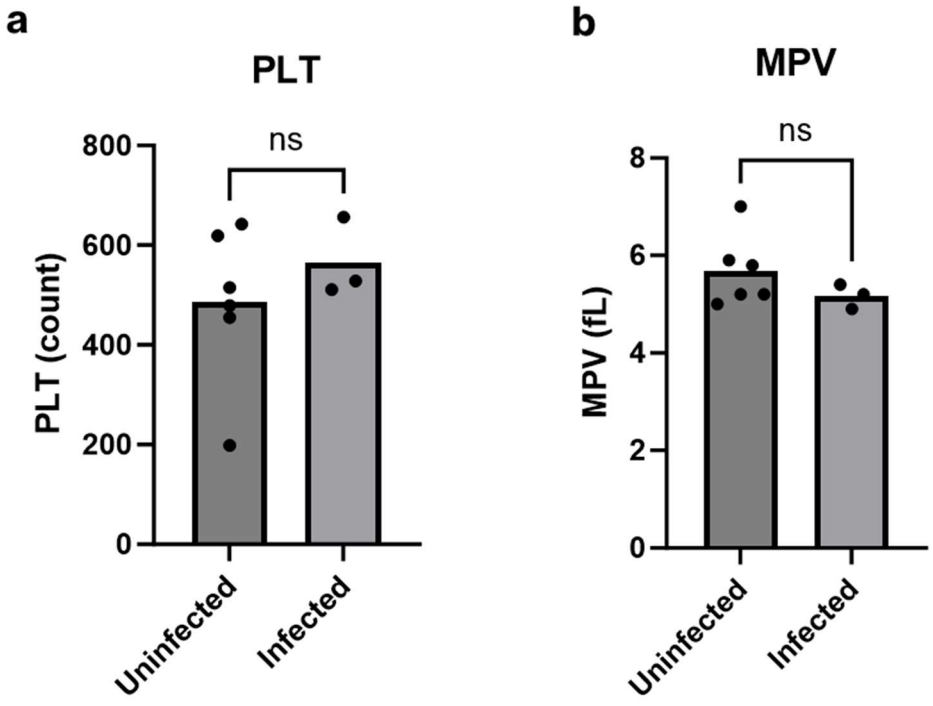


**Table 4.17. CBC analysis of uninfected and *C. neoformans* infected mice.** Blood samples were collected by cardiac puncture into tubes with EDTA and analysed using a CBC machine. (a) Platelet count (PLT) and (b) mean platelet volume (MPV) are plotted. Data points represent individual mice. n=3 for infected and n=6 for uninfected mice. Samples were collected from two independent experiments.

## 4.9 The role of complement in thrombosis and immune lesions in cryptococcal meningitis.

Since my RNA-seq data showed C3 is upregulated in the meninges at day 6, and C1q in late infection, I wanted to determine the function of these complement proteins in the meninges immune response (figure 4.3 and 4.6). Experiments from the Drummond lab have shown that C3 knockout mice have increased fungal burdens in the brain (figure 4.17a). C1q knockout mice however do not have significant differences in brain fungal burdens at day 6 post-infection, which reflects previous work using pulmonary *C. neoformans* infection where no differences in lung fungal burdens were observed[259] (figure 4.17b). I used the protocol I established for imaging meningeal whole mounts to determine if there were any changes in platelet (CD41) and leukocytes (CD45), as well as the *C. neoformans* fungus (GFP). I first imaged meninges from wild-type mice at late infection as I wanted to analyse tissue from day 6 and day 8/late infection samples in line with the sequencing data. Imaging showed similar patterns as in the d6 post-infection meninges, with extensive platelet recruitment and sterile clotting, as well as large lesions of GFP-*C. neoformans* in the tissue and in the dural venous sinuses, surrounded by CD45+ cells (figure 4.18). The large lesions seen reflect the increased fungal burden at late infection.

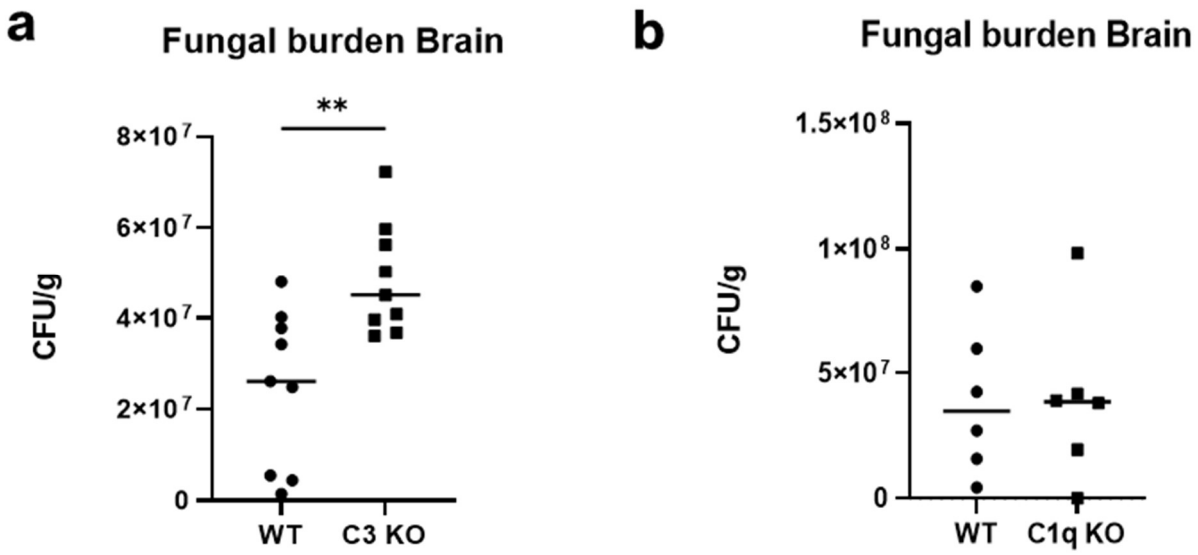


**Figure 4.18. CFU analysis of C3 and C1q knockout mice.** Brains were collected from wild-type and knockout mice at day 6 post-infection, and CFUs quantified. **(a)** CFU of C3 knockout (C3 KO) versus wild-type (WT). **(b)** CFU of C1q knockout (C1q KO) and wild-type mice. Each data point corresponds to an individual mouse. N=6 mice per condition for the C1q knockout experiments, and n=9 mice for the C3 knockout experiments. Data kindly provided by Dr Man Shun Fu.

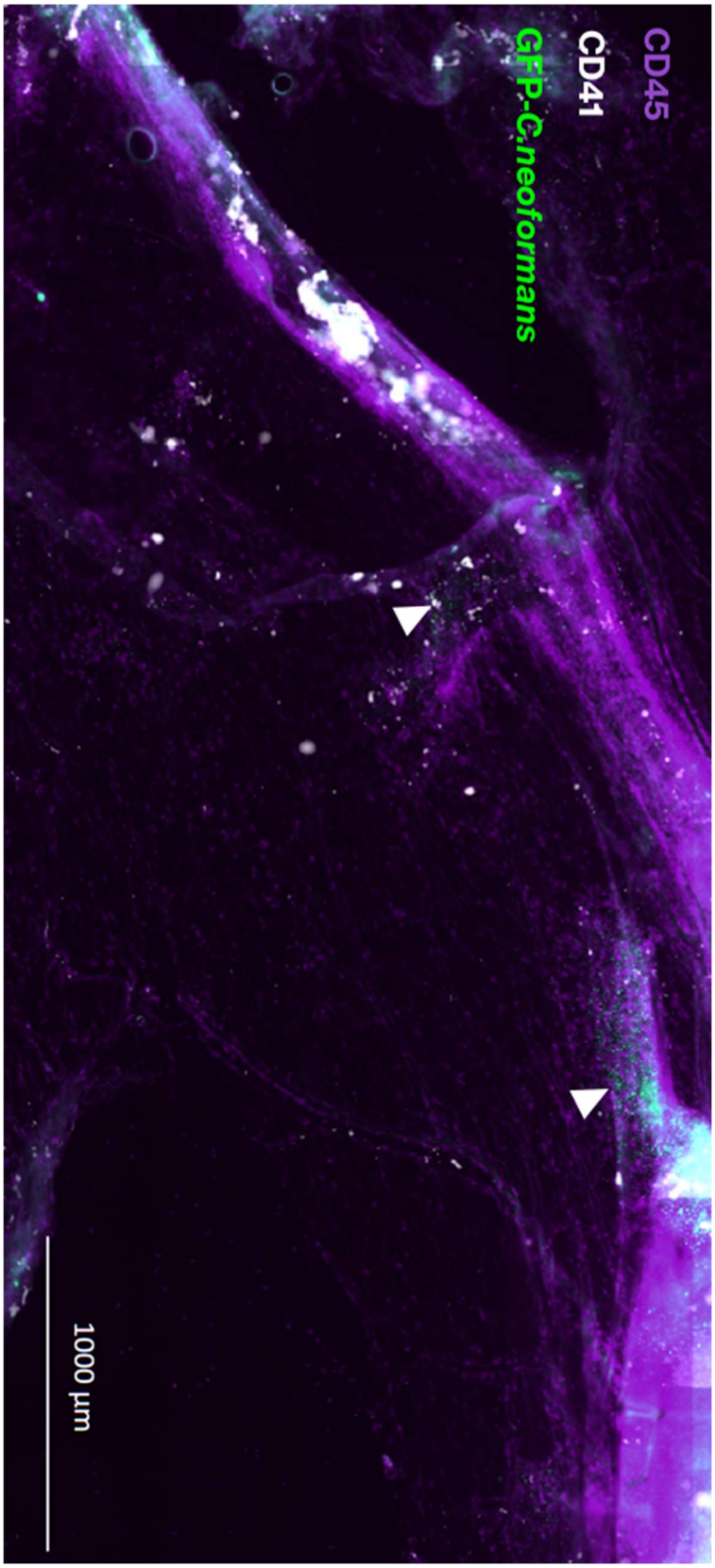


**Figure 4.19. Meningeal whole-mount imaging of the meninges at late infection.** Image taken at 20X on the Axio Slide scanner of the entire tissue, with a representative field of view shown. Staining for CD45-APC, CD41-PE and GFP-*C. neoformans* shown. Arrows indicate areas of fungal lesions.

I next looked at the meninges of C3 knockout mice at day 6. In these samples, some small fungal lesions could be seen in the tissue surrounded by CD45+ cells (figure 4.19a). However, extensive GFP+ and CD41+ cells could be seen in the anatomical area of the meninges behind the transverse sinus (figure 4.19b). This staining showed a large number of cells which did not appear to be clustered together (figure 4.19b). At day 8 post-infection, there appeared to be extensive bleeding around the superior sagittal sinus, with large numbers of individual platelets seen and few clots (figure 4.20). It was difficult to see where any GFP+ fungi were in this area as the bleeding caused extensive autofluorescence, however there did not appear to be fungal lesions in the wider tissue. Overall, these images indicate that whilst the fungal burden in the brains of C3 knockout mice increased, fewer fungi could be seen in the meninges than in the wild-type mice at day 6. Furthermore, at both day 6 and even more so at day 8, extensive bleeding could be seen with little platelet clotting.

At day 6 post-infection in the C1q knockout mice, few fungi could be seen in the meninges (figure 4.21b). Furthermore, CD45 and CD41 staining appeared lower than in the wild-type mice (figure 4.21a and b). However, at day 8, the meninges of C1q knockout mice contained large fungal lesions surrounded by extensive CD45+ staining, and some CD41+ platelets (figure 4.22). These images indicate that at day 6, C1q mice do not form fungal lesions and recruitment of platelets and leukocytes is reduced. However, by day 8, a large number of leukocytes can be found throughout the meninges, including surrounding large fungal lesions. Platelets appear to be interacting with the leukocytes in these lesions but are otherwise not seen extensively outside of the major blood vessels, and don't appear to form sterile clots.

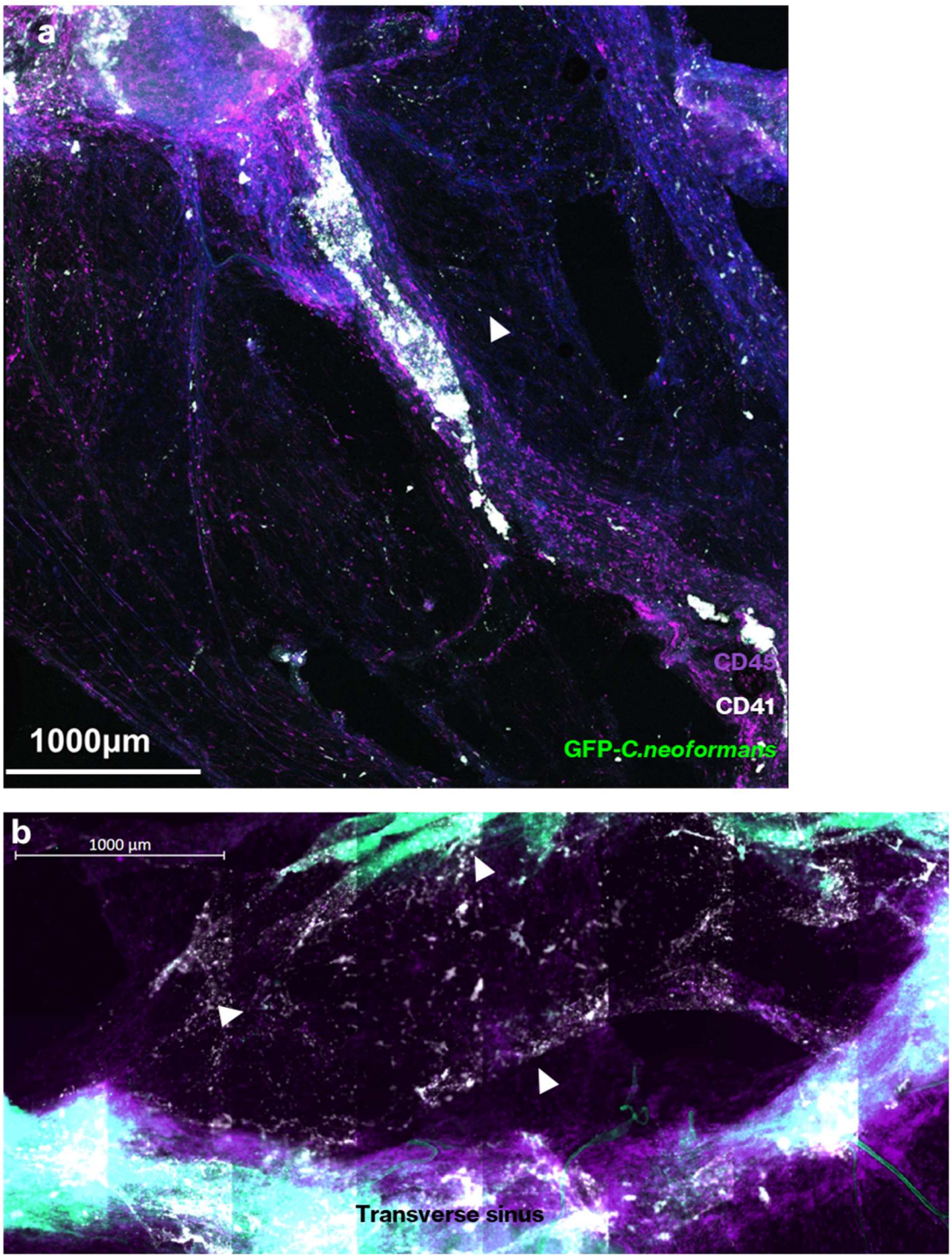


**Figure 4.20. Meningeal whole-mount imaging of the meninges at day 6 post-infection in C3 knockout mice. (a)** Arrows indicate areas of individual fungi in C3 KO meninges. Image taken at 10X on the LSM880 confocal. **(b)** The area above the transverse sinus, with CD41+ staining indicated by arrows. Image taken at 20X on the Axio Slide scanner. Staining for CD45-APC, CD41-PE and GFP-*C. neoformans* shown.

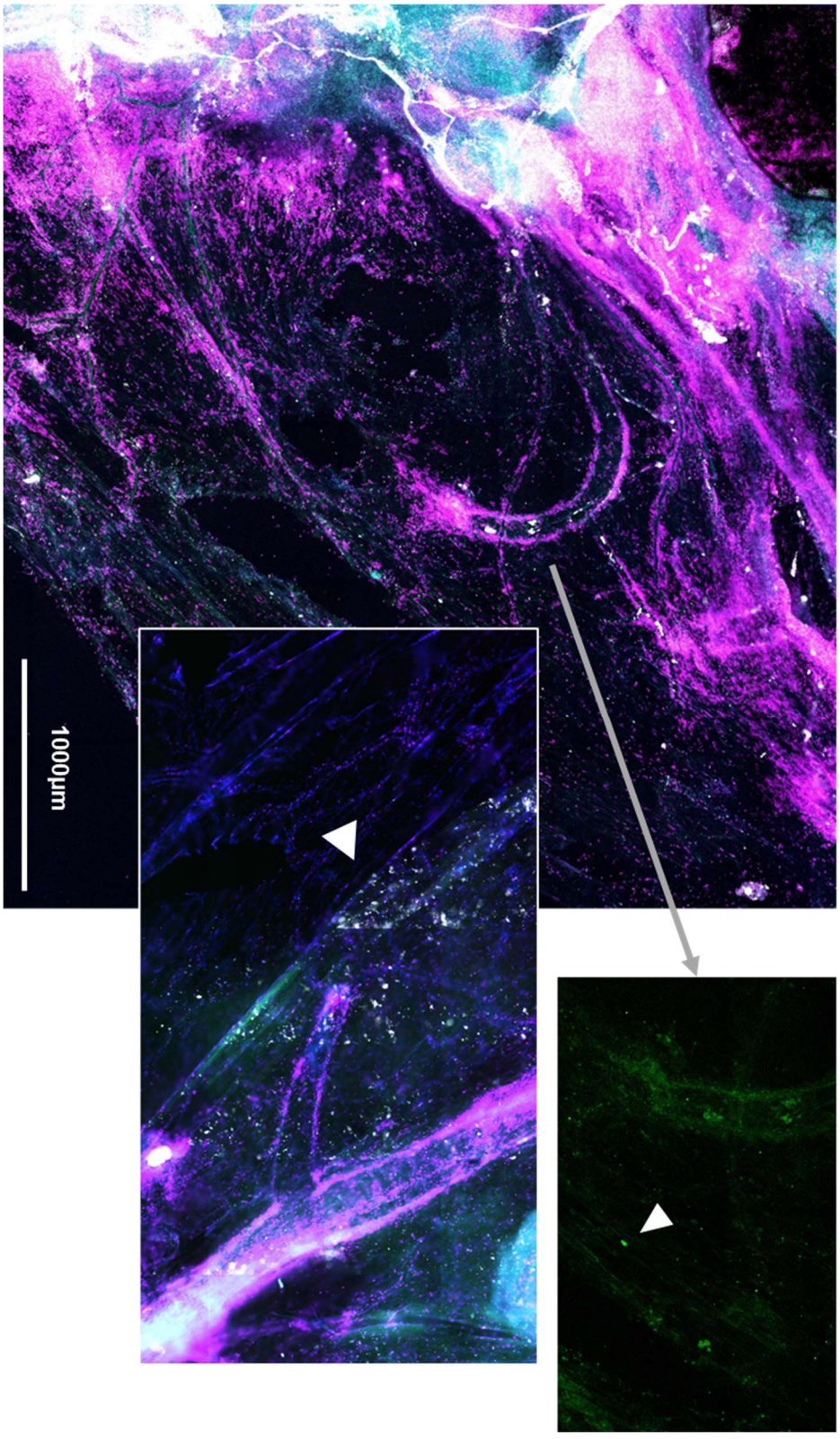


**Figure 4.21. Meningeal whole-mount imaging of the meninges at day 8 post-infection in C3 knockout mice.** Image taken at 10X on the LSM880 confocal. Staining for CD45-APC, CD41-PE and GFP-*C. neoformans* shown. Arrows indicate areas of bleeding and fungal infection.

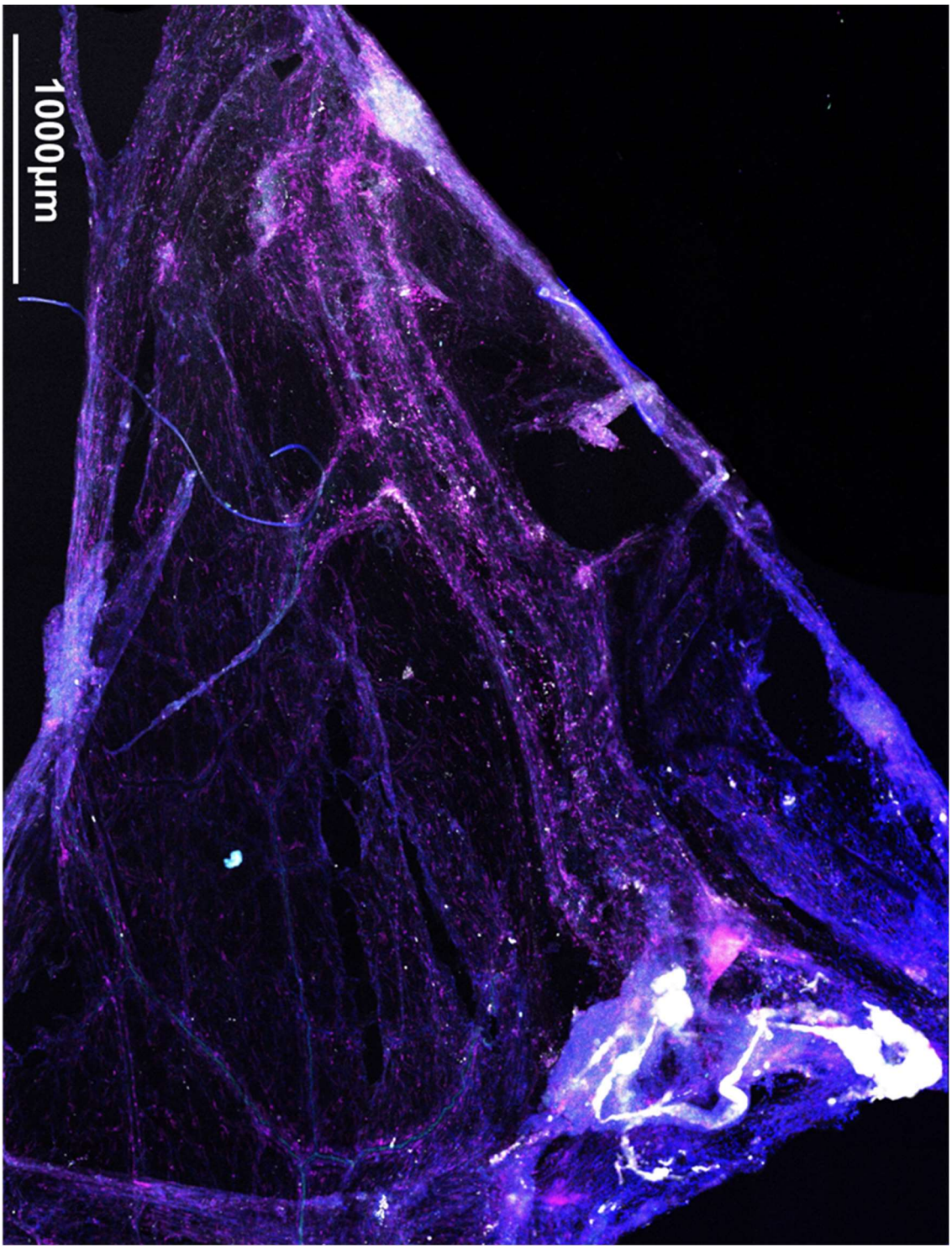


**Figure 4.22. Meningeal whole-mount imaging of the meninges at day 6 post-infection in C1q knockout mice.** Image taken at 10X on the LSM880 confocal. Staining for CD45-APC, CD41-PE and GFP-*C. neoformans* shown.

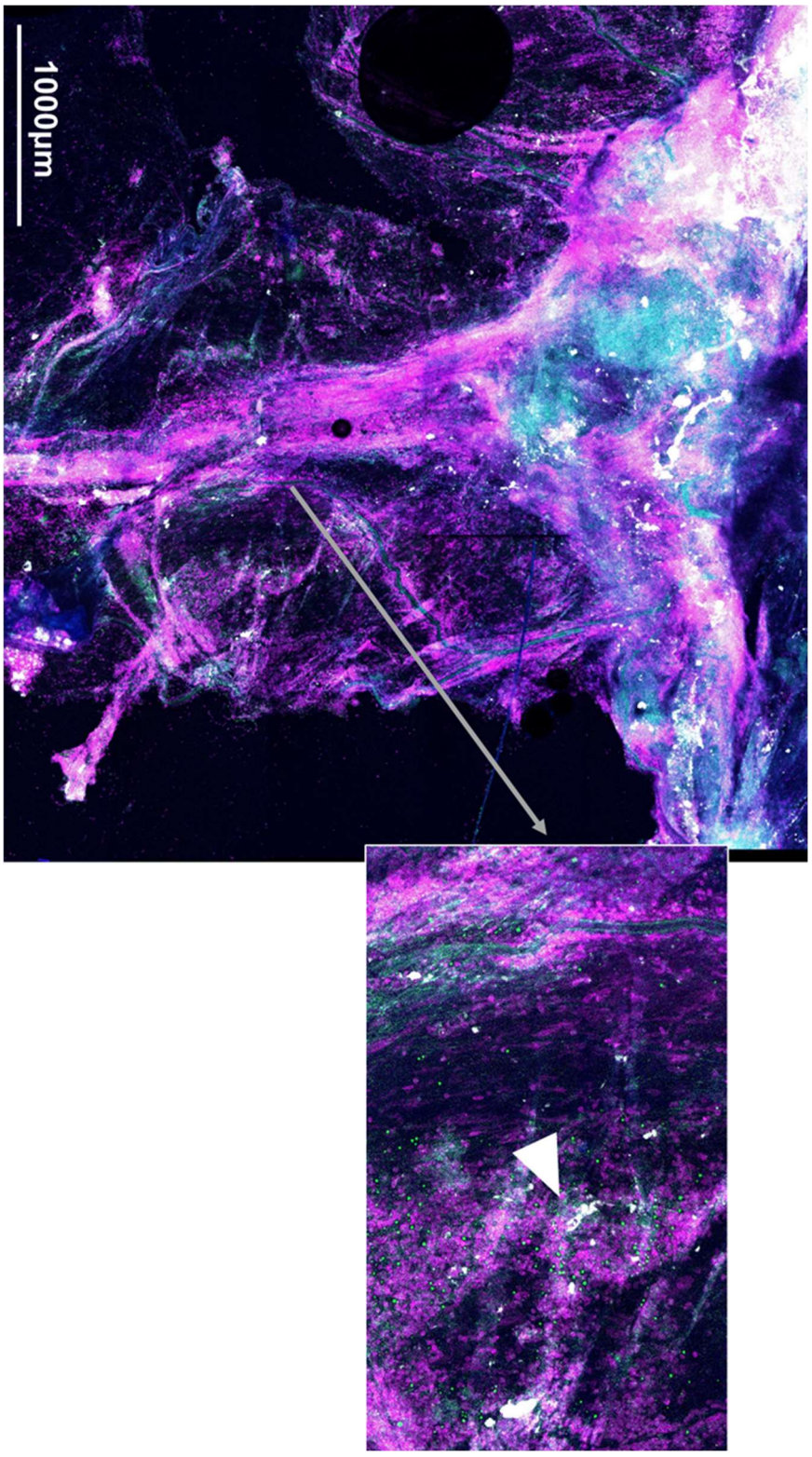


**Figure 4.23. Meningeal whole-mount imaging of the meninges at day 8 post-infection in C1q knockout mice** Image taken at 10X on the LSM880 confocal. Staining for CD45-APC, CD41-PE and GFP-*C. neoformans* shown. Arrows indicate fungal lesions.

## 4.10 Discussion

In this chapter, I have explored the inflammatory response to *C. neoformans* infection in the meninges, a tissue that has not been studied extensively despite its anatomical relevance to meningitis. Using bulk RNA-sequencing, I was able to analyse the overall transcriptomic changes in the meninges, which surprisingly showed no changes in early infection, but significant changes at day 6 and in late infection. Intravital imaging studies of this infection in the brain have found that fungi appear in the brain vasculature within minutes of infection and are arrested in the capillaries within 60 minutes[234]. In this study, a large number of yeasts was injected intravenously (a minimum of $1x10^6$ yeasts), whereas in my studies I injected $2x10^4$ yeast, thus in our model arrival in the CNS may be delayed. However, previous work in the Drummond lab has shown fungi are present in the brain at day 3 post-infection through CFU analysis, albeit at low numbers. It is therefore likely that the fungus is present in the meninges at day 3, thus the lack of genetic changes is suggestive of an immunosuppressive capability of the fungus. Future studies to corroborate this would be to perform meningeal whole mount imaging at the day 3 time point, and CFU analysis of the meninges over the course of infection to confirm whether genetic changes correlate with increasing fungal burden in the meninges. Another limitation of my current work in that I have only used an intravenous infection model. Whether an intranasal infection model would have a similar meningeal response is unknown, and as previously discussed in chapter 3, the fungus may enter the brain through the olfactory bulb in this model which may bypass the meninges.

A potential flaw of the intravital studies done thus far is the model requires thinning and removal of a small section of the skull, allowing imaging of the pia mater and the superficial brain vasculature [234]. This process therefore removes the dural and subarachnoid layers of the meninges. Whether this disrupts the meninges vasculature, and how this might

affect dissemination to the brain, is unknown. For my work, keeping the meninges intact is vital, thus intravital studies would ideally be performed using an alternative model. Other models have been explored, such as thinning of the skull without removing a section of the skull, or establishing a chronic brain window by insertion of a small coverslip, to enable recovery of the tissue prior to beginning the experiment and subsequent imaging of the same mouse across several time points[260]. Intravital imaging could provide valuable data on platelet and vascular interactions during cryptococcal meningitis, however this was beyond the scope of the current project due to the time and complexity of establishing the model.

The meningeal immunology field is increasingly moving towards considering the individual layers of the meninges as uniquely adapted for specific functions and respond differently to inflammatory stimuli[261]. For example, tissue-resident macrophages in the dural and subarachnoid layers have different renewal capacity and origin [261], and in *Trypanosoma brucei* infection, the parasite was found to be almost exclusively located in the dural layer[262]. The meningeal whole mounts I generated in this study will largely be formed of the dural layer, in line with similar published studies[263]. Other groups have been developed techniques to dissect the individual layers, including removal of the pia from the brain surface, and have performed analysis on specific regions within each layer[264], however this was beyond the scope of my study as it requires specialist training to master the dissection techniques. Further, our understanding of meningeal anatomy is still evolving, evidenced by the recent studies on skull bone marrow meningeal channels and a study that has suggested the subarachnoid space is composed of two layers[218,219,265]. Future work could however explore the other meningeal layers in more detail in the context of cryptococcal meningitis.

In this study, I identified the formation of lesions containing fungi, CD45+ cells and platelets as a key immune phenotype of the meningeal immune response. Further work is needed to determine the identity of the CD45+ cells in these lesions, albeit their rounded shape is indicative of them being monocytes or neutrophils. A recent study using an *in vivo* model of chronic *Trypanosoma brucei* infection found that ectopic lymphoid aggregates developed in the dural meninges, which are structures that resemble the germinal centres found in secondary lymphoid organs such as lymph nodes[263]. It would therefore be interesting to explore the lymphocyte response in the meninges during cryptococcal meningitis and whether the immune lesions I have identified have any components of ectopic lymphoid aggregates such as B cells, for example imaging whole mounts with markers such as B220. Another phenomenon to consider in my model is immuno-thrombosis. This is a mechanism where in the immune response to inflammatory stimuli such as infection, platelets, immune cells and coagulation factors aggregate to form a thrombus[266]. It was initially proposed that these immune thrombi would allow for pathogens to be trapped, however more recent studies have challenged this theory, for example in *Salmonella Typhimurium* infection *in vivo*, the spleen and liver contain many clots, but these thrombi contain very few bacteria[267]. In my data I see clotting occurring in the infected meninges, however these clots are sterile and are not apparently involved in 'trapping' the fungus, therefore they may be driven by other inflammatory signalling.

It is not clear whether the immune lesions seen in my data are beneficial or detrimental to the immune response to *C. neoformans*. However, the data from C3 knockout mice, in which the meninges appear almost sterile, and the fungal burdens are increased, would indicate that the lesions may be protective. For example, the lesions may contain the fungus to the meninges in a C3-dependent manner, thus in knockout mice more fungus is able to disseminate from the meninges to the brain. A previous study found that removal of arrested *C. neoformans* by neutrophils in the brain capillaries requires C3 deposition[233].

*In vitro* live cell imaging has further shown that neutrophil phagocytosis of *C. neoformans* requires the complement proteins C3 and C5a[268]. Another *in vivo* intravital imaging study used *Trypanosoma brucei* to study complement interactions by Kupffer cells (the tissue resident macrophages in the liver) and found that C3 deposition was vital for parasite capture and removal from the vasculature by Kupffer cells, mediated by the complement receptor CRIg[269].

Another theory is that C3 is required for lesion formation through its effect on platelet function. My data indicates that in the C3 knockout mice, platelet clotting is dysfunctional and therefore haemorrhaging occurs, reflecting a severe clinical manifestation of meningitis. Previous studies in C3 knockout mice have shown dysfunction in platelet clotting[270], which may explain the bleeding seen in my data. In human influenza infection, C3 has previously been shown to be released from platelet granules, which in turn drives neutrophil NETosis[271]. The immune lesions observed in my data could be the result of NETosis, and thereby the lack of C3 in the knockout mice would prevent platelet-driven neutrophil NET formation. However, other platelet-derived factors such as CXCL4 have also been shown to drive NETosis[272].

Early work in the *C. neoformans* field identified C1q as a potent opsonin for uptake of the fungus by monocytes[273]. Further, levels of C1q are elevated in the CSF of a subset of cryptococcal meningitis patients[274]. In my data, C1q proteins are elevated at late infection but not at day 6, thus presenting a role for C1q in late infection. Imaging analysis showed that at day 8 post-infection the meninges of C1q knockout mice contained large immune lesions and significant recruitment of rounded CD45+ cells. This aligns with a recent study of pulmonary *C. neoformans* infection in C1qa knockout mice, in which the knockout resulted in increased fungal burdens and pro-inflammatory cytokines in the lung[275], however another study showed no changes in lung fungal burden, albeit the knockout

mice did have increased pro-inflammatory cytokine signalling and neutrophil infiltration[259]. Whilst our lab did not see an increase in fungal burden in the brain at day 6, a future experiment would be to test this at late infection. It is possible that C1q is important for controlling the pro-inflammatory response, and therefore in the knockout mice excessive inflammation is seen. A role for C1q in clotting has also been explored, as C1q can interact with von-Willebrand factor and C1q knockout mice have reduced platelet aggregation[276]. My imaging data showed that at day 6, the meninges of C1q knockout mice appeared to have reduced platelet staining, therefore these mice may have delayed platelet recruitment, as at day 8 platelet staining was more apparent and could be seen within immune lesions. Quantification of images from WT and complement knockout mice is ongoing, which will confirm whether the differences described here are statistically significant.

To conclude, in this chapter I have begun to describe what happens in the meninges during cryptococcal meningitis, identifying significant platelet recruitment and clotting and the formation of inflammatory lesions that contain fungi and leukocytes. The complement proteins C1q and C3 have significant but differential roles in the meningeal immune response, and further work is needed to fully decipher these mechanisms.

# Chapter 5: Discussion

In this thesis I have explored the diversity and function of the CNS-specific innate immune response to a fungal pathogen. *Cryptococcus neoformans* is the major cause of fungal meningitis globally and is the top WHO priority fungal pathogen[14]. Whilst the main at-risk population for cryptococcal meningitis continues to be HIV/AIDS patients, the growing use of immune-modulating drugs is driving the emergence of new underlying risk factors for this disease[6]. Whilst a handful of anti-fungal drugs are available, these are not adequate to provide treatment, as (1) they are expensive and can have serious side-effects (2) there anti-fungal resistance is increasing (3) they do not prevent fungal infections[277]. Furthermore, conditions like C-IRIS show that even when the fungus is cleared, inflammatory disease can still occur[38], thus targeting the immune response in addition to the fungus itself could be more effective.

Whilst Th1 responses have been identified as beneficial in resolving *C. neoformans* infection, the lack of functional T cell responses in at-risk populations such as HIV/AIDS patients means immunotherapies may need to target other immune cell populations[278]. There is much to learn about the innate immune response to fungal infections, particularly within the tissues. Furthermore, despite the sophisticated borders in the brain, how a relatively large organism such as *C. neoformans* can overcome the resident immune cells which provide the first line of defence and disseminate to the brain is unknown. A major area of research in the neuroimmunology field is the heterogeneity of tissue-resident macrophages in the CNS. Elegant single-cell RNA-sequencing studies have enabled recent advances in this area, as sequencing analysis overcomes the difficulties of poorly defined and overlapping markers for the CNS myeloid populations. Studies have shown microglia form functional subsets depending on the inflammatory context, such as ageing

and neurodegenerative disease[184]. However, less is known about what happens in the context of infection.

The main focus of my thesis was to determine the heterogeneity of myeloid cells in an *in vivo* model of cryptococcal meningitis. Using single-cell RNA-sequencing, flow cytometry and functional assays I determined that microglial responses in *C. neoformans* infection are critically delayed, and that a unique population of microglia arises in infection which likely provides an intracellular niche for the fungus. This population, which we have termed infection-associated microglia (IAM), expresses receptors that have previously been shown to be involved in macrophage phagocytosis, namely GPR84 and MSR1. In this thesis I have begun to explore the function of these receptors in microglia by developing *in vitro* assays. Microglial proliferation increases exponentially at late infection coinciding with the onset of lethal inflammation, and this largely occurs in the IAMs population. Furthermore, the IAMs are likely involved in interactions with lymphocytes, as lymphocyte deficient mice lack the IAMs expansion at late infection.

IAMs as a host for intracellular fungi aligns with previous work from our lab showing *C. neoformans* uses microglia as a nutrient source of copper[135]. Further work is needed to understand how killing of the fungus by microglia is prevented once the fungus is phagocytosed. However, my current work has shown that IAMs upregulate Arginase, which metabolises arginine to urea and is associated with an M2 phenotype, as opposed to arginine metabolism by iNOS which results in the production of ROS which can be used to kill pathogens. This result was somewhat surprising given the number of IFN-γ regulated genes upregulated in the IAMs population, as IFN-γ signalling drives M1 responses. However, work in the macrophage field has already established that the M1/M2 paradigm is a spectrum, and to what extent microglia fit into this paradigm is being debated[279,280]. Work by the Drummond lab has also established that CD4 T cells are the

main source of IFN-γ in the brain, and the importance of this signalling in the establishment of IAMs is shown by our Rag2$^{-/-}$ data, where mice lacking lymphocytes did not have the proliferation of IAMs at late infection and there was a significant reduction in the intracellular fungi in IAMs. This latter result could be attributed to the lack of antibody responses in Rag2$^{-/-}$ mice, as opsonisation of the fungus promotes phagocytosis, so specific studies of CD4 depletion are needed. We also surprisingly observed a reduction in inflammatory monocyte recruitment in Rag2$^{-/-}$ mice. Our understanding of innate immune responses preceding adaptive immunity led us to assume that monocytes would arrive from the periphery to the brain first before recruiting T cells, however it seems instead that lymphocytes are required for the recruitment of monocytes. Furthermore, no significant differences in IAMs numbers were seen in the Rag2$^{-/-}$ mice at day 6 post-infection. Our current model is that *C. neoformans* entry into the CNS initially drives the formation of IAMs, with later recruitment of lymphocytes and the increasing inflammatory signalling in the brain driving the maintenance and expansion of IAMs. Inflammatory myeloid cells, including monocytes and macrophages, signal to recruit T cells to the brain, which in turn recruit further monocytes, driving a positive feedback loop.

In this thesis I have described the immune response in the tissue adjacent to the brain parenchyma, the meninges, in cryptococcal meningitis. Both RNA-seq data sets showed that responses to *C. neoformans* are delayed. Imaging analysis in both the brain and the meninges showed the fungi mostly localised to large lesions. It would be an interesting future experiment to perform light-sheet imaging analysis of the whole brain and skull to determine whether the lesions in the meninges are connected to those in the brain parenchyma. The sequencing analysis of the meninges revealed several genes involved in the extracellular matrix were altered during infection, therefore it may be possible that the physical barriers between the meninges and the brain is degraded by fungal infection.

The dynamics of the interaction between the brain and the meninges is still to be determined, in addition to exploring other brain borders such as the choroid plexus and perivascular spaces. As previously discussed, there are three main hypotheses regarding how the fungus arrives in the brain, one of which being the Trojan horse model of monocytes containing fungi disseminating from the lung and arriving in the brain where the fungi can escape[72]. However, it has also been shown that the skull bone marrow contains channels that connect it to the meninges and brain[218,219], and the skull bone marrow is a local source of monocytes for the brain, along with those derived from peripheral blood[281–284]. At day 6 post-infection, we see recruitment of inflammatory monocytes in the brain, and this is reduced in the Rag2$^{-/-}$ mice, however whether there are specific effects on peripheral or skull bone marrow derived macrophages is unknown. Applying the meningeal whole mount analysis to the Rag2$^{-/-}$ mice would begin to address this. It is clear from the present study that considering both lymphoid and myeloid responses is vital to developing an appropriate treatment strategy for *C. neoformans*, along with considering individual patient backgrounds.

In this thesis I also explored the role of complement signalling in cryptococcal meningitis. Whilst the Rag2$^{-/-}$ mouse data shows the importance of antibody opsonisation in promoting fungal uptake, opsonisation of the fungus can also occur through complement signalling, independent of lymphocytes, therefore this may explain why fungal uptake was completely eradicated in the Rag2$^{-/-}$ mice (along with uptake that occurs independently of opsonisation). Signalling by C1q and C3 has been shown to play a significant role in brain homeostasis and development by regulating synaptic pruning by microglia, and therefore elevation of these proteins is associated with neurodegeneration[285,286]. Microglia are the major expressors of the complement receptor CR3 in the brain, and microglial activation has been shown to increase CR3 expression thus driving phagocytosis by microglia[285,286]. Furthermore, microglia are the main producers of C1q in the brain[287]. It would therefore be

an interesting future study to determine the effects downstream of the meninges in the brain parenchyma of the C1q and C3 knockouts, such as whether microglial populations are altered in *C. neoformans* infection.

The study of the role of pathways such as the complement cascade is important to determine what regulates the activation, fungal uptake and killing by CNS macrophages. For example, in the present study I have identified the IAMs subset as a likely intracellular niche for the fungi, but treatment with anti-fungal drugs would likely only target extracellular fungi and therefore total elimination of the fungus may not be achieved. Understanding the mechanisms of IAMs signalling, such as how these cells are prevented from killing the fungi, could lead to the development of immune therapies to promote fungal killing by macrophages in the brain. This could therefore provide an adjunctive therapy for cryptococcal meningitis, whereby multiple immune-modulating drugs are used to treat the disease.

In summary, I have found extensive myeloid heterogeneity and host-fungal interactions occurring in the CNS mediated by pro-inflammatory cytokine signalling, phagocytic receptors, and lymphocyte recruitment. This work provides critical new advances for the field and lays groundwork for future studies aiming to understand how to prevent fungal dissemination into the brain and fungal immune escape, and how to target the fungus effectively with immunotherapy.

# References


1. Hain, S. & Drummond, R. A. Immunity to Fungal Infections. in *Encyclopedia of Infection and Immunity* (ed. Rezaei, N.) 445–461 (Elsevier, Oxford, 2022). doi:https://doi.org/10.1016/B978-0-12-818731-9.00102-6.

2. White, T. C. *et al.* Fungi on the skin: Dermatophytes and malassezia. *Cold Spring Harb Perspect Med* **4**, (2014).

3. Brown, G. D. *et al.* Hidden killers: Human fungal infections. *Science Translational Medicine* vol. 4 165rv13-165rv13 Preprint at https://doi.org/10.1126/scitranslmed.3004404 (2012).

4. Bongomin, F., Gago, S., Oladele, R. O. & Denning, D. W. Global and multi-national prevalence of fungal diseases – estimate precision. *Journal of Fungi* vol. 3 57 Preprint at https://doi.org/10.3390/jof3040057 (2017).

5. Denning, D. W. Global incidence and mortality of severe fungal disease. *Lancet Infect Dis* **0**, (2024).

6. Clark, C. & Drummond, R. The Hidden Cost of Modern Medical Interventions: How Medical Advances Have Shaped the Prevalence of Human Fungal Disease. *Pathogens* **8**, 45 (2019).

7. van Arkel, A. L. E. *et al.* COVID-19-associated pulmonary aspergillosis. *American Journal of Respiratory and Critical Care Medicine* vol. 202 132–135 Preprint at https://doi.org/10.1164/rccm.202004-1038LE (2020).

8. Lanternier, F. *et al.* Primary immunodeficiencies underlying fungal infections. *Current Opinion in Pediatrics* vol. 25 736–747 Preprint at https://doi.org/10.1097/MOP.0000000000000031 (2013).

9. Kozel, T. R. & Wickes, B. Fungal diagnostics. *Cold Spring Harb Perspect Med* **4**, (2014).

10. Benedict, K., Richardson, M., Vallabhaneni, S., Jackson, B. R. & Chiller, T. Emerging issues, challenges, and changing epidemiology of fungal disease outbreaks. *The Lancet Infectious Diseases* vol. 17 e403–e411 Preprint at https://doi.org/10.1016/S1473-3099(17)30443-7 (2017).

11. Rodrigues, M. L. & Albuquerque, P. C. Searching for a change: The need for increased support for public health and research on fungal diseases. *PLoS Negl Trop Dis* **12**, (2018).

12. Sabino, R., Veríssimo, C., Pereira, Á. A. & Antunes, F. Candida auris, an agent of hospital-associated outbreaks: Which challenging issues do we need to have in mind? *Microorganisms* vol. 8 Preprint at https://doi.org/10.3390/microorganisms8020181 (2020).

13. Lionakis, M. S., Iliev, I. D. & Hohl, T. M. Immunity against fungi. *JCI insight* vol. 2 Preprint at https://doi.org/10.1172/jci.insight.93156 (2017).

14. Fisher, M. C. & Denning, D. W. The WHO fungal priority pathogens list as a game-changer. **21**, (2023).

15. Coelho, C., Bocca, A. L. & Casadevall, A. The Intracellular Life of Cryptococcus neoformans. (2013) doi:10.1146/annurev-pathol-012513-104653.

16. Lin, X. & Heitman, J. The Biology of the Cryptococcus neoformans Species Complex. (2006) doi:10.1146/annurev.micro.60.080805.142102.

17. Temfack, E. *et al.* New Insights Into Cryptococcus Spp. Biology and Cryptococcal Meningitis. (1910) doi:10.1007/s11910-019-0993-0.

18. Hagen, F. *et al.* Importance of Resolving Fungal Nomenclature: the Case of Multiple Pathogenic Species in the Cryptococcus Genus . *mSphere* **2**, (2017).

19. Desnos-Ollivier, M., Patel, S., Raoux-Barbot, D., Heitman, J. & Dromer, F. Cryptococcosis serotypes impact outcome and provide evidence of Cryptococcus neoformans speciation. *mBio* **6**, (2015).

20. Cristina Francisco Auke de Jong Ferry Hagen, E. W. Cryptococcosis and Cryptococcus. *Mycopathologia* **186**,.

21. May, R. C., Stone, N. R., Wiesner, D. L., Bicanic, T. & Nielsen, K. Cryptococcus: from environmental saprophyte to global pathogen. *Nature Publishing Group* (2016) doi:10.1038/nrmicro.2015.6.

22. Library, W. O. & Barnett, J. A. A history of research on yeasts 14:1 medical yeasts part 2, Cryptococcus neoformans. *Yeast* **27**, 875–904 (2010).

23. Setianingrum, F., Rautemaa-Richardson, R. & Denning, D. W. Pulmonary cryptococcosis: A review of pathobiology and clinical aspects. *Med Mycol* **57**, 133–150 (2019).

24. Salazar, A. S. *et al.* Potential missed opportunities for diagnosis of cryptococcosis and the association with mortality: A cohort study. *EClinicalMedicine* **27**, (2020).

25. Williamson, P. R. *et al.* Cryptococcal meningitis: epidemiology, immunology, diagnosis and therapy. *Nat Rev Neurol* **13**, (2016).

26. Pasquier, E. *et al.* Long-term Mortality and Disability in Cryptococcal Meningitis: A Systematic Literature Review. *Clinical Infectious Diseases 1122 • CID* **2018**, 66 (2018).

27. Hevey, M. A. *et al.* Mortality Following Cryptococcal Infection in the Modern Antiretroviral Therapy Era. doi:10.1097/QAI.0000000000002095.

28. Sloan, D. J. & Parris, V. Cryptococcal meningitis: Epidemiology and therapeutic options. *Clinical Epidemiology* vol. 6 169–182 Preprint at https://doi.org/10.2147/CLEP.S38850 (2014).

29. Rajasingham, R. *et al.* Cryptococcal meningitis diagnostics and screening in the era of point-of-care laboratory testing. *J Clin Microbiol* **57**, (2019).

30. Anjum, S. H. *et al.* Neuroimaging of Cryptococcal Meningitis in Patients without Human Immunodeficiency Virus: Data from a Multi-Center Cohort Study. *Journal of Fungi* **9**, (2023).

31. Lee, W.-J. *et al.* Enlarged periventricular space and periventricular lesion extension on baseline brain MRI predicts poor neurological outcomes in cryptococcus meningoencephalitis. *Scientific Reports* | **11**, 6446 (123AD).

32. Xu, J. *et al.* Chemokine receptor CXCR3 is required for lethal brain pathology but not pathogen clearance during cryptococcal meningoencephalitis. *Sci. Adv* **6**, 2502–2519 (2020).

33. Dromer, F. *et al.* Epidemiology of HIV-associated cryptococcosis in France (1985-2001): comparison of the pre- and post-HAART eras. *AIDS* **18**, 555–562 (2004).

34. Temfack, E. *et al.* New Insights Into Cryptococcus Spp. Biology and Cryptococcal Meningitis. (1910) doi:10.1007/s11910-019-0993-0.

35. Williamson, P. R. *et al.* Cryptococcal meningitis: epidemiology, immunology, diagnosis and therapy. *Nat Rev Neurol* **13**, (2016).

36. Rezai, M. S. *et al.* Cryptococcosis and Deficiency of Interleukin12r. *Pediatr Infect Dis J* **27**, (2008).

37. Kawano, T. *et al.* T cell infiltration into the brain triggers pulmonary dysfunction in murine Cryptococcus-associated IRIS. doi:10.1038/s41467-023-39518-x.

38. Haddow, L. J. *et al.* Cryptococcal Immune Reconstitution Inflammatory Syndrome in HIV-1-infected individuals: Literature Review and Proposed Clinical Case Definitions. *Lancet Infect Dis* **10**, 791–802 (2010).

39. Salazar, F. & Brown, G. D. Antifungal Innate Immunity: A Perspective from the Last 10 Years. *Journal of Innate Immunity* vol. 10 373–397 Preprint at https://doi.org/10.1159/000488539 (2018).

40. Patin, E. C., Thompson, A. & Orr, S. J. Pattern recognition receptors in fungal immunity. *Seminars in Cell and Developmental Biology* vol. 89 24–33 Preprint at https://doi.org/10.1016/j.semcdb.2018.03.003 (2019).

41. Speakman, E. A., Dambuza, I. M., Salazar, F. & Brown, G. D. T Cell Antifungal Immunity and the Role of C-Type Lectin Receptors. *Trends in Immunology* vol. 41 61–76 Preprint at https://doi.org/10.1016/j.it.2019.11.007 (2020).

42. Zelensky, A. N. & Gready, J. E. The C-type lectin-like domain superfamily. *FEBS Journal* **272**, 6179–6217 (2005).

43. Drummond, R. A., Franco, L. M. & Lionakis, M. S. Human CARD9: A critical molecule of fungal immune surveillance. *Frontiers in Immunology* vol. 9 1836 Preprint at https://doi.org/10.3389/fimmu.2018.01836 (2018).

44. Lanternier, F. *et al.* Inherited CARD9 deficiency in otherwise healthy children and adults with Candida species-induced meningoencephalitis, colitis, or both. *Journal of Allergy and Clinical Immunology* **135**, 1558-1568.e2 (2015).

45. Rieber, N. *et al.* Extrapulmonary Aspergillus infection in patients with CARD9 deficiency. *JCI Insight* **1**, (2016).

46. Hu, X.-P. *et al.* Dectin-2 polymorphism associated with pulmonary cryptococcosis in HIV-uninfected Chinese patients. *Med Mycol* **53**, 810–816 (2015).

47. Kawasaki, T. & Kawai, T. Toll-like receptor signaling pathways. *Frontiers in Immunology* vol. 5 461 Preprint at https://doi.org/10.3389/fimmu.2014.00461 (2014).

48. Von Bernuth, H. *et al.* Pyogenic bacterial infections in humans with MyD88 deficiency. *Science (1979)* **321**, 691–696 (2008).

49. Moyes, D. L. *et al.* Candidalysin is a fungal peptide toxin critical for mucosal infection. *Nature* **532**, 64–68 (2016).

50. Kasper, L. *et al.* The fungal peptide toxin Candidalysin activates the NLRP3 inflammasome and causes cytolysis in mononuclear phagocytes. *Nat Commun* **9**, 1–20 (2018).

51. Drummond, R. A. *et al.* CARD9 + microglia promote antifungal immunity via IL-1β- and CXCL1-mediated neutrophil recruitment. *Nat Immunol* (2019) doi:10.1038/s41590-019-0377-2.

52. Briard, B. *et al.* Galactosaminogalactan activates the inflammasome to provide host protection. *Nature* **588**, 688–692 (2020).

53. Epelman, S., Lavine, K. J. & Randolph, G. J. Origin and Functions of Tissue Macrophages. *Immunity* vol. 41 21–35 Preprint at https://doi.org/10.1016/j.immuni.2014.06.013 (2014).

54. Gordon, S. & Plüddemann, A. Tissue macrophages: Heterogeneity and functions. *BMC Biology* vol. 15 1–18 Preprint at https://doi.org/10.1186/s12915-017-0392-4 (2017).

55. Wynn, T. A., Chawla, A. & Pollard, J. W. Macrophage biology in development, homeostasis and disease. *Nature* vol. 496 445–455 Preprint at https://doi.org/10.1038/nature12034 (2013).

56. Martinez, F. O. & Gordon, S. The M1 and M2 paradigm of macrophage activation: Time for reassessment. *F1000Prime Rep* **6**, (2014).

57. Italiani, P. & Boraschi, D. From monocytes to M1/M2 macrophages: Phenotypical vs. functional differentiation. *Frontiers in Immunology* vol. 5 514 Preprint at https://doi.org/10.3389/fimmu.2014.00514 (2014).

58. Becker, K. L., Ifrim, D. C., Quintin, J., Netea, M. G. & van de Veerdonk, F. L. Antifungal innate immunity: recognition and inflammatory networks. *Seminars in Immunopathology* vol. 37 107–116 Preprint at https://doi.org/10.1007/s00281-014-0467-z (2015).

59. Brown, G. D. Innate antifungal immunity: The key role of phagocytes. *Annu Rev Immunol* **29**, 1–21 (2011).

60. Warris, A. & Ballou, E. R. Oxidative responses and fungal infection biology. *Seminars in Cell and Developmental Biology* vol. 89 34–46 Preprint at https://doi.org/10.1016/j.semcdb.2018.03.004 (2019).

61. Rath, M., Müller, I., Kropf, P., Closs, E. I. & Munder, M. Metabolism via arginase or nitric oxide synthase: Two competing arginine pathways in macrophages. *Frontiers in Immunology* vol. 5 Preprint at https://doi.org/10.3389/fimmu.2014.00532 (2014).

62. Hardison, S. E. *et al.* Protective Immunity against Pulmonary Cryptococcosis Is Associated with STAT1-Mediated Classical Macrophage Activation. *The Journal of Immunology* **189**, 4060–4068 (2012).

63. Wager, C. M. L. *et al.* STAT1 signaling within macrophages is required for antifungal activity against Cryptococcus neoformans. *Infect Immun* **83**, 4513–4527 (2015).

64. Leopold Wager, C. M., Hole, C. R., Wozniak, K. L. & Wormley, F. L. Cryptococcus and phagocytes: Complex interactions that influence disease outcome. *Frontiers in Microbiology* vol. 7 105 Preprint at https://doi.org/10.3389/fmicb.2016.00105 (2016).

65. Hole, C. & Wormley, F. L. Innate host defenses against Cryptococcus neoformans. *Journal of Microbiology* **54**, 202–211 (2016).

66. Rosen, L. B. *et al.* Anti-granulocyte-macrophage colony stimulating factor autoantibodies in patients with cryptococcal meningitis. *J Immunol* **190**, 3959 (2013).

67. Borie, R. *et al.* Pulmonary alveolar proteinosis. *European Respiratory Review* **20**, 98–107 (2011).

68. Sun, D. *et al.* Fungal dissemination is limited by liver macrophage filtration of the blood. *Nat Commun* **10**, 1–14 (2019).

69. Osterholzer, J. J. *et al.* Role of dendritic cells and alveolar macrophages in regulating early host defense against pulmonary infection with Cryptococcus neoformans. *Infect Immun* **77**, 3749–3755 (2009).

70. Charlier, C. *et al.* Evidence of a role for monocytes in dissemination and brain invasion by Cryptococcus neoformans. *Infect Immun* **77**, 120–127 (2009).

71. Drummond, R. A. Neuro-immune mechanisms of anti-cryptococcal protection. *Journal of Fungi* vol. 4 Preprint at https://doi.org/10.3390/jof4010004 (2018).

72. Fu, M. S. & Drummond, R. A. The diverse roles of monocytes in cryptococcosis. *Journal of Fungi* vol. 6 1–14 Preprint at https://doi.org/10.3390/jof6030111 (2020).

73. Vinh, D. C. *et al.* Autosomal dominant and sporadic monocytopenia with susceptibility to mycobacteria, fungi, papillomaviruses, and myelodysplasia. *Blood* **115**, 1519–1529 (2010).

74. Meya, D. B. *et al.* Monocyte Phenotype and IFN-γ-Inducible Cytokine Responses Are Associated with Cryptococcal Immune Reconstitution Inflammatory Syndrome. **3**, 28 (2017).

75. Heung, L. J. & Hohl, T. M. Inflammatory monocytes are detrimental to the host immune response during acute infection with cryptococcus neoformans. *PLoS Pathog* **15**, e1007627 (2019).

76. 1☯, D. S. *et al.* VCAM1/VLA4 interaction mediates Ly6C low monocyte recruitment to the brain in a TNFR signaling dependent manner during fungal infection. (2020) doi:10.1371/journal.ppat.1008361.

77. Santiago-Tirado, F. H., Onken, M. D., Cooper, J. A., Klein, R. S. & Doering, T. L. Trojan horse transit contributes to blood-brain barrier crossing of a eukaryotic pathogen. *mBio* **8**, (2017).

78. Banchereau, J. *et al.* Immunobiology of Dendritic Cells. *Annu Rev Immunol* **18**, 767–811 (2000).

79. Eisenbarth, S. C. Dendritic cell subsets in T cell programming: location dictates function. *Nature Reviews Immunology* Preprint at https://doi.org/10.1038/s41577-018-0088-1 (2019).

80. Verma, A., Wüthrich, M., Deepe, G., Klein, B. & Giri, G. Adaptive immunity to fungi. *Cold Spring Harb Perspect Med* **5**, (2015).

81. Satpathy, A. T., Wu, X., Albring, J. C. & Murphy, K. M. Re(de)fining the dendritic cell lineage. *Nature Immunology* vol. 13 1145–1154 Preprint at https://doi.org/10.1038/ni.2467 (2012).

82. Bauman, S. K., Nichols, K. L. & Murphy, J. W. Dendritic Cells in the Induction of Protective and Nonprotective Anticryptococcal Cell-Mediated Immune Responses. *The Journal of Immunology* **165**, 158–167 (2000).

83. Osterholzer, J. J. *et al.* Role of Dendritic Cells and Alveolar Macrophages in Regulating Early Host Defense against Pulmonary Infection with Cryptococcus neoformans. *Infect Immun* **77**, 3749–3758 (2009).

84. Netea, M. G. *et al.* Trained immunity: A program of innate immune memory in health and disease. *Science (1979)* **352**, aaf1098–aaf1098 (2016).

85. Hole, C. R. *et al.* Induction of memory-like dendritic cell responses in vivo. doi:10.1038/s41467-019-10486-5.

86. Desai, J. V. & Lionakis, M. S. The Role of Neutrophils in Host Defense Against Invasive Fungal Infections. *Current Clinical Microbiology Reports* vol. 5 181–189 Preprint at https://doi.org/10.1007/s40588-018-0098-6 (2018).

87. Rosales, C. Neutrophil: A cell with many roles in inflammation or several cell types? *Frontiers in Physiology* vol. 9 113 Preprint at https://doi.org/10.3389/fphys.2018.00113 (2018).

88. Urban, C. F. & Nett, J. E. Neutrophil extracellular traps in fungal infection. *Seminars in Cell and Developmental Biology* vol. 89 47–57 Preprint at https://doi.org/10.1016/j.semcdb.2018.03.020 (2019).

89. Mambula, S. S., Simons, E. R., Hastey, R., Selsted, M. E. & Levitz, S. M. Human neutrophil-mediated nonoxidative antifungal activity against Cryptococcus neoformans. *Infect Immun* **68**, 6257–6264 (2000).

90. Aratani, Y. *et al.* Contribution of the myeloperoxidase-dependent oxidative system to host defence against Cryptococcus neoformans. *J Med Microbiol* **55**, 1291–1299 (2006).

91. Sun, D. *et al.* Real-time imaging of interactions of neutrophils with Cryptococcus neoformans demonstrates a crucial role of complement C5a-C5aR signaling. *Infect Immun* **84**, 216–229 (2015).

92. Zhang, M. *et al.* Real-time in vivo imaging reveals the ability of neutrophils to remove Cryptococcus neoformans directly from the brain vasculature. (2015) doi:10.1189/jlb.4AB0715-281R.

93. Mednick, A. J., Feldmesser, M., Rivera, J. & Casadevall, A. Neutropenia alters lung cytokine production in mice and reduces their susceptibility to pulmonary cryptococcosis. *Eur J Immunol* **33**, 1744–1753 (2003).

94. Wozniak, K. L., Kolls, J. K. & Wormley, F. L. Depletion of neutrophils in a protective model of pulmonary cryptococcosis results in increased IL-17A production by gamma/delta T cells. *BMC Immunol* **13**, 1 (2012).

95. Schmidt, S., Tramsen, L. & Lehrnbecher, T. Natural killer cells in antifungal immunity. *Frontiers in Immunology* vol. 8 22 Preprint at https://doi.org/10.3389/fimmu.2017.01623 (2017).

96. Pegram, H. J., Andrews, D. M., Smyth, M. J., Darcy, P. K. & Kershaw, M. H. Activating and inhibitory receptors of natural killer cells. *Immunology and Cell Biology* vol. 89 216–224 Preprint at https://doi.org/10.1038/icb.2010.78 (2011).

97. Li, S. S. *et al.* The NK receptor NKp30 mediates direct fungal recognition and killing and is diminished in NK cells from HIV-infected patients. *Cell Host Microbe* **14**, 387–397 (2013).

98. Tupin, E., Kinjo, Y. & Kronenberg, M. The unique role of natural killer T cells in the response to microorganisms. *Nature Reviews Microbiology* vol. 5 405–417 Preprint at https://doi.org/10.1038/nrmicro1657 (2007).

99. Kawakami, K. *et al.* Activation of Vα14+ natural killer T cells by α-galactosylceramide results in development of Th1 response and local host resistance in mice infected with Cryptococcus neoformans. *Infect Immun* **69**, 213–220 (2001).

100. Kawakami, K. *et al.* Monocyte Chemoattractant Protein-1-Dependent Increase of Vα14 NKT Cells in Lungs and Their Roles in Th1 Response and Host Defense in Cryptococcal Infection. *The Journal of Immunology* **167**, 6525–6532 (2001).

101. Templeton, S. *et al.* immunology of Cryptococcal infections: Developing a Rational Approach to Patient Therapy. **9**, 651 (2018).

102. Mukaremera, L. & Nielsen, K. Adaptive Immunity to Cryptococcus neoformans Infections. doi:10.3390/jof3040064.

103. Drummond, R. A., Gaffen, S. L., Hise, A. G. & Brown, G. D. Innate defense against fungal pathogens. *Cold Spring Harb Perspect Med* **5**, 1–19 (2015).

104. Jarvis, J. N. *et al.* Adjunctive interferon-γ immunotherapy for the treatment of HIV-associated cryptococcal meningitis: A randomized controlled trial. *AIDS* **26**, 1105–1113 (2012).

105. Chen, G. H. *et al.* The gamma interferon receptor is required for the protective pulmonary inflammatory response to Cryptococcus neoformans. *Infect Immun* **73**, 1788–1796 (2005).

106. Wiesner, D. L. *et al.* Chitin Recognition via Chitotriosidase Promotes Pathologic Type-2 Helper T Cell Responses to Cryptococcal Infection. *PLoS Pathog* **11**, 1–28 (2015).

107. Vignali, D. A. A., Collison, L. W. & Workman, C. J. How regulatory T cells work. *Nature Reviews Immunology* vol. 8 523–532 Preprint at https://doi.org/10.1038/nri2343 (2008).

108. Sato, K. *et al.* Production of IL-17A at Innate Immune Phase Leads to Decreased Th1 Immune Response and Attenuated Host Defense against Infection with Cryptococcus deneoformans. *The Journal of Immunology* **205**, 686–698 (2020).

109. Eschke, M. *et al.* A novel experimental model of Cryptococcus neoformans-related immune reconstitution inflammatory syndrome (IRIS) provides insights into pathogenesis. *Eur J Immunol* **45**, 3339–3350 (2015).

110. Neal, L. M. *et al.* Cd4+ T cells orchestrate lethal immune pathology despite fungal clearance during cryptococcus neoformans meningoencephalitis. *mBio* **8**, (2017).

111. Zhang, N. & Bevan, M. J. CD8+ T Cells: Foot Soldiers of the Immune System. *Immunity* vol. 35 161–168 Preprint at https://doi.org/10.1016/j.immuni.2011.07.010 (2011).

112. Kumaresan, P. R., da Silva, T. A. & Kontoyiannis, D. P. Methods of controlling invasive fungal infections using CD8+ T cells. *Frontiers in Immunology* vol. 8 1939 Preprint at https://doi.org/10.3389/fimmu.2017.01939 (2018).

113. Buchanan, K. L. & Doyle, H. A. Requirement for CD4+ T lymphocytes in host resistance against Cryptococcus neoformans in the central nervous system of immunized mice. *Infect Immun* **68**, 456–462 (2000).

114. Huffnagle, G. B., Lipscomb, M. F., Lovchik, J. A., Hoag, K. A. & Street, N. E. The role of CD4+ and CD8+ T cells in the protective inflammatory response to a pulmonary cryptococcal infection. *J Leukoc Biol* **55**, 35–42 (1994).

115. Lindell, D. M., Moore, T. A., McDonald, R. A., Toews, G. B. & Huffnagle, G. B. Generation of Antifungal Effector CD8 + T Cells in the Absence of CD4 + T Cells during Cryptococcus neoformans Infection . *The Journal of Immunology* **174**, 7920–7928 (2005).

116. Hauser, A. E. & Höpken, U. E. B Cell Localization and Migration in Health and Disease. in *Molecular Biology of B Cells: Second Edition* 187–214 (Elsevier Inc., 2015). doi:10.1016/B978-0-12-397933-9.00012-6.

117. Cyster, J. G. & Allen, C. D. C. B Cell Responses: Cell Interaction Dynamics and Decisions. *Cell* **177**, 524–540 (2019).

118. Casadevall, A. & Pirofski, L. A. Immunoglobulins in defense, pathogenesis, and therapy of fungal diseases. *Cell Host and Microbe* vol. 11 447–456 Preprint at https://doi.org/10.1016/j.chom.2012.04.004 (2012).

119. Plebani, A. & Lougaris, V. Agammaglobulinemia. in *Stiehm's Immune Deficiencies* 329–346 (Elsevier Inc., 2014). doi:10.1016/B978-0-12-405546-9.00013-3.

120. Diniz-Lima, I. *et al.* X-linked immunodeficient (XID) mice exhibit high susceptibility to Cryptococcus gattii infection. *Scientific Reports* | **11**, 18397 (123AD).

121. Rohatgi, S. & Pirofski, L. Molecular Characterization of the Early B Cell Response to Pulmonary Cryptococcus neoformans Infection . *The Journal of Immunology* **189**, 5820–5830 (2012).

122. Subramaniam, K. S. *et al.* The Absence of Serum IgM Enhances the Susceptibility of Mice to Pulmonary Challenge with Cryptococcus neoformans . *The Journal of Immunology* **184**, 5755–5767 (2010).

123. Szymczak, W. A. *et al.* X-linked immunodeficient mice exhibit enhanced susceptibility to Cryptococcus neoformans infection. *mBio* **4**, (2013).

124. Rivera, J., Zaragoza, O. & Casadevall, A. Antibody-mediated protection against Cryptococcus neoformans pulmonary infection is dependent on B cells. *Infect Immun* **73**, 1141–1150 (2005).

125. McClelland, E. E., Nicola, A. M., Prados-Rosales, R. & Casadevall, A. Ab binding alters gene expression in Cryptococcus neoformans and directly modulates fungal metabolism. *Journal of Clinical Investigation* **120**, 1355–1361 (2010).

126. Nabavi, N. & Murphy, J. W. Antibody-dependent natural killer cell-mediated growth inhibition of Cryptococcus neoformans. *Infect Immun* **51**, 556–562 (1986).

127. Di Mambro, T., Guerriero, I., Aurisicchio, L., Magnani, M. & Marra, E. The yin and yang of current antifungal therapeutic strategies: How can we harness our natural defenses? *Frontiers in Pharmacology* vol. 10 80 Preprint at https://doi.org/10.3389/fphar.2019.00080 (2019).

128. Maliehe, M. *et al.* Environmental Factors That Contribute to the Maintenance of Cryptococcus neoformans Pathogenesis. *Microorganisms* **8**, (2020).

129. Dambuza, I. M. *et al.* The Cryptococcus neoformans Titan cell is an inducible and regulated morphotype underlying pathogenesis. *PLoS Pathog* **14**, e1006978 (2018).

130. Piccioni, M. *et al.* A purified capsular polysaccharide markedly inhibits inflammatory response during endotoxic shock. *Infect Immun* **81**, 90–98 (2013).

131. De Leon-Rodriguez, C. M., Fu, M. S., Çorbali, M. O., Cordero, R. J. B. & Casadevall, A. The Capsule of Cryptococcus neoformans Modulates Phagosomal pH through Its Acid-Base Properties . *mSphere* **3**, (2018).

132. Gilbert, A. S., Wheeler, R. T. & May, R. C. Fungal pathogens: Survival and replication within macrophages. *Cold Spring Harb Perspect Med* **5**, (2015).

133. Kawakami, K., Zhang, T., Qureshi, M. H. & Saito, A. Cryptococcus neoformans inhibits nitric oxide production by murine peritoneal macrophages stimulated with interferon-γ and lipopolysaccharide. *Cell Immunol* **180**, 47–54 (1997).

134. Santangelo, R. *et al.* Role of Extracellular Phospholipases and Mononuclear Phagocytes in Dissemination of Cryptococcosis in A Murine Model. *Infect Immun* **72**, 2229–2239 (2004).

135. Mohamed, S. H. *et al.* Microglia are not protective against cryptococcal meningitis. *Nature Communications 2023 14:1* **14**, 1–15 (2023).

136. Dang, E. V. *et al.* Secreted fungal virulence effector triggers allergic inflammation via TLR4. *Nature* **608**, 161 (2022).

137. Voelz, K., Johnston, S. A., Rutherford, J. C. & May, R. C. Automated Analysis of Cryptococcal Macrophage Parasitism Using GFP-Tagged Cryptococci. *PLoS One* **5**, 15968 (2010).

138. Maler, M. D. *et al.* Key Role of the Scavenger Receptor MARCO in Mediating Adenovirus Infection and Subsequent Innate Responses of Macrophages. *mbio.asm.org* **8**, 670–687.

139. Fejer, G. *et al.* Nontransformed, GM-CSF-dependent macrophage lines are a unique model to study tissue macrophage functions. doi:10.1073/pnas.1302877110.

140. Onyishi, C. U. *et al.* Toll-like receptor 4 and macrophage scavenger receptor 1 crosstalk regulates phagocytosis of a fungal pathogen. doi:10.1038/s41467-023-40635-w.

141. Stephens, M. False discovery rates: a new deal. *Biostatistics* **18**, 275–294 (2017).

142. GitHub - kevinblighe/EnhancedVolcano: Publication-ready volcano plots with enhanced colouring and labeling. https://github.com/kevinblighe/EnhancedVolcano?tab=readme-ov-file.

143. Barres, B. A. Perspective The Mystery and Magic of Glia: A Perspective on Their Roles in Health and Disease. doi:10.1016/j.neuron.2008.10.013.

144. Vidal-Itriago, A. *et al.* Microglia morphophysiological diversity and its implications for the CNS. *Front Immunol* **13**, 997786 (2022).

145. Ginhoux, F. & Guilliams, M. Review Tissue-Resident Macrophage Ontogeny and Homeostasis. doi:10.1016/j.immuni.2016.02.024.

146. Butovsky, O. & Weiner, H. L. Microglial signatures and their role in health and disease. *Nat Rev Neurosci* doi:10.1038/s41583-018-0057-5.

147. Bennett, F. C. *et al.* A combination of ontogeny and CNS environment establishes microglial identity. *Neuron* **98**, 1170 (2018).

148. Cronk, J. C. *et al.* Peripherally derived macrophages can engraft the brain independent of irradiation and maintain an identity distinct from microglia. *Journal of Experimental Medicine* **215**, 1627–1647 (2018).

149. Colonna, M. & Butovsky, O. Microglia Function in the Central Nervous System During Health and Neurodegeneration. (2017) doi:10.1146/annurev-immunol.

150. Borst, K., Dumas, A. A. & Prinz, M. Microglia: Immune and non-immune functions. *Immunity* vol. 54 2194–2208 Preprint at https://doi.org/10.1016/j.immuni.2021.09.014 (2021).

151. Rodríguez, A. M., Rodríguez, J. & Giambartolomei, G. H. Microglia at the Crossroads of Pathogen-Induced Neuroinflammation. *ASN Neuro* **14**, (2022).

152. Dobri, A. M., Dudău, M., Enciu, A. M. & Hinescu, M. E. CD36 in Alzheimer's Disease: An Overview of Molecular Mechanisms and Therapeutic Targeting. *Neuroscience* **453**, 301–311 (2021).

153. Gratuze, M., Leyns, C. E. G. & Holtzman, D. M. New insights into the role of TREM2 in Alzheimer's disease. *Molecular Neurodegeneration 2018 13:1* **13**, 1–16 (2018).

154. Laye, S., Michelucci alessandromichelucci, A., Sousa, C., Biber, K. & Michelucci, A. Cellular and Molecular Characterization of Microglia: A Unique Immune Cell Population. *Front. Immunol* **8**, (2017).

155. Jung, S. *et al.* Analysis of Fractalkine Receptor CX3CR1 Function by Targeted Deletion and Green Fluorescent Protein Reporter Gene Insertion. *Mol Cell Biol* **20**, 4106 (2000).

156. Cardona, A. E. *et al.* Control of microglial neurotoxicity by the fractalkine receptor. *Nature Neuroscience 2006 9:7* **9**, 917–924 (2006).

157. Wieghofer, P., Knobeloch, K. P. & Prinz, M. Genetic targeting of microglia. *Glia* **63**, 1–22 (2015).

158. Prinz, M., Jung, S. & Priller, J. Microglia Biology: One Century of Evolving Concepts. *Cell* **179**, 292–311 (2019).

159. Saederup, N. *et al.* Selective Chemokine Receptor Usage by Central Nervous System Myeloid Cells in CCR2-Red Fluorescent Protein Knock-In Mice. *PLoS One* **5**, (2010).

160. Faust, T. E. *et al.* A comparative analysis of microglial inducible Cre lines. *CellReports* **42**, 113031 (2023).

161. Yona, S. *et al.* Fate Mapping Reveals Origins and Dynamics of Monocytes and Tissue Macrophages under Homeostasis. *Immunity* **38**, 79–91 (2013).

162. Buttgereit, A. *et al.* Sall1 is a transcriptional regulator defining microglia identity and function. *Nature Immunology 2016 17:12* **17**, 1397–1406 (2016).

163. Kim, J. S. *et al.* A Binary Cre Transgenic Approach Dissects Microglia and CNS Border-Associated Macrophages. *Immunity* **54**, 176-190.e7 (2021).

164. Eme-Scolan, E. & Dando, S. J. Tools and Approaches for Studying Microglia In vivo. *Front Immunol* **11**, 583647 (2020).

165. Mercurio, D. *et al.* Protein Expression of the Microglial Marker Tmem119 Decreases in Association With Morphological Changes and Location in a Mouse Model of Traumatic Brain Injury. *Front Cell Neurosci* **16**, (2022).

166. Ruan, C. & Elyaman, W. A New Understanding of TMEM119 as a Marker of Microglia. *Front Cell Neurosci* **16**, (2022).

167. Guttenplan, K. A. & Liddelow, S. A. Astrocytes and microglia: Models and tools. *Journal of Experimental Medicine* **216**, 71–83 (2019).

168. Elmore, M. R. P. *et al.* CSF1 receptor signaling is necessary for microglia viability, which unmasks a cell that rapidly repopulates the microglia-depleted adult brain. *Neuron* **82**, 380 (2014).

169. Hume, D. A. *et al.* Phenotypic impacts of CSF1R deficiencies in humans and model organisms. *J Leukoc Biol* **107**, 205–219 (2020).

170. Mohamed, S. H. *et al.* CSF1R inhibition by PLX5622 reduces pulmonary fungal infection by depleting MHCIIhi interstitial lung macrophages. *bioRxiv* 2022.11.18.517077 (2022) doi:10.1101/2022.11.18.517077.

171. Lee, S. C., Dickson, D. W. & Casadevall, A. Pathology of cryptococcal meningoencephalitis: Analysis of 27 patients with pathogenetic implications. *Hum Pathol* **27**, 839–847 (1996).

172. Koutsouras, G. W., Ramos, R. L. & Martinez, L. R. Role of microglia in fungal infections of the central nervous system. *Virulence* **8**, 705 (2017).

173. Neal, L. M. *et al.* CD4+ T Cells Orchestrate Lethal Immune Pathology despite Fungal Clearance during Cryptococcus neoformans Meningoencephalitis. *mBio* **8**, (2017).

174. Xu, J. *et al.* Chemokine receptor CXCR3 is required for lethal brain pathology but not pathogen clearance during cryptococcal meningoencephalitis. *Sci Adv* **6**, 2502–2519 (2020).

175. Drummond, R. A. *et al.* CARD9+ Microglia Promote Antifungal Immunity via IL-1β and CXCL1-mediated Neutrophil Recruitment. *Nat Immunol* **20**, 559 (2019).

176. Drummond, R. A. *et al.* CARD9-Dependent Neutrophil Recruitment Protects against Fungal Invasion of the Central Nervous System. *PLoS Pathog* **11**, (2015).

177. Batista, S. J. *et al.* Gasdermin-D-dependent IL-1α release from microglia promotes protective immunity during chronic Toxoplasma gondii infection. *Nature Communications 2020 11:1* **11**, 1–13 (2020).

178. Garber, C. *et al.* T cells promote microglia-mediated synaptic elimination and cognitive dysfunction during recovery from neuropathogenic flaviviruses. *Nature Neuroscience 2019 22:8* **22**, 1276–1288 (2019).

179. Waltl, I. *et al.* Microglia have a protective role in viral encephalitis-induced seizure development and hippocampal damage. *Brain Behav Immun* **74**, 186–204 (2018).

180. Tan, Y. L., Yuan, Y. & Tian, L. Microglial regional heterogeneity and its role in the brain. *Molecular Psychiatry 2019 25:2* **25**, 351–367 (2019).

181. Ribeiro Xavier, A. L., Kress, B. T., Goldman, S. A., De Lacerda Menezes, J. R. & Nedergaard, M. A Distinct Population of Microglia Supports Adult Neurogenesis in the Subventricular Zone. *Journal of Neuroscience* **35**, 11848–11861 (2015).

182. Bisht, K. *et al.* Capillary-associated microglia regulate vascular structure and function through PANX1-P2RY12 coupling in mice. *Nature Communications 2021 12:1* **12**, 1–13 (2021).

183. Wlodarczyk, A. *et al.* A novel microglial subset plays a key role in myelinogenesis in developing brain. *EMBO J* **36**, 3292 (2017).

184. Stratoulias, V., Venero, J. L., Tremblay, M. & Joseph, B. Microglial subtypes: diversity within the microglial community. *EMBO J* **38**, (2019).

185. Krasemann, S. *et al.* The TREM2-APOE pathway drives the transcriptional phenotype of dysfunctional microglia in neurodegenerative diseases. *Immunity* **47**, 566 (2017).

186. Butovsky, O. & Weiner, H. L. Microglial signatures and their role in health and disease. *Nature Reviews Neuroscience 2018 19:10* **19**, 622–635 (2018).

187. Keren-Shaul, H. *et al.* A Unique Microglia Type Associated with Restricting Development of Alzheimer's Disease. *Cell* **169**, 1276-1290.e17 (2017).

188. Sousa, C. *et al.* Single-cell transcriptomics reveals distinct inflammation-induced microglia signatures. *EMBO Rep* **19**, (2018).

189. Pulido-Salgado, M., Vidal-Taboada, J. M., Barriga, G. G. D., Solà, C. & Saura, J. RNA-Seq transcriptomic profiling of primary murine microglia treated with LPS or LPS + IFNγ. *Scientific Reports 2018 8:1* **8**, 1–21 (2018).

190. Van Den Brink, S. C. *et al.* Single-cell sequencing reveals dissociation-induced gene expression in tissue subpopulations. *Nature Methods 2017 14:10* **14**, 935–936 (2017).

191. Ferrington, D. A. & Gregerson, D. S. Immunoproteasomes: Structure, Function, and Antigen Presentation. *Prog Mol Biol Transl Sci* **109**, 75 (2012).

192. Wang, J., Wu, X., Simonavicius, N., Tian, H. & Ling, L. Medium-chain Fatty Acids as Ligands for Orphan G Protein-coupled Receptor GPR84*. *Journal of Biological Chemistry* **281**, 34457–34464 (2006).

193. Mancini, S. J. *et al.* On-target and off-target effects of novel orthosteric and allosteric activators of GPR84. doi:10.1038/s41598-019-38539-1.

194. Yue, S. *et al.* Activation of the Immune-Metabolic Receptor GPR84 Enhances Inflammation and Phagocytosis in Macrophages. **9**, 1419 (2018).

195. Luscombe, V. B., Lucy, D., Bataille, C. J. R., Russell, A. J. & Greaves, D. R. 20 Years an Orphan: Is GPR84 a Plausible Medium-Chain Fatty Acid-Sensing Receptor? doi:10.1089/dna.2020.5846.

196. Jenkins, L. *et al.* Discovery and Characterization of Novel Antagonists of the Proinflammatory Orphan Receptor GPR84. *Cite This: ACS Pharmacol. Transl. Sci* **2021**, 1598–1613 (2021).

197. Zhang, Q. *et al.* GPR84 signaling promotes intestinal mucosal inflammation via enhancing NLRP3 inflammasome activation in macrophages. doi:10.1038/s41401-021-00825-y.

198. Bouchard, C., Pagé, J., Bédard, A., Tremblay, P. & Vallières, L. G protein-coupled receptor 84, a microglia-associated protein expressed in neuroinflammatory conditions. *Glia* **55**, 790–800 (2007).

199. Nicol, L. S. C. *et al.* The Role of G-Protein Receptor 84 in Experimental Neuropathic Pain. (2015) doi:10.1523/JNEUROSCI.3558-14.2015.

200. Onyishi, C. U. *et al.* Toll-like receptor 4 and macrophage scavenger receptor 1 crosstalk regulates phagocytosis of a fungal pathogen. *Nat Commun* **14**, (2023).

201. Suzuki, M. *et al.* Medium-chain fatty acid-sensing receptor, GPR84, is a proinflammatory receptor. *J Biol Chem* **288**, 10684–10691 (2013).

202. Gudgeon, J., Marín-Rubio, J. L. & Trost, M. The role of macrophage scavenger receptor 1 (MSR1) in inflammatory disorders and cancer. *Front Immunol* **13**, 1012002 (2022).

203. Lipovsky, M. M. *et al.* Phagocytosis of NonopsonizedCryptococcus neoformansby Swine Microglia Involves CD14 Receptors. *Clin Immunol Immunopathol* **84**, 208–211 (1997).

204. Liu, Y. J. *et al.* Cspg4high microglia contribute to microgliosis during neurodegeneration. *Proc Natl Acad Sci U S A* **120**, e2210643120 (2023).

205. Rath, M., Müller, I., Kropf, P., Closs, E. I. & Munder, M. Metabolism via Arginase or Nitric Oxide Synthase: Two Competing Arginine Pathways in Macrophages. *Front Immunol* **5**, (2014).

206. Maric-Biresev, J. *et al.* Loss of the interferon-γ-inducible regulatory immunity-related GTPase (IRG), Irgm1, causes activation of effector IRG proteins on lysosomes, damaging lysosomal function and predicting the dramatic susceptibility of Irgm1-deficient mice to infection. *BMC Biol* **14**, 1–20 (2016).

207. Pilla-Moffett, D., Barber, M. F., Taylor, G. A. & Coers, J. Interferon-inducible GTPases in host resistance, inflammation and disease. *J Mol Biol* **428**, 3495 (2016).

208. Abstract, G. Human GBP1 Differentially Targets Salmonella and Toxoplasma to License Recognition of Microbial Ligands and Caspase-Mediated Death. *CellReports* **32**, 108008 (2020).

209. Rafeld, H. L., Kolanus, W., Van Driel, I. R. & Hartland, E. L. Interferon-induced GTPases orchestrate host cell-autonomous defence against bacterial pathogens. *Biochem Soc Trans* **49**, 1287 (2021).

210. Jarvis, J. N. *et al.* Adjunctive Interferon-γ Immunotherapy for the Treatment of HIV-associated Cryptococcal Meningitis: A Randomized Controlled Trial. *AIDS* **26**, 1105 (2012).

211. Xu, J. *et al.* CCR2 Signaling Promotes Brain Infiltration of Inflammatory Monocytes and Contributes to Neuropathology during Cryptococcal Meningoencephalitis. *mBio* **12**, 1076–1097 (2021).

212. Moseman, E. A., Blanchard, A. C., Nayak, D. & McGavern, D. B. T cell engagement of cross-presenting microglia protects the brain from a nasal virus infection. *Sci Immunol* **5**, 1817 (2020).

213. Eschke, M. *et al.* A novel experimental model of Cryptococcus neoformans-related immune reconstitution inflammatory syndrome (IRIS) provides insights into pathogenesis. *Eur J Immunol* **45**, 3339–3350 (2015).

214. Aggarwal, N., Barclay, W. & Shinohara, M. L. Understanding mechanisms underlying the pathology of immune reconstitution inflammatory syndrome (IRIS) by using animal models. *Curr Clin Microbiol Rep* **5**, 201 (2018).

215. Khaw, Y. M. *et al.* Th1-Dependent Cryptococcus-Associated Immune Reconstitution Inflammatory Syndrome Model With Brain Damage. *Front Immunol* **11**, 529219 (2020).

216. Rustenhoven, J. & Kipnis, J. Brain borders at the central stage of neuroimmunology. *Nature* **612**, 417 (2022).

217. Louveau, A., Harris, T. H. & Kipnis, J. Revisiting the Mechanisms of CNS Immune Privilege. (2015) doi:10.1016/j.it.2015.08.006.

218. Herisson, F. *et al.* Direct vascular channels connect skull bone marrow and the brain surface enabling myeloid cell migration. doi:10.1038/s41593-018-0213-2.

219. Mazzitelli, J. A. *et al.* Skull bone marrow channels as immune gateways to the central nervous system. *Nature Neuroscience* | **26**, (2023).

220. Mazzitelli, J. A. & Smyth, L. C. D. ✉. Cerebrospinal fluid regulates skull bone marrow niches via direct access through dural channels. doi:10.1038/s41593-022-01029-1.

221. Cugurra, A. *et al.* Skull and vertebral bone marrow are myeloid cell reservoirs for the meninges and CNS parenchyma. *Science (1979)* **373**, (2021).

222. Louveau, A. *et al.* CNS lymphatic drainage and neuroinflammation are regulated by meningeal lymphatic vasculature. doi:10.1038/s41593-018-0227-9.

223. Pasciuto, E. *et al.* Microglia Require CD4 T Cells to Complete the Fetal-to-Adult Transition. *Cell* **182**, 625 (2020).

224. Vu, K., Eigenheer, R. A., Phinney, B. S. & Gelli, A. Cryptococcus neoformans Promotes Its Transmigration into the Central Nervous System by Inducing Molecular and Cellular Changes in Brain Endothelial Cells. *Infect Immun* **81**, 3139 (2013).

225. Chen, S. H. M. *et al.* Cryptococcus neoformans induces alterations in the cytoskeleton of human brain microvascular endothelial cells. *J Med Microbiol* **52**, 961–970 (2003).

226. Strickland, A. B. & Shi, M. Mechanisms of fungal dissemination. *Cell Mol Life Sci* **78**, 3219 (2021).

227. Kim, J. *et al.* Fungal brain infection modelled in a human-neurovascular-unit-on-a-chip with a functional blood–brain barrier. *Nature Biomedical Engineering 2021 5:8* **5**, 830–846 (2021).

228. Chen, Y. *et al.* Quantitative analysis reveals internalization of Cryptococcus neoformans by brain endothelial cells in vivo. *Cell Microbiol* **23**, e13330 (2021).

229. Cain, M. D., Salimi, H., Diamond, M. S. & Klein, R. S. Mechanisms of Pathogen Invasion into the Central Nervous System. *Neuron* **103**, 771–783 (2019).

230. Kaufman-Francis, K. *et al.* The Early Innate Immune Response to, and Phagocyte-Dependent Entry of, Cryptococcus neoformans Map to the Perivascular Space of Cortical Post-Capillary Venules in Neurocryptococcosis. *Am J Pathol* **188**, 1653–1665 (2018).

231. Santiago-Tirado, F. H., Onken, M. D., Cooper, J. A., Klein, R. S. & Doering, T. L. Trojan horse transit contributes to blood-brain barrier crossing of a eukaryotic pathogen. *mBio* **8**, (2017).

232. Yang, X., Wang, H., Hu, F., Chen, X. & Zhang, M. Nonlytic exocytosis of Cryptococcus neoformans from neutrophils in the brain vasculature. *Cell Commun Signal* **17**, (2019).

233. Zhang, M. *et al.* Real-time in vivo imaging reveals the ability of neutrophils to remove Cryptococcus neoformans directly from the brain vasculature. *J Leukoc Biol* **99**, 467–473 (2016).

234. Shi, M. *et al.* Real-time imaging of trapping and urease-dependent transmigration of Cryptococcus neoformans in mouse brain. *J Clin Invest* **120**, 1683 (2010).

235. Shi, M. & Mody, C. H. Fungal Infection in the Brain: What We Learned from Intravital Imaging. *Front Immunol* **7**, 292 (2016).

236. Fu, M. S. *et al.* Cryptococcus neoformans urease affects the outcome of intracellular pathogenesis by modulating phagolysosomal pH. *PLoS Pathog* **14**, (2018).

237. Gibson, J. F. *et al.* Blood vessel occlusion by Cryptococcus neoformans is a mechanism for haemorrhagic dissemination of infection. *PLoS Pathog* **18**, (2022).

238. Davis, J. M., Huang, M., Botts, M. R., Hull, C. M. & Huttenlocher, A. A Zebrafish Model of Cryptococcal Infection Reveals Roles for Macrophages, Endothelial Cells, and Neutrophils in the Establishment and Control of Sustained Fungemia. *Infect Immun* **84**, 3047 (2016).

239. Nielson, J. A. & Davis, J. M. Roles for Microglia in Cryptococcal Brain Dissemination in the Zebrafish Larva. *Microbiol Spectr* **11**, (2023).

240. van der Meijden, P. E. J. & Heemskerk, J. W. M. Platelet biology and functions: new concepts and clinical perspectives. *Nat Rev Cardiol* **16**, 166–179 (2019).

241. Assinger, A., Schrottmaier, W. C., Salzmann, M. & Rayes, J. Platelets in sepsis: An update on experimental models and clinical data. *Front Immunol* **10**, 1687 (2019).

242. Mezger, M. *et al.* Platelets and Immune Responses During Thromboinflammation. *Front Immunol* **10**, 1731 (2019).

243. Eberl, C. *et al.* Candida: Platelet Interaction and Platelet Activity in vitro. *J Innate Immun* **11**, 52–62 (2019).

244. Tischler, B. Y., Tosini, N. L., Cramer, R. A. & Hohl, T. M. Platelets are critical for survival and tissue integrity during murine pulmonary Aspergillus fumigatus infection. *PLoS Pathog* **16**, e1008544 (2020).

245. Krijgsveld, J. *et al.* Thrombocidins, microbicidal proteins from human blood platelets, are C- terminal deletion products of CXC chemokines. *Journal of Biological Chemistry* **275**, 20374–20381 (2000).

246. Ghuman, H. *et al.* Mucor circinelloides induces platelet aggregation through integrin αIIbβ3 and FcγRIIA. *Platelets* **30**, 256–263 (2019).

247. Speth, C., Rambach, G. & Lass-Flörl, C. Platelet immunology in fungal infections. *Thromb Haemost* **112**, 632–639 (2014).

248. Speth, C., Rambach, G., Lass-Florl, C., Dierich, M. P. & Wurzner, R. The role of complement in invasive fungal infections. *Mycoses* **47**, 93–103 (2004).

249. Gundlach, J. P. *et al.* Lethal thrombosis of the iliac artery caused by Aspergillus fumigatus after liver transplantation: Case report and review of the literature. *BMC Surg* **19**, 200 (2019).

250. Sherif, R. & Segal, B. H. Pulmonary aspergillosis: Clinical presentation, diagnostic tests, management and complications. *Curr Opin Pulm Med* **16**, 242–250 (2010).

251. Fréalle, E. *et al.* In vitro coagulation triggers anti-Aspergillus fumigatus neutrophil response. *Future Microbiol* **13**, 659–669 (2018).

252. Rayes, J. *et al.* The podoplanin-CLEC-2 axis inhibits inflammation in sepsis. *Nat Commun* **8**, 1–14 (2017).

253. Carestia, A., Mena, H. A., Olexen, C. M., Jenne, C. N. & Carrera Silva, E. A. Platelets Promote Macrophage Polarization toward Pro-inflammatory Phenotype and Increase Survival of Septic Mice. *Cell Rep* **28**, 896–908 (2019).

254. Jafari, M. & Ansari-Pour, N. Why, When and How to Adjust Your P Values? *Cell Journal (Yakhteh)* **20**, 604 (2019).

255. Lui, H. *et al.* Progranulin Deficiency Promotes Circuit-Specific Synaptic Pruning by Microglia via Complement Activation. *Cell* **165**, 921 (2016).

256. Ma, K. *et al.* CTSB is a negative prognostic biomarker and therapeutic target associated with immune cells infiltration and immunosuppression in gliomas. *Sci Rep* **12**, (2022).

257. Gonzalez-Leal, I. J. *et al.* Cathepsin B in Antigen-Presenting Cells Controls Mediators of the Th1 Immune Response during Leishmania major Infection. *PLoS Negl Trop Dis* **8**, (2014).

258. Hain, S. & Drummond, R. A. Meningeal Whole Mounts for Imaging CNS Fungal Infection. *Methods in Molecular Biology* **2667**, 113–121 (2023).

259. Xu-Vanpala, S. *et al.* Functional heterogeneity of alveolar macrophage population based on expression of CXCL2. *Sci Immunol* **5**, (2020).

260. Cramer, S. W. *et al.* Through the looking glass: a review of cranial window technology for optical access to the brain. *J Neurosci Methods* **354**, 109100 (2021).

261. Derk, J., Jones, H. E., Como, C., Pawlikowski, B. & Siegenthaler, J. A. Living on the Edge of the CNS: Meninges Cell Diversity in Health and Disease. *Front Cell Neurosci* **15**, (2021).

262. Coles, J. A. *et al.* Intravital Imaging of a Massive Lymphocyte Response in the Cortical Dura of Mice after Peripheral Infection by Trypanosomes. *PLoS Negl Trop Dis* **9**, 3714 (2015).

263. Quintana, J. F. *et al.* The murine meninges acquire lymphoid tissue properties and harbour autoreactive B cells during chronic Trypanosoma brucei infection. *PLoS Biol* **21**, (2023).

264. DeSisto, J. *et al.* Single-Cell Transcriptomic Analyses of the Developing Meninges Reveal Meningeal Fibroblast Diversity and Function. *Dev Cell* **54**, 43 (2020).

265. Møllgård, K. *et al.* A mesothelium divides the subarachnoid space into functional compartments. *Science (1979)* **379**, 84–88 (2023).

266. Rayes, J., Bourne, J. H., Brill, A. & Watson, S. P. The dual role of platelet-innate immune cell interactions in thrombo-inflammation. *Res Pract Thromb Haemost* **4**, 23 (2020).

267. Beristain-Covarrubias, N. *et al.* Salmonella-induced thrombi in mice develop asynchronously in the spleen and liver and are not effective bacterial traps. *Blood* **133**, 600 (2019).

268. Sun, D. *et al.* Real-Time Imaging of Interactions of Neutrophils with Cryptococcus neoformans Demonstrates a Crucial Role of Complement C5a-C5aR Signaling. *Infect Immun* **84**, 216 (2016).

269. Liu, G. *et al.* CRIg plays an essential role in intravascular clearance of bloodborne parasites by interacting with complement. *Proc Natl Acad Sci U S A* **116**, 24214–24220 (2019).

270. Heurich, M. & McCluskey, G. Complement and coagulation crosstalk – Factor H in the spotlight. *Immunobiology* **228**, 152707 (2023).

271. Koupenova, M. *et al.* The role of platelets in mediating a response to human influenza infection. *Nature Communications 2019 10:1* **10**, 1–18 (2019).

272. Wienkamp, A. K., Erpenbeck, L. & Rossaint, J. Platelets in the NETworks interweaving inflammation and thrombosis. *Front Immunol* **13**, 953129 (2022).

273. Monocytes, H., Bobak', D. A., Washburn, R. G. & Frank, M. M. C1q enhances the phagocytosis of Cryptococcus neoformans blastospores by human monocytes. *The Journal of Immunology* **141**, 592–597 (1988).

274. Shen, L. *et al.* Increased activity of the complement system in cerebrospinal fluid of the patients with Non-HIV Cryptococcal meningitis. *BMC Infect Dis* **17**, 1–7 (2017).

275. Zhao, X. *et al.* C1q Confers Protection Against Cryptococcal Lung Infection by Alleviating Inflammation and Reducing Cryptococcal Virulence. *Open Forum Infect Dis* **10**, (2023).

276. Donat, C. *et al.* Complement C1q Enhances Primary Hemostasis. *Front Immunol* **11**, 527652 (2020).

277. Roemer, T. & Krysan, D. J. Antifungal drug development: challenges, unmet clinical needs, and new approaches. *Cold Spring Harb Perspect Med* **4**, (2014).

278. Wüthrich, M., Filutowicz, H. I., Warner, T., Deepe, G. S. & Klein, B. S. Vaccine immunity to pathogenic fungi overcomes the requirement for CD4 help in exogenous antigen presentation to CD8+ T cells: Implications for vaccine development in immune-deficient hosts. *Journal of Experimental Medicine* **197**, 1405–1416 (2003).

279. Paolicelli, R. C. *et al.* Microglia states and nomenclature: A field at its crossroads. *Neuron* **110**, 3458 (2022).

280. Ransohoff, R. M. A polarizing question: do M1 and M2 microglia exist? *Nature Neuroscience 2016 19:8* **19**, 987–991 (2016).

281. Chen, H. *et al.* Ly6C-high monocytes alleviate brain injury in experimental subarachnoid hemorrhage in mice. *J Neuroinflammation* **20**, 1–17 (2023).

282. Kolabas, Z. I. *et al.* Distinct molecular profiles of skull bone marrow in health and neurological disorders. *Cell* **186**, 3706 (2023).

283. Cugurra, A. *et al.* Skull and vertebral bone marrow are myeloid cell reservoirs for the meninges and CNS parenchyma. *Science* **373**, (2021).

284. Schneider, C. A. *et al.* Imaging the dynamic recruitment of monocytes to the blood–brain barrier and specific brain regions during Toxoplasma gondii infection. *Proc Natl Acad Sci U S A* **116**, 24796–24807 (2019).

285. Stephan, A. H., Barres, B. A. & Stevens, B. The Complement System: An Unexpected Role in Synaptic Pruning During Development and Disease. *https://doi.org/10.1146/annurev-neuro-061010-113810* **35**, 369–389 (2012).

286. Hong, S. *et al.* Complement and microglia mediate early synapse loss in Alzheimer mouse models. *Science (1979)* **352**, 712–716 (2016).

287. Fonseca, M. I. *et al.* Cell-specific deletion of C1qa identifies microglia as the dominant source of C1q in mouse brain. *J Neuroinflammation* **14**, 1–15 (2017).